# UNCLASSIFIED

AD NUMBER

ADB157529

NEW LIMITATION CHANGE

TO

Approved for public release, distribution unlimited

FROM

Distribution authorized to U.S. Gov't. agencies and their contractors; Critical Technology; APR 1991. Other requests shall be referred to Wright Lab., WL/FIMT. Wright-Patterson AFB, OH 45433-6503.

AUTHORITY

AFRL/WSC ltr, 1 Feb 2010

THIS PAGE IS UNCLASSIFIED

②

AFFTC-TR-91-15

A
F
F
T
C

X-29 HIGH ANGLE-OF-ATTACK
FLYING QUALITIES

AD INEXPLORATA

DTIC
ELECTE
AUG 2 8 1991
S D D

FREDRICK R. WEBSTER
Project Engineer

DANA PURIFOY, MAJOR, USAF
Project Pilot

JULY 1991

FINAL REPORT

CRITICAL TECHNOLOGY

Distribution authorized to U.S. Government Agencies and their contractors (Test and Evaluation), April 1991. Other requests for this document shall be referred to WL/FIMT, Wright-Patterson AFB, Ohio 45433-6523

CONTROLLING OFFICE: WL/FIMT, WRIGHT-PATTERSON AFB, OHIO 45433-6523

AIR FORCE FLIGHT TEST CENTER
EDWARDS AIR FORCE BASE, CALIFORNIA
AIR FORCE SYSTEMS COMMAND
UNITED STATES AIR FORCE
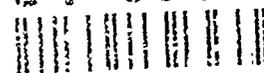
This Technical Report (AFFTC-TR-91-15, X-29 High Angle-of-Attack Flying Qualities) was submitted under Job Order Number A83007 by the Commander, 6510 Test Wing, Edwards Air Force Base, California, 93523-5000.

Prepared by:

This report has been reviewed and is approved for publication: 09 July 1991

Fredrick R. Webster
AFFTC Lead Engineer

Robert D. Evans
Chief, Research Projects Division
6510 Test Wing
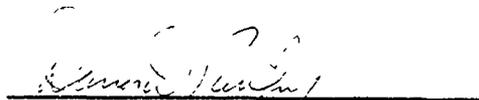
Dana Purifoy
Major, USAF
AFFTC Project Pilot

Roger C. Crane
Chief Engineer, 6510 Test Wing
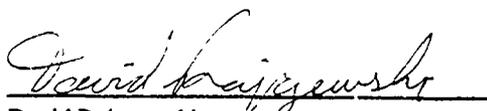
David Rajczewski
Captain, USAF
Project Engineer
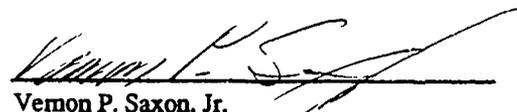
Vernon P. Saxon, Jr.
Colonel, USAF
Commander, 6510 Test Wing
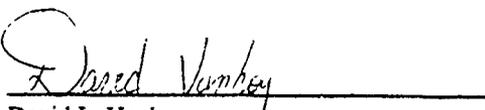
David L. Vanhoy
Project Engineer
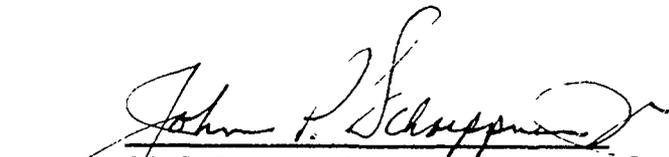
John P. Schoeppner, Jr.
Major General, USAF
Commander, AFFTC

REPORT DOCUMENTATION PAGE

Public reporting burden for this collection of information is estimated to average 1 hour per response, including the time for reviewing instructions, searching existing data sources, gathering and maintaining the data needed, and completing and reviewing the collection of information. Send comments regarding this burden estimate or any other aspect of this collection of information, including suggestions for reducing this burden to Washington Headquarters Services, Directorate for Information Operations and Reports, 1215 Jefferson Davis Highway, Suite 1204, Arlington, VA 22202-4302, and to the Office of Management and Budget, Paperwork Reduction Project (0704-0188), Washington, DC 20503.

1. AGENCY USE ONLY (Leave blank)	2. REPORT DATE	3. REPORT TYPE AND DATES COVERED
	June 1991	Final, 23 May 1989 to 21 February 1991

4. TITLE AND SUBTITLE

X-29 High Angle-of-Attack Flying Qualities

5. FUNDING NUMBERS

JON: A83007

6. AUTHOR(S)

Webster, Fredrick R.
Purifoy, Dana, Major, USAF

7. PERFORMING ORGANIZATION NAME(S) AND ADDRESS(ES)

AFFTC, 6510 Test Wing
Edwards AFB, California 93523-5000

8. PERFORMING ORGANIZATION REPORT NUMBER

AFFTC-TR-91-15

9. SPONSORING/MONITORING AGENCY NAME(S) AND ADDRESS(ES)

WL/FIMT
Wright-Patterson AFB, Ohio 45433-6503

10. SPONSORING/MONITORING AGENCY REPORT NUMBER

11. SUPPLEMENTARY NOTES

12a. DISTRIBUTION/AVAILABILITY STATEMENT CRITICAL TECHNOLOGY

Distribution authorized to U.S. Government agencies and their contractors (Test and Evaluation), April 1991. Other requests for this document shall be referred to WL/FIMT, Wright-Patterson AFB, Ohio 45433-6503.

12b. DISTRIBUTION CODE

13. ABSTRACT (Maximum 200 words)

This program was conducted to evaluate the X-29 configuration at high angle of attack. The flight test objectives were to evaluate the high angle of attack (AOA) flying qualities and to conduct a limited military utility and agility metric test effort with the X-29 number two research aircraft (USAF S/N 820049). These objectives were met. The X-29 was an advanced technology demonstrator aircraft which incorporated a forward swept wing, a thin supercritical airfoil, an aeroelastically tailored composite wing cover, full span flaperons providing variable camber, variable incidence close coupled canards, high longitudinal static instability, a three surface longitudinal control configuration, and a triplex digital flight control system.

14. SUBJECT TERMS			15. NUMBER OF PAGES
research aircraft X-29 high AOA	forward swept wing canard stability derivative canard configuration flying qualities	static stability control derivative	
			16. PRICE CODE

17. SECURITY CLASSIFICATION OF REPORT	18. SECURITY CLASSIFICATION OF THIS PAGE	19. SECURITY CLASSIFICATION OF ABSTRACT	20. LIMITATION OF ABSTRACT
UNCLASSIFIED	UNCLASSIFIED	UNCLASSIFIED	SAR

PREFACE

The X-29 high angle-of-attack (AOA) program was a research effort conducted to evaluate the X-29 aircraft at high AOA. Grumman Aerospace Corporation (GAC) of Bethpage, New York, was contracted to design two X-29 aircraft. The second of these aircraft (X-29 USAF S/N 820049) was modified with a spin chute, subsystems upgrades, and a new flight control system for high AOA flight test. Overall program management was the responsibility of the Wright Laboratory Flight Dynamics Directorate, Wright-Patterson AFB, Ohio. The NASA Ames-Dryden Flight Research Facility (ADFRF) was responsible for flight test management and safety of flight. The Air Force Flight Test Center (AFFTC) was a Participating Test Organization under Job Order Number A83007. The program was conducted in accordance with Program Management Directive 9024 (8/63245F) dated 22 March 1990.

Technical data on stability, control, flight control systems, and flying qualities were obtained. Limited military utility and agility metric tests were also conducted. High AOA agility metric results were documented in AFFTC-TIM-91-02, X-29 High Angle-of-Attack Agility Flight Test Results (Reference 1).

Testing began on 23 May 1989 and ended 21 February 1991 at NASA ADFRF, Edwards AFB, California. The aircraft (X-29 USAF S/N 820049) flew 85 flights totaling 70.9 flight hours.

The X-29 high AOA program was a result of a team effort involving personnel from the AFFTC, NASA, GAC and Honeywell. The authors wish to thank Paul Pellicano and Joseph Krummenacker of GAC for their contributions to the test program and the preparation of this report

EXECUTIVE SUMMARY

This report documents the high angle-of-attack (AOA) flying qualities of the X-29 aircraft. The program was conducted with the second X-29 aircraft (USAF S/N 820049) between May 1989 and February 1991. Eighty-five flights totaling 70.9 flight hours were conducted. The NASA Ames-Dryden Flight Research Facility was responsible for flight test management and safety of flight. The Air Force Flight Test Center was a Participating Test Organization. Overall program management was the responsibility of the Wright Laboratory Flight Dynamics Directorate through the X-29 Advanced Development System Program Office

The flight test objectives were to expand the technical evaluations and to conduct military utility and agility metric testing of the X-29 configuration above 20 degrees AOA. The flight test objectives were met. Technical evaluations consisted of stability, control, aerodynamic analysis, and comparisons with predictions. Military utility tests consisted of limited qualitative evaluations of two representative types of air-to-air engagements utilizing high AOA. Agility metric tests were conducted at 200 KCAS above 15 degrees AOA

The X-29 exhibited good stability, control, and maneuverability up to 45 degrees AOA for the lateral-directional axis and to 50 degrees AOA for the longitudinal axis. Aircraft control was precise in all three axes. As AOA increased, the aircraft stability and control degraded gradually Slow but well coordinated velocity-vector rolls were demonstrated using full-lateral stick inputs with feet on the floor Full pedal-rudder roll capability was also demonstrated. Beneficial differences in aerodynamics from predictions allowed increasing the roll rate by 40 to 60 percent below 35 degrees AOA with use of the in flight variable gain capability. Predicted large amplitude wing rock above 30 degrees AOA did not materialize Mild wing rock was encountered above 37 degrees AOA but was considered inconsequential to

lateral-directional maneuvering. Lateral-directional maneuvering above 45 degrees AOA was not possible due to insufficient rudder control power.

Aerodynamic full nosedown recovery moments were up to 50 percent less than predicted above 50 degrees AOA. No hung stalls occurred, but nosedown recovery capability from above 50 degrees AOA was marginal at aft centers of gravity. Aerodynamic yaw asymmetries and the lack of rudder control power above 50 degrees AOA degraded the recoveries to lower AOA. Repeated recoveries from approximately 55 degrees AOA were made ahead of 447 inches center of gravity; however, recoveries with centers of gravity aft of 446 inches were marginal

The AOA envelope was cleared to 50 degrees AOA for all centers of gravity and to 55 degrees for centers of gravity at or ahead of 446 inches. Full-lateral stick or full-rudder pedal inputs were cleared. The envelope was not cleared for combined lateral-stick and rudder-pedal inputs.

The pilots overall qualitative assessments of the X-29 flying qualities indicated that it flew better in the 25- to 45-degree AOA range than current operational fighters. The improvements included precise AOA tracking, loaded rolling capability to 45 degrees AOA, and gradual degradation of aircraft control as AOA increased. These characteristics made the X-29 a natural aircraft to fly up to 45 degrees AOA

Results from the military utility maneuvers indicated the need for cockpit displays at high AOA which would provide the attacking aircraft flight path relative to the target as well as accurate target range and closure rate. Limited military utility tests with the increased roll-rate capability showed promise. The military utility tests accomplished indicated that the maneuvers performed should provide a starting point for future high AOA military utility evaluations.

TABLE OF CONTENTS

LIST OF ILLUSTRATIONS

LIST OF ILLUSTRATIONS (Continued)

LIST OF ILLUSTRATIONS (Continued)

LIST OF ILLUSTRATIONS (Continued)

APPENDIX C

LIST OF ILLUSTRATIONS (Continued)

LIST OF ILLUSTRATIONS (Concluded)

LIST OF TABLES

INTRODUCTION

GENERAL

This report presents results of the flying qualities testing of the X-29 aircraft at high angle-of-attack (AOA). The program was conducted with the second X-29 aircraft (USAF Serial Number 820049) from May 1989 to February 1991. The NASA Ames-Dryden Flight Research Facility (ADFRF) was responsible for flight test management and safety of flight. The Air Force Flight Test Center (AFFTC) was a Participating Test Organization (PTO). The program consisted of an integrated test team of AFFTC, NASA, Grumman, and Honeywell engineers and technicians. The program required 85 flights for a total of 70.9 flight hours. The program consisted of high AOA envelope clearance, stability, control, and flying qualities evaluations. Limited military utility and agility metric tests were also performed. The agility metric test results are documented in AFFTC TIM-91-02, *X-29A High Angle-of-Attack Agility Flight Test Results* (Reference 1).

BACKGROUND

The X-29 high AOA program was managed by the Wright Laboratory X-29 Advance Development Program Office (ADPO). Tests were conducted under Program Management Directive 9024(8/63245F), Advance Fighter Technology Integration which was dated 22 March 1990. The high AOA program was the last part of the X-29 follow-on program designed to evaluate the X-29 configuration which consisted of eight technologies. The technologies were a forward swept wing, variable incidence close coupled canards, high static longitudinal instability, three surface pitch control, full span flaperons providing variable camber capability, thin supercritical airfoil, aeroelastic tailored composite wing cover, and a triplex digital flight control system (FCS) with specific high AOA control laws.

The planned test program was to be conducted in two phases with differing airspeed regions. The first phase was limited to 0.6 Mach number above 10 degrees AOA and would take place between May 1989 and July 1990. The second phase would include an upgraded control system capable of flight to 0.9 Mach number above 10 degrees AOA. Flight testing for the second phase was scheduled for late

summer of 1990. Program budget cuts precluded completion of the 0.6 Mach number envelope expansion in late spring of 1990 and resulted in a restructuring of the program. Flight testing was halted for the spring and early summer of 1990 as funds for flight testing the aircraft were unavailable.

Limited funding was identified in Fiscal Year 1991 for resumption of high AOA flight testing. The program was restructured to achieve 0.75 Mach number above 10 degrees AOA and to conduct limited military utility and agility metric tests within the cleared envelope The FCS modifications with airspeed capability above 0.6 Mach number and flight-test defined upgrades were designed during the summer of 1990. High AOA flight testing resumed in October of 1990 with a reduced program aimed at expanding the envelope to 0.75 Mach number above 27,000 feet pressure altitude and to 300 KCAS between 17,000 and 27,000 feet pressure altitude. Twelve military utility and agility metric flights were planned between 1 January and 15 February 1991, following envelope expansion. Program funds for further flight testing expired on 22 February 1991.

FLIGHT TEST OBJECTIVES

The restructured program flight test objectives were:

1. Clear a maneuvering envelope to maximum AOA within a 0.75 Mach number/300 KCAS envelope between 17,000 and 40,000 feet pressure altitude;

2. Obtain technical data on stability, control, and aerodynamics and perform comparisons with predictions;

3. Obtain agility metric test data at 20,000 feet pressure altitude; and

4. Obtain limited military utility test data from perch set-up tracking and basic fighter maneuvers (BFMs).

The X-29 high AOA flight test objectives were met.

AIRCRAFT DESCRIPTION

The X-29 was a single seat, forward swept wing (FSW) research aircraft with a takeoff gross weight of approximately 18,000 pounds. The wings were thin supercritical airfoils with a forward sweep of 34 degrees at the quarter chord and were covered with aeroelastically tailored composite skins as means of controlling structural divergence. The nearly coplanar, variable incidence close coupled canards were the primary pitch control surfaces. The canards provided the high level of static instability (approximately 35 percent unstable at low AOA and high subsonic speed) as well as the means for controlling the instability. Canard control power was augmented by a two segment full span flaperon and an aft body strake flap. All three surfaces acted in conjunction to provide control of the highly unstable configuration. The flaperon and strake also worked independently from the canard in a slow trim mode, Automatic Camber Control (ACC), to minimize induced drag at low AOA and maximize lift above 15 degrees AOA during steady-state conditions.

Lateral control was provided by full span asymmetric deflection of the flaperon. Directional control was provided by a conventional rudder.

The Grumman design incorporated existing aircraft hardware to reduce development costs. This hardware included a modified F-5A nose section, F-16 main gear, emergency power unit (EPU) and surface actuators, and F-14 flight sensors and Honeywell HDP5301 flight control computers. The X-29 was powered by an F-18 General Electric (GE) F-404-GE-400 afterburning engine with a maximum thrust rating of 16,000 pounds at sea level static conditions. The aircraft was equipped with three air data probes; two fuselage-mounted side probes and a noseboom probe. Three independent vanes mounted on the noseboom were also used for AOA data.

A triplex fly-by-wire flight control system was used to provide the stability, control, handling qualities, and optimal surface trim configuration. The system had a primary digital mode (Normal Digital) and a dissimilar analog backup mode (Analog Reversion). The control laws were specifically redesigned for the high AOA program to provide good flying qualities, departure resistance, and spin prevention. The design was accomplished to 0.75 Mach number above 10 degrees AOA. The X-29 with the high AOA control laws had a limited airspeed envelope above 10 degrees AOA compared to the low AOA flight control system. However, the low AOA control laws were limited to 20 degrees AOA.

The second X-29 (USAF S/N 820049) was also equipped with a spin recovery parachute; enlarged cockpit AOA; yaw rate and sideslip gauges; and subsystems modifications designed for high AOA flight. Appendix A contains a detailed aircraft description. Appendix D contains a full detailed FCS and control law description.

FLIGHT CONTROL SYSTEM DESCRIPTION

The X-29 high AOA FCS was designed by a combined AFFTC and NASA ADFRF team. The design was added to an earlier low AOA version of the aircraft control laws, the BLOCKVIII-AD software. Modifications were implemented above 15 degrees AOA which helped to minimize the budget and time requirements for verification and validation (V and V) and low AOA envelope expansion. Control laws below 10 degrees AOA remained the same as the already proven software from the previous low AOA X-29 flight test program. The new high AOA control laws were faded in between 10 and 15 degrees AOA.

Three flight control system software releases were flown during the test program. These were BLOCKIX-AA (the original release), BLOCKIX-AA01 (longitudinal command changes), and BLOCKIX-AA02 (new gains and software to allow flight above 10 degrees AOA above 0.6 Mach number). Functional descriptions of the high AOA FCS are contained in Appendix D and References 2 and 3.

The longitudinal axis required little modification from the low AOA system originally designed by Grumman. The high AOA control laws were a pitch rate command system with a weak AOA feedback to provide positive apparent speed stability to the pilot above 15 degrees AOA. Gravity vector compensation to the pitch rate command was removed above 15 degrees AOA due to redundancy management concerns about nuisance failure indications with the attitude and heading reference system (AHRS). Negative AOA and load factor limiters were added to aid in preventing tumble entries. Positive AOA limiters were not used.

The lateral-directional control laws required extensive modification to meet flying qualities design

requirements above 15 degrees AOA. Modifications included:

1. Linear lateral stick command gearing;

2. Increased gain roll damper using roll rate feedback;

3. Elimination of the lateral integrator,

4. Addition of washed-out stability axis yaw rate to the rudder feedback path;

5. Aileron to rudder interconnect modifications in the direct path and the addition of a washed-out parallel path;

6. AOA and airspeed gain scheduling;

7. Simplification of lateral command and feedback architecture, and

8. Spin prevention logic above 40 degrees AOA (later changed to 50 degrees) with pilot override capability.

The lateral command system was designed to provide velocity vector rolls with minimal sideslip using simple architecture. Major modifications were required to provide appropriate command and feedback balance. The low AOA control laws had a complicated optimal control type structure where all lateral-directional states were fed back to both aileron and rudder. Optimal control theory was not used in the design of the X-29 high AOA control laws.
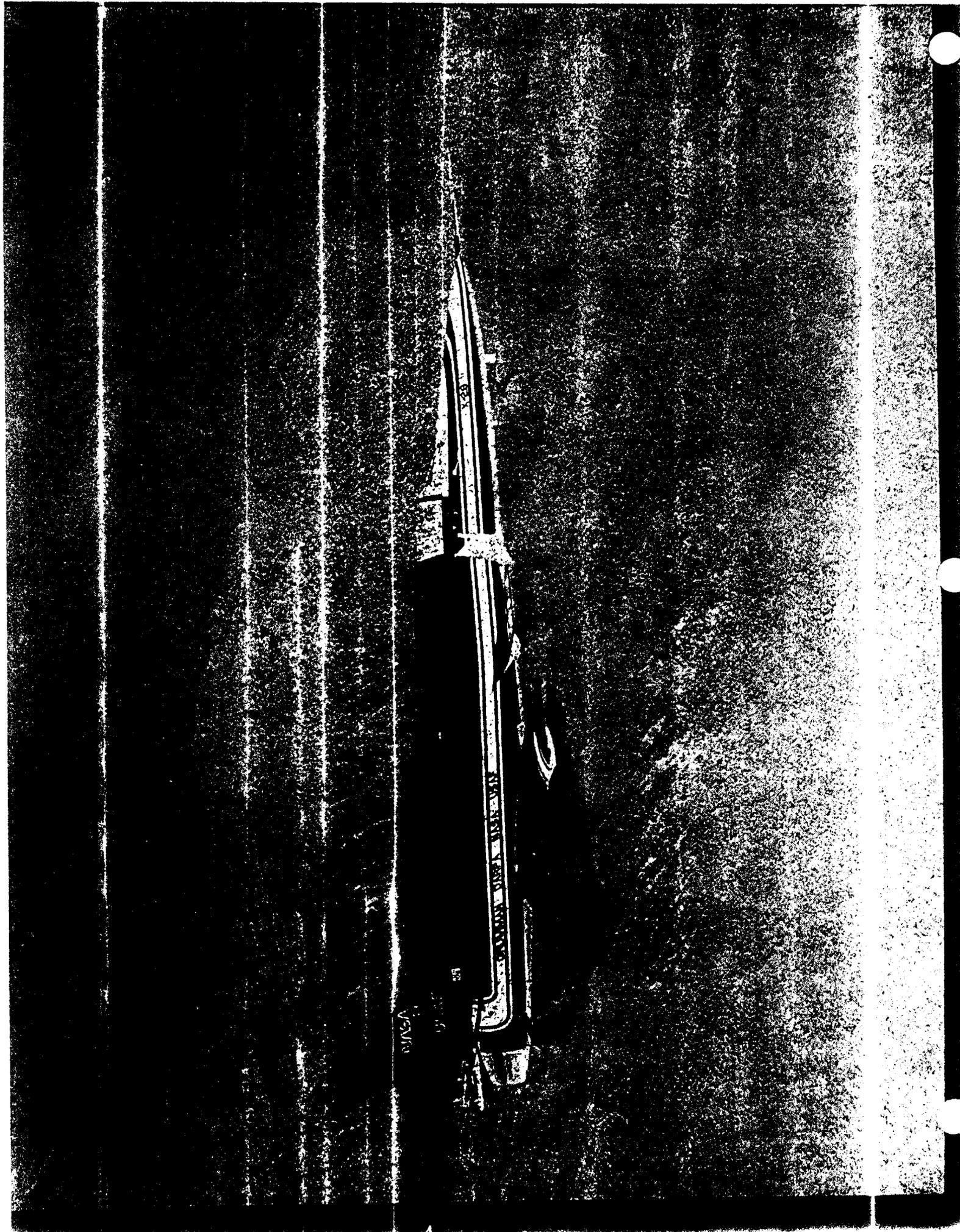
TEST AND EVALUATION

PREDICTED FLYING QUALITIES

Ground-based flying qualities predictions included static and dynamic wind tunnel, spin tunnel, free flight model, radio controlled drop model, and rotary balance tests. An aerodynamic mathematical model was developed from these tests for use in 6-degree of freedom (DOF) simulation. The expected flying qualities were generated using simulation with high angle-of-attack (AOA) control laws, free flight, and drop model tests.

The X-29 forward swept wing (FSW) design was predicted to maintain low but effective aileron control power up to 90 degrees AOA. Rudder power was predicted to remain high to 25 degrees AOA and then decrease to zero by approximately 45 degrees AOA. Lateral static stability, or dihedral effect, was predicted to be good above 10 degrees AOA and body axis directional stability was predicted to be positive to approximately 45 degrees AOA. The stable dihedral effect acted through a large inertia ratio ($I_{zz}/I_{xx} = 10$) to provide a stable directional divergence parameter (DDP or $Cn\beta dyn$) to above 70 degrees AOA, indicating the configuration would be resistant to rapid nose slice departures. Lateral dynamic stability, or roll damping, was predicted to be unstable between 20 and 50 degrees AOA and to become stable above 60 degrees. Wind tunnel tests indicated that the source of the roll instability was the nose vortex system generated by the modified F-5A forebody. Vortices provided a roll moment forcing function which was interpreted as a roll damping term for mathematical modeling purposes.

At low AOA and subsonic airspeed, the X-29 was predicted to be statically unstable in the longitudinal axis, with an approximate negative static margin of 35 percent. Static instability was predicted to decrease with AOA and become stable above approximately 60 degrees. The canard was predicted to provide ample power for controlling both the instability and inertial coupling.

Early design phase simulation, free flight, and drop model tests indicated the need for a high gain aileron-based roll damper to fully suppress a predicted divergent wing rock, which was a result of the unstable aerodynamic roll damping. Low gains or the lack of a roll damper could result in roll departures above 25 degrees AOA. The X-29 system could not incorporate the gain level required for complete wing rock suppression due to limited actuator bandwidth and rate limits. The final control law design for the X-29 was predicted to exhibit bounded wing rock above 30 to 35 degrees AOA, increasing in amplitude to a maximum at approximately 45 degrees AOA and then damp out by 60 degrees as aerodynamic roll damping became stable.

Real-time simulation using the predicted aerodynamics indicated that lateral-directional maneuvering capability existed to approximately 45 degrees AOA where rudder power was lost. High levels of roll coordination were required to minimize adverse sideslip and potential roll reversals due to high stable dihedral effect. The predicted high AOA roll performance was limited by the coordinating power of the rudder rather than aileron control power. Wing rock onset above 30 degrees AOA was predicted to degrade roll maneuvering to the point that little useful capability was available between 35 and 45 degrees AOA, although limited ability was present. Lack of rudder power was predicted to prevent lateral-directional maneuvering above 45 degrees AOA.

Wind tunnel and drop model tests demonstrated the potential for zero sideslip yawing moment asymmetries above 45 degrees AOA. Predicted rudder power was insufficient to counter yaw moments generated by the asymmetries above 45 degrees AOA. The magnitude of the asymmetries varied and could not be accurately predicted. The impact on trim or longitudinal maneuvering above 45 degrees AOA was predicted to be dependent upon the magnitude of the asymmetry.

Longitudinal control power was predicted to be sufficient for pitch stabilization and to counter noseup inertial coupling generated during velocity vector rolls. Potential longitudinal trim to 70 degrees AOA was predicted in the absence of yaw asymmetries or lateral-directional instabilities. Positive AOA hung stalls were not indicated by the predicted wind tunnel aerodynamic data or simulation.

The vertical spin tunnel predicted two upright and one inverted spin mode (Reference 4):

1. Upright fast flat (AOA = 85 degrees, 3 seconds per turn);

2. Upright slow oscillatory (AOA = 54 to 100 degrees, 4 seconds per turn); and

3. Inverted (AOA = -75 degrees, 4 seconds per turn).

Both upright modes were predicted to have slow to nonexistent aerodynamic recovery characteristics. The inverted mode recovered quickly with neutral or opposite rudder. Wind tunnel tests also indicated that no sustained spin could be entered with full antispin aileron and rudder, suggesting the possibility of a spin prevention system (as opposed to recovery) which was later incorporated into the flight control system (FCS).

Wind tunnel tests also showed the possible existence of a nosedown autorotative pitch tumble mode as a result of the high longitudinal static instability. An active strake flap was predicted to eventually damp the mode but not necessarily prevent rapid nosedown departures. Simulation with predicted aerodynamics indicated that aggravated roll departures, which generated negative AOA from kinematic coupling, could result in severe nosedown departures or potential tumble entries. Simulation tumble entries produced negative load factors at initial departure entry which ranged from 1 to 6 g's, depending on airspeed. The simulator aerodynamic model was only valid to -50 degrees AOA and investigation of the tumble characteristics with the simulation was not possible. Limited radio controlled drop model tests to evaluate the mode and entry conditions were inconclusive due to the low number of flights attempted, limited maneuver types performed and lack of center of gravity (cg) variation. No tumbles or evere nosedown departures similar to the simulator were encountered with the drop model; however, no attempts to kinematically couple to high negative AOA at aft cg were performed. The tumble mode was investigated in the vertical wind tunnel with free to pitch models (Reference 5). Lateral-directional aerodynamic or coupling affects on the tumble mode were not predicted. The results of this study indicated

that the nosedown pitch rate was oscillatory and peaked at 200 degrees per second.

Full lateral stick or full rudder pedal maneuvering was predicted to be possible without departure of the aircraft below 45 degrees AOA. Lateral stick aileron rolls were predicted to be well coordinated with sideslips less than 5 degrees. Full pedal rudder rolls were predicted to produce up to 8 degrees sideslip without departures. Sideslip excursions above 30 degrees AOA and 5 degrees sideslip were predicted as a result of body axis static directional instability. The excursions were not considered departures since they were slow and easily controlled with opposite rudder. Rapid noseslice departure as a result of the body axis yaw instability was prevented by predicted strong stable dihedral effect.

Full cross-control inputs below 45 degrees AOA produced little lateral-directional motion using the simulation with predicted aerodynamics. Roll due to dihedral and aileron essentially cancelled. The canard countered inertial pitch coupling during full cross-controlled rolling pullouts and no departure tendencies were predicted.

Sustained full cross controls above 50 degrees AOA were predicted to result in a flat spin which was unrecoverable when fully developed. The spin prevention logic prevented development of the spin without full pilot cross-control input.

Full coordinated rudder and aileron inputs were predicted to be the most likely maneuver for departures to occur below 45 degree AOA. The aileron input and dihedral effect combined to produce large roll and yaw rates. Inertial coupling to all three axes was severe and recoveries were not consistent. Full nosedown stick inputs phased properly with abrupt full coordinated inputs were predicted to cause kinematic coupling to negative AOA and could occasionally result in tumble entries. Autoroll susceptibility was predicted with the simulator using predicted aerodynamics. Autorolls would usually self recover within two full rolls. Rudder opposite yaw rate combined with slow neutralization of longitudinal stick was predicted to be the most effective recovery technique from any simulation departure or autoroll condition.

6

TEST CONDUCT

General:

The flight test program was divided into two test phases:

1. Envelope expansion; and

2. Military utility and agility metric tests within the cleared envelope.

Each had different flight test philosophies, requirements, and procedures.

Envelope expansion of AOA was conducted in a careful buildup. Angle of attack, airspeed, and maneuver restrictions were applied. Analysis of flight data prior to the next expansion point was conducted. The analysis provided an understanding of differences from predictions and possible results for the next expansion point. Identification of potential stability problems and expected characteristics using a simulator with flight updated aerodynamics was a primary tool for the process.

Military utility and agility metric maneuvers were conducted within the cleared envelope. Extensive safety analysis between flights was not required unless unexpected aircraft response was encountered. Postflight analysis between flights was minimal and consisted primarily of confirming maneuver quality. Real-time monitoring consisted of maneuver quality and limit compliance checks. Higher flight rates were possible during the evaluation flights compared to expansion flights.

Envelope Expansion Maneuvers:

Envelope expansion maneuvers were divided into integrated test blocks (ITBs) which defined the maneuver buildup process at a given AOA and airspeed. The ITBs were designed to progress from relatively benign to more aggressive maneuvers. Slightly different ITBs were defined for 1-g flight and accelerated maneuvers.

Table 1 lists the various ITBs used during envelope expansion. The ITB-1 maneuvers were designed to provide limited aerodynamic and controllability information when at a test point for the first time. The ITB-2 maneuvers expanded the maneuvering to greater limits. The ITB-3 maneuvers

were designed for large amplitude and aggravated inputs. The aggravated inputs (cross control and full proverse inputs) were deleted from the ITB-3 maneuvers due to schedule constraints and were not performed. Table 2 outlines the uses of the maneuvers in postflight analysis and aerodynamic model updating.

Integrated Test Block maneuvers were performed in sequence at 5-degree AOA intervals. When results warranted, the interval was reduced to 2 degrees AOA. A limit of 10 degrees AOA expansion without postflight analysis was imposed during the initial expansion. Successful completion of the ITB-1 maneuvers was required prior to performing ITB-2 maneuvers and successful ITB-2 completion prior to ITB-3 maneuvers. A 10-degree AOA buffer was maintained between sequential ITB maneuvers. The ITB-1 maneuvers had to be successfully completed at 10 degrees higher AOA prior to performing an ITB-2 at a given AOA. A similar AOA buffer was used between ITB-2 and ITB-3 maneuvers. Rules concerning AOA expansion limits without postflight analysis (10 degrees) were relaxed during lower altitude expansion to AOAs already cleared at higher altitude. Angle-of-attack intervals of 5 degrees and ITB order were adhered to.

Figure 1 presents the initial expansion and data analysis process. The simulator aerodynamic model was updated with the most recent flight data and extrapolated to the next expansion point. Both expected and worst case extrapolations were made and evaluated on the simulator prior to flight. Limits, expected results, real-time stability and departure susceptibility indicators, and maneuver sequence were defined by the simulation process.

The process was shortened for the low altitude expansion below 25,000 feet pressure altitude. The aircraft characteristics at high AOA and an initial flight updated simulator aerodynamic model had been defined from high AOA testing at altitude. Simulation was still performed prior to flight, but postflight data analysis and simulator updating were not required unless unexpected adverse results occurred. The ITBs were modified in accordance with Table 1. Modifications were based on lessons learned during the higher altitude expansion. The availability of a flight updated simulation which more closely represented the aircraft and a knowledge of aerodynamic characteristics allowed the abbreviated expansion maneuvers and process.

Table 1
INTEGRATED TEST BLOCKS
(ITBs)

ONE-G MANEUVERING		
ITB-1	ITB-2	ITB-3
Stabilized Points	0/90/0 Aileron Roll	360° Aileron Roll
Push-Over	0/60/0 Rudder Roll	(Full Input)[1]
Fast/Slow Pitch Doublet	Wings-Level Sideslip	
Fast Lateral Pulse	(10° β)	
Fast Rudder Pulse		
Yaw/Roll Doublet		
0/60/0 Aileron Roll		
0/30/0 Rudder Roll		
(1/2 Input)		
Wings-Level Sideslip		
(5° β)		
WINDUP TURNS		
ITB-1	ITB-2	ITB-3
Stabilized Points	Stabilized Points	360° Aileron Roll
Fast/Slow Pitch Doublet	0/60/0 Aileron Roll	(Full Input)[1]
Fast Lateral Pulse	0/30/0 Rudder Roll	
Fast Rudder Pulse	(Full Input)	
0/60/0 Aileron Roll		
0/30/0 Rudder Roll		
(1/2 Input)		

Notes: 1. For expansion below 25,000 feet, doublets and sideslips were eliminated from ITB-1s.

2. For expansion below 25,000 feet, ITB-3s were eliminated.

3 No abrupt entry coupled maneuvers were performed.

[1] Proverse and cross control inputs were not accomplished.

Table 2
MANEUVER USE

Maneuver	Post Flight Analyses Tools	Answers
ITB-1 Stabilized Point (5 sec) Push-Over/Pull-Up	Total Coefficient*	De~ons~rate nose-down recovery capability
Stabilized Point (60 sec)	Total Coefficient INS Batch Sim	Real time check of longitudinal trim surfaces Post flight calculation of ΔC_m, C_{no}, C_{lo} Real time check of wing rock amplitude and freq. Provide time history to match wing rock Real time check of control surfaces limit cycles
Pitch Doublets (slow/fast)	MMLE Total Coefficient	$C_{m\alpha}$, C_{md_c}
Yaw/Roll Doublets	MMLE Total Coefficient	$C_{l\beta}$, C_{lp}, $C_{n\beta}$, C_{nd_r}, C_{ld_a}
Lateral Raps (sm&lg) Rudder Raps	MMLE Total Coefficient	C_{nd_r}, C_{ld_r}, C_{ld_a}, C_{nd_a}
Slow, Wings-Level Sideslips (±5 deg β)	Total Coefficient Batch Sim	Real time check of stability/linearity of Cl & Cn vs β Cross comparison & linearity determination of C_{ld_a}, $C_{l\beta}$, C_{ld_r}, C_{nd_r}, $C_{n\beta}$, C_{nd_a}
Aileron Roll (0/60/0) Rudder Roll (0/30/0) (1/2 Amplitude, L&R)	Total Coefficient Batch Sim	Check/determination of derivatives
ITB-2 Slow, Wings-Level Sideslips (±10 deg β)	Total Coefficient Batch Sim	Provides same data as small sideslip but over larger β range
Aileron Roll (0/90/0) Rudder Roll (0/60/0) 360 deg Rolls (Full Amplitude)	Total Coefficient Batch Sim	Final check/determination of derivatives

* For an explanation of the Total Coefficient Matching Method see Appendices C and E.
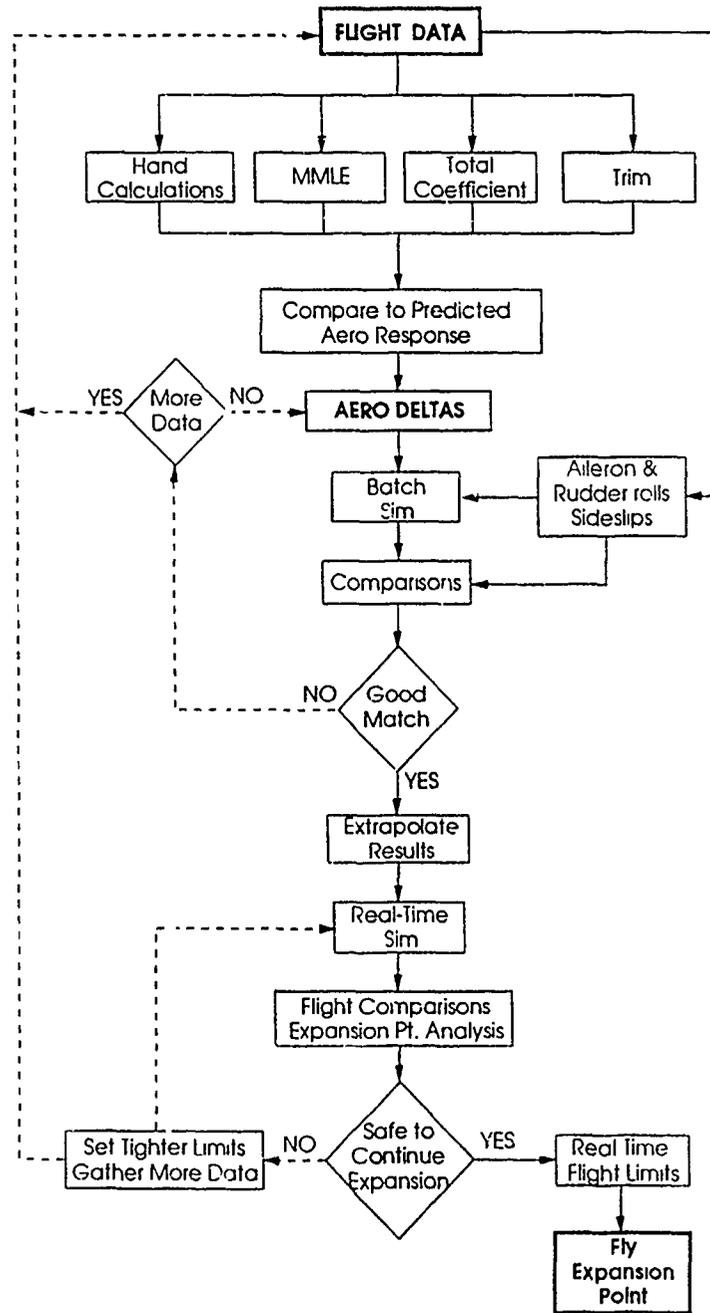
Figure 1 Expansion and Analysis Process

10

Military Utility Piloted Evaluation Maneuvers:

Tracking From A Perch Setup.

Tracking maneuvers were entered from a perch setup with the attacking aircraft approximately 2,000 feet aft and 500 feet laterally offset from the target. The target aircraft initiated a constant airspeed descending turn between 25 and 40 degrees AOA. The attacking aircraft acquired and tracked the target through various maneuvers. The maneuvers included roll reversals called by the attacker, random roll reversals initiated by the target, straight ahead pull-ups to maximum AOA, and roll to wings level followed by a pull to maximum AOA. The attacking aircraft would attempt to track the target during the maneuvers.

Both the X-29 and F-18 served as target and attack aircraft to acquire qualitative comparative pilot comments. Pilot ratings were not attempted since desired and adequate performance levels were not established. The X-29 did not have a head-up display (HUD) or a gunsight installed. This limited the ability to assess the tracking performance.

Neutral Basic Fighter Maneuvering.

The neutral basic fighter maneuver (BFM) setup was initiated with the X-29 and the opponent F-18 laterally separated by 1,000 feet and flying on opposite headings at approximately 250 KCAS. When the aircraft passed, both aircraft initiated a one-circle fight using a 25- to 40-degree AOA turn. Both aircraft attempted to maneuver to a slow speed firing advantage or until maneuver termination.

## AERODYNAMIC DATA COMPARISONS

General:

This section compares the predicted and flight updated simulation aerodynamic mathematical model (Reference 6). The predicted model was continually updated as a part of the envelope expansion program. Updates were further refined during subsequent testing and analysis. Methods for updating a nonlinear aerodynamic model with linear and piece-wise linear flight data were developed. A description of the update methods, parameters, application equations, model validation, and limitations is contained in Appendix C

The model was updated beyond the limits of the flight data by following predicted trends. Changes were implemented in a manner which preserved the predicted nonlinear characteristics by applying increments to the predicted model. The predicted model tables and functions were not modified.

The flight updated aerodynamic model was generated using a variety of methods for extracting the aerodynamics. Determination of the control power derivatives from varying magnitude surface pulses was the first step. Surface pulses of sufficiently high frequency to provide state accelerations but small changes in the actual states were the best maneuvers for control power estimation. Varying the magnitude of the pulses allowed estimation of nonlinear characteristics. Linear parameter estimation of the stability derivatives about a trim condition using classical surface doublet inputs followed the determination of the control derivatives. The combined stability and control derivatives about the trim condition were used as the first indicator of the overall trend for the nonlinear variation of the model. An initial model update was derived using the linear parameter estimation data as the variation from predictions. Batch simulation overplot comparisons with flight dynamics using larger amplitude maneuvers than the doublets or pulses were then used to further refine the flight updated model. Valid linear parameter estimation data about trim conditions were obtained in 5-degree AOA intervals up to 45 degrees AOA; however, the quality degraded above 35 degrees AOA. Two repeats of the pulses and doublets were obtained at each expansion AOA. Wings level sideslips, aileron and rudder rolls were available for batch simulation comparisons in 5-degree AOA intervals up to 45 degrees AOA. These maneuvers were performed for one-half and full pilot control inputs. The flight model was considered valid when a majority of the larger amplitude batch simulation overplots and real-time simulation dynamics consistently matched flight results within engineering judgment limits.

Parameter comparisons presented in this section (and Appendix B) are between the predicted mathematical aerodynamic model and the flight updated version. Parameter comparisons are for a 1-g trim condition presented in Figure 2, between 38,000 and 25,000 feet pressure altitude. The updated model covers the full flight test envelope. Data presented are representative of variations between predicted and flight updated aerodynamics.

X-29 USAF S/N 820049
1 G ACC TRIM
MIL POWER   XCG=449 in
ALT= 38K to 25K ft
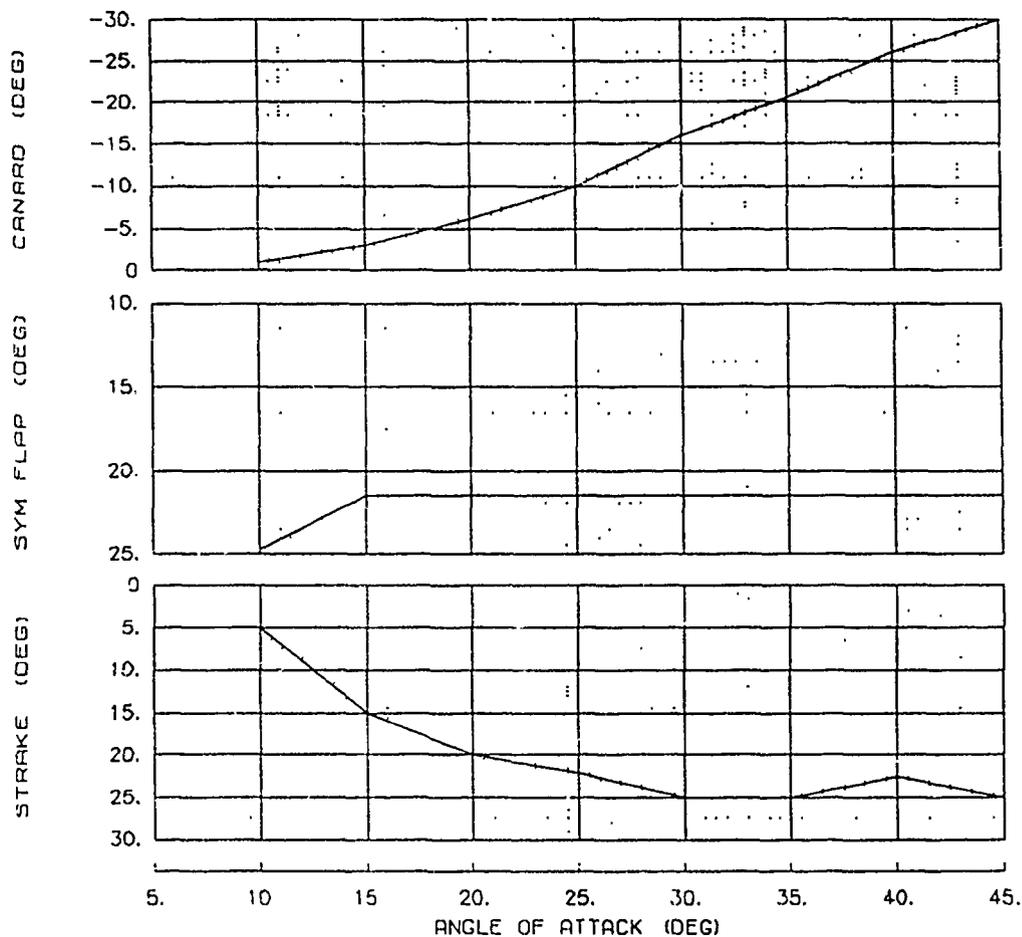
NOTES:

1. DATA ARE AVERAGES OF FLIGHT TRIMS.

2. DATA TAKEN DURING DESCENDING SLOW DECELERATION MANEUVERS.

Figure 2 One-G Flight ACC Trim

12

Longitudinal Stability and Control Parameters:

Figure 3 presents comparisons of linearized longitudinal static instability (Cmα) and longitudinal control power (Cmδc) between the predicted and flight updated models. Figure B1 presents a similar comparison with the flight parameter estimation data. Parameter estimation data were generated using the well known Modified Maximum Likelihood methodology of Reference 7. Longitudinal parameter estimation data were usually derived at trim conditions which were different from those of Figure 2 due to the unique longitudinal trim characteristics of the X-29. See the Longitudinal Stability and Control section and Figure 12 of this report for a description of the X-29 trim characteristics.

Longitudinal static instability was predicted to decrease with AOA and to become stable between 55 and 65 degrees AOA, varying with canard position. Both longitudinal static instability and control power were higher than predicted to 40 degrees AOA. The trends with AOA were well predicted. Static instability reduced with AOA and canard power remained relatively constant. Parameter estimation data above 45 degrees AOA were not obtained. Estimation of control power was limited to the canard since adequate separate surface inputs were not available. As a consequence, differences in longitudinal control power were attributed to the canard. Estimated parameters were derived from standard longitudinal pulses and doublets.

Predicted longitudinal static instability and canard power were nonlinear with canard deflection. The model updating techniques held the predicted nonlinear trend intact such that the updated model would also reflect the nonlinear characteristics. Figure 3 also presents an example of the nonlinearity for both the predicted and updated models at 35 degrees AOA. In general, canard power and static instability increased with trailing edge up (TEU) deflection. The nonlinearities in control power and static instability with canard position made comparison of longitudinal parameter data difficult. The X-29 trimmed differently depending on multiple variables discussed in the Longitudinal Stability and Control section. The canard position for which parameter estimation data were obtained was often more TEU than that shown in Figure 2. The nonlinear character of the predicted data with canard position required an incremental update method using the differences between flight and

predictions at comparable canard trim conditions. The nonlinearity also presented problems with updating control power and static instability separately. Changes in canard power would also modify static instability since the update model used both canard and AOA as independent variables. The resulting flight updated model had a higher linearized static instability below 25 degrees AOA than was indicated by the parameter estimation data of Figure B1. The nonlinear variation of static instability with canard position was also affected (Figure 3) and may not be representative of actual values when far off the canard trim positions. The flight update increment tables did not contain sufficient canard break points (see Appendix C) to model the characteristics at all conditions.

Figure 4 presents a time history comparison of flight computed, predicted, and flight updated model total pitching moment coefficient. Flight data were computed and corrected for thrust and inlet affects as described in Appendix E. Model data were generated by driving both the predicted and flight updated aerodynamic models with flight measured inputs. The aircraft exhibited more noseup pitching moment at a given AOA and surface position than was predicted. Comparison of flight computed and predicted model total aerodynamic pitching moment across the envelope shows the trend.

Full Nosedown Pitching Moment:

Figure 5 presents a comparison of available full nosedown aerodynamic pitching moment coefficient between the predicted and flight updated aerodynamic models. Flight data for the cases where full nosedown pitch control surface deflection was encountered are also presented. Figure B2 presents an expanded comparison of full nosedown pitching moment coefficient between the predicted and flight updated aerodynamic models.

The aircraft had no hung stall up to 67 degrees AOA (limit of flight data), although the noseup difference between the flight data and predictions increased with AOA. Full nosedown aerodynamic pitching moment was significantly reduced from predictions. The minimum nosedown aerodynamic pitching moment (Cm*) was approximately one-half of predictions between 55 and 67 degrees AOA. The low Reynolds Number (RN of 0.6×10^6 per foot) wind tunnel data more accurately reflected the flight value for Cm* than did the high Reynolds Number (RN above 1.4×10^6 per foot) data. The reasons for the large

X-29 USAF S/N 820049
1 G ACC TRIM
MIL POWER   XCG=449 in
## AERO MODEL COMPARISONS
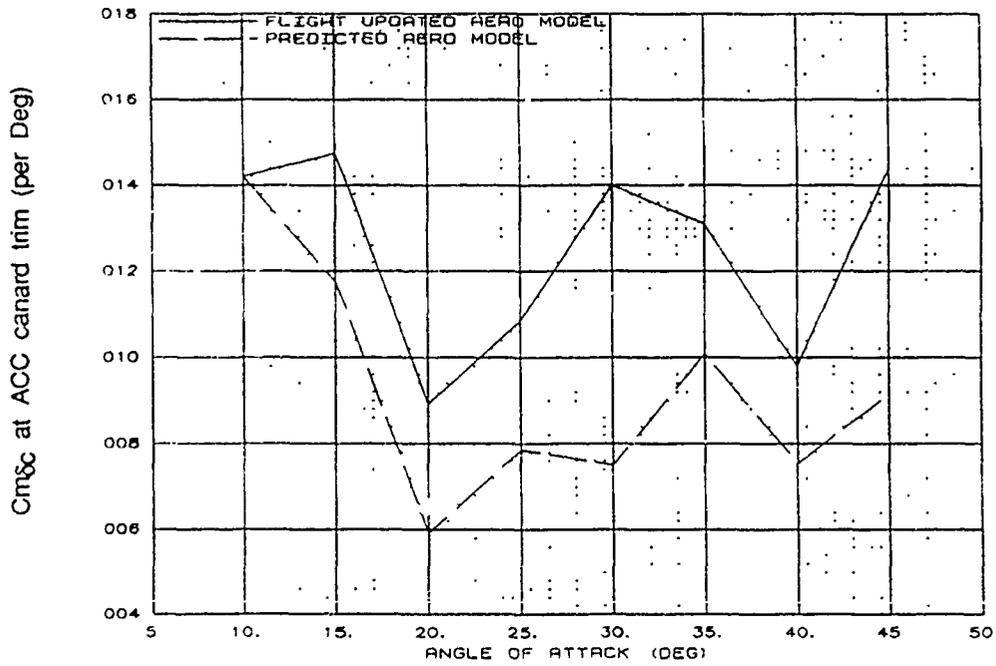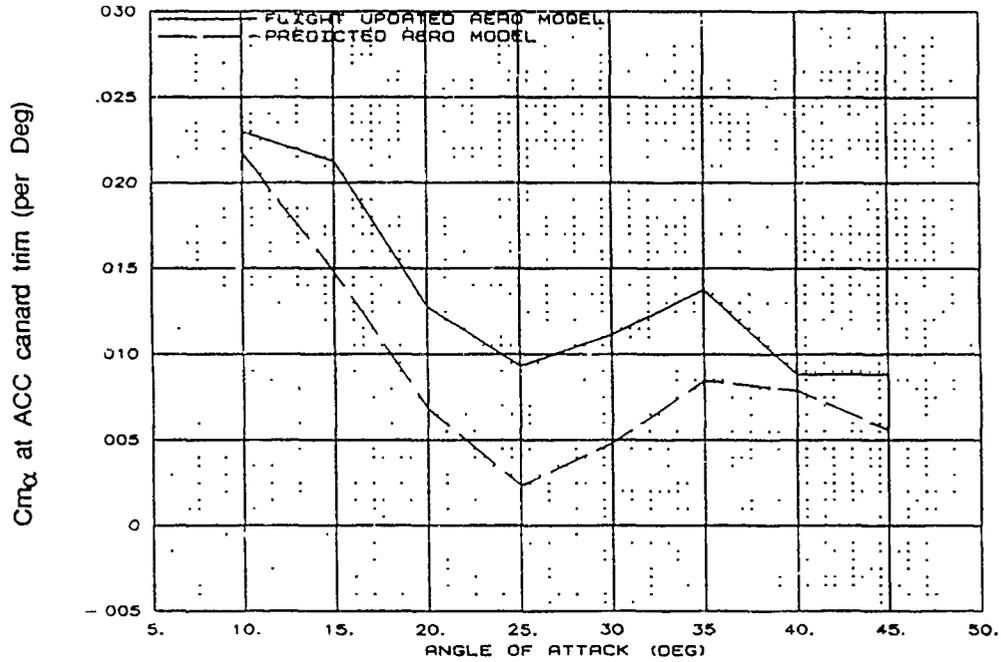
Figure 3 Longitudinal Stability and Control Parameters

14
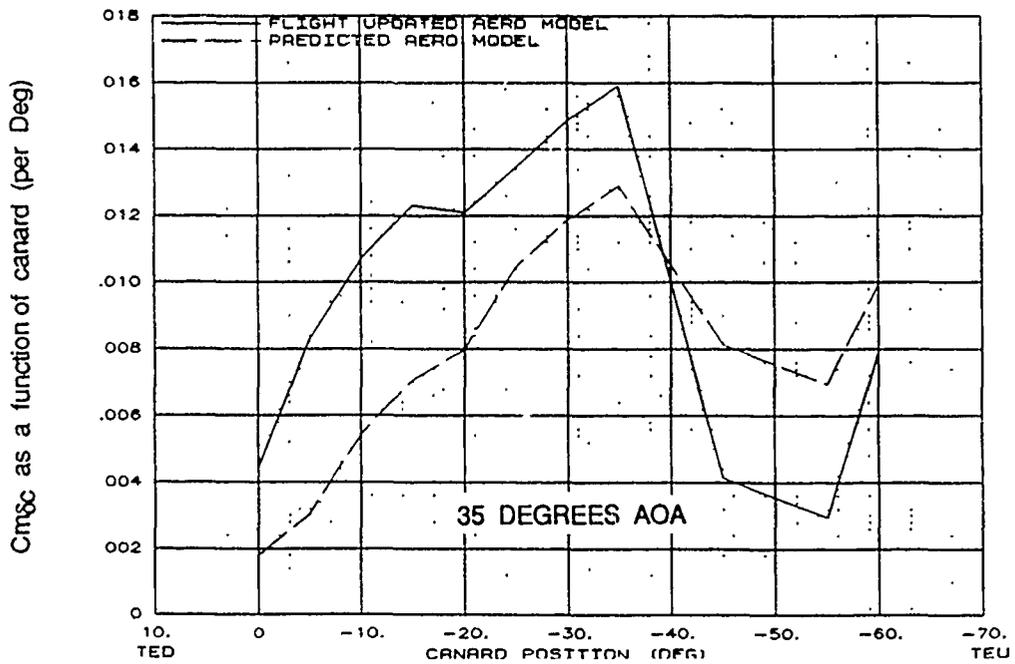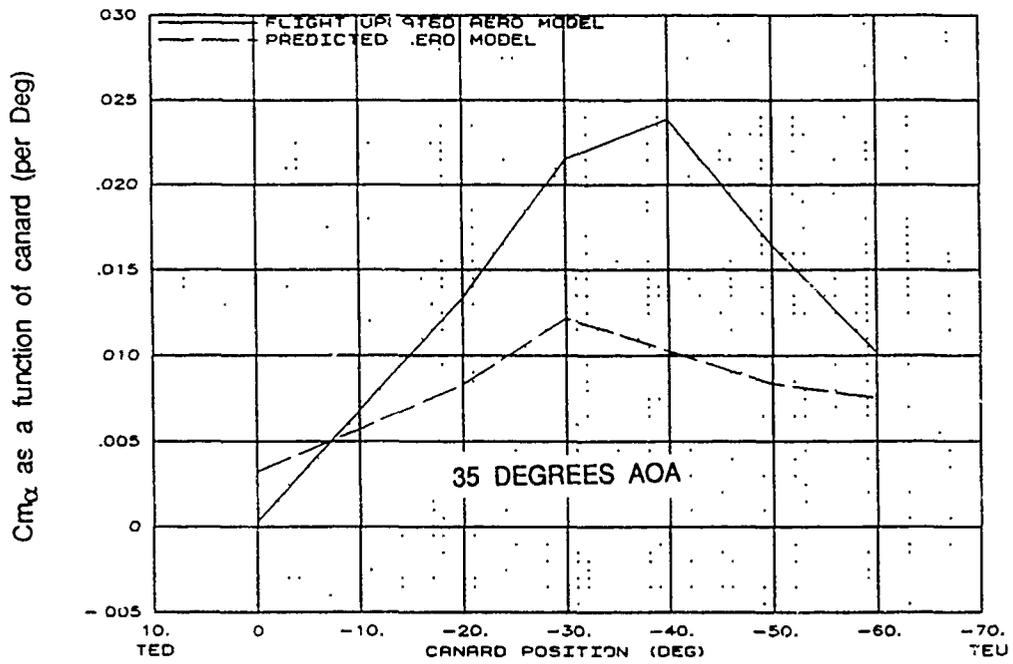
Figure 3 Longitudinal Stability and Control Parameters (Concluded)

X-29 USAF S/N 820049
MIL POWER   XCG=445.4 in
1 G PULL UP TO 36 DEG AOA
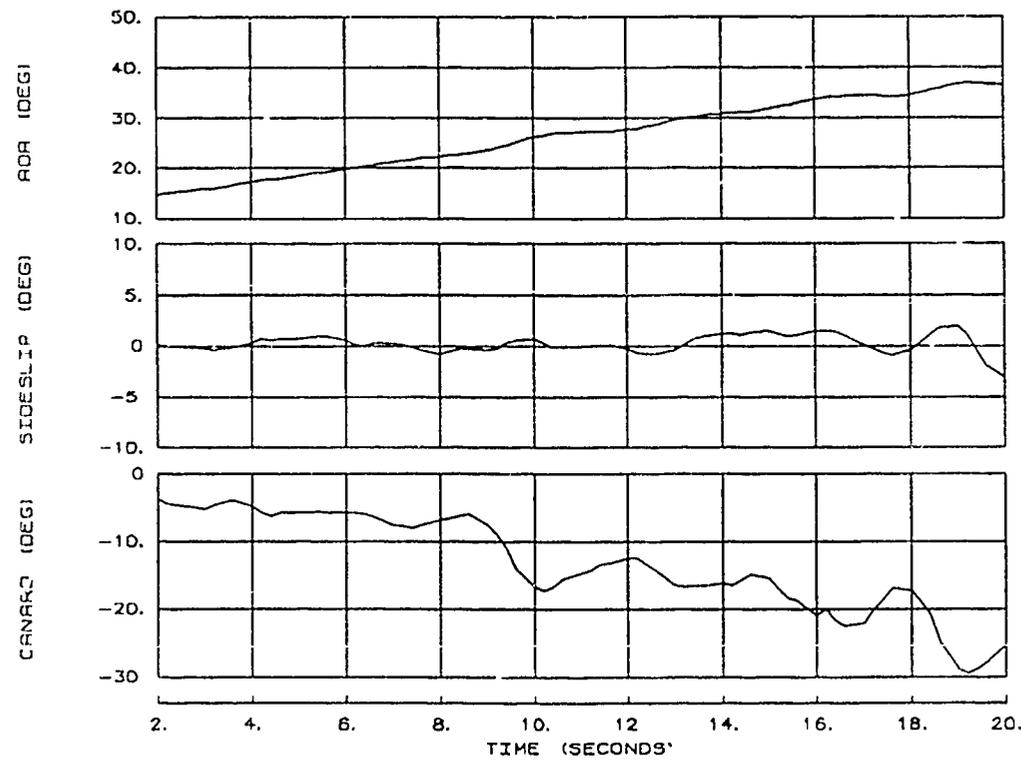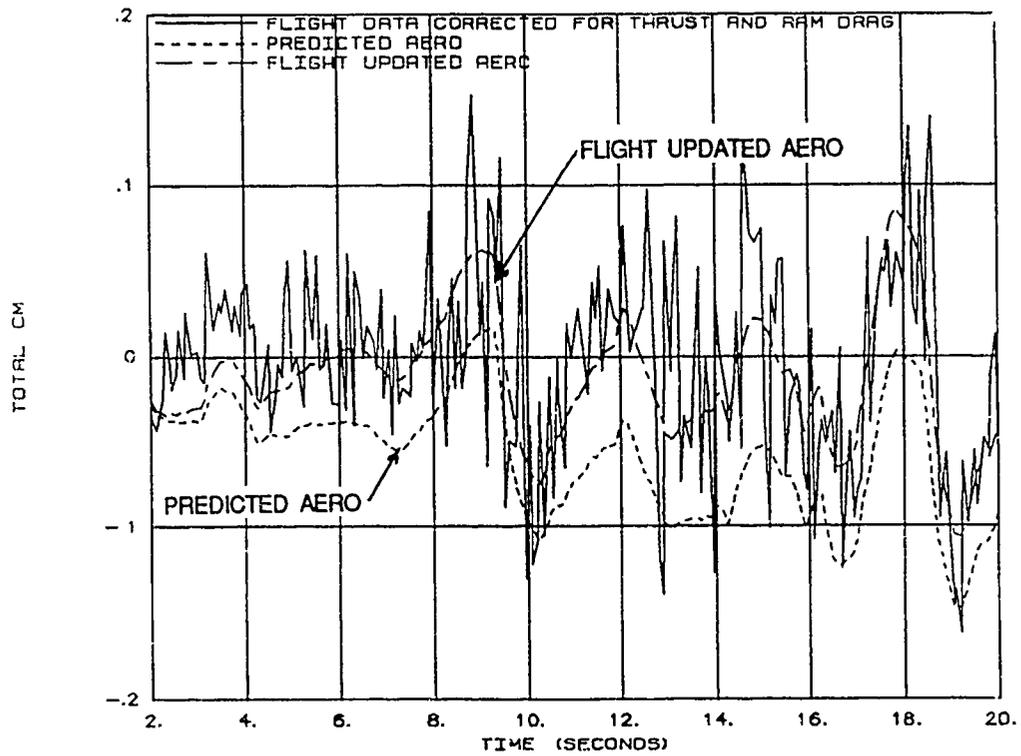
Figure 4 Total Pitching Moment Coefficient Comparison

X-29 USAF S/N 820049
POWER OFF   XCG=449 in
CANARD=-57 deg   SYM FLAP=21.5 deg   STRAKE=30 deg
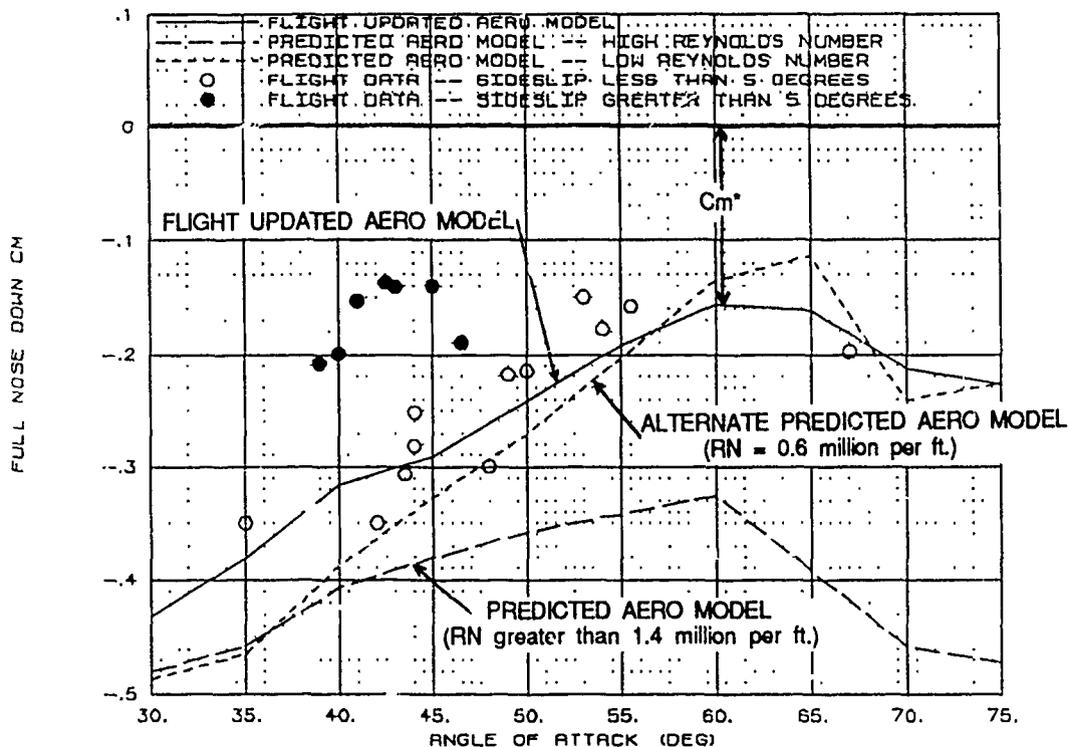
NOTES:

1. PREDICTED AERO MODEL HAD A REYNOLDS NUMBER
   GREATER THAN 1.4 MILLION PER FOOT.

2. ALTERNATE PREDICTED AERO MODEL HAD A REYNOLDS
   NUMBER OF 0.6 MILLION PER FOOT.

3. UPDATED AERO MODEL WAS BASED ON FLIGHT DATA FOR
   SIDESLIP LESS THAN 5 DEGREES.

Figure 5 Full Nose Down Pitching Moment

difference were not determined but were attributed to a change in basic pitching moment (Cmo) or Cmα with AOA. Flight data indicated a slight stable slope similar to predictions between 60 and 67 degrees AOA. Data beyond 67 degrees AOA were not obtained. Differences between the flight and predicted pitching moment above 67 degrees AOA were held constant for the model updating process. Care should be exercised when extrapolating the model results above the AOA for accurate flight data. The shape and magnitude of the pitching moment curve above stall AOA has significant influence on spin, departure, and hung stall susceptibility.

Significant data scatter in full nosedown aerodynamic pitching moment was evident between 39 and 50 degrees AOA. Maneuvers with full nosedown commands generally resulted during yaw excursion recoveries from above 45 degrees AOA. Yaw excursions are discussed in detail in the Lateral-Directional Stability and Control section of this report. Significant sideslip, aerodynamic hysteresis, or nose vortex effects may have been present. Definition of the potential factors impacting the data in this region was not accomplished.

Lift and Drag Characteristics:

Figure 6 presents a comparison of flight computed, predicted, and flight updated aerodynamic model lift and drag coefficients. Flight data were computed using a simplified thrust model and ram drag model (see Appendix E). The predicted and flight updated model data were generated by driving the two models with the appropriate flight measured data.

An increase in lift coefficient at a given AOA over predictions was evident during 1 g maneuvers. Differences were less pronounced for airspeeds above approximately 150 KCAS at similar AOA. The lift coefficient trends with AOA and the AOA for maximum lift were close to predictions. Flight computed drag coefficients were close to predictions at all airspeeds. Lift, and to a lesser extent drag, at high AOA were strong functions of canard, symmetric flaperon, and strake positions. The canard was predicted to be a large contributor to total aircraft lift due to its large surface area which was 20 percent of the wing area. The update to the aerodynamic model only accounts for differences as a function of AOA and airspeed

The lift and drag coefficients were derived using a simplified thrust model which was estimated to be accurate within 15 percent. The GE-F-404-400 engine installed in the X-29 was not instrumented for accurate in-flight thrust computations. The engine thrust model also contained the predicted ram drag characteristics as a function of flight condition and power setting. Angle-of-attack effects on engine power and ram drag were not measured in flight nor predicted.

## Lateral-Directional Stability and Control Parameters:

Figure 7 presents a comparison between the predicted and flight updated aerodynamic model for linearized lateral-directional static stability parameters. Figures B3 through B11 present the total nonlinear variation of yaw and rolling moment coefficients with sideslip. All comparisons are for the 1-g trim condition of Figure 2. Flight values of sideslip from which aerodynamic model updates were determined ranged from approximately 15 degrees at 10 degrees AOA to 5 degrees at 45 degrees AOA. Data above 45 degrees AOA were generated without benefit of linear parameter estimation and the flight model updates relied upon batch simulation overplotting of flight and simulated dynamics.

The directional divergence parameter (DDP or Cnβdyn) was lower than predicted but still stable below 35 degrees AOA and higher than predicted between 35 and 45 degrees AOA. Stable Cnβdyn is an indicator of nose-slice departure resistance and computed with a combination of body axis static directional stability (Cnβ) and dihedral effect (Clβ). The reduction in Cnβdyn below 35 degrees AOA was due to a combination of lower body axis directional stability and dihedral effect. The lower dihedral effect provided the largest contribution due to a large inertia ratio. The increase in Cnβdyn above 35 degrees AOA was due to both an increase in body axis static directional stability and stable dihedral effect.

Both dihedral effect and body axis static stability were nonlinear with sideslip. Figures B4 through B8 show that the reduction in linearized dihedral occurs about sideslip angles less than 5 degrees. The slope of rolling moment with sideslip was close to predicted above approximately 5 degrees sideslip. The total value of rolling moment was still lower than predicted

18

X-29 USAF S/N 820049

1 G to 63 deg AOA
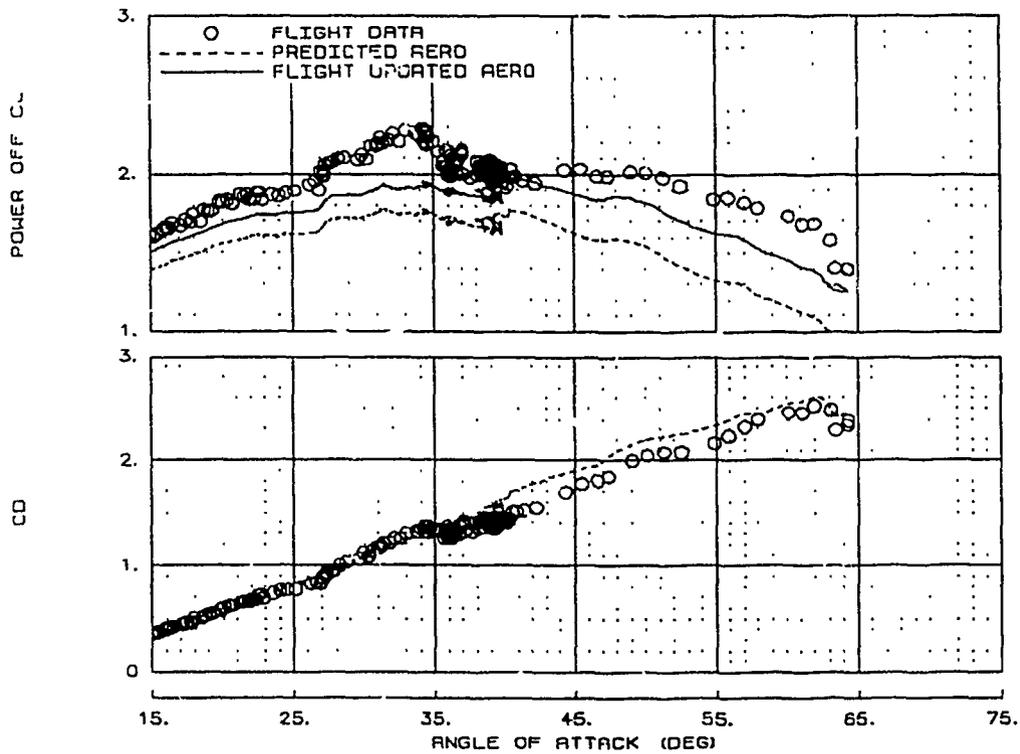

1 G to 55 deg AOA

Figure 6 Lift and Drag Comparison

19
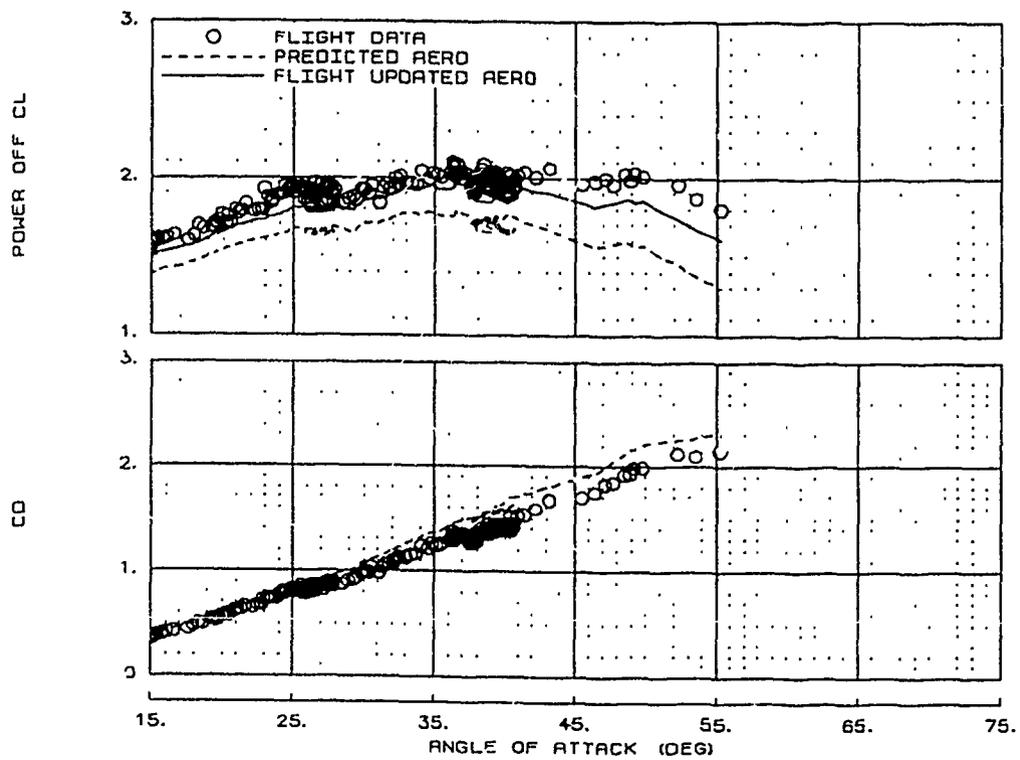
WIND UP TURN TO 40 DEGREES AOA WITH A 250 KCAS ENTRY
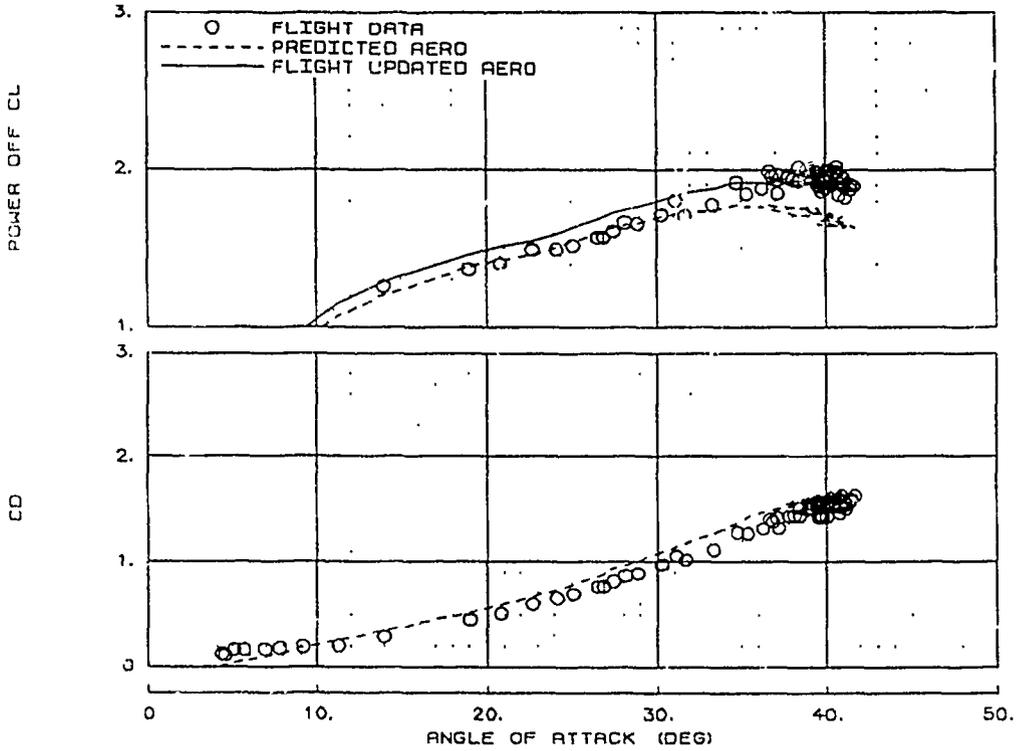
NOTE:

DATA COMPUTED USING GE-F404-400 ENGINE
SPECIFICATION MODEL.

Figure 6 Lift and Drag Comparison (Concluded)

20

X-29 USAF S/N 820049
1 G ACC TRIM   XCG=449 in
MACH=0.3   ALT=30K ft
AERO MODEL COMPARISONS

$$Cn_{\beta dyn} = Cn_\beta \cos(\alpha) - (Izz/Ixx)\, Cl_\beta \sin(\alpha)$$

Figure 7 Lateral-Directional Static Stability

21
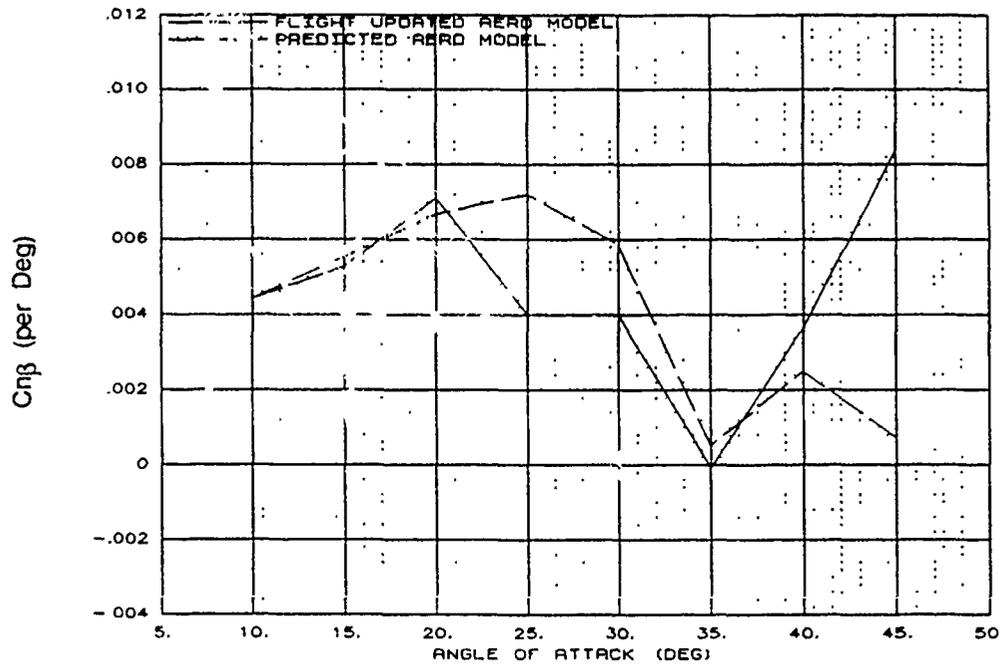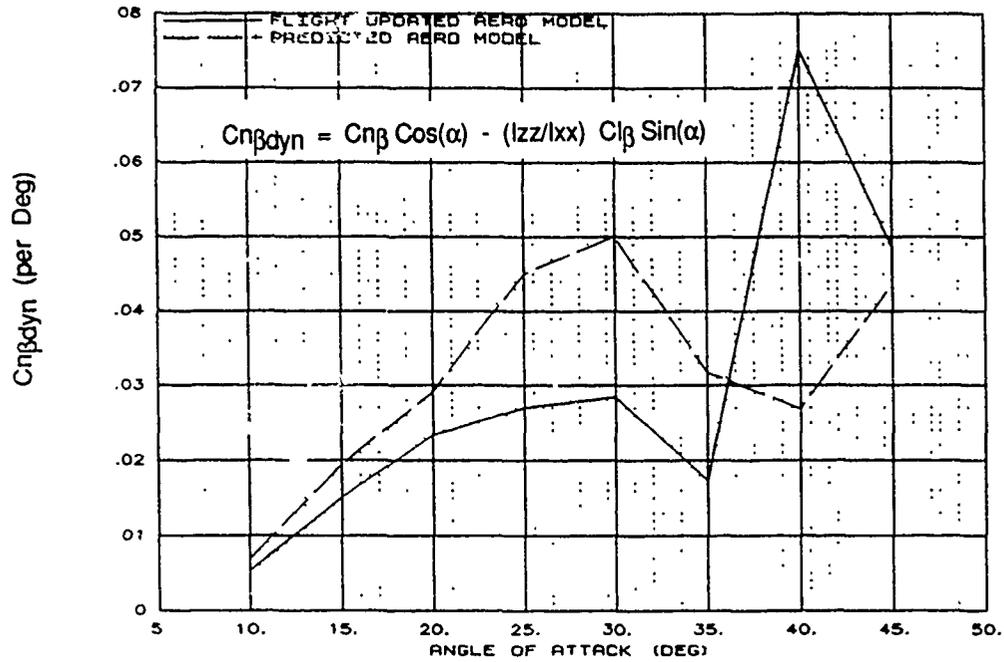
Figure 7 Lateral-Directional Static Stability (Concluded)
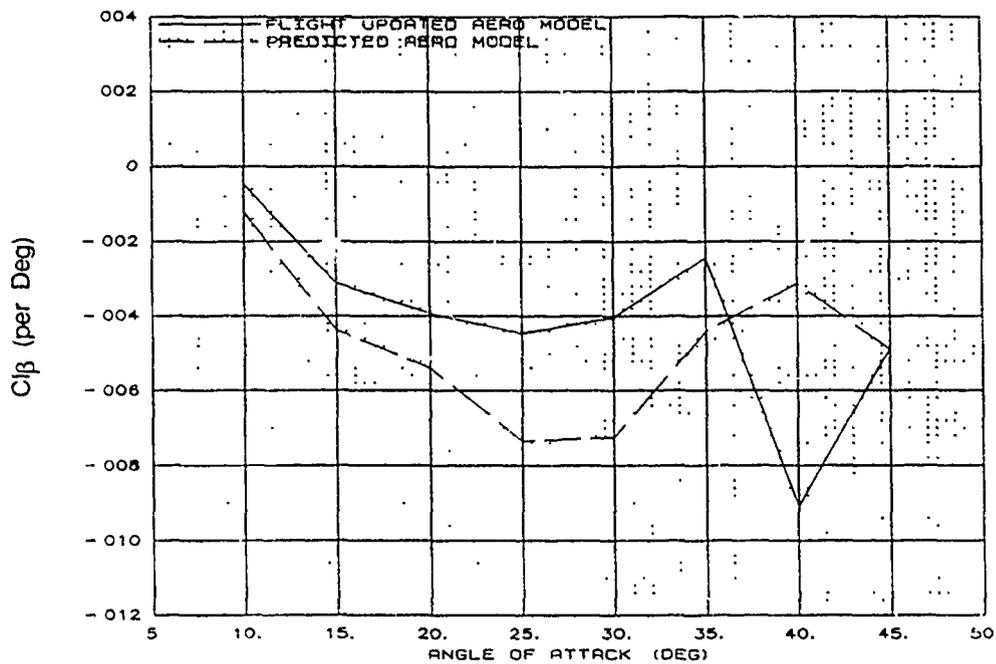
NOTES:

1. ALL DATA ARE FOR THE BODY AXIS.

2. DATA WAS COMPUTED FROM THE PREDICTED AND THE FLIGHT UPDATED AERO MODELS.

3. LINEARIZATION INCREMENT WAS +/- 2 DEGREES ABOUT 0 DEGREES SIDESLIP.

22

at a given sideslip due to slope differences about zero sideslip.

Figure 8 presents a comparison of linearized aileron and rudder power ($Cl\delta a$ and $Cn\delta r$, respectively). Figures B3 through B11 present total nonlinear yaw and rolling moment comparisons between the predicted and flight updated aerodynamic model as functions of surface deflection and AOA. All comparisons are for the 1-g automatic camber control (ACC) trim condition of Figure 2. Aileron and rudder power were derived from lateral stick and rudder pedal pulses ranging from one-half to full input. Rudder and aileron data were gathered across the deflection range (30 and 17.5 degrees, respectively) up to 45 degrees AOA. Linear parameter estimation data were not available above 45 degrees AOA. The flight updates above 45 degrees AOA relied upon batch simulation overplot comparisons between flight and simulated dynamics.

Aileron power was lower than predicted between 10 and 40 degrees AOA for deflections less than 5 degrees. Aileron power was nonlinear with deflection, gaining power at higher deflections. Flight values for aileron power followed the predicted trends with deflection but also exhibited a higher degree of nonlinearity.

Rudder power was higher than predicted between 10 and 35 degrees AOA. Rudder power was also higher than predicted for deflections above 15 degrees (see Figures B8 through B11) between 35 and 50 degrees AOA.

Both aileron and rudder power trends with AOA were similar to predictions. Aileron power about zero deflection remained low but constant above 30 degrees AOA and rudder power was negligible above 45 degrees AOA.

Figure 9 presents a comparison between the flight updated and predicted roll damping (Clp) as a function of AOA and sideslip. The predicted values were unstable between 20 and 50 degrees AOA with a strong stabilizing influence due to sideslip. Flight data at zero sideslip was more unstable than predicted between 20 and 35 degrees AOA and less unstable above 35 degrees. The stabilizing influence of sideslip was larger than predicted.

Figure 10 presents the average zero sideslip yaw asymmetry (Cno) encountered in flight. The potential presence of asymmetries as a consequence of the nose vortex system was predicted above 45 degrees AOA. The vortical and separated flow typically resulted in inaccurate predictions for magnitude and direction, although the potential presence of asymmetries was predicted. Nose-right asymmetries were encountered between approximately 40 and 48 degrees AOA. By 50 degrees AOA the asymmetry had reversed, becoming nose-left. The yaw asymmetry indicated in Figure 10 for the flight updated aerodynamic model represents an average of the characteristics which produced the most consistent comparisons between flight and batch simulation dynamics. The asymmetry magnitudes, onset, and reversal AOA were not always repeatable; however, the trend of nose-right between 40 and 48 degrees AOA and nose-left above 50 degrees AOA was consistent.

Summary:

A nonlinear flight test based update of the X-29 high AOA simulation aerodynamic model was accomplished. The update was successful in providing characteristics closer to the actual aircraft than the predicted model. Differences between flight and the updated aerodynamic model exist. The difference was greatest in the pitch axis above 45 degrees AOA. The model shows greater nosedown recovery moment than was encountered in flight. Uncertainty in the flight pitching moment data between 40 and 50 degrees AOA may be attributable to sideslip affects, aerodynamic hysteresis, rate affects, and vortex asymmetry uncertainties.

Significant differences between predicted and actual aircraft aerodynamics were present. The ground-based predictive methods adequately determined the stability and control trends with AOA, but the accuracy of individual aerodynamic parameter predictions was low. High AOA aerodynamic prediction had a higher degree of uncertainty compared to low AOA prediction capability.

The largest difference from prediction was a large reduction in full nosedown aerodynamic control power above 45 degrees AOA. The minimum value of full nosedown control power (Cm^*) between 50 and 70 degrees AOA was 50 percent of prediction. The low Reynolds number wind tunnel data more accurately reflected the correct value for Cm^* than did the high Reynolds number predicted data.

23

X-29 USAF S/N 820049
1 G ACC TRIM   XCG=449 in
MACH=0.3   ALT=30K ft
AERO MODEL COMPARISONS

Figure 8 Lateral-Directional Control Power
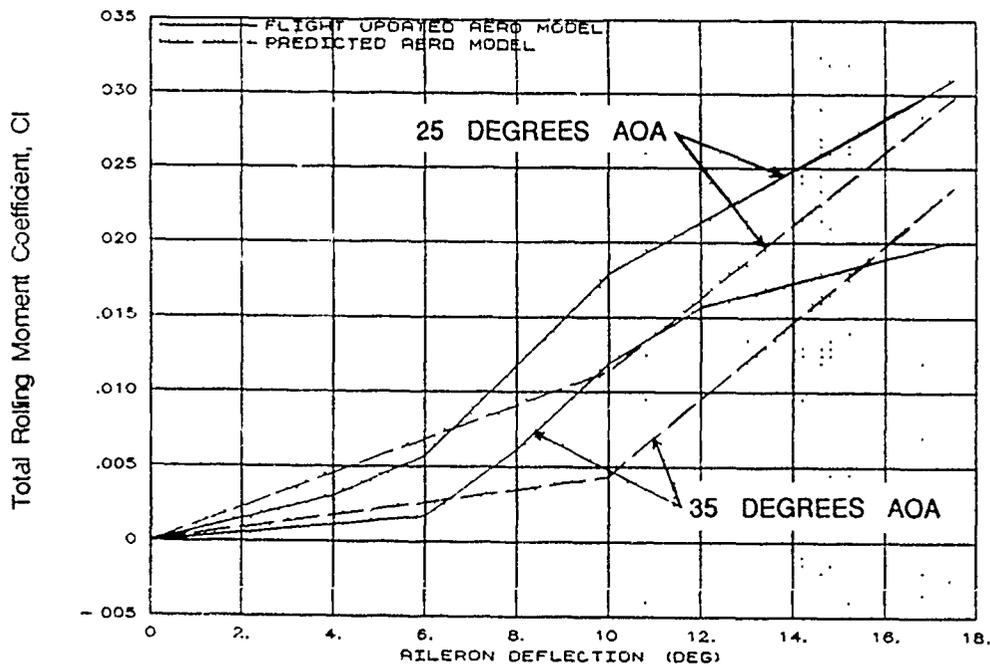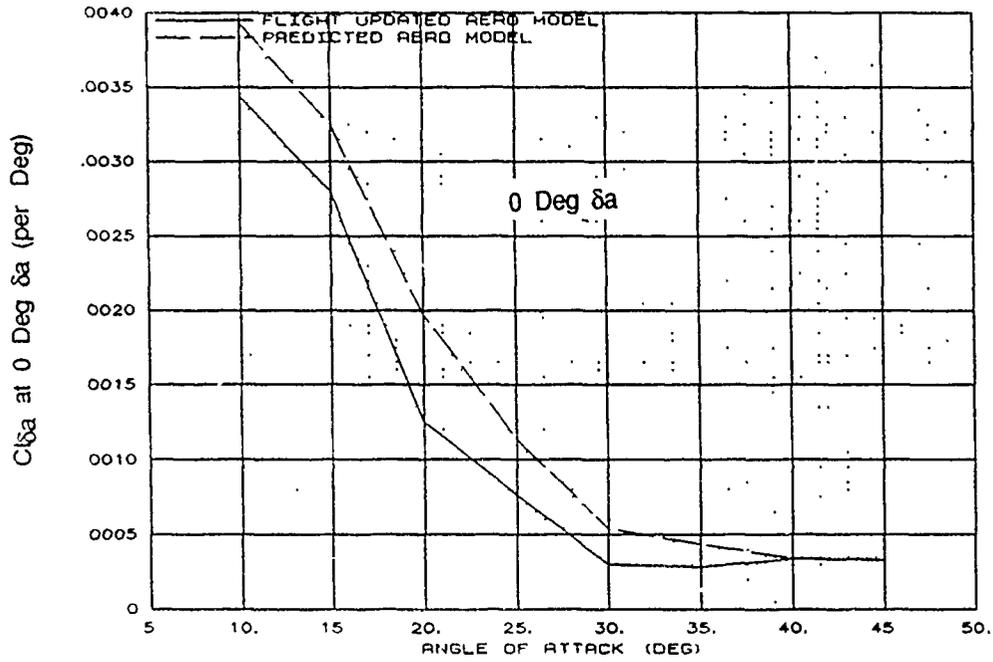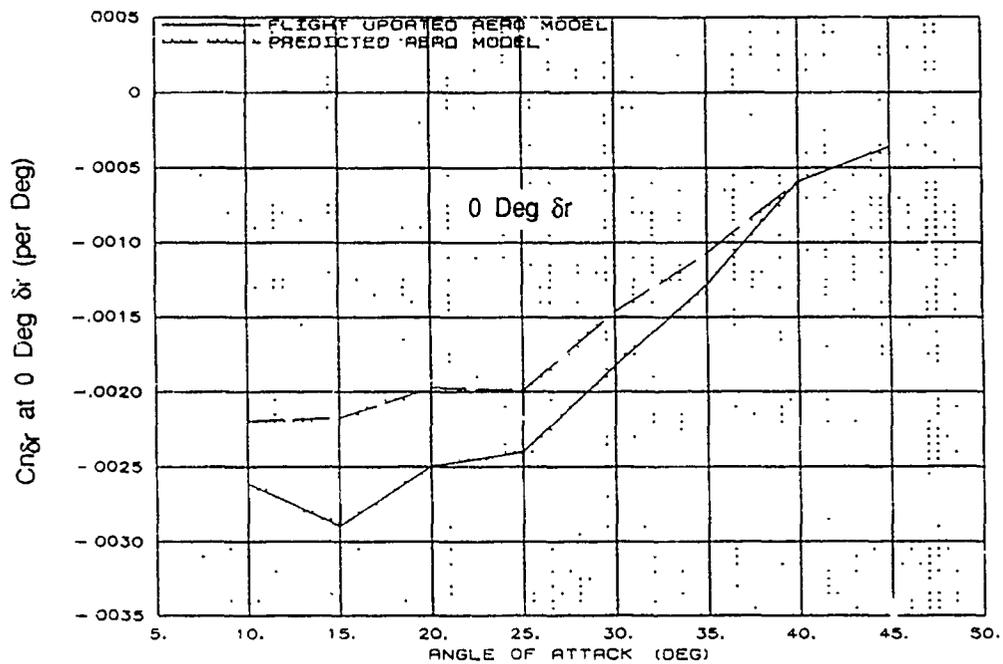
Figure 8 Lateral-Directional Control Power (Concluded)

NOTES:

1. ALL DATA ARE FOR THE BODY AXIS.

2. DATA WAS COMPUTED FROM THE PREDICTED AND THE
   FLIGHT UPDATED AERO MODELS.

3. LINEARIZATION INCREMENT WAS +/- 2 DEGREES
   ABOUT 0 DEGREES AILERON AND RUDDER DEFLECTION.

25

X-29 USAF S/N 820049
1 G ACC TRIM   XCG=449 in
MACH=0.3   ALT=30K ft
AERO MODEL COMPARISONS


Figure 9 Aerodynamic Roll Damping

26
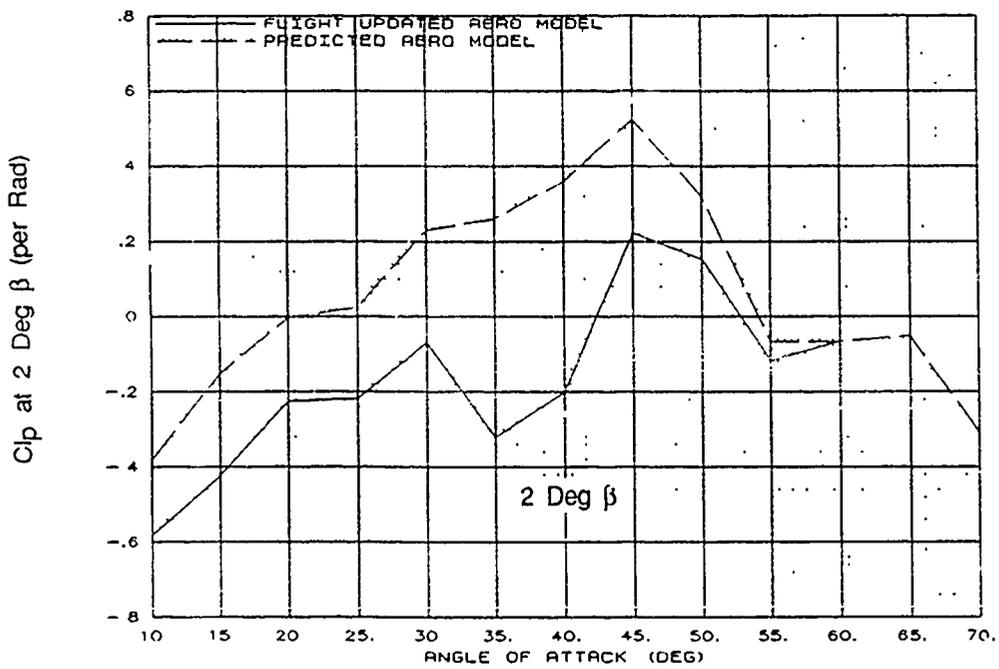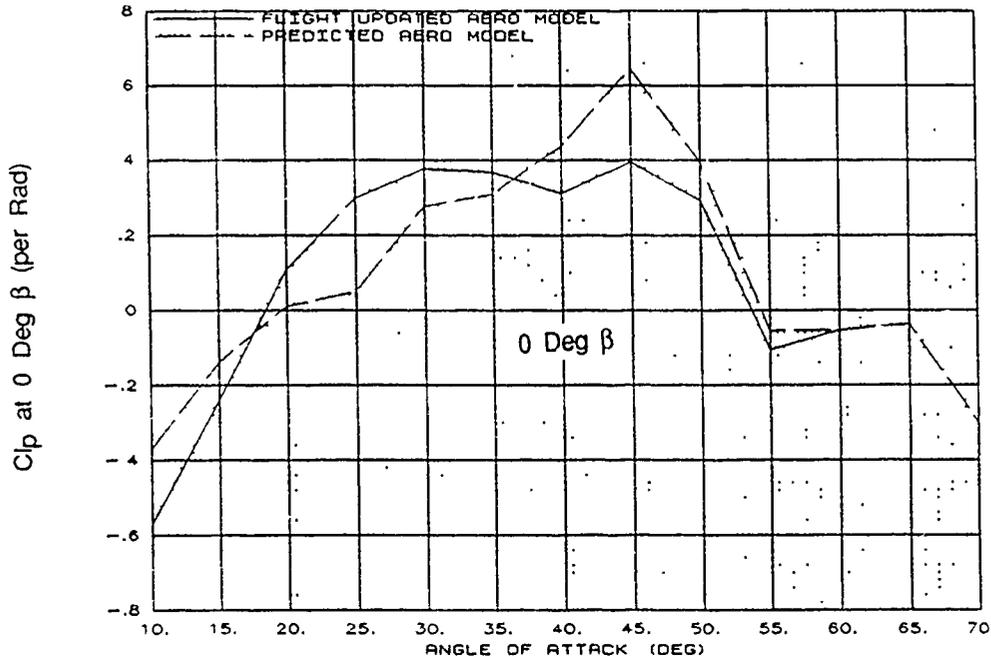
Figure 9 Aerodynamic Roll Damping (Concluded)

NOTES:

1. ALL DATA ARE FOR THE BODY AXIS.

2. DATA WAS COMPUTED FROM THE PREDICTED AND THE
   FLIGHT UPDATED AERO MODELS.

X-29 USAF S/N 820049
1 G ACC TRIM   XCG=449 in
MACH=0.3   ALT=30K ft
### AERO MODEL COMPARISONS
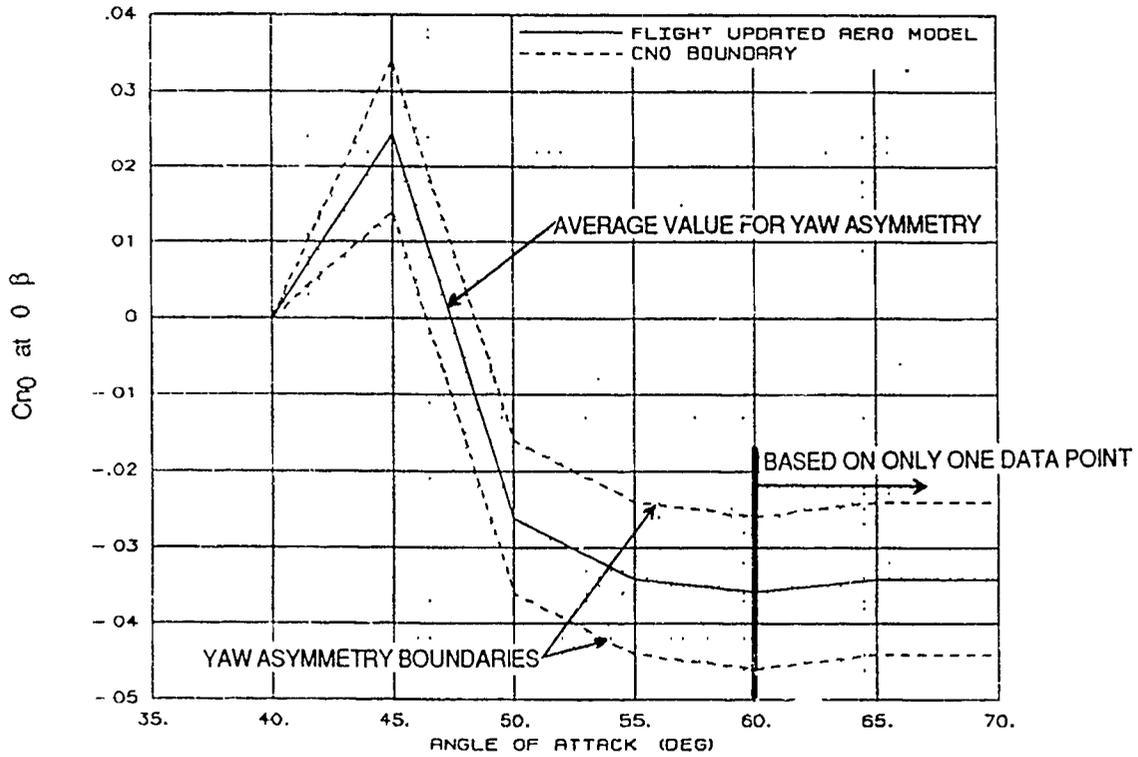
Figure 10 Average Yaw Asymmetry

28

The predicted aileron control power characteristics for the FSW were confirmed to 45 degrees AOA. Differences from predictions existed, but the general character and trends were as anticipated

The predicted high canard control power below 45 degrees AOA was confirmed. Flight values of control power were higher than predicted around trim positions. Full nosedown recovery moments at -57 degrees trailing edge up (TEU) canard were less than predictions; however, this may have been the result of changes in static instability (Cmα) or basic pitching moment (Cmo) rather than changes in surface control power.

The lift coefficient trends and maximum lift AOA predicted for the configuration were confirmed. Lift coefficients and slope with AOA were higher than predicted during slow speed (1-g) maneuvering near the ACC trim conditions and the maximum lift coefficient was greater than 2.0. Lift was close to predicted during higher speed (above 150 KCAS) dynamic maneuvering. The drag was close to predicted at all conditions tested

LONGITUDINAL STABILITY AND CONTROL

Trim:

The X-29 exhibited unique longitudinal trim characteristics as a consequence of three-surface pitch control, FCS control law interactions, and nonlinear longitudinal stability and control parameters. The three-surface pitch control provided a theoretical infinite number of trim conditions at a given AOA and airspeed. The actual trim was dependent on the control law architecture and aerodynamic nonlinearities

The ACC canard trim mode of the longitudinal control laws took advantage of the multiple surfaces to position the canard for maximum total aircraft lift, while maintaining sufficient control power for stabilization. The canard was slowly forced to a predetermined trim position by integration of an error signal to the symmetric flaperon until flaperon position saturation (21.5 degrees trailing edge down [TED] above 15 degrees AOA). Canard positioning commands were then transferred to the strake. The ACC worked through a slow outer-loop control law and only achieved full scheduled canard trim during sustained steady-state conditions. Longitudinal

command and stabilization had priority over ACC commands and provided the initial surface trim based on balancing commanded and actual pitch rate. The initial trim prior to full ACC canard schedule implementation was dependent on the rate at which AOA and airspeed were attained. Slow entry rates provided initial trim closer to the ACC schedule than did rapid entries. Flight test efficiency during high sink rate conditions often required entering maneuvers prior to achieving full ACC trim.

Figure 11 presents a comparison of flight, flight updated simulation and predicted simulation ACC trim surface positions during a slow 1-g deceleration to 45 degrees AOA. Figures B12 and B13 present similar data for other cg conditions. Flight and simulation trim data were obtained during descending (38,000 to 25,000 feet pressure altitude) slow decelerations in military power.

The canard was maintained on the ACC schedule by trimming of the strake since the flaperon was saturated by 10 degrees AOA. Strake trim was more TED compared to simulation predictions due to the overall noseup aerodynamic pitching moment differences from predictions discussed in the Aerodynamic Data Comparison section of this report (Figures 4 and 5).

Figure 12 presents a comparison of the flight ACC trim canard from Figure 2 and the initial canard trim positions encountered during longitudinal pulses and doublets. The initial canard trim positions are for a large range of cg. The initial canard trim (prior to full ACC scheduling) averaged 5 degrees more TEU than did the ACC trim conditions. The value of canard trim impacted the parameter estimation results for static instability and canard power as discussed in the Aerodynamic Data Comparison section of this report.

Longitudinal Maneuvering:

General.

The X-29 high AOA longitudinal control laws used a pitch rate command and stabilization system. A low frequency, weak AOA feedback was implemented to provide positive apparent speed stability to the pilot through increased aft stick force with AOA. The AOA feedback provided little short period stabilization. The pure pitch rate command system required varying degrees of aft stick force to maintain normal load factor depending on aircraft attitude as well as airspeed.

29

**X-29 USAF S/N 820049**
1 G ACC TRIM
MIL POWER   XCG=449 in
ALT=38K TO 25K ft
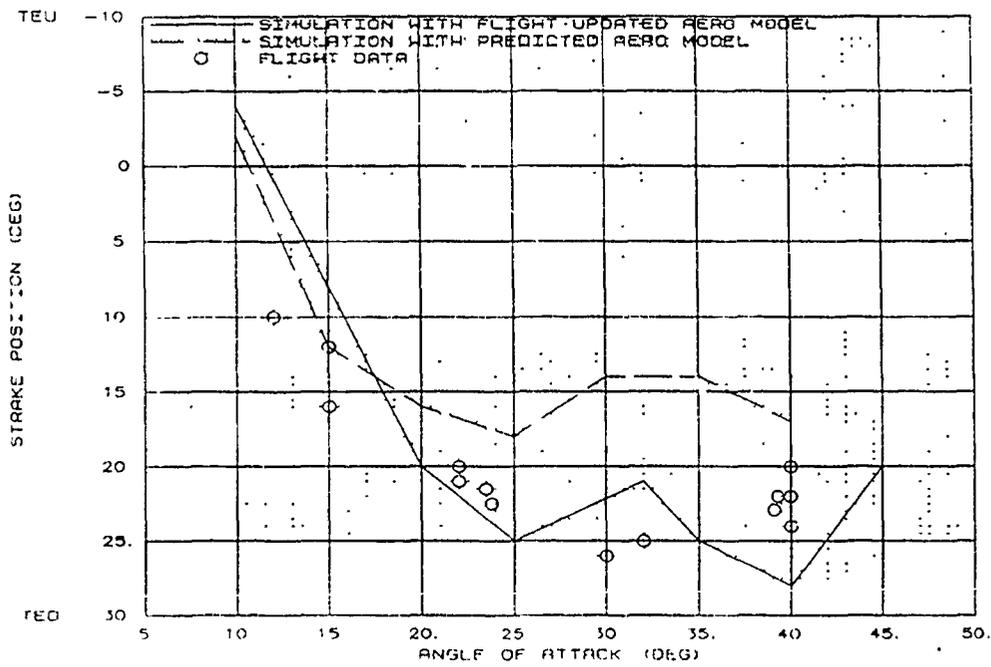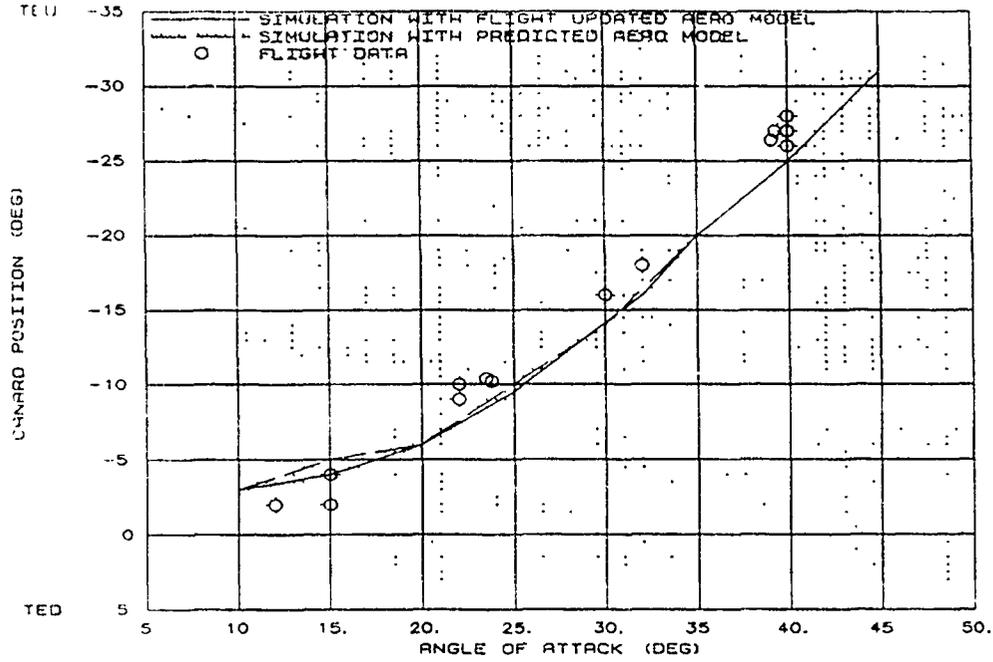
Figure 11 One-G ACC Trim Comparison

X-29 USAF S/N 820049
INITIAL and 1 G ACC TRIM
ACC TRIM XCG=449 in
**INITIAL TRIM XCG=446 to 451 in**
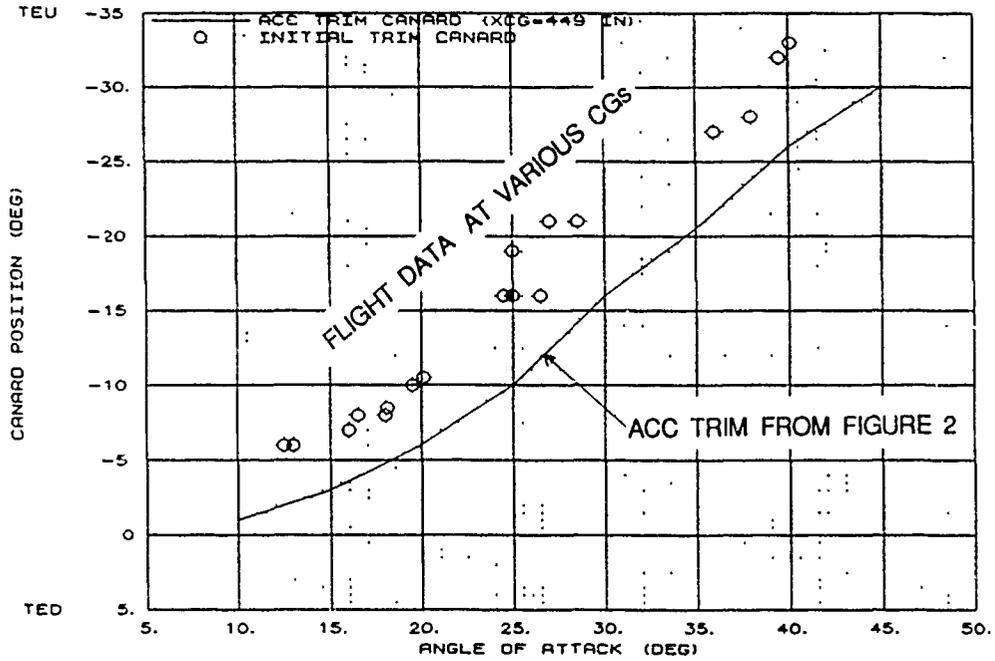
Figure 12 Initial Canard Trim

Active pilot control of AOA was required during lateral-directional maneuvering since automatic compensation for kinematic coupling or gravity vector orientation was not provided. The system was simple and relatively unmodified from the low AOA control laws

Pitch Rate Capability.

Figure 13 presents maximum pitch rates attained during full aft stick pitch attitude captures entered from 170 to 210 KCAS at 20,000 feet pressure altitude. The maximum rates were comparable to other current fighter type aircraft. High AOA basic fighter maneuvers (BFMs) performed against an F-18 target aircraft indicated that although maximum pitch rate capability was similar to current aircraft, increased pitch rate would be desirable at high AOA for nose-pointing purposes. The extent to which the X-29 pitch rate command could be increased was a function of the longitudinal instability and canard actuator rate capability. The high static instability required rapid positioning of available control power to maintain adequate stability. Although high aerodynamic control power existed, maximum pitch rate ability (from a stability maintenance point of view) was dictated by the canard rate limit.

Figure 14 summarizes the results of a limited simulation effort to study the feasibility of longitudinal command gain increases below 200 KCAS. The study was not exhaustive and only considered effects on stability Handling characteristics or other pilot-in-the loop sensitivity studies were not accomplished. The data were gathered from abrupt aft stick inputs from wings level at 150 and 200 KCAS, 20,000 feet pressure altitude with an aft cg of 450 inches. Inputs were neutralized at 40 degrees AOA. Maximum pitch rate, TEU canard rates to stop pitchup, TEU canard position saturation time, and AOA overshoots beyond 40 degrees were measured The study was performed with the flight updated aerodynamic model. The results indicated a 30-percent increase in pitch rate command capability may have been feasible at 200 KCAS and below. Canard rate limits, excessive AOA overshoots, or prolonged canard position saturation after longitudinal stick neutralization were not present with the simulation for a 30-percent command gain increase.

Pitch Rate and AOA Control.

Figure B14 presents a time history of a pitch attitude capture performed during agility metric studies (Reference 1). The maneuver called for capturing a pitch attitude within an error band of ±2 degrees. Pitch attitude was easily captured and maintained within the specified limits. Figure 15 presents the times to capture and pitch through various pitch attitudes during maximum command inputs at 200 KCAS at approximately 20,000 feet pressure altitude. The time to pitch-through was close to the time to capture an equal pitch attitude, demonstrating good control of both pitch attitude and rate. Good pitch attitude and rate control below 45 degrees AOA was accomplished using a simple pitch rate command control law architecture.

The pitch rate command system required pilot compensation to maintain AOA as aircraft attitude and corresponding gravity vector orientation changed. Kinematic coupling of AOA and sideslip during lateral-directional maneuvering could change AOA without significant pitch rate changes. High pitch attitude maneuvers at low airspeed could result in AOA changes without large rate or attitude variations. Pilots were aided in AOA control during expansion maneuvers with an AOA error indication on the attitude direction indicator (ADI) director bars. The ADI error indicator was used in fine control of AOA during critical data gathering and envelope expansion maneuvers. Overall AOA control with or without the ADI error indicator was considered good to 45 degrees AOA. Angle-of-attack control was considered better than the simulation with either the predicted or initial flight updated aerodynamic models. The final simulation aerodynamic update model reflected some increase in AOA control compared to previous versions.

Pitch Inertial Coupling.

The X-29 FCS was designed to roll about the velocity vector at high AOA. Velocity vector rolls required combined roll and yaw rates in the same direction which imparted a noseup inertial coupling moment. Figure B15 presents a time history of typical X-29 longitudinal inertial coupling characteristics during a 1-g velocity vector roll at 30 degrees AOA.

X-29 USAF S/N 820049
MAX POWER   ALT=20K ft
BLOCKIX-AAO2 CONTROL LAWS
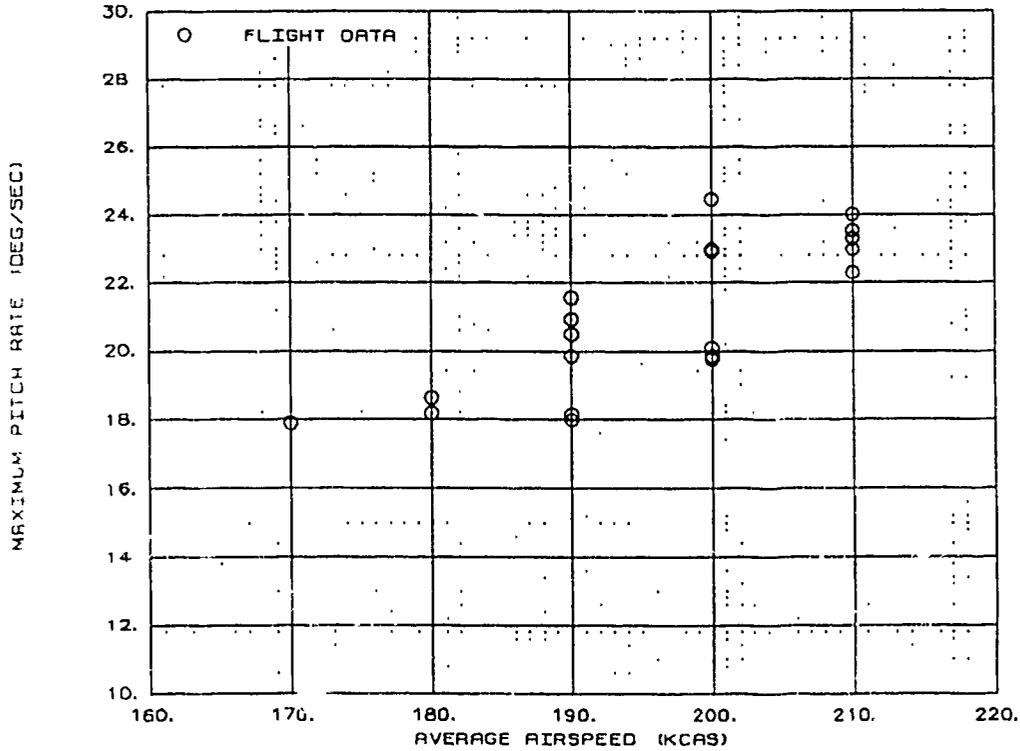
NOTES:

1. AIRSPEED WAS AVERAGE VALUE TO THE NEAREST 10 KCAS FOR EACH MANEUVER.

2. CENTER OF GRAVITY VARIED FROM 447 IN. TO 450 IN.

Figure 13 Maximum Pitch Rates at 20,000 Feet

Figure 14 Simulation Longitudinal Command Gain Study

X-29 USAF S/N 820049
MAX POWER   ALT=20K ft   XCG=450 in
BLOCKIX-AAO2 CONTROL LAWS

TIME TO PITCH THROUGH A PITCH ANGLE CHANGE
ABRUPT CONTROL STICK INPUTS ONLY,   1G

Figure 15 Pitch Capture Summary

35
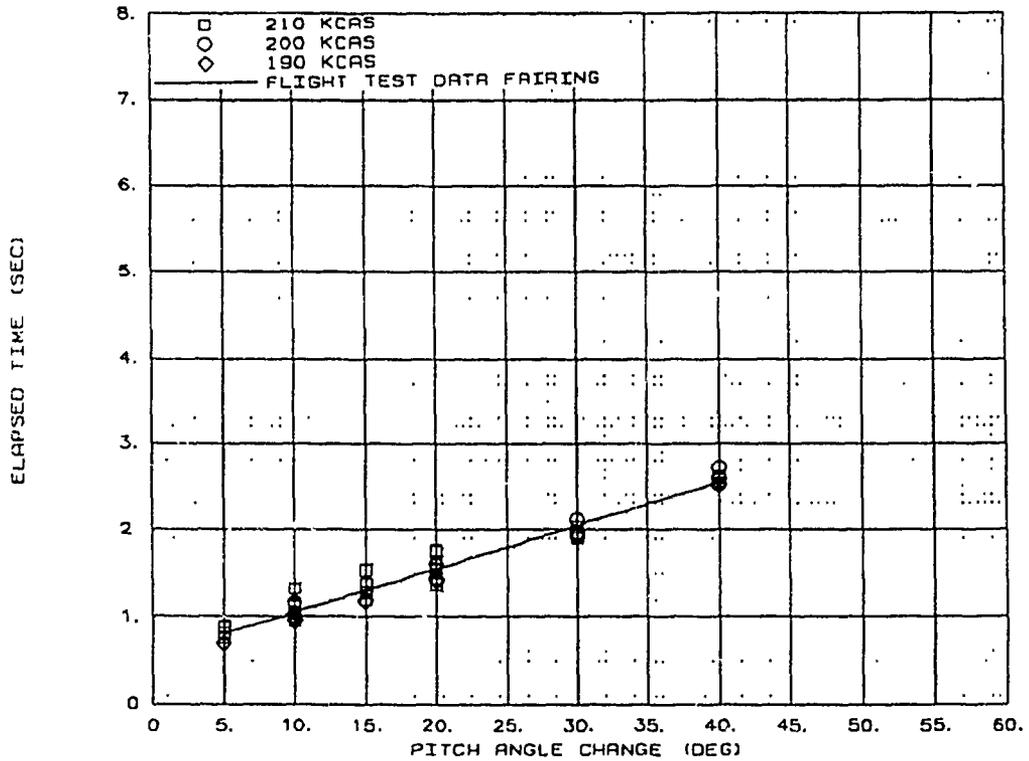
TIME TO CAPTURE A PITCH ANGLE GHANGE, 1G
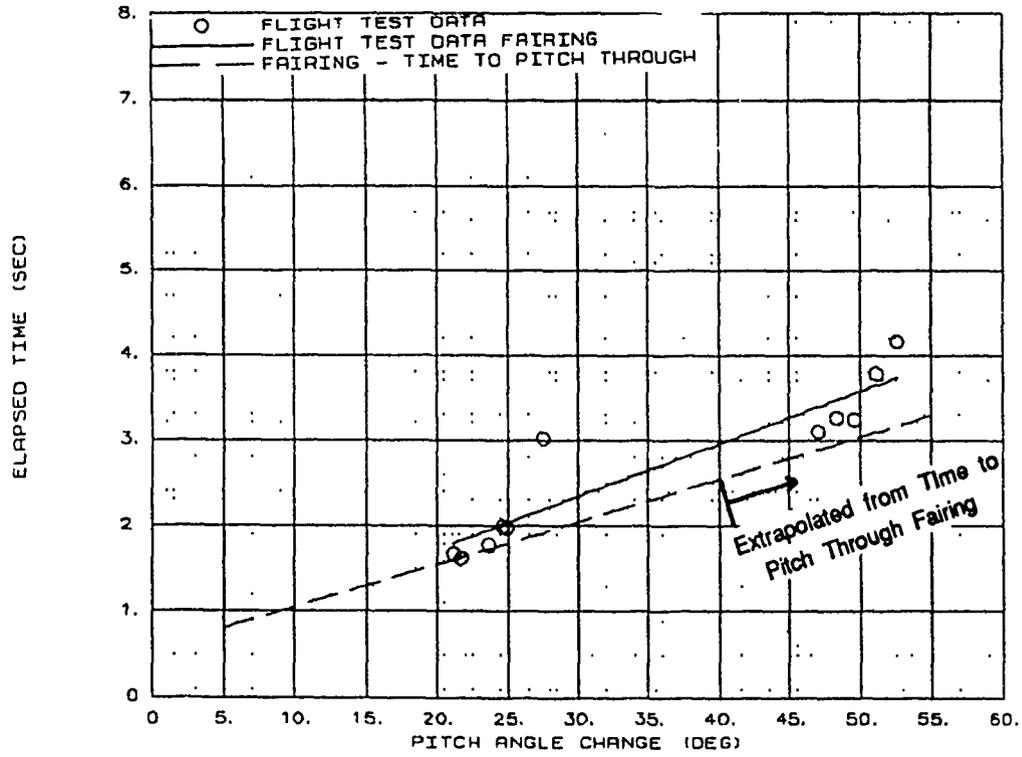
Figure 15 Pitch Capture Summary (Concluded)

36

Inertial coupling was controlled with small canard inputs. Canard unload (TEU movement) produced the required nosedown aerodynamic control of velocity vector roll induced inertial coupling. Unloading the canard allowed for maintaining high control power by avoiding local surface stall.

Directional asymmetries above 45 degrees AOA produced yaw rates (see Lateral-Directional Stability and Control section) which were not controllable with available rudder power. Longitudinal inertial coupling was generated by uncontrolled rates above 50 degrees AOA and was usually noseup. The impact of the inertial coupling on recovery from above 50 degrees AOA was cg sensitive. Figure 16 presents a comparison between a forward cg (445 inches) pitchup maneuver to 67 degrees AOA and a similar maneuver to 55 degrees AOA at a farther aft cg (447 inches). Figures B16 and B17 present full time histories of the two maneuvers. Both maneuvers encountered full nosedown aerodynamic surface positions during recovery to below 40 degrees AOA. Inertial coupling with the forward cg case was controlled with the available nosedown aerodynamic pitching moment. The maneuver at the farther aft cg location encountered a minor AOA hangup during recovery. Inertial coupling induced noseup pitching moments were sufficient to momentarily overcome full nosedown aerodynamic capability. Phasing of the inertial coupling component between the two maneuvers varied, although both encountered maximum inertial coupling moments between 40 and 45 degrees AOA.

The susceptibility to pitch inertial coupling was due to the low aerodynamic nosedown recovery moment above 45 degrees AOA. Low full nosedown aerodynamic moments degraded recovery characteristics in the presence of noseup inertial coupling. Consistent recoveries from above 55 degrees AOA were not demonstrated as only one maneuver was performed. Recovery from the single maneuver was excellent, however, different phasing of inertial coupling could have resulted in a less satisfactory recovery. Multiple recoveries from maneuvers between 50 and 55 degrees AOA were demonstrated for cg locations ahead of 447 inches; however, maneuvers aft of 446 inches cg demonstrated marginal recovery ability.

Figure 17 presents a comparison of the X-29 flight value of Cm* at 65 degrees AOA and the proposed minimum Cm* criteria of Reference 8. The X-29 flight value of Cm* occurred at 65 degrees AOA. Pitch

recovery was marginal above 50 degrees AOA and aft of 446 inches cg in the presence of noseup inertial coupling. The full nosedown flight value of pitching moment coefficient at 50 degrees AOA is also indicated in Figure 17. The value of the pitching moment coefficient at 50 degrees AOA was more nosedown than the value of Cm* taken at 65 degrees AOA. The data indicate that the proposed criteria was not conservative for the X-29 in the presence of noseup inertial coupling.

Figure 18 presents the required nosedown aerodynamic pitching moment coefficient to control noseup inertial coupling moments. The unique roll and yaw rate combination for stability axis or velocity vector rolls produced noseup inertial moments. The nosedown aerodynamic moment (-Cmic) required to control the inertial coupling due to velocity vector rolls is presented in the first part of the figure as a function of stability axis roll rate, AOA, and airspeed. The inertial coupling control requirements are also compared to the a...lable aircraft nosedown moments as a function of AOA and cg. The second part of Figure 18 presents similar data for the general inertial coupling case where yaw and roll rate products (PR) of the same sign were used to compute the required nosedown aerodynamic control (-Cmic) for noseup inertial coupling. The majority of the maneuvers with the X-29 encountered noseup inertial coupling.

The first part of Figure 18 shows that the available aerodynamic nosedown pitching moment for control of noseup inertial coupling between 30 and 45 degrees AOA exceeds the available stability axis roll rate capability of the aircraft. The maximum stability axis roll rate reduced from 40 degrees per second at 30 degrees AOA to approximately 10 degrees per second between 40 and 45 degrees AOA (see Figures 20 through 23 of the Lateral-Directional Stability and Control section of this report). No velocity vector rolls above 45 degrees AOA were possible due to lack of rudder power. Even with yaw control, however, little capability would have existed due to low nosedown aerodynamic recovery moments. Stability axis roll rates beyond 20 degrees per second across the cg range would not have been possible above 50 degrees AOA due to the low nosedown pitching moment capability.

The second part of Figure 18 showing the general inertial coupling characteristics indicates that a combined roll and yaw rate product above 800 degrees^2 per second^2 (28.3 degrees per second^2) at 60 degrees AOA would exceed available nosedown

X-29 USAF S/N 820049
MIL POWER

Xcg = 445 inches

smooth AOA recovery

full nose-down canard

nose-down pitch rate

Xcg = 447 inches

AOA hang up

full nose-down canard

nose-up pitch rate due
to inertial coupling

Figure 16 Inertial Coupling During Recovery From Above 50 Degrees AOA

Figure 17 Comparison of X-29 Data With the Proposed Cm* Criteria

100 KEAS

Stability Axis Roll Rate (deg/s)

Required to Overcome Velocity Vector Roll Induced Nose-Up Inertial Coupling

PSTAB = 10
PSTAB = 20
PSTAB = 30
PSTAB = 40
PSTAB = 50

XCG = 451
XCG = 445

Available Nose-Down Aerodynamic Cm

PITCHING MOMENT COEFFICIENT, Cm

ANGLE OF ATTACK (DEG)

150 KEAS

Stability Axis Roll Rate (deg/s)

Required to Overcome Velocity Vector Roll Induced Nose-Up Inertial Coupling

PSTAB = 20
PSTAB = 50

XCG = 451
XCG = 445

Available Nose-Down Aerodynamic Cm

PITCHING MOMENT COEFFICIENT, Cm

ANGLE OF ATTACK (DEG)

Figure 18 Pitch Inertial Coupling Departure Susceptibility

aerodynamic recovery capability at full forward cg (445 inches). This value reduced to approximately 300 degrees^2 per second^2 (17.3 degrees^2 per second^2) for the aft cg of 451 inches. Data from the Lateral-Directional Stability and Control section of this report show that combined yaw and roll rates of 25 to 30 degrees per second were regularly encountered above 50 degrees AOA.

Summary:

The X-29 exhibited good pitch and AOA control below 50 degrees AOA. The maximum pitch rate capability was comparable to other modern fighter type aircraft up to 45 degrees AOA. Angle-of-attack control during three-axis maneuvering was considered good, with acceptable pilot workload. Good stability and control characteristics below 50 degrees AOA were achieved with a simple pitch rate command flight control system.

No hung stalls were encountered to the 67 degrees AOA tested. Nosedown recoveries from above 50 degrees AOA were degraded aft of 446 inches center of gravity due to low aerodynamic recovery moments and nosecup coupling to the pitch axis. Multiple maneuvers and recoveries from between 50 to 55 degrees AOA were demonstrated with the center of gravity ahead of 447 inches; however, recoveries were marginal for centers of gravity aft of 446 inches. The AOA envelope was considered cleared to 50 degrees for all centers of gravity and to 55 degrees for centers of gravity at or ahead of 446 inches. Fifty-five degrees was considered the maximum cleared AOA. Clearance above 55 degrees AOA would require further envelope expansion since only one maneuver above 55 degrees was accomplished during the program.

The proposed Cm* criteria of Reference 8 was not conservative for the X-29 in the presence of nosecup inertial coupling. Marginal recovery was encountered above 50 degrees AOA, which had a more nosedown recovery pitching moment than the Cm* value taken at 65 degrees AOA. The marginal recovery was a result of nosecup inertial coupling.

Lateral-directional maneuvering capability was not available above 45 degrees AOA due to the lack of

rudder power, however, lateral-directional maneuvering would have been limited by the available nosedown aerodynamic pitch control power above 45 degrees AOA even if rudder or yaw control power were available. Future programs designed to provide the X-29 with lateral-directional maneuvering above 45 degrees AOA will have to address the low longitudinal recovery capability. Stability axis roll rates above 20 degrees per second across the center of gravity range will not be possible above 50 degrees AOA without providing increased nosedown pitching moment capability.

# LATERAL-DIRECTIONAL STABILITY AND CONTROL

General:

The lateral-directional stability and control envelope expansion and testing were done using separate lateral stick and rudder pedal inputs. Combined lateral stick and rudder pedal inputs to test departure susceptibility with aggravated inputs were not accomplished below 45 degrees AOA. Some combined inputs were used above 45 degrees AOA to control directional asymmetries but were not intended for departure susceptibility evaluations. The flight updated simulation indicated that cross-control inputs below 45 degrees AOA would not produce departures. The same simulation did indicate that departures were possible below 45 degrees AOA with full lateral stick and rudder pedal inputs in the same direction (proverse inputs).

Envelope expansion for the BLOCKIX-AA and BLOCKIX-AA01 flight control system software releases performed full stick bank-to-bank and 360-degree aileron rolls. The BLOCKIX-AA02 flight control system release used full stick bank-to-bank aileron rolls for the envelope expansion. No 40-degree aileron rolls were performed during the envelope expansion of the BLOCKIX-AA02 software. Some 360-degree roll maneuvers at 15 and 25 degrees AOA and 200 KCAS were performed for agility metric data. All software performed full pedal rudder rolls and 1-g wings-level sideslips below 40 degrees AOA during the envelope expansion.

Steady Sideslip and Static Stability:

Figure 19 presents a comparison between flight, original, and updated simulation of full pedal, 1-g wings-level sideslips. Aileron and rudder ratios with sideslip were taken at 2 degrees positive (left pedal) sideslip. Figures B18 through B24 present a full comparison between flight, predicted, and the updated simulation of rudder and aileron deflection during sideslips.

Rudder per sideslip was less than predicted below 40 degrees AOA due to the increase in rudder power and reduced body axis static stability and dihedral effect. Rudder with sideslip was stable with small sideslips below 40 degrees AOA. Static instability above 4 degrees positive sideslip (left pedal) was indicated between 30 and 35 degrees AOA. The instability was due to destabilization of body axis yawing moment (see Figure B7). Opposite rudder countered the momentary sideslip excursion. Departures in regions with low body axis stability were prevented by high stable dihedral effect and rudder control power.

Aileron per sideslip was less than predicted below 40 degrees AOA and close to predicted at 40 degrees. The differences from prediction were due to reduced stable dihedral effect and increased aileron power for deflections above approximately 5 degrees aileron. Dihedral effect at 10 degrees AOA was neutral to slightly unstable (see Figure B3).

Stable aileron deflection with sideslip increased with AOA as dihedral effect became more stable.

Maximum sideslip during wings-level sideslips was higher than predicted due to an increase in rudder power and a decrease in stable dihedral effect and body axis static stability. Maximum sideslip was limited by lateral command authority above 25 degrees AOA, since strong dihedral effect resulted in high aileron requirements

Maximum sideslip during wings-level or steady-heading sideslips should not be confused with overall maximum sideslip. The high stable dihedral effect required aileron into sideslip above 10 degrees AOA to maintain steady conditions. The control laws had a large aileron to rudder interconnect (ARI) gain which detracted from the rudder pedal command during steady sideslips. Maximum sideslip at or below 25 degrees AOA during steady sideslips was less than 10

degrees and decreased with AOA above 30 degrees. Sideslips of 15 degrees or greater were possible with pure rudder pedal commands such as those during a rudder roll.

Lateral-Directional Maneuvering:

General.

Flight control system modifications were made during the course of the program which affected the roll capability of the aircraft. The FCS software releases were tested at differing altitudes and airspeeds which also affected roll performance. The initial FCS software releases (BLOCKIX-AA and BLOCKIX-AA01) were tested above 25,000 feet pressure altitude. The second release (BLOCKIX-AA01) contained a pitch command gain increase and affected the roll performance by obtaining a given AOA at higher airspeed. The third release (BLOCKIX-AA02) contained roll rate feedback gain reductions and variable command gain capability (lateral and ARI) The BLOCKIX-AA02 release was tested above 17,000 feet pressure altitude to 300 KCAS and 0.75 Mach number. Envelope expansion of the BLOCKIX-AA02 release performed full stick bank-to-bank rolls and reversals. The BLOCKIX-AA and BLOCKIX-AA01 releases tested full stick 360-degree and bank-to-bank rolls.

The X-29 control laws were designed to provide velocity vector rolls with lateral stick commands only. The control law architecture was simple but appropriately gain scheduled with AOA and airspeed. Rudder rolls were possible with pure pedal inputs as a result of stable dihedral effect. Velocity vector rolls were required to prevent large adverse sideslip which could cause roll hesitation or reversal through strong stable dihedral effect. Roll coordination was supplied for aileron rolls through a high gain ARI and washed-out stability axis yaw rate feedback to the rudder.

Initial FCS Releases (BLOCKIX-AA and BLOCKIX-AA01).

Figure 20 presents steady-state stability axis roll rates $(P\cos(\alpha) + R\sin(\alpha))$ for the BLOCKIX-AA01 software releases. The BLOCKIX-AA data were only obtained to 160 KCAS and are not presented. Data for Figure 20 are fairings from Figures B25 through B27 for full stick 360-degree rolls. Coordination data are also presented in Figures B25 through B27. Figures

X-29 USAF S/N 82C049
1 G ACC TRIM
## MIL POWER   FLIGHT XCG
RATIO AT 2 DEG POSITIVE SIDESLIP (S/S)
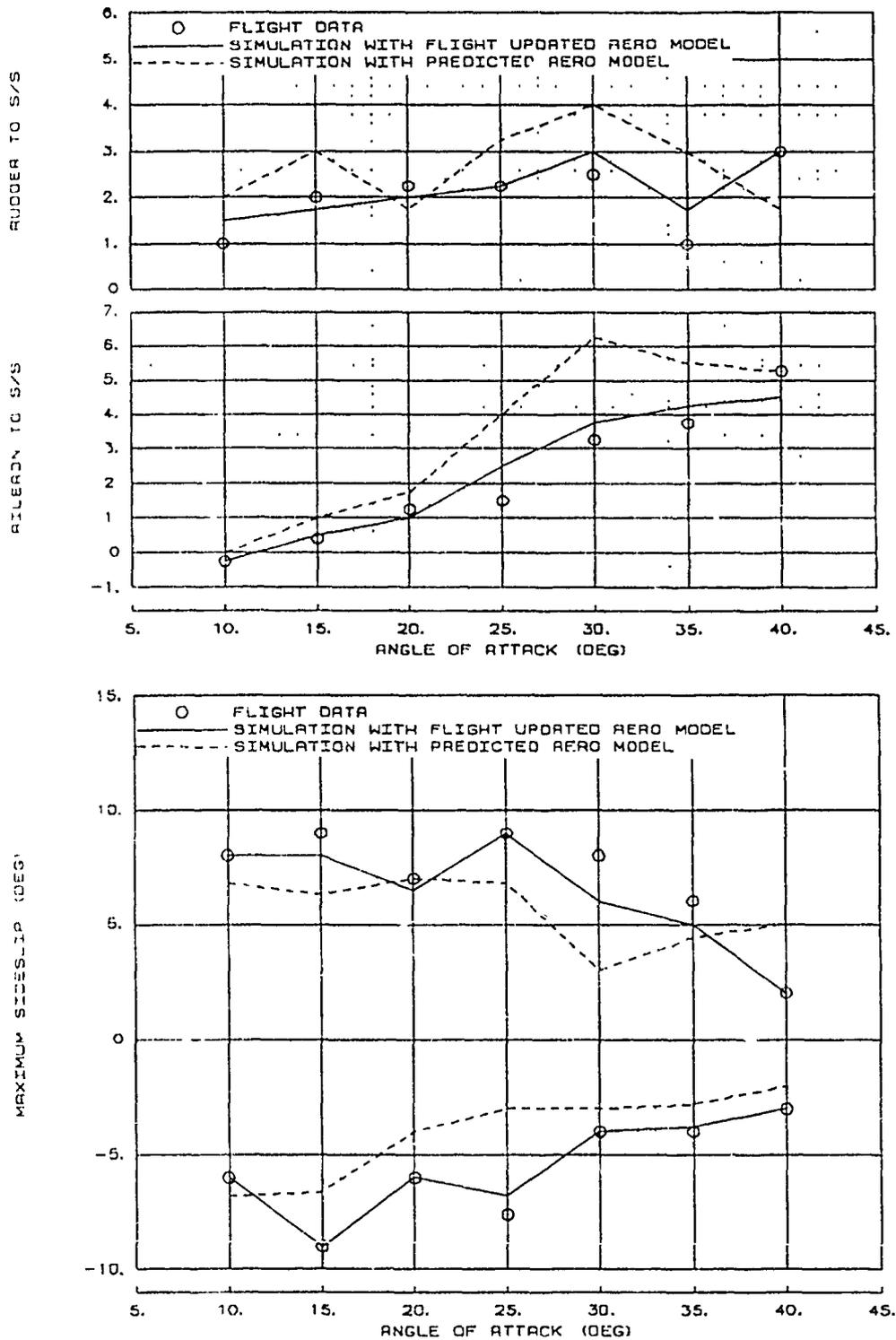
Figure 19 Wings-Level Sideslip Summary

44

X-29 USAF S/N 820049
MIL POWER   ALT=38K TO 25K ft
## BLOCKIX-AA01 CONTROL LAWS
FULL LATERAL STICK DEFLECTION
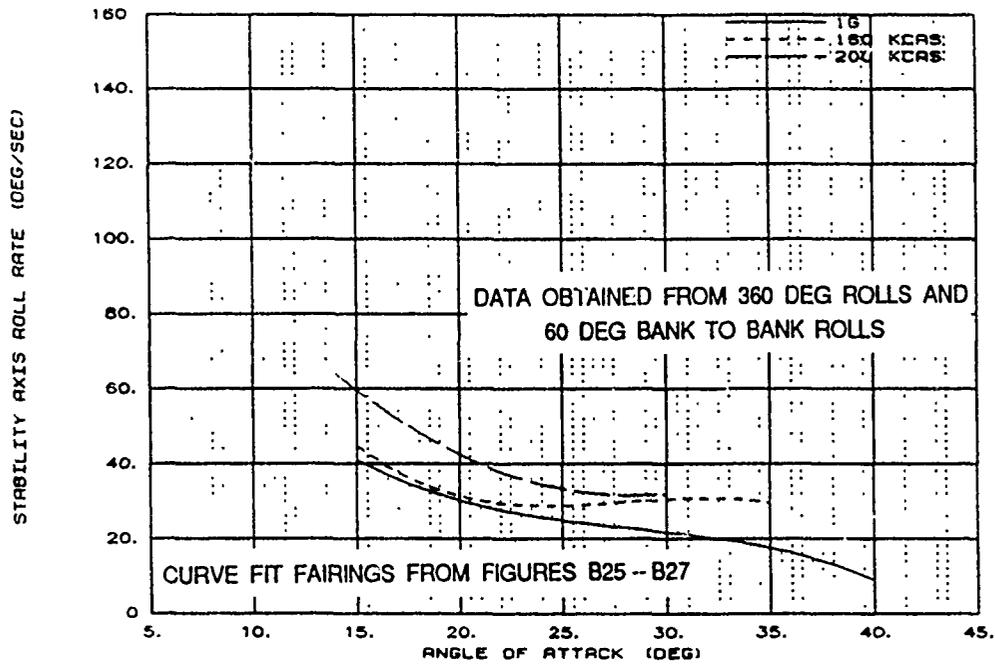
Figure 20 BLOCKIX-AA01 Roll Performance Summary

B41 and B42 present representative time histories of aileron roll maneuvers with the BLOCKIX-AA01 software release.

The X-29 initial software releases exhibited slow but well coordinated aileron rolls to 40 degrees AOA. At 45 degrees AOA, mild lateral maneuvering was possible while maintaining full left rudder pedal to offset directional yaw asymmetries which are discussed further in the Directional Asymmetry section of this report Lateral-directional maneuvering above 45 degrees AOA was not possible due to lack of rudder power and the presence of yaw asymmetries. An increase in the utility of the 35 to 45 degree AOA range for lateral-directional maneuvering compared to simulations with the predicted aerodynamic model was noted Wing rock was predicted to degrade lateral-directional maneuvering above approximately 35 degrees AOA. Mild wing rock was present above 37 degrees AOA but was of smaller magnitude than predicted and was not considered detrimental to lateral-directional maneuvering.

Aileron rolls were well coordinated with less than 5 degrees of sideslip below 40 degrees AOA. Roll coordination degraded above 30 degrees AOA. Severe roll hesitations or reversals were not present. Mild roll hesitations were encountered above 35 degrees AOA as a consequence of wing rock and low rudder power. The mild roll hesitations were not considered significantly detrimental to lateral-directional maneuvering.

Lateral maneuvering about the full left pedal condition at 45 degrees AOA during 1-g flight was limited to bank-to-bank rolls Coordination was dependent on the direction of initial stick input. Left lateral stick input while maintaining left rudder pedal followed by a right stick reversal allowed for mild bank to-bank rolls (± 30 degrees bank). Right lateral stick inputs while maintaining left rudder pedal followed by left stick reversals generated large adverse sideslips but did not result in departure. Maneuver transients between 40 and 45 degrees AOA during higher airspeed maneuvers showed increased lateral-directional maneuvering ability compared to the 1-g cases

Active pilot control of AOA during roll maneuvers was required Control requirements were minimal and the workload was not considered excessive. Well coordinated rolls limited kinematic coupling of

sideslip and AOA. Pilot compensation to maintain AOA was primarily due to changing aircraft attitude and airspeed.

Upgraded FCS Release (BLOCKIX-AA02).

Figure 21 presents peak stability axis roll rates for the BLOCKIX-AA02 software release between 17,000 and 25,000 feet pressure altitude up to 300 KCAS. Data for Figure 21 are fairings from Figures B28 through B32 for full stick 60-degree roll attitude bank-to-bank rolls. Coordination data are also presented in Figures B28 through B32. Figures B43 and B44 present representative time histories of bank-to-bank rolls. The BLOCKIX-AA02 software release contained roll rate feedback gain reductions and an increased airspeed envelope compared to BLOCKIX-AA01. The BLOCKIX-AA01 software also moved the spin prevention logic onset AOA from 40 to 50 degrees.

Stability axis roll rates were increased 10 to 15 percent above 160 KCAS compared to the BLOCKIX-AA01 release. The increase was due to reduced roll rate feedback gains compared to the BLOCKIX-AA01 release. Gain reductions were made to increase stability axis roll rates and reduce the potential for lateral limit cycles above 200 KCAS Roll coordination remained good. Control of the yaw asymmetry and mild maneuvering at 45 degrees AOA was more consistent with the absence of spin prevention logic inputs.

Command Gain Changes.

The BLOCKIX-AA02 software release had variable lateral command (K13) and ARI (K27) gains. Gain combinations were preselected and initiated by the pilot with thumbwheel (TW) inputs on the cockpit FCS control panel Flight tests were accomplished for two principal combinations:

1. 50 percent K13 and 40 percent K27 increase (TW47)

2 75 percent K13 and 80 percent K27 increase (TW53)

Both combinations were designed to increase stability axis roll rates. Tests and clearance were performed between 17,000 and 25,000 foot pressure altitude to 250 KCAS.
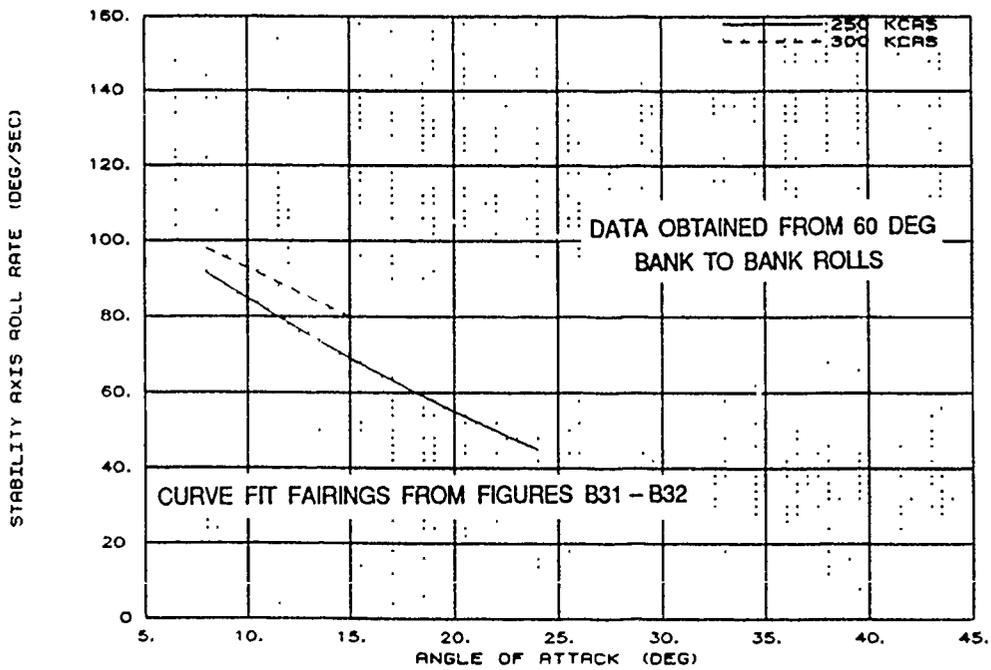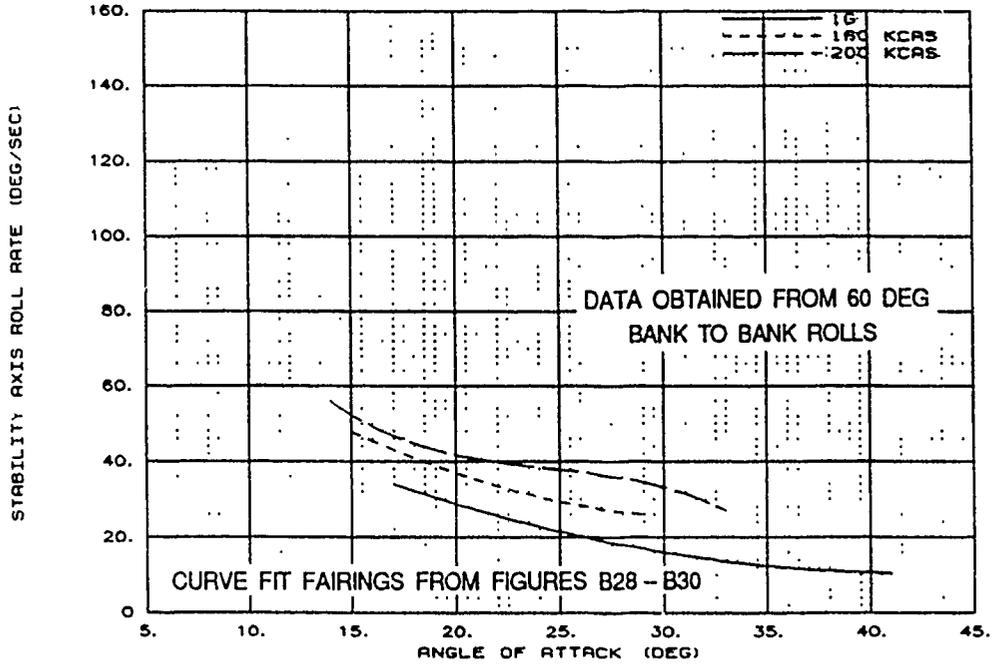
Figure 21 BLOCKIX-AA02 Roll Performance Summary

Momentary aileron and rudder position saturation were encountered with both TW combinations above 10 degrees AOA below 200 KCAS. Saturation times varied and were more often encountered during the roll reversal than with the initial inputs. Saturation times for the TW47 combination ranged from 0.5 to 1.5 seconds and from 1 0 to 2.0 seconds with the TW53 combination. Position saturation duration was dependent upon the time to achieve 60 degrees of bank angle change and thus tended to increase as roll rates decreased with AOA.

Figures 22 and 23 present the maximum stability axis roll rate for the TW47 and TW53 variations, respectively. Data for Figures 22 and 23 are data fairings from Figures B33 through B40 for full stick 60-degree roll attitude bank-to-bank rolls. Figures B33 through B40 also present roll coordination data. Figures B45 through B49 present representative time histories of bank-to-bank rolls with the TW combinations

The TW47 combination provided a 40- to 60-percent increase in stability axis roll rate over the baseline gains at 25 degrees AOA for airspeeds of 160 KCAS or greater One-g rates were comparable to the baseline gains Thumbwheel 47 encountered uncommanded roll reversal above 30 degrees AOA during 1-g maneuvering. Uncommanded roll reversals above 30 degrees AOA with airspeeds of 140 KCAS or above were not encountered with the TW47 combination. Higher airspeed maneuvers were performed from noselow windup turns at higher true airspeeds which reduced the total force contribution (aerodynamic and gravity) to adverse sideslip and corresponding uncommanded roll reversal tendencies.

The TW53 combination provided stability axis roll rate increases of 80 to 100 percent over the baseline gains at 25 degrees AOA for airspeeds of 160 KCAS or greater The 1-g rates were comparable to the baseline gains at 25 degrees AOA The TW53 combination experienced uncommanded roll reversal at 30 degrees AOA during 1-g maneuvers. Uncommanded roll reversal tendencies reduced with airspeed. However, the TW53 combination experienced mild uncommanded roll reversals above 30 degrees AOA for airspeeds above 140 KCAS. The higher command gains of the TW53 configuration produced prolonged aileron saturation at 30 degrees AOA and above. The rudder was not able to provide sufficient coordinating yaw rates to combat adverse sideslip

The TW53 combination produced higher stability axis roll rates than did the TW47 combination. Degradation in coordination capability led to increased susceptibility to uncommanded roll reversal or hesitation. The TW47 combination was considered the better of the two, providing a significant increase in stability axis roll rate with minimal degradation due to adverse sideslip and roll reversal.

Angle-of-attack control with both thumbwheel combinations was degraded from the baseline gain systems. Kinematic coupling of AOA and sideslip occurred with less precise roll coordination. Pilot workload to maintain AOA during roll maneuvers was higher than with the baseline gain systems. The increased workload was not considered objectionable and did not detract from the increased roll rate performance of the TW47 combination.

Figure 24 illustrates the differences between predicted and flight aerodynamic roll coordination ability. Increased stability axis roll rate and coordination capability compared to predictions were due to a more favorable aerodynamic yaw to roll control power ratio and reduced dihedral effect. The more favorable ratio reduced adverse sideslip above 23 degrees AOA. The lower dihedral effect reduced uncommanded roll reversal tendencies below 37 degrees AOA and made the aircraft more tolerant of adverse sideslip. The strong roll damping stabilizing influence of sideslip prevented roll departures in the absence of roll damping augmentation with position saturated ailerons. Uncommanded roll reversal and hesitation at or above 30 degrees AOA were a consequence of the inability of the rudder to provide sufficient control power for coordination of available roll rates.

The ability to control sideslip buildup during high AOA rolls was dependent on roll to yaw inertias and the aerodynamic ratio of rudder to aileron power. The magnitude of aerodynamic rudder to aileron power ratio required for coordination increased as the tangent of AOA. Uncommanded roll reversals or hesitations as a consequence of adverse sideslip were dependent on aileron power, dihedral effect and roll damping. Sideslip generation potential was estimated by the indicated computations and assumptions shown in Figure 24, using the yaw to roll aerodynamic moment ratio (Cn/Cl) for full aileron and rudder deflection. Aerodynamic yaw to roll ratios falling below the tangent of AOA line indicate adverse sideslip potential. Ratios above the line imply proverse potential Exact

48

X-29 USAF S/N 820049
MIL POWER   ALT=25K TO 17K ft
BLOCKIX-AA02 TW 47 CONTROL LAWS
### FULL LATERAL STICK DEFLECTION
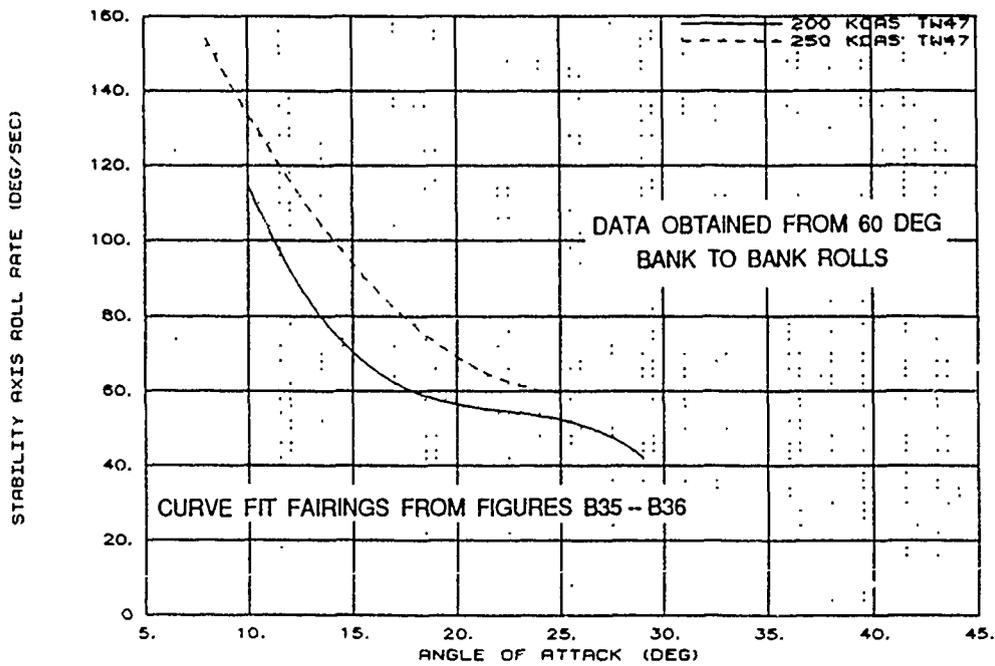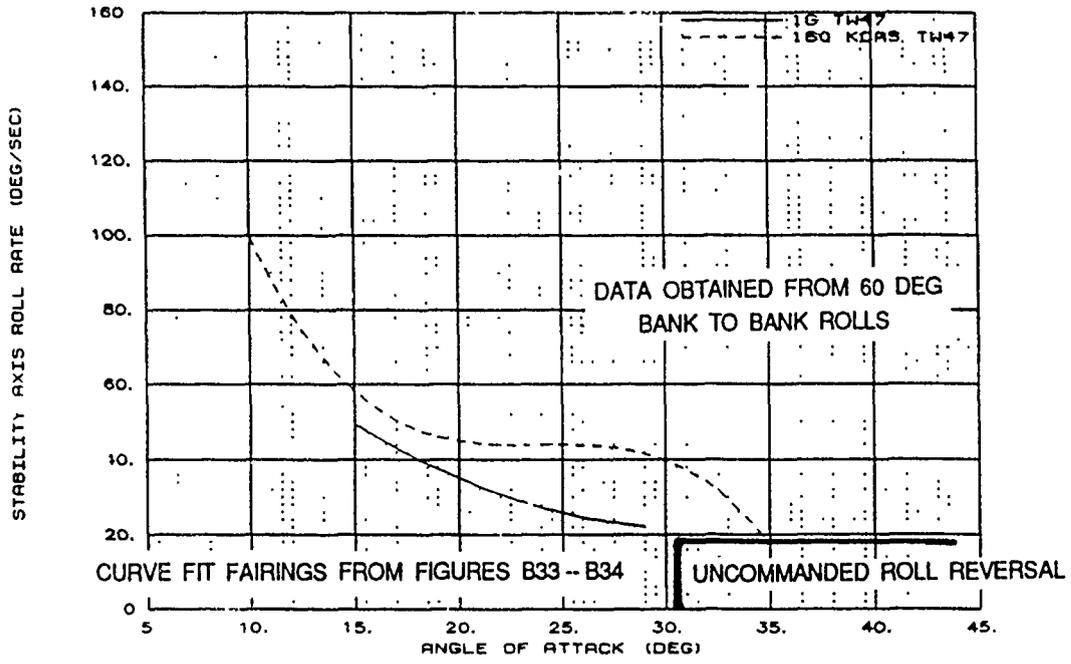
Figure 22 BLOCKIX-AA02 TW47 Roll Performance Summary

X-29 USAF S/N 820049
MIL POWER ALT=25K TO 17K ft
## BLOCKIX-AA02 TW 53 CONTROL LAWS
FULL LATERAL STICK DEFLECTION
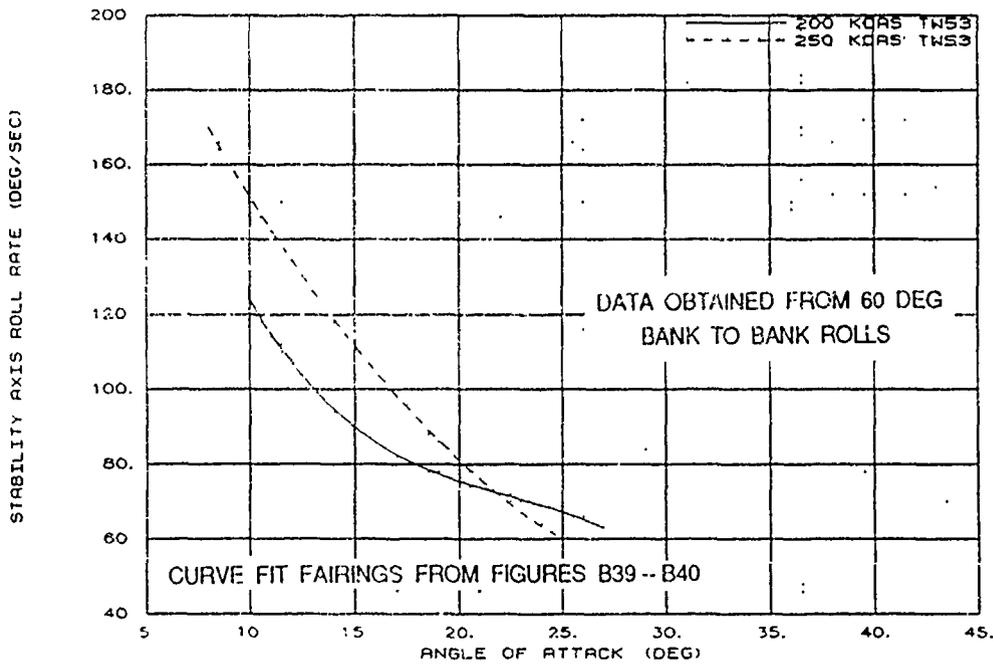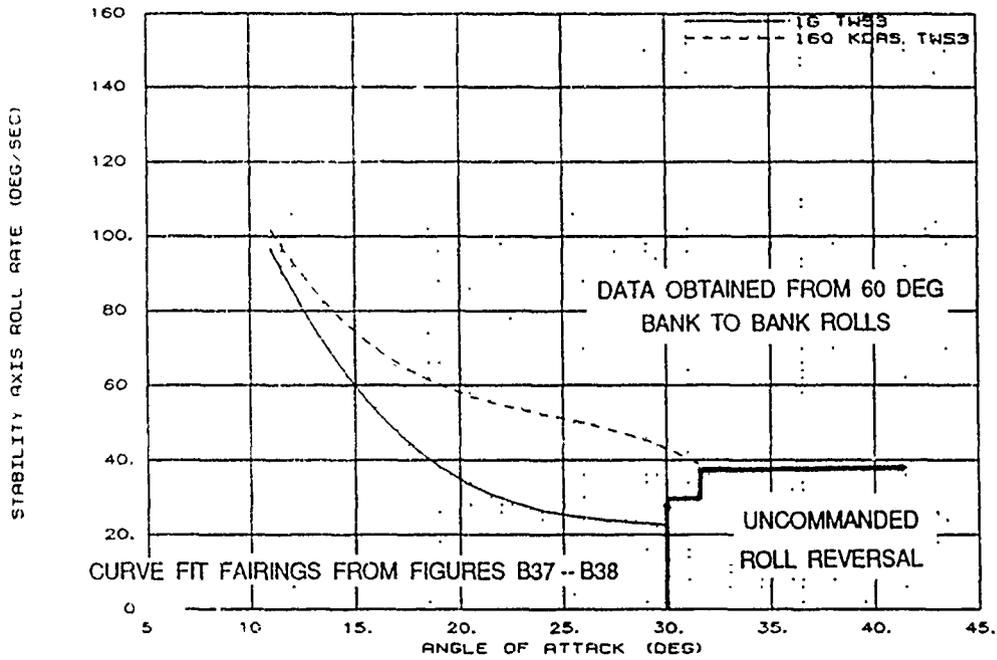
Figure 23 BLOCKIX-AA02 TW53 Roll Performance Summary

X-29 USAF S/N 820049
1 G ACC TRIM   XCG=449 in
FULL RUDDER and FULL AILERON
AERO MODEL DATA
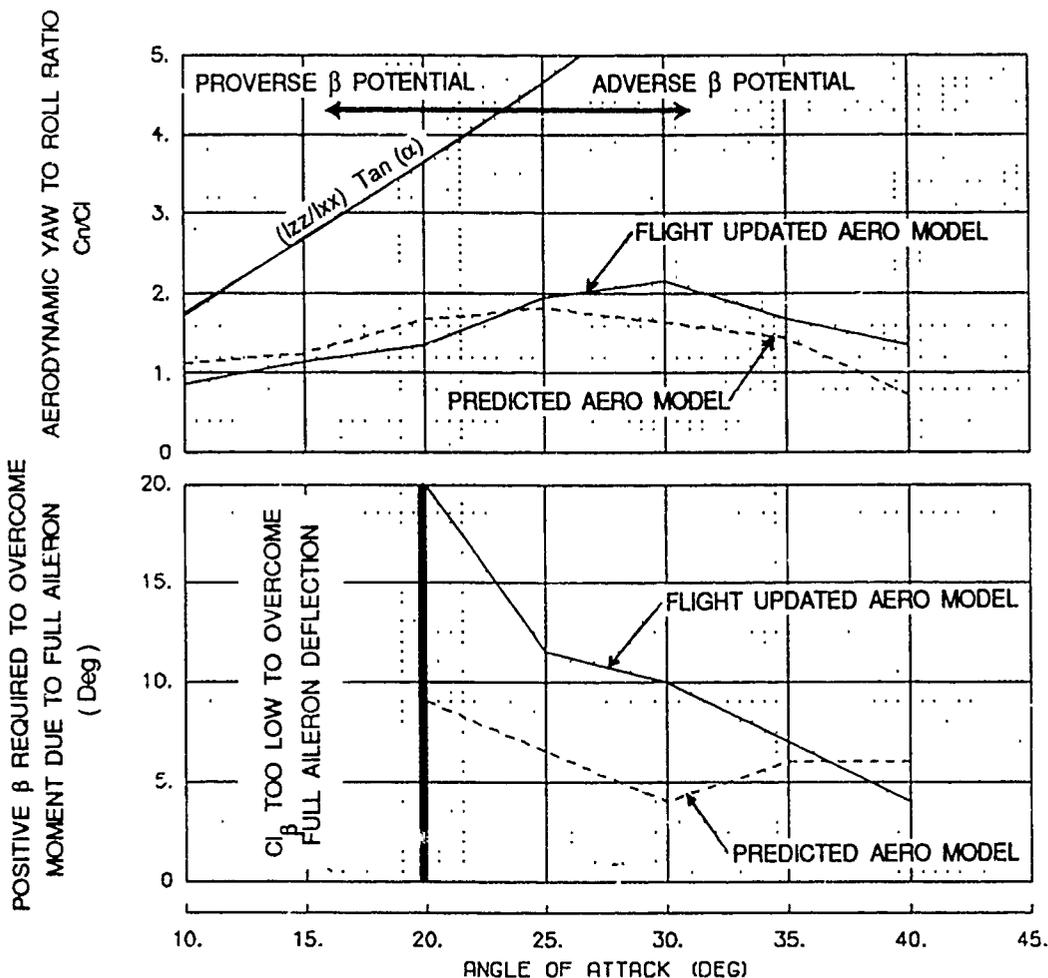
For perfect coordination, sideslip buildup from kinematic coupling must be minimized:

$$\dot{\beta} = p \sin(\alpha) - r\cos(\alpha) \quad \text{(A)}$$

assume
$$\dot{\beta} = \ddot{\beta} = \dot{\alpha} = 0.0 \quad \text{(B)}$$

differentiating (A) and applying (B) :

$$0.0 = \dot{p}\sin(\alpha) - \dot{r}\cos(\alpha)$$

$$\dot{p} = \frac{Clqsb}{Ixx} \quad \text{and} \quad \dot{r} = \frac{Cnqsb}{Izz}$$

substituting :

$$\frac{\dot{r}}{\dot{p}} = \tan(\alpha) \quad \text{and} \quad \frac{Cn}{Cl} = \left[\frac{Izz}{Ixx}\right]\tan(\alpha)$$

Figure 24 Roll Reversal and Coordination Potential

51

sideslip generation cannot be determined with this analysis, but the relative location compared to the tangent AOA line can compare capability. Computation of sideslip potential for full X-29 aileron and rudder deflection indicated a more favorable aerodynamic yaw to roll ratio for the aircraft than with predicted aerodynamics. Uncommanded roll reversal tendencies can be compared by the amount of adverse sideslip required to overcome rolling moments from full aileron deflection. The second part of Figure 24 shows a comparison between the predicted and flight updated aerodynamic model of the sideslip required to overcome full aileron deflection. The aircraft had higher resistance to uncommanded roll reversal onset compared to prediction, due to a reduction in dihedral effect. Increased adverse sideslip compared to predictions was required to overcome rolling moment due to full aileron.

Rudder Rolls.

Body axis roll rates during full pedal rudder rolls were similar to those obtained during aileron rolls with the baseline gains. Yaw rates and sideslip generated were higher than simulation predictions due to the increased rudder power and reduced static stability. No rudder roll capability was present at 10 degrees AOA due to the lack of dihedral effect. Stable dihedral effect rapidly increased with AOA and rudder rolls were possible above approximately 12 degrees AOA. No rudder roll ability existed above 45 degrees AOA due to the lack of rudder power. Yaw instabilities were present between 30 and 35 degrees AOA for sideslips above approximately 4 degrees. Sideslip would increase with no increase in rudder input due to unstable body axis static stability. The instability was not noticeable to the pilot until approximately 8 degrees sideslip due to the slow nature of the divergence. The instability did not interfere with transient maneuvering through the region. Sideslip excursions were more prevalent with left pedal inputs due to aerodynamic asymmetrics with sideslip. Excursions were sensed by the pilot and controlled with opposite rudder. Figure B50 presents a representative time history of a rudder roll.

No departures occurred during the full pedal rudder roll maneuvers performed below 45 degrees AOA. Rudder roll maneuvers were usually aborted if 10 degrees or more sideslip were encountered. Transient sideslips above 15 degrees were possible with abrupt rudder inputs.

Angle-of-attack control during rudder rolls was more difficult than with aileron rolls. The aircraft rolled using a combination of proverse sideslip and stable dihedral effect which produced an AOA increase through kinematic coupling. Higher pilot workload was required to maintain AOA during rudder rolls compared to aileron rolls. The workload was not considered objectionable, but caution was required when performing rudder rolls above 35 degrees AOA to avoid AOA increases to above 45 degrees.

Aileron saturation from the high gain roll damper system was common during full pedal rudder rolls. Momentary roll rate increases occurred during saturation since the aileron was no longer providing roll damping and high sideslip was present. No roll departures were encountered with aileron saturation due to the large stabilizing influence of sideslip on aerodynamic roll damping. The overall rudder roll ability of the X-29 was considered good below 40 degrees AOA.

Wing Drop:

High frequency (2 to 3 hertz) low magnitude, random bank angle disturbances were encountered between 20 and 30 degrees AOA and were most noticeable during 1-g flight. The high gain roll damper could not respond with sufficient magnitude to oppose the moments. The phenomena was termed wing drop to differentiate from the wing rock mode which would be present without the high gain roll damper. Wing rock with X-29 USAF S/N 820003 without the high AOA FCS was encountered above 15 degrees AOA and was cyclical at a frequency of 0.5 hertz. In contrast, wing drop encountered with X-29 USAF S/N 820049 with the high AOA FCS above 20 degrees AOA was random and at higher frequencies.

The wing drop was noticeable in the cockpit and degraded the ability to accurately hold bank angle while between 20 and 30 degrees AOA. The magnitude of the wing drop reduced by 25 degrees AOA, although some random rolling moments continued to a lesser degree at all AOAs. The wing drop was considered objectionable within the 20- to 25-degree AOA region, but did not severely impact maneuvering.

Wing drop was attributed to random flow separation. Increasing the roll rate feedback gain to counter the wing drop was not feasible due to the frequency of the wing drop. The wing drop frequency

was at the outer range of the actuator bandwidth (3 hertz). The gain levels required to damp the wing drop would have created lateral limit cycle susceptibility. Increase in the already high roll rate feedback gain would also have reduced steady roll rates.

Wing Rock:

Wing rock onset occurred at approximately 37 degrees AOA. Magnitude increased to a peak value of 16 degrees bank angle between 50 and 55 degrees AOA. Mild cyclic roll oscillations of 2 degrees bank angle were present as low as 30 degrees AOA but were of insufficient magnitude to be considered sustained wing rock by the pilot. The small random wing drop was also noticeable at 30 degrees AOA. The wing rock damped out with as little as 2 degrees of sideslip due to the large stabilizing influence of sideslip on aerodynamic roll damping. Aileron inputs larger than 10 degrees also damped wing rock as aileron power increased with deflection. The damping influence of increased aileron deflection was more pronounced with right (positive) than with left (negative) aileron.

Figure 25 presents a comparison of flight and predicted wing rock characteristics. Figure B51 presents a representative time history example of wing rock The magnitude of the wing rock was less than predicted. Preflight predictions indicated that the wing rock would severely degrade lateral-directional maneuvering above approximately 35 degrees AOA. The flight wing rock magnitude was considered a minor annoyance and did not significantly impact lateral-directional maneuvering ability.

The reduction in wing rock magnitude from predictions was due to a lower level of unstable roll damping above 30 degrees AOA. Zero sideslip magnitudes of aerodynamic roll damping were less unstable than predicted The strong stabilizing influence of sideslip produced a net increase from predicted roll damping since sideslip from kinematic coupling was present during wing rock. Differences in aileron power from predictions did not significantly affect the wing rock onset characteristics Aileron power was close to or equal to predicted for deflections less than 5 degrees above 35 degrees AOA. Aileron power increased from predictions with deflection above 35 degrees AOA. The increase in aileron power may have contributed to the decreased magnitude of the developed wing rock as higher aileron deflections were commanded with the higher oscillatory roll rates.

Prediction and mathematical modeling of wing rock characteristics for the X-29 were difficult due to the source of the roll instability. The modified F-5A nose section was predicted to produce a cyclical rolling moment which was mathematically modeled for simulation as an unstable roll damping term. Wind tunnel forced oscillation tests indicated that roll damping magnitudes were a strong function of both roll rate and frequency which were not possible to adequately model. Predicted sideslip effects on roll damping were derived empirically from time history matching of free flight and drop model tests. The preflight predictions contained a wide range of sources beyond simulation, including free flight and drop model tests. All prediction sources indicated that substantial wing rock would be present above 30 to 35 degrees AOA.

Directional Asymmetries:

Yaw asymmetries were encountered above approximately 40 degrees AOA (Figure 10). Asymmetries were nose-right between 40 and 48 degrees AOA. The asymmetry changed to nose-left above approximately 48 degrees AOA. The asymmetry remained nose-left up to 67 degrees AOA, which was the limit of flight test data. The magnitude above 50 degrees AOA was higher than below 50 degrees AOA. Onset AOA and magnitude were not always consistent; however, the nose-right asymmetry was well established by 45 degrees AOA and nose-left by 50 degrees. The asymmetries were attributed to an asymmetric vortex system generated by the modified F-5A forebody section.

Full left rudder at 45 degrees AOA could control the asymmetry if applied prior to reaching 5 degrees per second yaw rate. Combined yaw and roll rates of 15 to 20 degrees per second could be reached without early application of opposing rudder. Delaying rudder input to beyond 5 degrees per second yaw rate provided insufficient opposing moment for complete control but did prevent further rate increase. Limited control of the asymmetries between 45 and 50 degrees AOA was possible using aileron, rudder, and asymmetry reversal to control yaw rates. Control was not as consistent as with the 45 degree AOA case. Figures B52 through B54 present time history examples of the control of the asymmetry between 40 and 50 degrees AOA.

The asymmetry was well established in the nose-left direction above 50 degrees AOA. Full rudder or full aileron were insufficient to prevent left yaw rates

X-29 USAF S/N 820049
1 G ACC TRIM   FLIGHT CG
MIL POWER   ALT=25K TO 38K ft
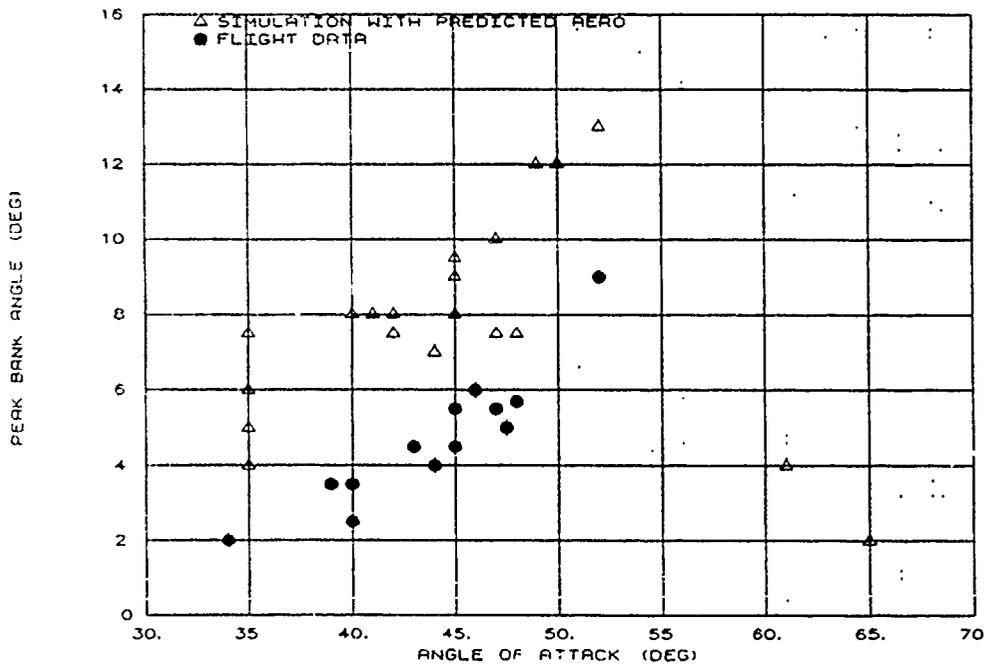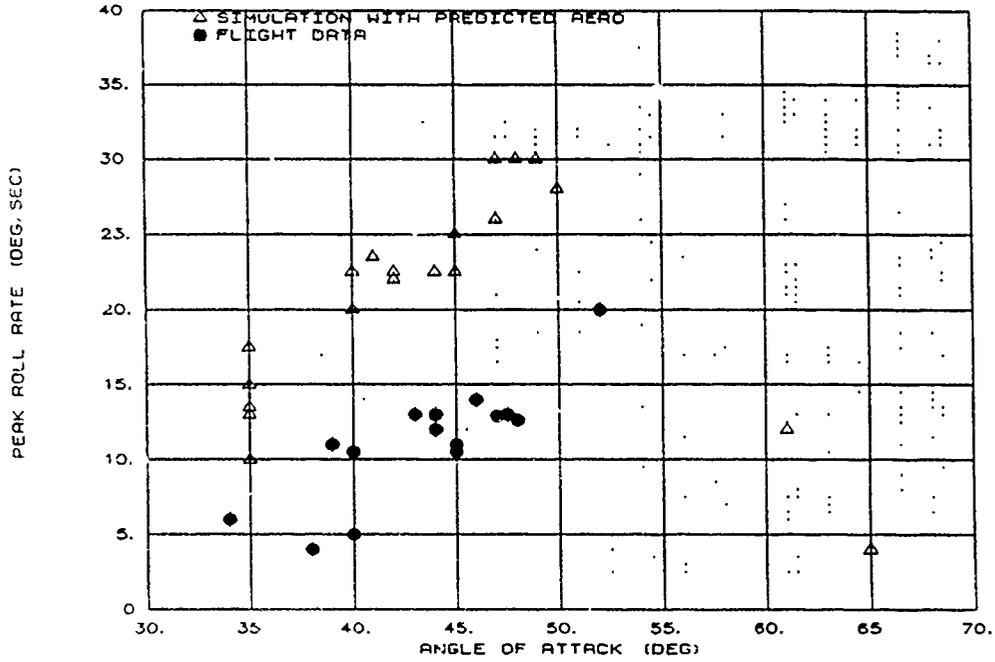
Figure 25 Flight and Predicted Wing Rock Characteristics
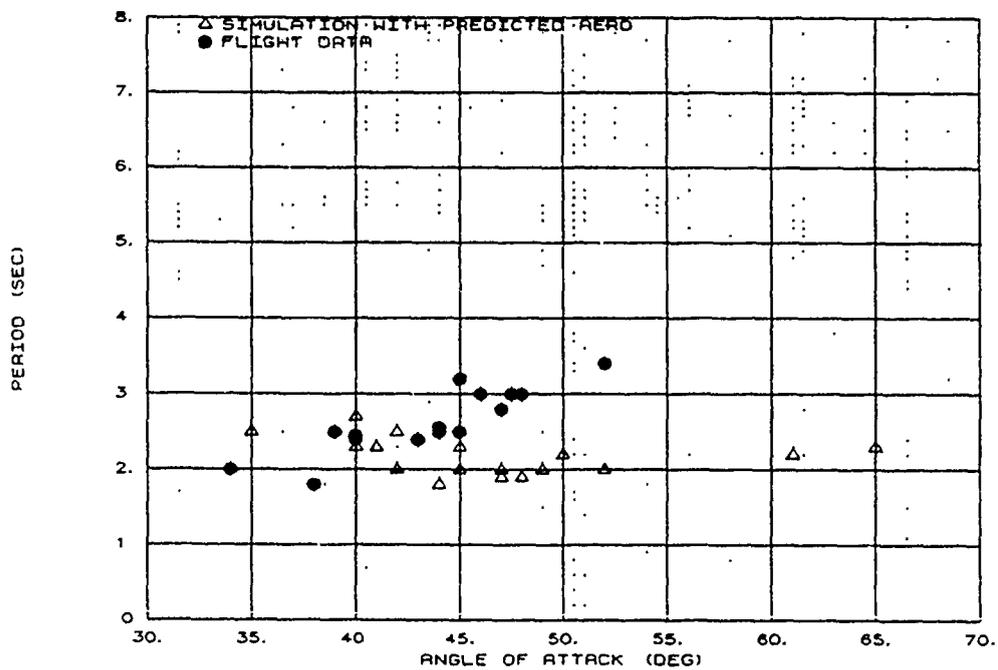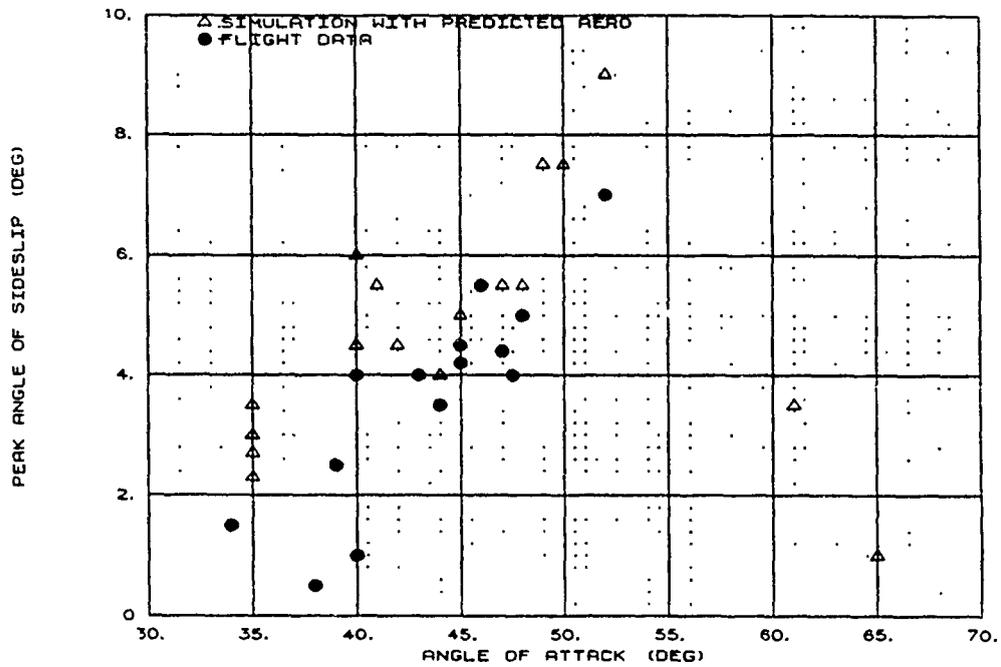
Figure 25 Flight and Predicted Wing Rock Characteristics (Continued)
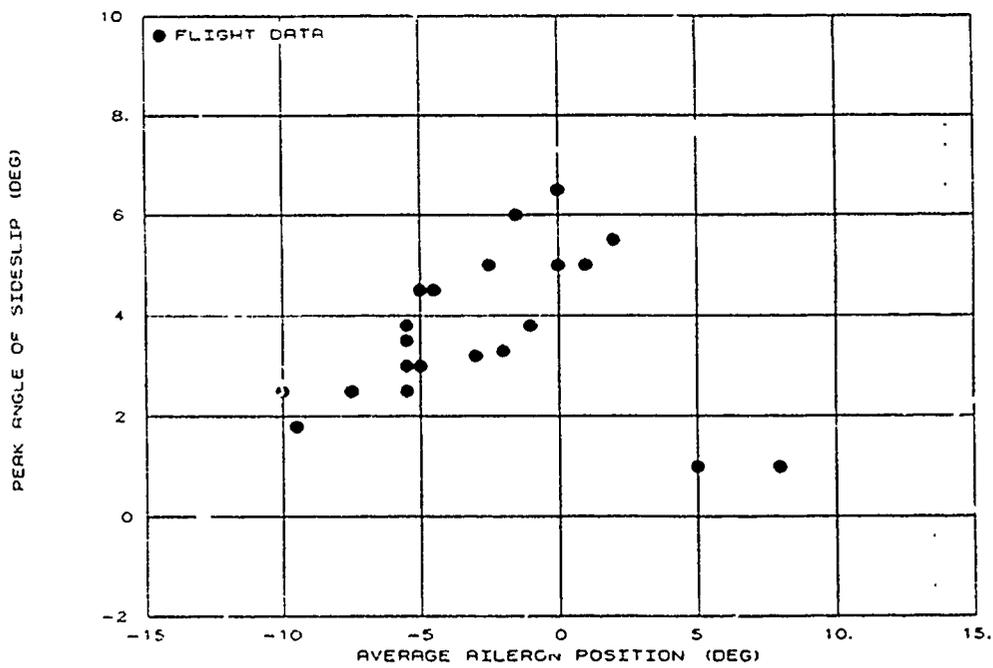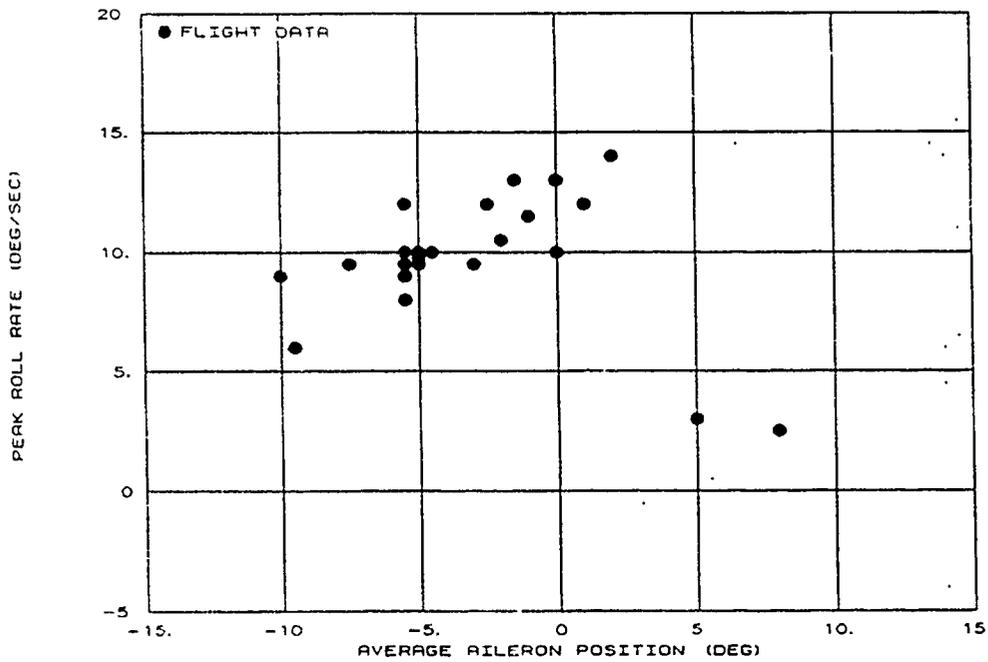
Figure 25 Flight and Predicted Wing Rock Characteristics (Continued)
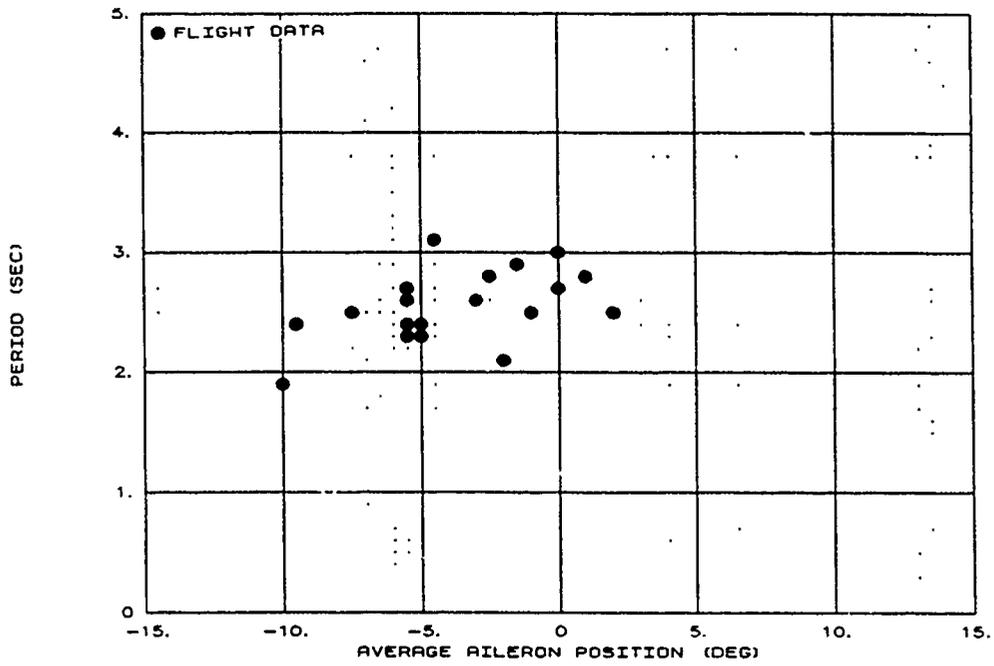
Figure 25 Flight and Predicted Wing Rock Characteristics (Concluded)

from developing Combined yaw rates and sideslip-induced roll rates of 25 to 30 degrees per second were routinely encountered. Recoveries to AOA below 40 degrees were initiated at 15 degrees per second yaw rate Rates continued to increase or hold constant until significantly below 40 degrees AOA. Peak yaw rates were sensitive to recovery technique. Full right rudder opposing the yaw rate above 50 degrees AOA did little to stop the onset due to lack of rudder power, however, holding full right rudder until lower AOA enhanced recovery as rudder power was regained Pilot pitch inputs could also affect the speed and ease of recovery. Rapid stick neutralization or inputs forward of neutral could produce sufficient nosedown pitch rates to inertially couple to the yaw axis and momentarily increase yaw rate and sideslip. Slow neutralization of longitudinal control, combined with holding full right rudder until AOA, yaw rate, and sideslip were reduced, was the most effective recovery technique.

Summary:

The lateral-directional maneuvering envelope was cleared for full separate lateral stick or rudder pedal inputs below 45 degrees AOA. Combined lateral stick and rudder pedal inputs to test aggravated input departure susceptibility were not accomplished. The envelope was not cleared for combined lateral-directional inputs.

The X-29 exhibited good lateral-directional maneuvering and stability characteristics up to 45 degrees AOA. The lateral directional maneuvering capability below 45 degrees AOA was better than predicted. The maneuvering characteristics were achieved with a simple FCS control law architecture which was appropriately gain scheduled. The addition of variable in-flight gain feature allowed the test program to take advantage of beneficial aerodynamics and to maximize the roll performance of the aircraft between 25 and 35 degrees AOA

Slow, but well coordinated, lateral stick only roll maneuvers were demonstrated to 40 degrees AOA. Mild bank-to-bank rolls were possible while holding full left rudder pedal at 45 degrees AOA. Rudder rolls provided roll rates comparable to lateral stick only maneuvers No departures were encountered during either lateral stick or rudder roll maneuvers performed below 45 degrees AOA Full rudder inputs between 30 and 35 degrees AOA required caution as mild

directional instability was encountered. The instability was c .ollable with opposite rudder. No lateral-directional maneuvering capability existed above 45 degrees AOA due to lack of rudder power and directional aerodynamic asymmetries.

Significant increases (40 to 60 percent with TW47 and 80 to 100 percent with TW53 at 25 degrees AOA) in stability axis roll rate between 15 and 35 degrees AOA were demonstrated with the variable gain feature. The TW47 increase in lateral command and ARI gains was considered the best combination tested, providing increased roll rate with minimal degradation of coordination. Beneficial aerodynamic changes from predictions below 45 degrees AOA allowed the FCS m lification to achieve significant performance increases.

Mild wing rock was encountered between 37 and 55 degrees AOA. Predicted degradation of lateral-directional maneuvering above 30 degrees AOA due to large amplitude wing rock did not occur. Wing rock was present but of sufficiently small amplitude to be considered little more than an annoyance. Wing rock quickly damped with small sideslip angles, large aileron inputs, or during maneuvering

Directional asymmetries were encountered above 40 degrees AOA. Asymmetries were initially nose-right between 40 and 48 degrees AOA and became nose-left above 50 degrees. Full left rudder could control asymmetries at 45 degrees AOA. Control of the asymmetries between 45 and 50 degrees AOA was marginal. Asymmetries were uncontrollable above 50 degrees AOA and resulted in combined left yaw and roll rates of 25 to 30 degrees per second. Maintaining full right rudder and slow neutralization of longitudinal stick was the most effective recovery technique

ENERGY MANEUVERABILITY AND INSTANTANEOUS TURN PERFORMANCE

Figure 26 presents specific excess energy and maximum instantaneous turn performance at 20,000 feet pressure altitude. Data were for test day conditions. Low speed turn rate and radius were comparable to current fighter aircraft. Large negative specific excess energy was present due to high drag above 25 degrees

X-29 USAF S/N 820049
GW =15500 lbs   XCG=450 in
MAX AB
TEST DAY CONDITIONS
PRESSURE ALTITUDE = 20,000 ft
STATIC TEMPERATURE = 454° R (6.5° HOT)

NOTE: DATA NOT STANDARDIZED

NOTE: DATA NOT STANDARDIZED

NOTE: DATA NOT STANDARDIZED
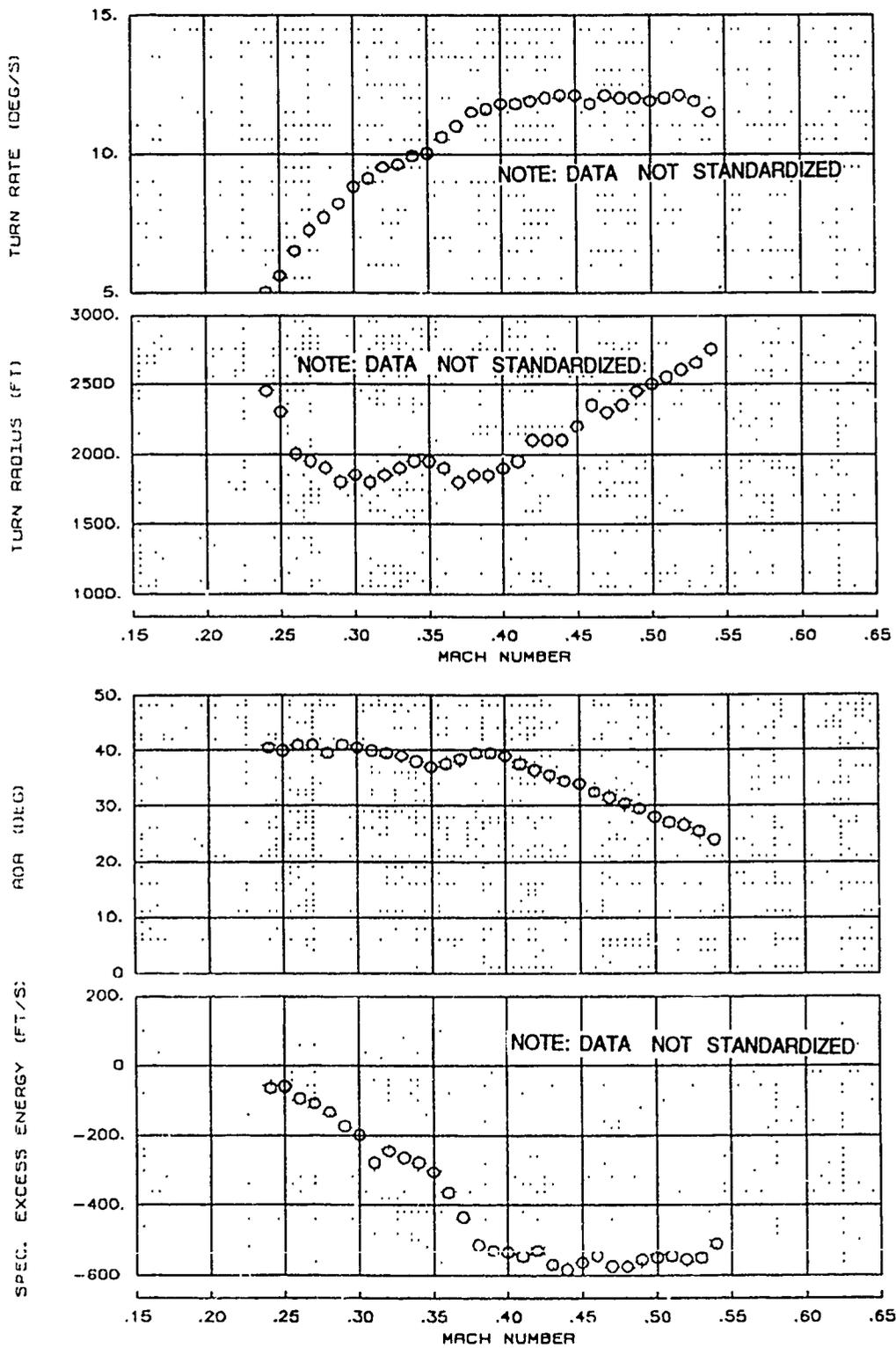
Figure 26 Instantaneous Turn Performance and Specific Excess Energy

AOA and relatively low thrust to weight (0.97 static sea level, fuel weight of 16,500 pounds).

The potential command increases mentioned in the Longitudinal Stability and Control section of this report would increase the available normal load factor below 40 degrees AOA and enhance turn rate and radius above approximately 120 KCAS. However, the enhancement would be achieved at the cost of increased negative specific excess energy due to achieving higher AOA and associated drag at a given airspeed

QUALITATIVE FLYING QUALITIES ASSESSMENT

Longitudinal:

Longitudinal control appeared positive and precise up to 67 degrees AOA. The low aerodynamic recovery capability from above 55 degrees AOA at mid cg was not evident from the cockpit. The momentary AOA hangup during the mid-cg maneuver to 55 degrees AOA was not apparent to the pilot. Recovery to low AOA from maneuvers above 50 degrees did not appear questionable from the cockpit.

Longitudinal control was good during maneuvering below 45 to 50 degrees AOA There were no natural or pilot induced oscillations noted. Light airframe buffet began at approximately 15 degrees AOA and remained nearly constant with AOA during 1-g flight An increase in buffet level was noted during accelerated maneuvering Heavy buffet was encountered when flying above 190 KCAS and 30 degrees AOA; however, at no time was the pilot able to use buffet intensity as a method to judge AOA.

Accurate AOA control was possible by using the error indicator on the ADI director bars The pilot was able to easily attain the target AOA and subsequently track within 1 degree The onset of a small lateral acceleration was an indication that AOA greater than 45 degrees had been achieved Longitudinal control was precise enough to reduce AOA when this cue was encountered Overall, the aircraft had no undesirable longitudinal flying qualities below 50 degrees AOA

Lateral-Directional:

Lateral control was available throughout the flight envelope and permitted maneuvers up to 45 degrees AOA Roll was slow but precise, with good

coordination. The aircraft was generally flown without rudder pedal inputs. Roll onset and steady rate capability were slow for the BLOCKIX-AA01 and -AA02 software releases without the command gain changes. The command gain increases (TW47 and TW53) produced significant rate and onset improvements below approximately 35 degrees AOA. The TW47 configuration was considered the best overall combination.

The rudder roll ability was good to 35 degrees AOA. Roll rates were comparable to those during lateral stick only velocity vector rolls. At 30 degrees AOA the small yaw divergence which was apparent in the data was not visible to the pilot until approximately 8 degrees sideslip. The divergence was not rapid and did not affect transient maneuvering through the 30 to 40 degree AOA region. The divergence was controllable with opposite rudder.

At 20 to 30 degrees AOA in 1-g flight, small random bank angle variations of 2 to 3 degrees occurred. The bank angle variations appeared to be a combination of the previously mentioned wing drops and small cyclic beginnings of wing rock. Damping the motion with lateral inputs was not possible. The wing drop did not interfere with overall aircraft control due to the small magnitude. The motion was not apparent during maneuvering.

Small amplitude wing rock (±4 degrees bank) was encountered at approximately 40 degrees AOA. The wing rock presented some minor problems in stabilizing AOA, but disappeared during maneuvering. The wing rock had no significant adverse impact on the lateral-directional flying qualities.

At 45 degrees AOA, a nose-right yaw motion developed which required full left rudder and approximately one-third left lateral stick to control. The onset of the motion was predictable and a good indication of AOA. By 50 degrees AOA the motion reversed and could not be controlled, which resulted in a slow nose-left yaw as the AOA was increased above 50 degrees.

Lateral-directional control degraded gracefully with AOA. No sudden loss of control was encountered. Aircraft control and maneuverability degradation with AOA was predictable and repeatable. Overall, the aircraft had no undesirable lateral-directional flying qualities up to 45 to 50 degrees AOA.

Summary:

The pilot's overall qualitative assessment of the X-29 was that it flew better in the 25 to 45 degree AOA range than any current operational fighter. The improvements included precise AOA tracking, good loaded rolling capability with the FCS command gain increases, and gradual degradation of aircraft control as AOA increased. These characteristics made the X-29 a natural aircraft to fly up to 45 degrees AOA.

MILITARY UTILITY

Background:

The military utility evaluation for the X-29 consisted of:

1. Agility metric maneuvers

2. Tracking from a perch setup

3. Basic fighter maneuvers (BFM)

The majority of the military utility flights were dedicated to agility metric maneuvers. Six flights were devoted to agility metrics. Limited agility metric data were gathered for 200 KCAS entries at 20,000 feet pressure altitude. The results of the evaluation are reported separately in Reference 1.

An initial attempt was made to define a set of offensive and defensive high AOA tracking maneuvers which would provide qualitative military utility evaluations of the X-29. Portions of five flights with the airspeed limited BLOCKIX-AA01 software release were dedicated to tracking exercise experiments. The software was limited to 200 KCAS above 10 degrees AOA and 25,000 feet pressure altitude.

The extended airspeed and altitude envelope of the BLOCKIX AA02 software release allowed revisiting the piloted evaluation issue. Project pilots defined BFM evaluations to be performed against an F-18. Portions of three flights were flown with the baseline BLOCKIX-AA02 software and one flight with the lateral command gain increases.

Maneuvering Limitations:

The X-29 was limited to 6.5 g equivalent load factor below 20 degrees AOA and 5.0 g equivalent load factor above 20 degrees AOA. Equivalent load factor was defined as actual load factor for a 15,000 pound aircraft, which was the original midfuel design weight. The X-29 USAF S/N 820049 weighed 16,500 pounds at midfuel weight. Equivalent load factor was reached at lower actual load factor for aircraft weights above 15,000 pounds. The FCS longitudinal command system was capable of exceeding the equivalent load factor limits above approximately 250 KCAS. Limits were maintained by pilot control as opposed to automatic FCS limiting.

Envelope expansion results produced BFM limitations of 40 degrees AOA and 10 degrees sideslip. Stricter maneuvering limitations were set for BFM to allow sufficient safety margin for overshoots while maneuvering "head out of the cockpit". Airspeed limitations were 300 KCAS or 0.75 Mach number above 10 degrees AOA. Maneuvers were limited to aileron or rudder only inputs since combined inputs were not cleared during envelope expansion.

Tail fin fatigue life considerations did not play a role in the envelope limitations except in defining maneuver buildup requirements. Some maneuvers which used large amounts of tail fatigue life were not attempted.

Tracking From A Perch Setup.

During high AOA tracking, the X-29 pilot often had difficulty determining overtake on the target. The visual cues for angular overtake normally used at low AOA were not sufficient at high AOA. Specifically, the larger angular difference between the nose of the aircraft and the velocity vector would cause the pilot to misjudge the aircraft flightpath relative to the target. The pilot falsely believed that the flightpath was directed towards the target, when actually it was directed behind the target. As a result, the attacker would often unnecessarily lag the target during reversals. It was not generally possible to regain nose position for a weapons deployment following the lag. The tendency to excessively lag was increased by the lack of positive target information when the target passed out of sight under the attacker's nose. Appropriate displays showing the attacker's flightpath and the target state were required to avoid the problem. The X-29 did not have such displays.

The slant range between the target and the attacking aircraft was more critical in determining the nature of the engagement than at low AOA.

Conventional tracking maneuvers (attacker behind target) needed to be initiated with less than 2,000 feet separation. At greater ranges, the target was able to generate sufficient heading changes during a high AOA turn to preclude a conventional tracking solution. However, the high AOA defensive turn by the target stopped angular movement relative to the attacker and allowed an excellent opportunity for the attacking aircraft to point and shoot. The attacker could continue to point until minimum gun range. A high AOA defensive turn was only effective if the attacker was inside 2,000 feet slant range.

The tracking exercises provided useful lessons learned and limited qualitative information on the military utility of the X-29 at high AOA. The low airspeed for entry (200 KCAS or less) and lack of appropriate displays limited the utility of the maneuvers.

Neutral BFM Maneuvering

The BFM to an initial firing solution against an F-18 showed promise for piloted evaluations of both the envelope and the X-29 within the envelope. Three partial flights with the basic BLOCK IX-AA02 command gains and one flight with the thumbwheel increases were performed. Limited military utility data were obtained with the BFM maneuvers.

Although little time was available for evaluation, initial comments indicated that the roll performance available with the increased lateral command gains could prove a significant advantage at high AOA. The X-29 was able to perform a loaded roll at a sufficiently high rate to obtain improved angular position on the F-18 which had to unload to roll. The X-29 was able to continue to roll and turn as the F-18 had to reduce AOA and turn capability to change the plane of the maneuver.

Summary:

Limited military utility tests were accomplished using tracking exercises from a perch setup and neutral BFM engagements. Both evaluations used an F-18 adversary aircraft. Results indicated the need for cockpit displays tailored for high AOA which would provide both attacking and target aircraft information. Displays should include the attacking aircraft flight path relative to the target as well as accurate target range and closure rate information.

Flight control system in-flight gain changes provided an initial look at an increased roll rate capability which showed promise for further evaluation, however, the program was ended before a full evaluation was accomplished. The military utility tests accomplished indicated that the maneuvers performed should provide a starting point for future high AOA military utility evaluations.

OTHER FLIGHT TEST CONSIDERATIONS

Spin Chute:

The second X-29, USAF S/N 820049, was equipped with a mortar deployed, 19-foot diameter, ribbon type spin recovery parachute. Spin chute jettison was accomplished with a mechanical primary and a pyrotechnic backup system. The chute was sized for fully developed spin recoveries in the NASA Langley Research Center vertical spin tunnel. Appendix A contains a detailed description of the chute and operating mechanisms.

Three test deployments, following extensive contractor ground tests, were accomplished. A high speed taxi deployment and jettison were performed at 90 KEAS. Two in-flight deployments and jettisons at 180 and 120 KEAS were performed. No emergency jettison system deployment tests were conducted by the test team due to potential hardware damage from using the pyrotechnic jettison system. The contractor performed extensive ground tests of the emergency jettison system prior to aircraft delivery.

The taxi test provided data for engine plume effects on the chute loads during deployment. Chute loads during the taxi deployment were twice the anticipated aerodynamic loads. The test was performed at military power and the additional load was attributed to engine plume effects on the chute.

The first in flight deployment was at 180 KEAS, 20,000 feet pressure altitude. The jettison at 10 degrees AOA produced an unanticipated nosedown transient to -1 degree AOA. Jettison at 10 degrees AOA was performed to minimize transients, assuming the chute was aligned with the velocity vector. The jettison was performed at military power. Postflight analysis indicated that the chute was captured by the engine plume, which realigned the risers away from the velocity vector in a direction to produce a significant

noseup pitching moment. The transient upon jettison was due to the sudden release of the large chute induced moment. The magnitude of the moment was larger than anticipated due to the entrapment in the exhaust plume.

The second deployment and jettison were performed at 120 KEAS and 20,000 feet pressure altitude. The jettison was performed with flight idle power at 10 degrees AOA. Flight idle power was used to avoid chute entrapment in the exhaust plume and subsequent jettison transients. The jettison was successfully completed without any major pitch transients. Jettison procedures were modified to release in-flight idle power only.

Engine Operation:

The X-29 F404-GE-400 (F404)[1] engine demonstrated excellent performance during the program. Initial expansion was performed at military power with fixed throttle to avoid engine stall or stagnation. Military power did not provide the maximum stall margin but was required to provide maximum hydraulic flow rates. High flow rates were desired to maintain surface actuator rate capability in case of departure.

Throttle transients and afterburner (AB) use were cleared throughout the AOA and sideslip envelope after the initial AOA expansion. Afterburner clearance was conducted with throttle cancellations to military and flight idle power to 45 degrees AOA. Full dry power throttle transients were performed to similar conditions. No engine stalls or safety of flight anomalies were encountered during the test program.

Afterburner light would not occur above 12 degrees AOA below 150 KCAS. The suspected cause was an out of tolerance afterburner flame holder. Failure of afterburner light with the F404 was not a dangerous condition since the engine control unit would shut off AB fuel flow if no light was detected.

Vertical Tail Buffet:

High levels of vertical tail buffet (120 g's acceleration) were encountered above 25 degrees AOA and 150 KCAS. The source of the buffet was attributed to the forebody or canard vortex system impinging on

the vertical tail. Buffet intensity increased with AOA and airspeed. The buffet magnitude required the initiation of a fin fatigue analysis and a corresponding fatigue tracking mechanism.

The high levels of vertical tail buffet produced a high frequency (approximately 16 hertz) feedback to the roll axis. The roll rate combined with high gains produced large aileron commands which affected the left outboard flaperon actuator hydrologic redundancy management. Initial nuisance trips of the primary system were encountered routinely above 150 KCAS and 25 degrees AOA. When a primary trip was declared, the remaining two servos were monitored with a simplified actuator model in the FCS computers. The high aileron commands generated by the tail buffet occasionally exceeded the rate limit of the simplified model and declared a secondary trip of the actuator. The actuator was still operational with the third servo. Either primary or secondary nuisance trips were reset after maneuver recovery to restore full operational and failure detection capability. All trips occurred on the left outboard flaperon actuator. Other actuators were not affected. The trips occurred with several actuator combinations installed at the left outboard station, indicating that the condition was environmentally generated.

The BLOCKIX-AA02 software contained a roll axis analog notch filter and roll rate feedback gain reductions to solve the nuisance trip problem. The simplified FCS actuator model was also modified to more accurately represent the true rate capability. The initial model contained a low rate limit which was not representative of the actual limit. Only one primary trip at approximately 160 KCAS was encountered after the modifications. No secondary trips were experienced.

Air Data System:

The X-29 was equipped with a National Advisory Committee for Aeronautics (NACA) noseboom and two side fuselage-mounted pitot probes. Consideration of the potential for pitot stall at high AOA was given in the design of the FCS control laws. The FCS gains did not vary below 100 KCAS. The noseboom was anticipated to provide the least stall susceptibility. All FCS airspeed data were taken from the noseboom

[1] The X-29 F404-GE-400 engine will be referred to as F404 throughout this report.

source above 15 degrees AOA for the BLOCKIX-AA and AA01 software releases.

Figure 27 presents a comparison of the noseboom and inertial navigation system (INS) computed incompressible dynamic pressure. The noseboom pitot stall began at approximately 30 to 40 degrees AOA and was completely stalled by 50 degrees AOA. The side mounted fuselage probes followed similar patterns with initial stall beginning at approximately 30 degrees AOA. The BLOCKIX-AA02 software raised the AOA for sole use of the noseboom in the FCS to 40 degrees AOA. The differences between the side probes and the noseboom were insufficient to result in nuisance air data redundancy management trips.

The stall of the pitot probes also affected postflight data analysis. Accurate dynamic pressure was required to determine aerodynamic characteristics. The INS computed dynamic pressure (Appendix E) was used for postflight data processing above 30 degrees AOA.

The noseboom sideslip vane encountered an instability at approximately 65 degrees AOA. The instability can be seen in Figure B16. The INS sideslip was more accurate for this region.

LESSONS LEARNED

Flight Test Related:

The spin chute was trapped in the exhaust plume during in-flight jettisons in military power. The entrapment realigned the parachute risers and produced a significant unanticipated nosedown transient on jettison. Jettisons in flight idle power did not entrap the chute and jettisons were essentially transient free at 10 degrees AOA.

Pitot tube stall began at moderate AOA, 30 to 35 degrees, and developed into a full stall by 50 degrees. Valid dynamic pressure and airspeed are required for derivation of aerodynamic coefficients. Errors in dynamic pressure can result in significant flight derived aerodynamic coefficient errors. The INS was used to derive both true airspeed and dynamic pressure for use when the pitot tube began to stall. The INS gave more consistent and believable airspeed results above 30 to 35 degrees AOA

Sideslip vane instabilities were encountered at approximately 65 degrees AOA. The instabilities produced large errors in vane measured sideslip.

Real-time and batch simulation for pilot and engineer training, flight planning, and aerodynamic model updating was an invaluable tool. Extrapolation of the derived flight aerodynamics to the next test point allowed the preparation of expected and worst case scenarios and pertinent critical parameters prior to flying a new test point.

Simulation was used as another engineering tool and should not be considered an answer in and of itself. Simulation results can give valuable as well as erroneous information. The simulation results must be integrated with other test results and used as part of the decision making process.

Variable gain capability with the FCS allowed the rapid evaluation of various gain combinations with a single software release. The capability reduced the required test and evaluation time for gain changes. A significant increase in roll performance without resorting to another software release was realized with the variable gain feature

Aerodynamic Modeling Related:

Nonlinear and complicated aerodynamic models can be updated from flight test results in a timely manner. The X-29 flew two expansion flights per week on a single fly day. The simulation was usually updated with the best available results prior to the next fly day the following week. The ability to rapidly update a simulation model relied heavily on flight data turnaround. The X-29 usually had postflight second generation data within 24 hours after the flight.

Nonlinear aerodynamic flight test data required more effort than linear estimation. Developing a nonlinear flight update procedure required an intimate knowledge of the nonlinear nature of the predicted aerodynamic model. Simply analyzing local stability and control derivatives was insufficient. A knowledge of predicted nonlinear trends was required in order to establish extrapolations of localized results across a broader range of flight conditions.

64

X-29 USAF S/N 820049
1 G PULLUP TO 67 DEG AOA   XCG=445 in
MIL POWER   ALT=32K ft
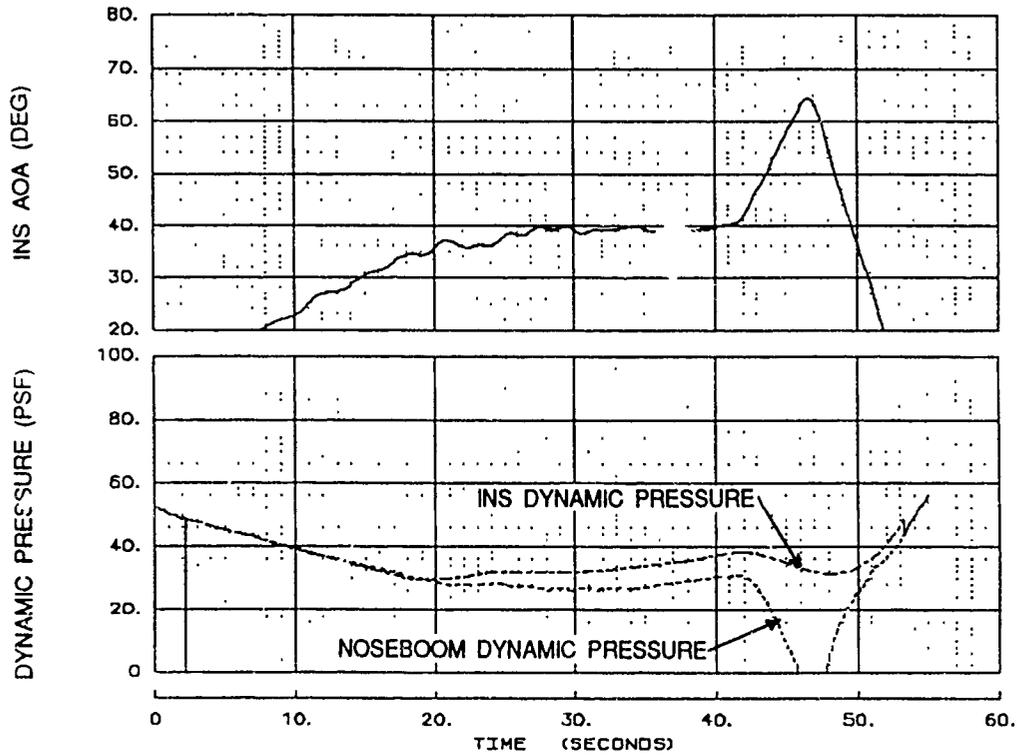
Figure 27 Noseboom Pitot Tube Stall

Updating a nonlinear data base with pure linear flight test results should not be attempted across large variations from trim. Applying pure linear modifications to a nonlinear model can unreasonably distort results. Updates should be made in a piece-wise linear fashion and forced to follow predicted trends where flight data are not available.

The best results for the initial flight derivative estimations were obtained by developing appropriate maneuvers. Adding high frequency control raps to the classic doublets proved an excellent maneuver for estimating stability and control derivatives. The raps added information which simplified sorting out potential tradeoffs between stability and control parameters. Varying the magnitude of the raps aided in identifying control power nonlinearities. Using larger amplitude maneuvers (sideslips, rudder rolls, aileron rolls, etc.) provided information for aerodynamics beyond the linear estimation range. Another useful tool was computing total flight aerodynamic force and moment coefficients for comparison with predicted results. Predicted aerodynamics were easily generated from the simulation aerodynamic model driven with flight test measured inputs. A direct comparison of the total flight and predicted coefficients could be made and large differences readily identified.

A large update matrix with appropriate independent variable break points was required. Even with the large size of the matrix developed for the X-29, modeling could have improved with additional break points. The number of break points required was a function of the degree of nonlinearity for the updated variable. Numerous modifications to the breakpoints were made during the course of the program. Early identification of predicted regions of high aerodynamic nonlinearity helped establish the initial set of break points, however, time would have been saved by including more points than were initially thought necessary.

Flight Control System Related:

Good high AOA stability, control, and maneuvering capability was demonstrated with simple control law architecture combined with appropriate gain scheduling. A knowledge of high AOA flight mechanics and classical control law design were used

with extensive 6 degree of freedom (DOF) simulation for the control law design. Initial gains were established and then appropriately tuned with the simulator. Extensive linear analysis was not used as the high AOA region was highly nonlinear. Modern or optimal control theory was not applied nor required. The structure of the control laws were dictated by flight mechanics requirements and not by restrictions imposed by questionable linearization.

Series gains with common independent variables should be collapsed to a single gain. Assumptions of linear variations of the gains when multiplied together are valid only at common break points. Multiplication of gains at conditions in between break points will not give anticipated results. Assumed linear variations will, in fact, be a polynomial variation. The order of the polynomial will be the number of series gains multiplied together. Variations from the linear assumption can be large and have significant impact on desired characteristics.

A parallel washed-out ARI circuit was useful in the X-29 for improving coordination during rapid reversals as well as steady-state rolling. The wash-out circuit provided an additional rudder input to initiate, stop, or reverse a maneuver. The additional rudder command aided in overcoming the large yaw to roll inertia of the X-29. Less rudder was required to coordinated steady rolls due to propelling rotational aerodynamics. The washed-out ARI circuit also allowed the use of lower R-$\beta\alpha$ feedback gains which was desirable in lowering autoroll susceptibility.

Six DOF simulation was invaluable in the high AOA control law process. The simulation allowed rapid adjustment of initial gains and structure based on the full nonlinear nature of the aerodynamics and equations of motion. An understanding of the nonlinear relationship was felt to be essential for a successful design.

Attention must be paid in the design process to sensor performance, especially at high AOA where air data probes and vane values of flow angles can be erroneous. Sensors which operate reasonably well at low AOA may become unreliable at high AOA. This will have implications for both redundancy management logic as well as control law performance.

CONCLUSIONS

AERODYNAMICS

A nonlinear flight test based update of the simulation aerodynamic model was successful in providing characteristics closer to the actual aircraft than the original predicted model.

The ground-based predictive methods adequately determined the stability and control trends with angle of attack (AOA), but the accuracy of individual aerodynamic parameter predictions was low. The greatest difference was noted in the longitudinal axis. High AOA aerodynamic prediction methods had a higher degree of uncertainty compared to low AOA prediction capability.

STABILITY AND CONTROL

Good longitudinal stability, control, and maneuvering characteristics below 50 degrees AOA (55 degrees ahead of 446 inches center of gravity) were achieved with a simple pitch rate command flight control system. The maximum pitch rate capability was comparable to other modern fighter type aircraft. Angle-of-attack control during 3-axis maneuvering was considered good, with acceptable pilot workload.

Good lateral-directional stability, control, and maneuvering characteristics up to 45 degrees AOA were achieved with a simple flight control system architecture which was appropriately gain scheduled. The addition of a variable in-flight gain feature allowed the test program to maximize the roll performance of the aircraft between 25 and 35 degree AOA

The AOA envelope was cleared to 50 degrees for all centers of gravity and to 55 degrees for centers of gravity at or ahead of 446 inches. Clearance above 55 degrees AOA would require further testing since only one maneuver above 55 degrees was accomplished. The lateral-directional maneuvering envelope was cleared for full separate lateral stick or rudder pedal inputs below 45 degrees AOA. The envelope was not cleared for combined lateral stick and rudder pedal inputs

The proposed minimum nosedown aerodynamic pitching moment (Cm*) criteria of Reference 8 was not conservative for the X-29 in the presence of noseup inertial coupling. Marginal recovery was encountered above 50 degrees AOA, which had a more nosedown recovery pitching moment than the Cm* value taken at 65 degrees AOA.

Future programs designed to provide the X-29 with lateral-directional maneuvering above 45 degrees AOA will have to address the low longitudinal recovery capability. Stability axis roll rates above 20 degrees per second across the center of gravity range will not be possible above 50 degrees AOA without providing increased nosedown pitching moment capability.

FLYING QUALITIES

The pilot's overall qualitative assessment of the X-29 indicated that it flew better in the 25 to 45 degree AOA range than current operational fighters. The improvements included precise AOA tracking, loaded rolling capability to 45 degrees AOA, and gradual degradation of aircraft control as AOA increased. These characteristics made the X-29 a natural aircraft to fly up to 45 degrees AOA.

MILITARY UTILITY

Results from the military utility maneuvers indicated the need for cockpit displays at high AOA which would provide the attacking aircraft flightpath relative to the target, as well as accurate target range and closure rate.

Flight control system in-flight gain changes provided an initial look at an increased roll rate capability which showed promise, however, the program was ended before a full evaluation was accomplished. Limited military utility tests were accomplished with the increased roll rate capability. The military utility tests accomplished indicated that the maneuvers performed should provide a starting point for future high AOA military utility evaluations.

USAF

REFERENCES

1 Butts, Stuart L., Captain, USAF, *X-29A High Angle-of-Attack Agility Flight Test Results*, AFFTC-TIM-91-02, AFFTC, Edwards AFB, CA, May 1991.

2. Butts. Stuart L., First Lieutenant., USAF, *Flying Qualities Evaluation of the X- 29A Research Aircraft*, AFFTC-TR-89-08. AFFTC, Edwards AFB, CA, May 1989.

3. *Computer Control Law Specification, X-29 Internal Document*, X-29-003 REV C, NASA ADFRF, Edwards AFB, CA, September 1989.

4. Moore, M., GAC Memo: *Notes on Spin Chute System Review with Ray Whipple on January 20, 1987*, GAC Engineering Memo No. 712/ENG-M-87-038, May 1987.

5. Fears, S.C., *Investigation of the Tumbling Phenomen Using Computer Simulation*. Masters Thesis, George Washington University, September 1985.

6. Krummenacker, J. and Pellicano, P., *Evolution of the X-29 Aerodynamic Math Model (AERO9B)*, Grumman Aircraft Systems, Edwards AFB, CA, May 1991.

7. Murray, James E. and Maine, Richard E., *pEst Version 2.1 Users Manual*, NASA TM 88280, NASA ADFRF, Edwards AFB, CA. September 1987.

8 Nguyen, L.T. and Foster, J.V., *Development of a Preliminary High Angle-of-Attack Nose-Down Pitch Control Requirement for High-Performance Aircraft*. NASA Tech Memorandum 1012684, NASA Langley Research Center, February 1990.

9. Hakabone, Thomas C., Captain. USAF, *Performance Evaluation of the X- 29A Research Aircraft*, AFFTC-TR-87-51, AFFTC, Edwards AFB, CA, March 1988.

10 Tippy, D. Kurt, *The INS Wind Calibration In Climb Algorithm*, SFTE 16th Annual Symposium, August 1985.

11 Rajczewski, David, Captain, USAF, *X-29A High AOA Flight Test Air Data Comparisons of an INS and Noseboom Probe*, SFTE 21st Annual Symposium, 10 August 1990.

12. Pellicano, P., et el, *X-29 High Angle-of-Attack Flight Test Procedures. Results and Lessons Learned*. SFTE 21st Annual Symposium, August 1990

70
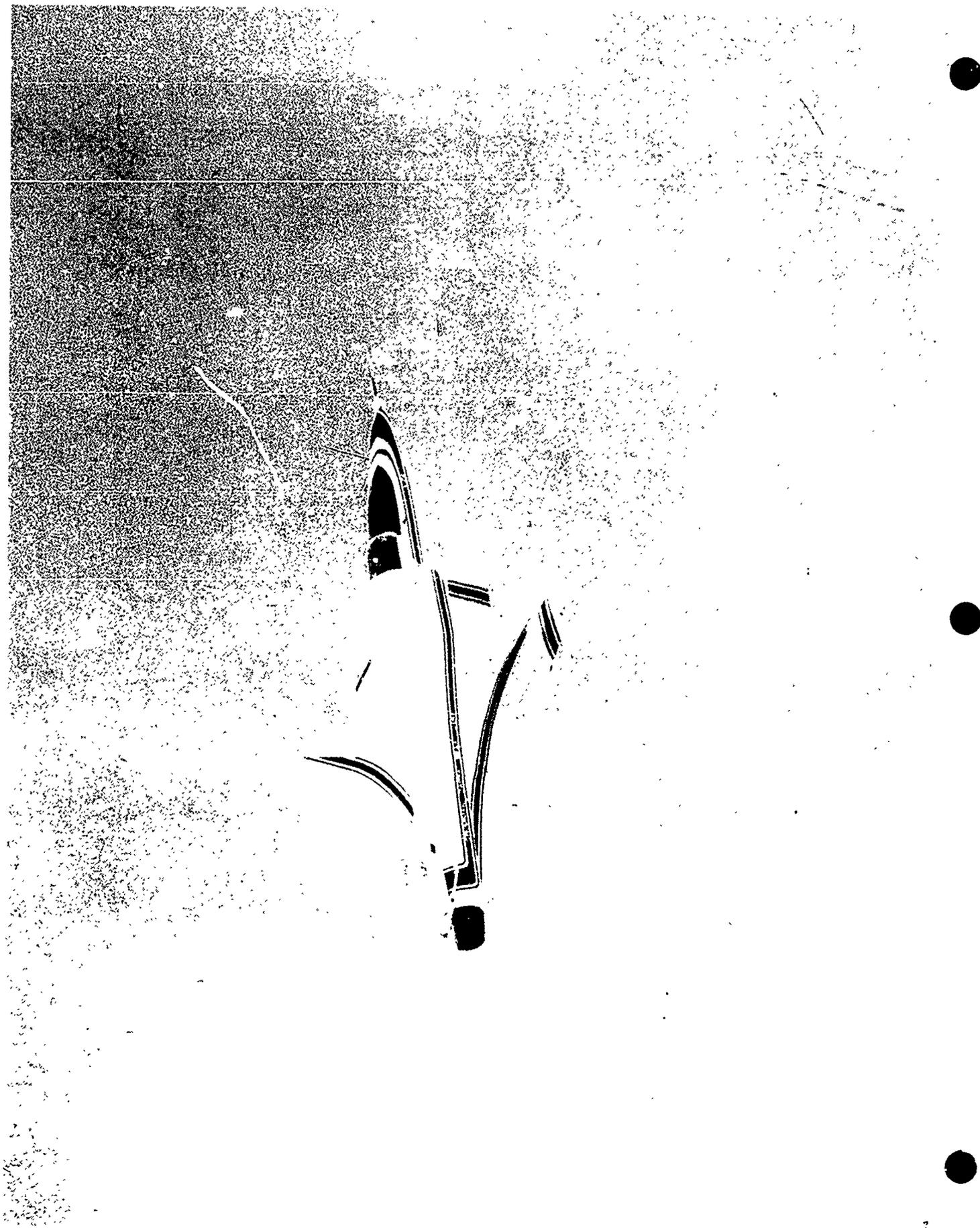
APPENDIX A
AIRCRAFT DESCRIPTION

This page intentionally left blank.

AIRCRAFT DESCRIPTION

GENERAL

To reduce technical risks and investment costs, the design of the X-29 used flight-proven, "off-the-shelf" equipment wherever possible. The aircraft used a modified F-5A forebody and cockpit; main landing gear, an emergency power unit, jet fuel starter, and actuators from a USAF F-16; and U.S. Navy F-14 rate gyros. A flight-proven General Electric F404-GE-400 engine with afterburner provided approximately 16,000 pounds of thrust at sea level.

The second X-29, USAF S/N 820049, was identical to the first X-29, USAF S/N 820003, except for modifications incorporated to permit safe operation in the high angle-of-attack (AOA) flight envelope. The following changes were implemented:

1. Two additional noseboom angle-of-attack vanes were added aft the existing vane for air data redundancy.

2. A spin-recovery parachute system (spin chute) was installed.

3. A Litton LN-39 inertial navigation system was installed for reliable angle of attack, sideslip, and air data at high AOA.

4. Two modifications were made to the environmental control system to increase operating efficiency during high angle-of-attack flight; an external exhaust scoop was installed at the primary/secondary heat exchanger ram outlet to maintain proper pressure differential; and the precooler ejectors were modified to permit operation in flight and maintain a favorable bleed air flow.

5. The emergency power unit circuitry was revised to permit operation in the bleed air mode. The modification was incorporated to decrease startup time at high altitude flight conditions.

6. The wing surface pressure ports and wing deflection instrumentation were not installed on the second X-29.

7 Additional cockpit instrumentation was installed to decrease pilot workload including:

a. Large AOA and yaw rate indicators in the center of the main instrument panel.

b. A single-needle gross-scale altimeter to complement the primary altimeter.

c. Spin recovery lights to indicate proper rudder pedal and lateral stick directions in the event of pilot disorientation during a spin.

d. The attitude director indicator (ADI) was modified so that its needles could be controlled from the ground via the remote augmented vehicle (RAV) facility. The needles were modulated to aid the pilot in holding conditions and performing maneuvers.

A more comprehensive description of the design and ground testing of these modifications is contained in Grumman Report No. 712/CDM-M90-001, Final Report: *X-29A-2 High Alpha Modification Design And Analysis.*

SPIN CHUTE

A spin recovery parachute system was installed on the X-29 USAF S/N 820049. The system was intended for use in the event of an inadvertent, uncontrollable spin. Many of the X-29 spin chute system components were similar to those on spin chute systems used on other aircraft test programs. The mortar fired parachute system was part of a standardized family of parachute systems used on more than a dozen flight test aircraft. The spin chute arming mechanism was schematically identical to that used on the Grumman F-14 aircraft. Similarly, the cockpit arrangement was also based on the F-14 configuration.

The spin chute consisted of a mortar ejected spin recovery parachute, an arming and jettison linkage, a pyrotechnic emergency jettison system, a passive jettison system, a structural support truss, and an

electrical system which provided pyro initiation, cockpit indication, and in-flight system readiness test features The arrangement of the spin chute modifications on the aft portion of the aircraft is shown in Figure A1. Additional detail is shown is Figure A2. Cockpit modifications are shown in Figure A3.

Based on spin tunnel tests at NASA Langley, a 19-foot nominal diameter parachute with a 75-foot towline was selected. Drag coefficient of this parachute, based on the 19-foot laid-out-flat diameter, was 0.508. The design conditions were: a dynamic pressure of 110 psf, an equivalent airspeed of 180 knots, and a total force of 19 000 pounds The configuration is shown in Figure A4 The mortar deployed spin chute system chosen was the Mitsubishi XT-2 spin chute manufactured by Irvin Industries Inc It was modified in accordance with Grumman Specification No 712DCV025 and used on the X-29

The parachute was deployed from the aircraft via the parachute mortar assembly The primary mortar assembly components were the mortar body, the breech, two mortar deployment cartridges, the sabot, and the extended cover The arrangement of these components is shown in Figure A5

Reliability of function was the foremost design consideration To enhance reliability, the dual-port breech had two identical cartridges, each containing one-half of the total propellant, ignition of one would reliably ignite the other Each cartridge contained two bridgewires, either of which would ignite it.

The spin chute electrical system was redundant and controlled the firing of the chute deploy pyros and the back-up jettison pyros There were two bridgewires in each pyro and there were two pyros in the deploy circuit and two in the jettison circuit When the pyro-arm switch located on the spin chute status panel, was in the secure position, the pyro bridgewires were shorted to ground This was to prevent electromagnetic interference (EMI) from supplying the energy to fire the initiators When the switch was placed in the arm position, the grounding was removed and the pyros were connected to the pyro-test switch, the deploy switch, and the jettison switch

When the pyro-test switch was selected, voltage was supplied through a light, a current limiting resistor, and the same circuit used for the actual firing The current in this test was limited to less than 40 milliamps In addition, all spin chute status panels

lighted when the pyro-test switch was selected. This allowed check out of the pyro circuits and the status panel lights from the cockpit.

When the chute deploy button was pressed, voltage from two independent circuit breakers was supplied through four different circuits to the four bridgewires in the two deploy pyros. The chute jettison circuit operated in the same way except it was activated by the emergency jettison switch located on the throttle quadrant. Normal jettison and emergency jettison functions are illustrated in Figure A6.

EMERGENCY POWER UNIT

The emergency power unit (EPU) was a self-contained, stored energy system that provided for simultaneous generation of emergency hydraulic and electrical power. It was designed for the F-16 and installed in both X-29 aircraft. The EPU was used to maintain control of the aircraft in case of failure of the main electrical system generator, failure of the main hydraulic system pumps, loss of engine power, or power takeoff (PTO) shaft failure. Power for driving the 23-gpm hydraulic pump and the 5-kw electrical generator was derived by converting monopropellant fuel (70 percent hydrazine and 30 percent water) and/or by engine bleed air The monopropellant automatically augmented the engine bleed air mode whenever the EPU output power demand exceeded the bleed air capability. The EPU would provide power for about 7 minutes using monopropellant only, and would provide power for an unlimited duration on engine bleed air.

Concern was raised that EPU start-up time, which was critical due to the high degree of longitudinal instability, would be increased by EPU oil churning induced by extreme attitudes inherent in a high AOA program To minimize this risk, EPU circuitry was modified on X-29 USAF S/N 820049. The modification allowed the EPU to run in bleed air mode during high AOA maneuvering. If a failure occurred, the monopropellant augmentation mode would be initiated immediately and no EPU spin-up time would be required.

ENVIRONMENTAL CONTROL SYSTEM

Review of the X-29 USAF S/N 820003 flight data at sustained AOA above 15 degrees showed a rise in environmental control system (ECS) turbine speed and

degraded cooling to the flight control computers. This was attributed to the lack of ram air to the two heat exchangers, degrading their capacity to cool the engine bleed air. Further impacting the ECS performance at high AOA was the EPU, which would be extracting 45 percent of the total bleed air. Studies of ECS operation indicated that modification was required to enable the ECS to operate at higher angles of attack. These changes made for the X-29 USAF S/N 820049 were:

1 Cockpit switches were incorporated to turn on the ejectors of both heat exchangers in flight to induce additional flow through the heat exchangers.

2. An exhaust fairing was installed for the primary/secondary heat exchanger ram air outlet.

3. Four additional temperature sensors were added for ECS monitoring and data analysis.

DESCRIPTION COMMON TO BOTH X-29 USAF S/Ns 820049 AND 82003

Figure A7 presents a schematic drawing of the X-29 research aircraft. Further aircraft information is presented in Table A1. A detailed description of the X-29 flight control system is contain ! in Appendix D. Figure A8 presents the X-29 sign convention.

The X-29 fuselage structure consisted of a modified F-5A forward section which included the avionics compartment, cockpit, and nose landing gear doors. New aspects of the structure included the canards, the forward engine inlet duct section, the mid and aft fuselage sections, the main landing gear doors, the fuselage strakes, the vertical tail, and the forward swept wing. Sufficient fuselage strength was provided to permit the addition of a spin chute. The wing structural box had hard points for attaching two external stores pylons under each wing and a sidewinder missile launcher adapter at each wing tip. External stores were not carried during any flight testing.

The F-5A forward fuselage had several structural modifications to adapt it fc · use on the X-29. The nose cap v as replaced with one incorporating nose strakes and a flight test noseboom. Forward engine inlet duct supports were also added. The side panels were modified for the inlet diverter ramps. The cockpit floor was modified to accommodate new control devices.

The forward duct section consisted of conventional aluminum alloy skin, frame, and longeron. Key elements were the duct lip and splitter, the canard support and actuator access, fuselage side mounting points, diverter inlet ducts, and diverter support struts and attachments.

Each of the canards was a one piece assembly that included formed aluminum alloy covers and ribs, machined aluminum alloy leading and trailing edges, and a machined titanium torque shaft/spar. The canards were the primary pitch control surfaces and were driven by two F-16A flaperon integrated servo actuators (ISAs).

The forward swept wing consisted of a continuous, tip-to-tip, 26-foot span main box structure. The wing featured a primary box comprised of aeroelastically tailored graphite-epoxy composite covers which were bolted to a titanium front spar and five aluminum intermediate and aft spars. The wing leading edge was fixed and made of detachable aluminum segments Dual-hinged, trailing-edge flaperons provided high lift during takeoff and landing, lateral control, and variable camber to maximize the lift over drag. The tip caps, gloves, leading edges, trailing edges, and flaperons were attached to the main box structure. The main box upper and lower structure covers consisted of conventional 0/90/±45 degree, laminated assemblies made from graphite-epoxy tape. Primary graphite-epoxy tape plies outboard of wing station 64 were oriented 9 degrees forward of the wing box centerline axis to provide the required beneficial aeroelastic coupling between bending and twist deflections of the wing. Plies were arranged to provide linear stress and strain behavior and eliminate complex splicing due to ply direction changes across the aircraft centerline and at the sweep-change station (wing station 64). The main box structure supported the other wing components and transmitted applied loads to the fuselage. The main substructure consisted of 6 spars and 12 ribs.

The dual-hinged full span flaperon flap-tab system consisted of three flaps and three tab segments per side. The flaperons were actuated by four F-16A rudder ISAs at wing stations 58 and 127.

Each fuselage strake included an integral fuel tank and a hinged trailing edge flap. The strakes used a built-up construction with a formed sheet of aluminum

alloy and machined parts using conventional channel seal techniques to assure tank integrity. The strake flaps were used symmetrically as longitudinal control surfaces. These flaps were driven by two actuators designed and produced specifically for the X-29 aircraft.

The vertical tail consisted of the fin box, the leading edge and actuator support structure, the rudder, the actuator fairings, and a tip cap. The rudder was supported by hinges and by a bearing below the actuator. The rudder was driven by an F-16A rudder integrated servo actuator.

The aircraft was powered by a single F404-GE-400 turbofan engine with an afterburner which provided approximately 16,000 pounds of sea level uninstalled static thrust. Engine airflow was provided through two simple-fixed geometry inlets integrated into each side of the fuselage aft of the cockpit. The inlets had large radius edges which permitted a wide range of acceptable angles of free stream flow incidence. The exhaust nozzle was the same as used with the F404 engine on the F-18 aircraft. Engine starting and secondary power systems used the same aircraft mounted accessory drive (AMAD) unit as used on the F-16 aircraft. The AMAD unit was driven by a PTO shaft made of composite materials. In the event of a failure causing the loss of aircraft power, an F-16 EPU was installed to supply power to the aircraft.

The landing gear of the X-29 was a conventional tricycle configuration consisting of right and left pneudraulic shock strut main gear and a single-wheel pneudraulic shock strut nose gear. All major components within the landing gear system were flight qualified off-the-shelf hardware. The landing gear arrangement provided a turnover angle of 55 degrees, ensuring good ground stability for the aircraft. The main gear used the body mounted side articulating F-16A main gear assembly. The existing nose gear installed in the F-5A nose section was used without change. The nose wheel steering actuator was an integral part of this assembly. The existing F-5A steering control system was used without change. A new main gear wheel was installed that was compatible with the existing main landing gear axle and the Ply Rating tubeless tire. The brakes were operated by the conventional toe-type brake pedals from the existing F-5A nose section using transducers and electric brake valves to meter the hydraulic pressure to the brakes.

The hydraulic power supply consisted of two F-16A 3,000 psi type II hydraulic pumps supplying separate flight and combined hydraulic systems. The flight hydraulic system powered the primary flight control surfaces. The combined hydraulic system also supplied power to the primary flight control dual-tandem actuators and, in addition, supplied all utility subsystems such as the landing gear, wheel brakes, nose wheel steering, and jet fuel starter motor. All utility subsystems were isolated during "wheels-up" flight to protect the integrity of the primary flight control systems. Alternate power for emergency main landing gear extension was supplied by stored pneumatic energy. The alternate mechanical release system for the F-5A nose gear was retained without change. Accumulators provided alternate power for park and emergency wheel brakes. In the event of hydraulic system failure (pump, AMAD, gear box, gear train, PTO shaft, or engine failure), hydraulic power to the flight hydraulic system would have been provided by a 22-gallon per minute Vickers pump powered by the F-16A EPU.

The aircraft fuel system employed a number of components which were in current production. Fuel was contained in four interconnected fuselage tanks. Two tanks were light weight bladder cells and were located in the main landing gear wheel well. Two tanks were internal types located in the strakes. The bladder tanks used for engine feed were subdivided for negative g operation. An automatic internal fuel system management scheme, which employed electric boost pump transfer, engine feed, and a gravity interconnect between tanks, required no pilot attention during flight. Pressure fueling was provided through a single fueling and defueling adapter located in the main landing gear well.

The X-29 electrical system consisted of three power sources, an F-16A 40/50 kw integrated drive generator driven directly from the AMAD as the primary generating system; an emergency 5 kw alternating current (ac) generator powered by an F-16 EPU, and the batteries. The ac sources fed two buses. The main and essential direct current (dc) power was derived from the ac through two transformer rectifiers (TRs). The TRs fed the main and essential dc buses while the battery energized the battery bus. The electrical system provided a fail-safe capability through the use of the EPU generator. The battery provided an additional backup source of electrical power to the FCS in case of a dual generator failure.

The X-29 environmental control system used the F-5A air conditioning and pressurization system as it was installed in the forward fuselage section. The system was modified to accommodate the higher bleed air supply pressure and temperature available from the F404 engine and the forced air cooling required by the FCCs. The breathing oxygen system of the X-29 used the F-5A system as it was installed in the forward fuselage section.

The standard F-5A ejection seat was replaced with an F-5A qualified MKGRQ7A ejection seat.

Table A1

GENERAL X-29 NUMBER TWO INFORMATION

Wing

Reference Area	185.00 ft^2
Exposed Area	188.84 ft^2
Span	27.20 ft
Mean Aerodynamic Chord (MAC)	7.22 ft
Aspect Ratio	4.0
Leading Edge Sweep	-29.27 deg
1/4 Chord Sweep	-33.73 deg
Taper Ratio	0.40
Dihedral Angle	0.0 deg
Flaperon Area	14.32 ft^2
Flaperon Deflection	25 deg TED (+)
	10 deg TEU (-)
Strake Flap Area	5.21 ft^2
Strake Flap Deflection	30 deg TED (+)
	30 deg TEU (-)

Canard

Reference Area	37.00 ft^2
Exposed Area	35.96 ft^2
Span (1 Canard)	3.69 ft
MAC	5.46 ft
Aspect Ratio	1.47
Leading Edge Sweep	42.00 deg

78

Table A1 (CONTINUED)

GENERAL X-29 NUMBER TWO INFORMATION

1/4 Chord Sweep	23.08 deg
Taper Ratio	0.318
Deflection	30 deg TED (+)
	60 deg TEU (-)

Vertical Tail

Reference Area	33.75 ft^2
Exposed Area	32.51 ft^2
Span	6.67 ft
MAC	5.54 ft
Aspect Ratio	2.64
Leading Edge Sweep	47.00 deg
1/4 Chord Sweep	41.05 deg
Taper Ratio	0.306
Rudder Area	7.31 ft^2
Rudder Deflection	30 deg TEL (+)
	30 deg TER (-)

Engine	F404-GE-400
Inlet	
Capture Area	650 in^2
Throat Area	473.5 in^2
Fuel	JP-5

Table A1 (CONCLUDED)

GENERAL X-29 NUMBER TWO INFORMATION

Zero Fuel Weight and Balance

Gross Weight	14,583 lb
x_{cg} Fuselage Station	451.6 in (-8.9% MAC)
I_{xx}	4,541 slug - ft^2
I_{yy}	51,746 slug - ft^2
I_{zz}	56,931 slug - ft^2
I_{xz}	2,559 slug - ft^2

Fuel Tank Capacities

Feed Tank	1,830 lb
Forward Tank	1,810 lb
Strake Tank	340 lb
Total	3,980 lb

X-29 SPIN CHUTE
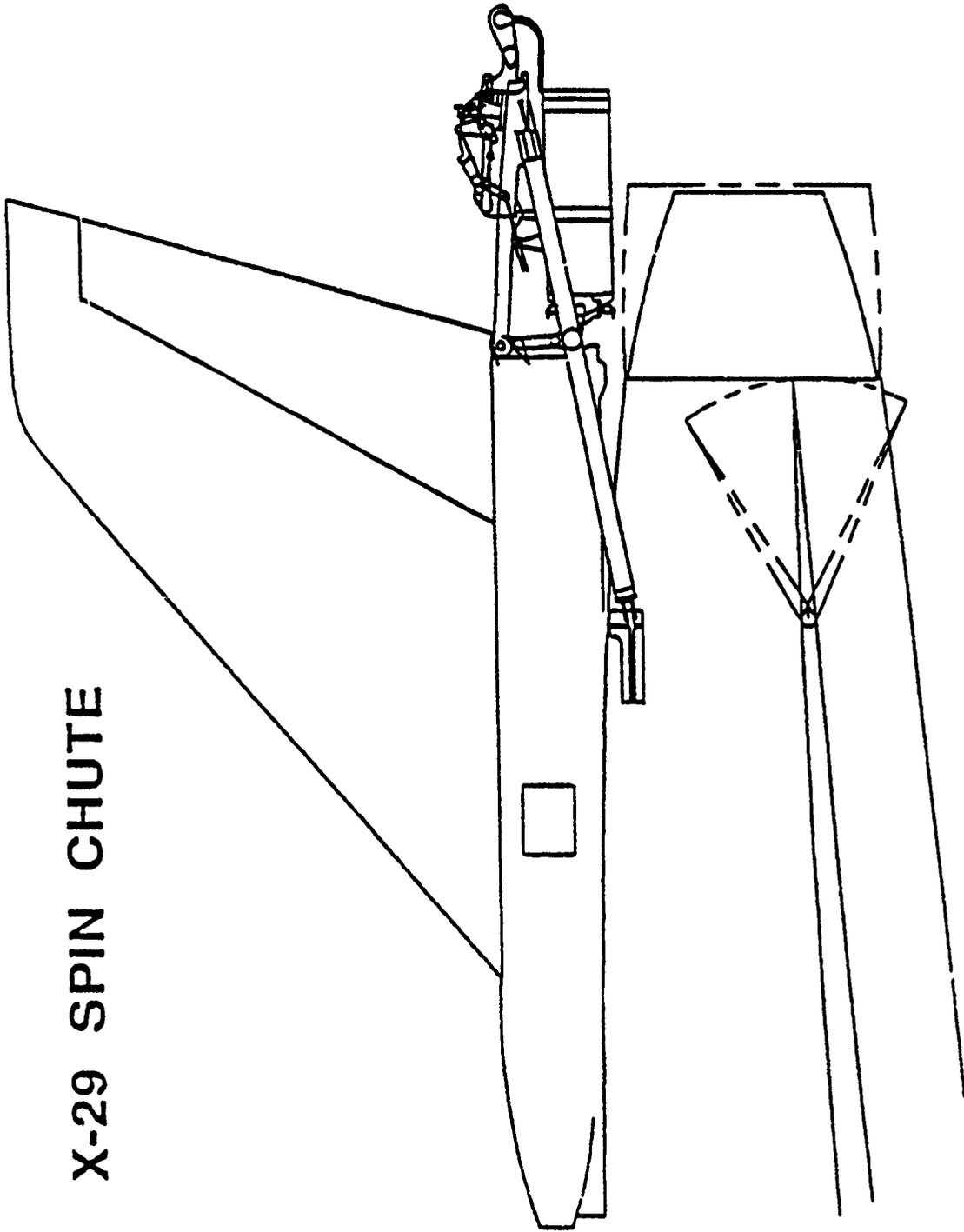
Figure A1 Spin Chute Placement

81
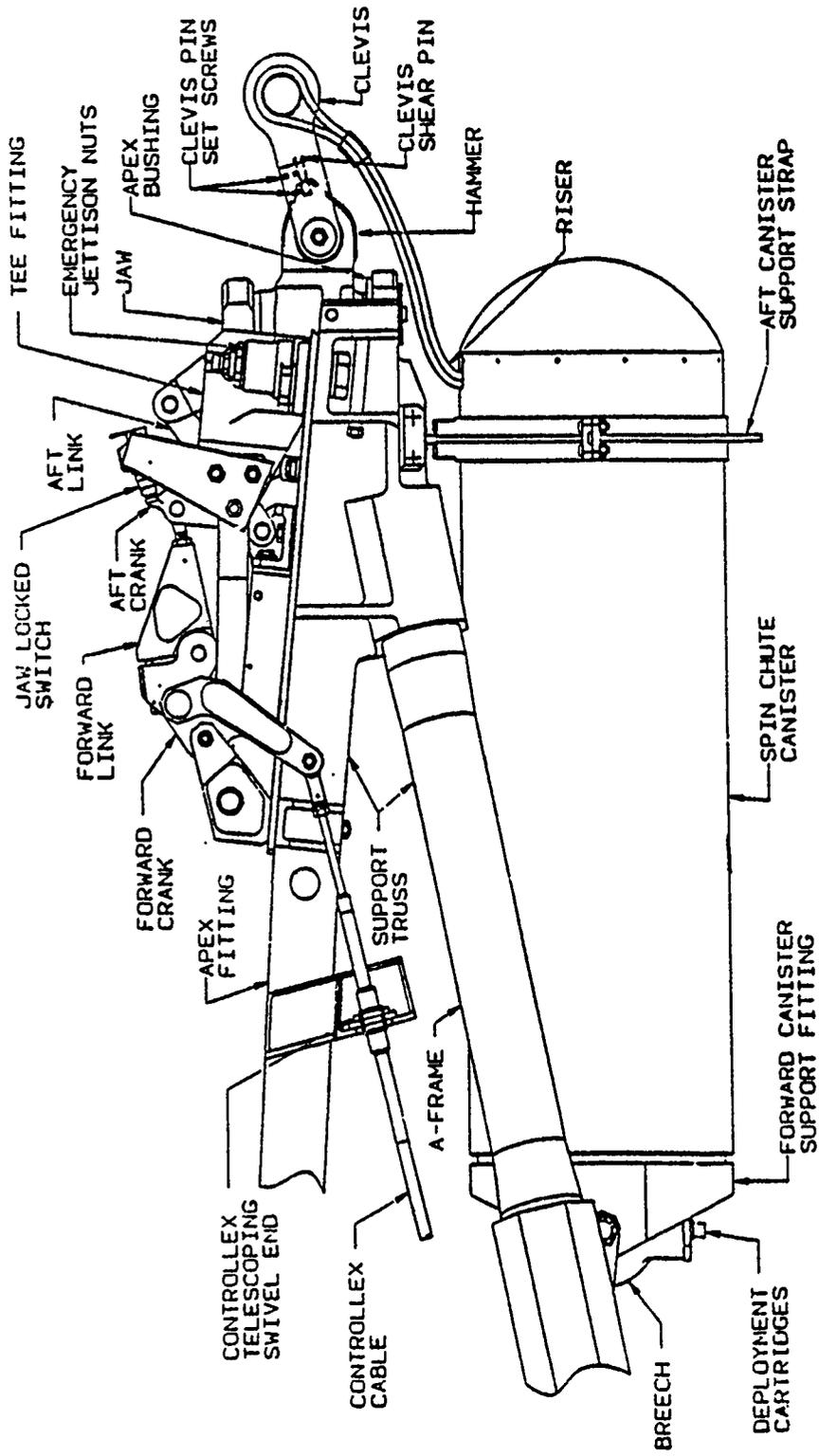
Figure A2 Spin Chute Mechanism

82

CHUTE DEPLOY CONTROL

CHUTE LOCK/
JETTISON HANDLE
(PRIMARY)

YAW
RATE

ADI

CHUTE STATUS PANEL

CHUTE JETTISON
SWITCH (SECONDARY)
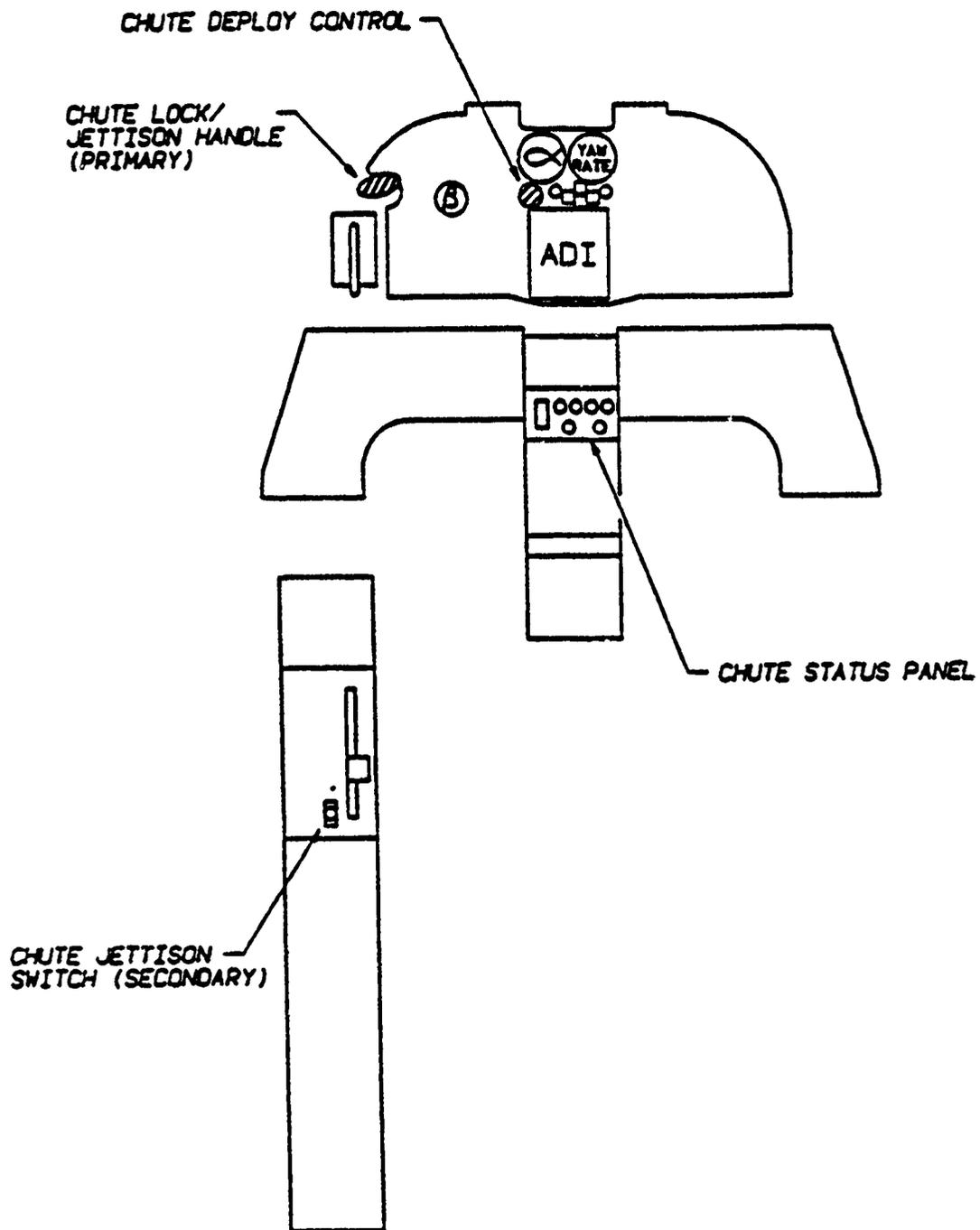
Figure A3   Cockpit Modifications
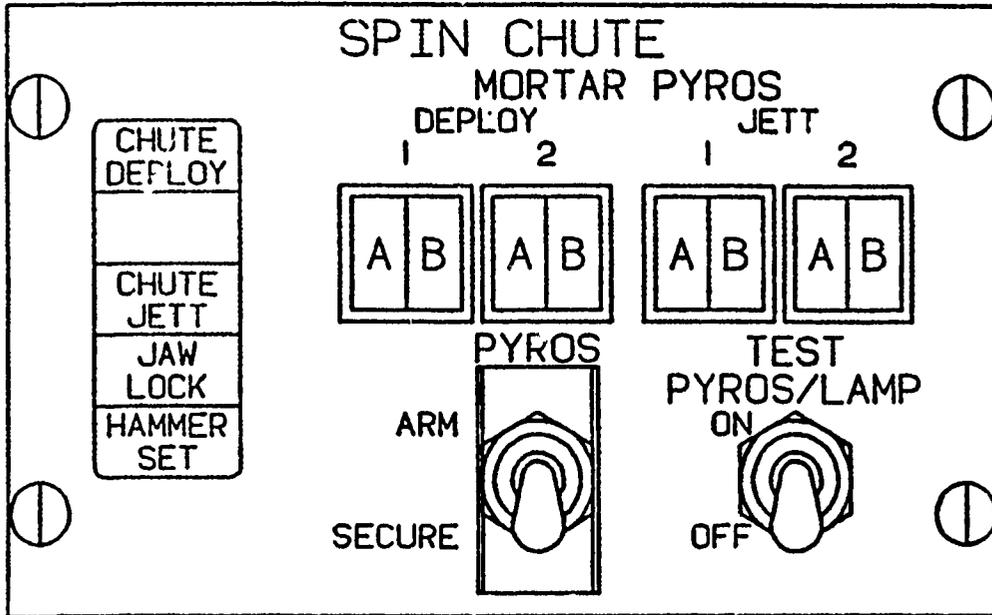
Spin Chute Status Panel

Figure A3 Cockpit Modifications   (Concluded)

CANISTER COVER

DEPLOYMENT BAG

SUSPENSION
LINES (24)

PARACHUTE
Do = 19.0 ft

75
FEET

RISER

A/C ATTACH

CANISTER
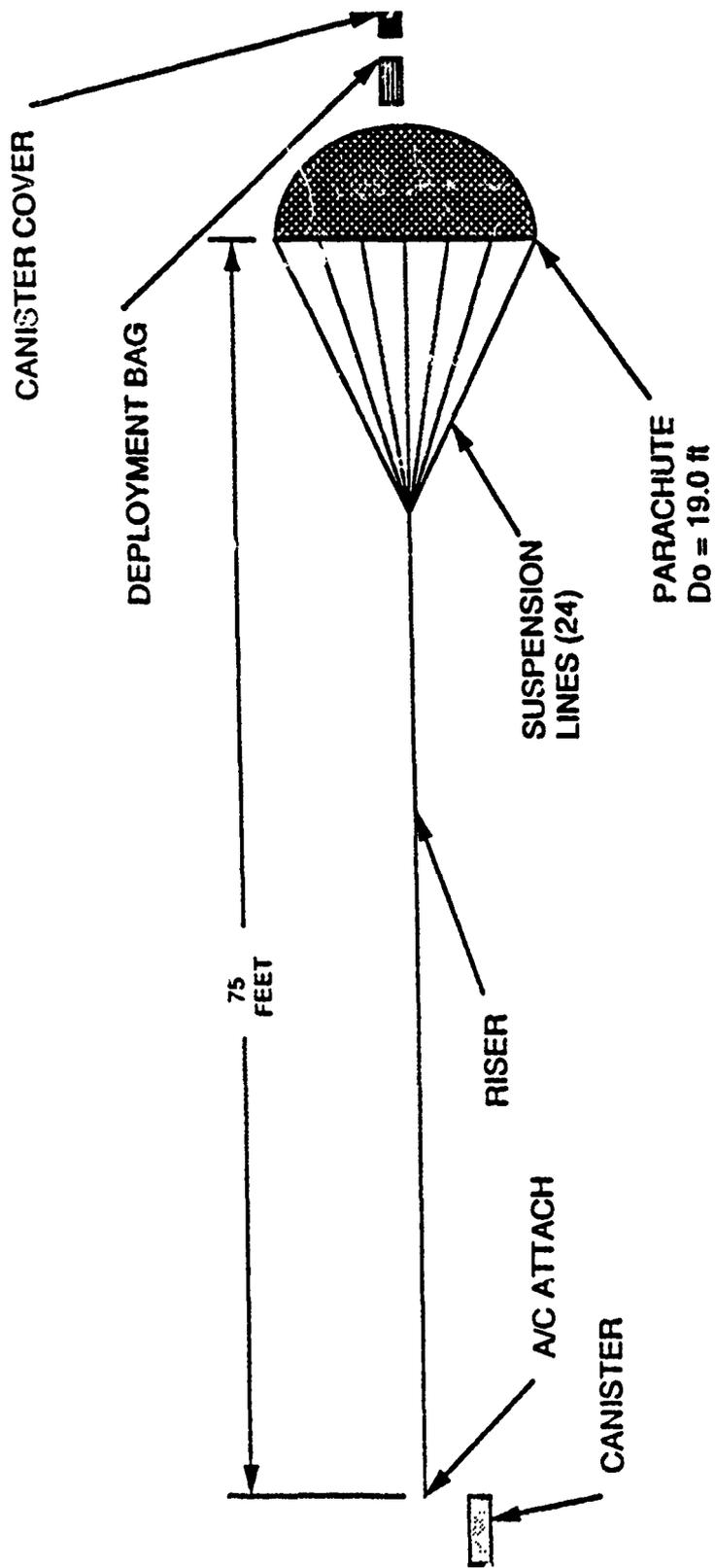
Figure A4 Parachute Configuration

RISER

RISER END LOOP

RISER
EXIT
SLOT

SABOT ASSY

BREECH

MORTAR BODY

SHEAR RIVETS

EXTENDED COVER
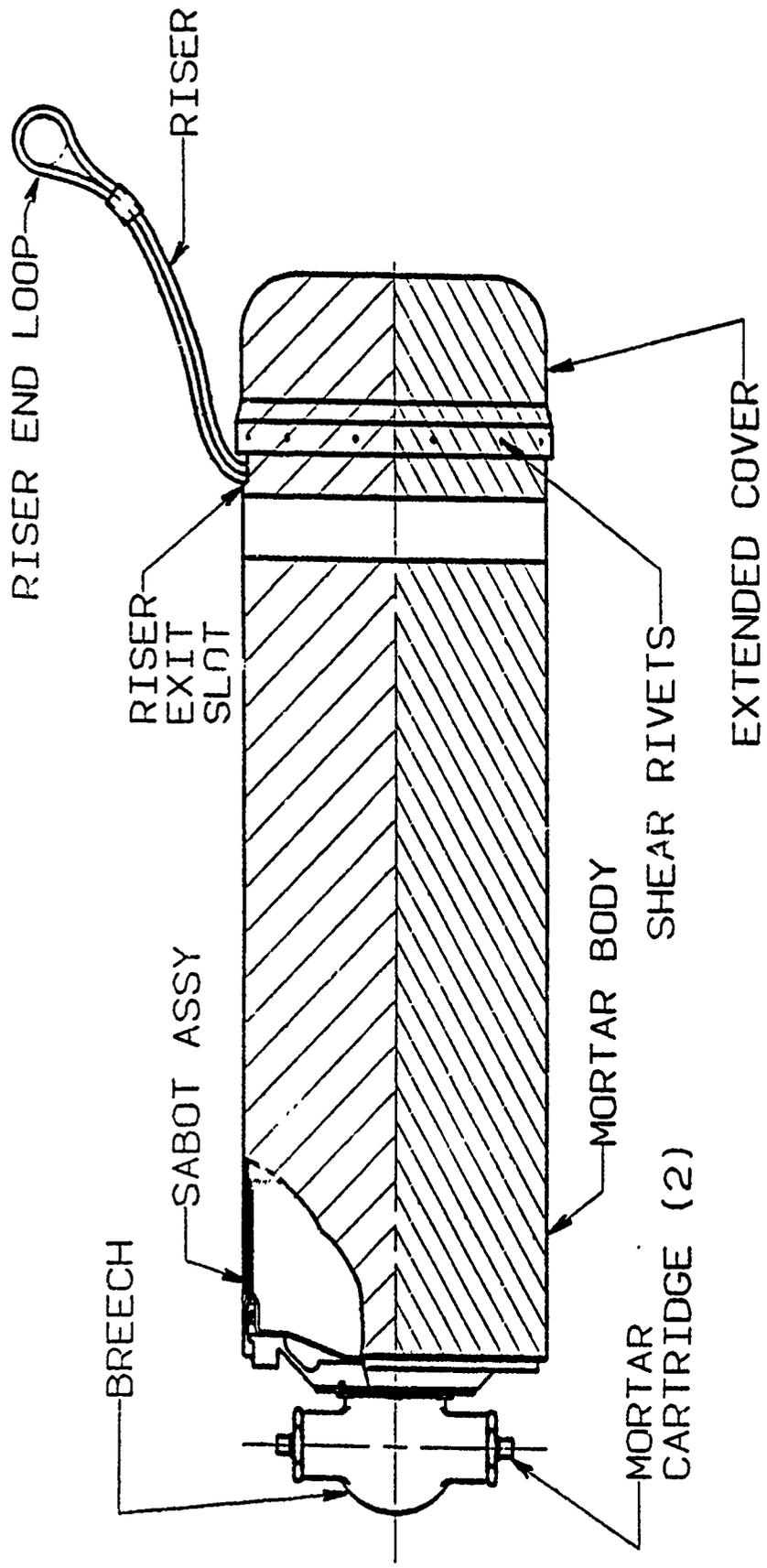
MORTAR
CARTRIDGE (2)

Figure A5   Mortar Assembly

86
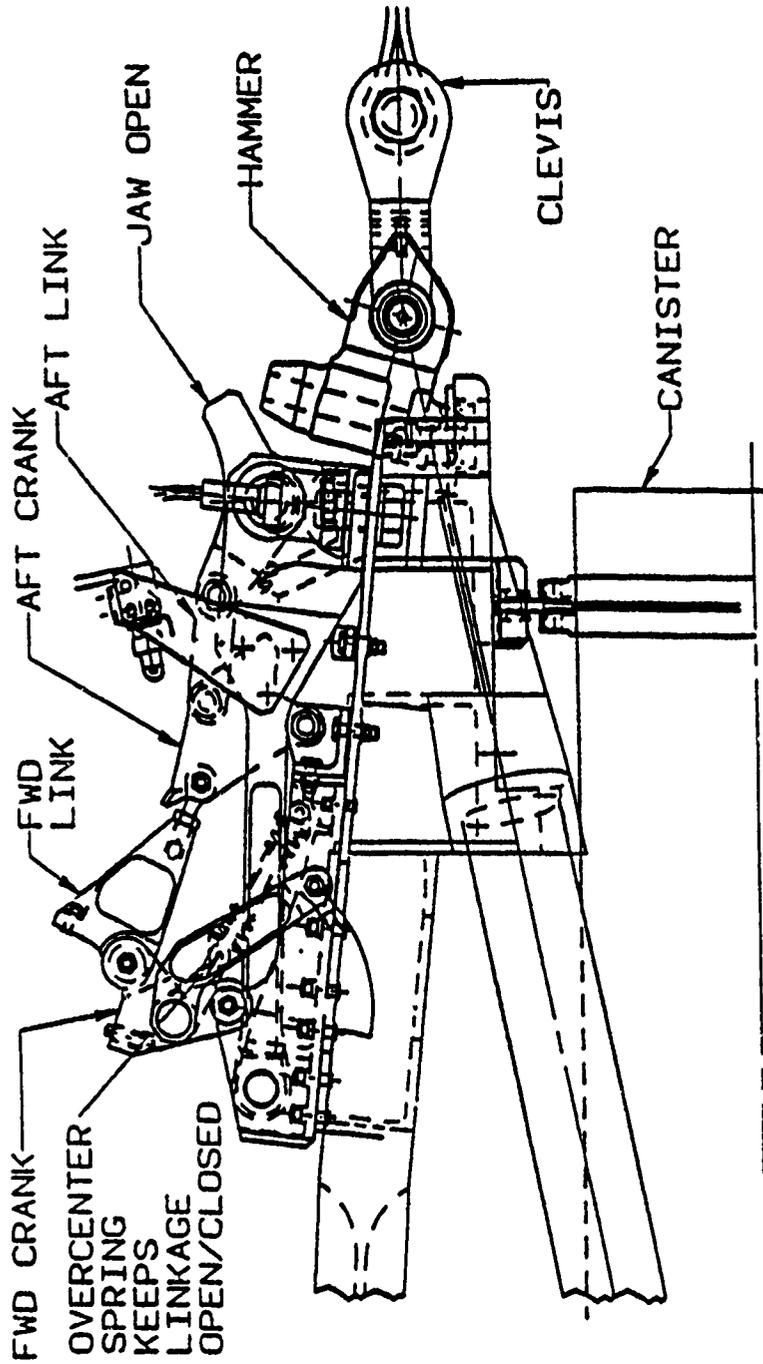
Mechanical Jettison Mechanics

Figure A6 Jettison Assembly

JAW OPEN

HAMMER

AFT LINK

AFT CRANK

CLEVIS

FWD LINK

CANISTER

FWD CRANK

OVERCENTER
SPRING
KEEPS
LINKAGE
OPEN/CLOSED

87

PYROTECHNIC
RELEASE
NUT

"T" FTG

"T" FTG
STRAPS

BATHTUB FTG

"T" FTG
PIVOT
POINT
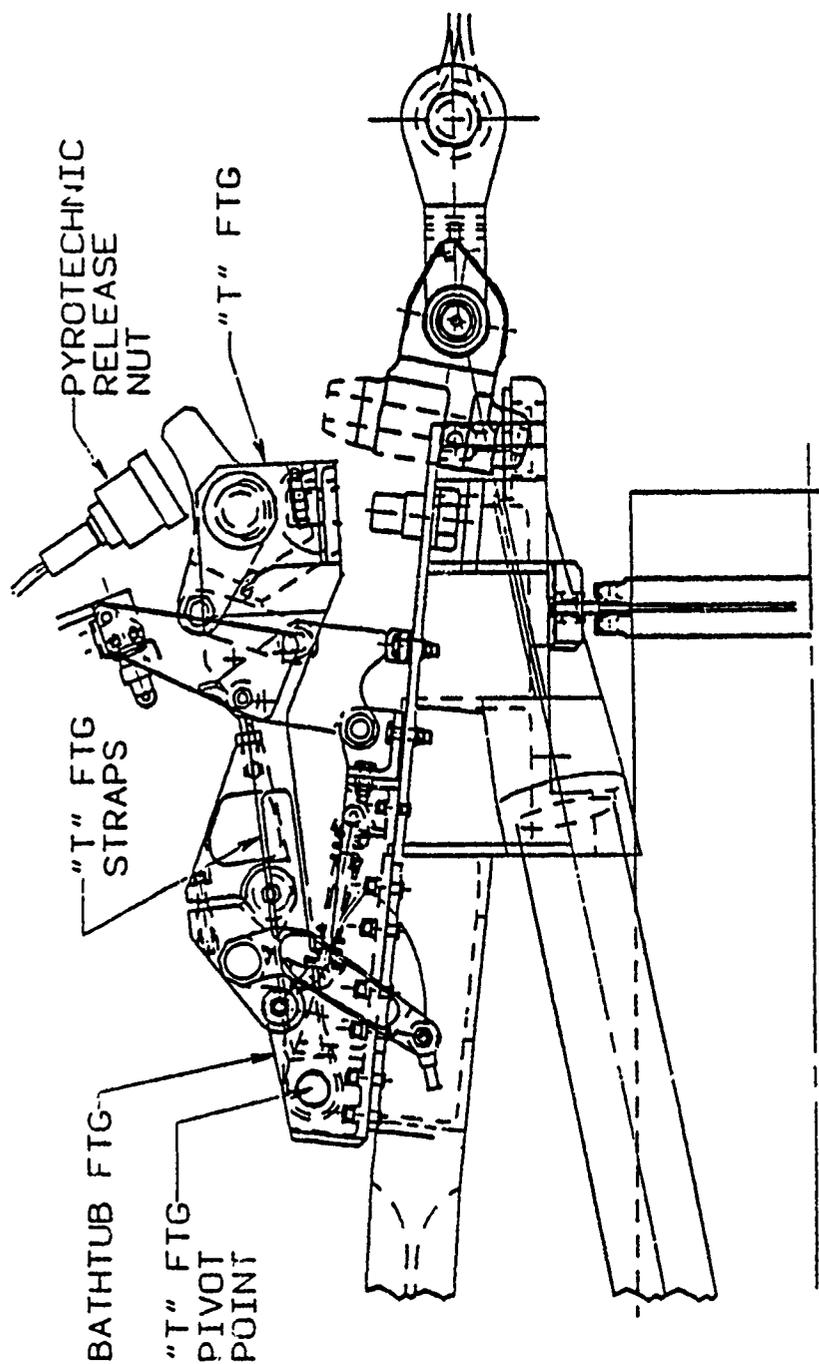
Emergency Jettison Mechanics

Figure A6 Jettison Assembly (Concluded)

88

326.44 IN.SPAN
(27 FT.2.44 IN.)

C/L AIRPLANE

WS 127.0   WS 127.0

WING REF.PLANE
W.L.61.0 AT 70% C

90.9 IN
(7 FT.6.9 IN.)

Figure A7   X-29 Aircraft Schematic

89

Figure A7 X-29 Aircraft Schematic (Continued)

90
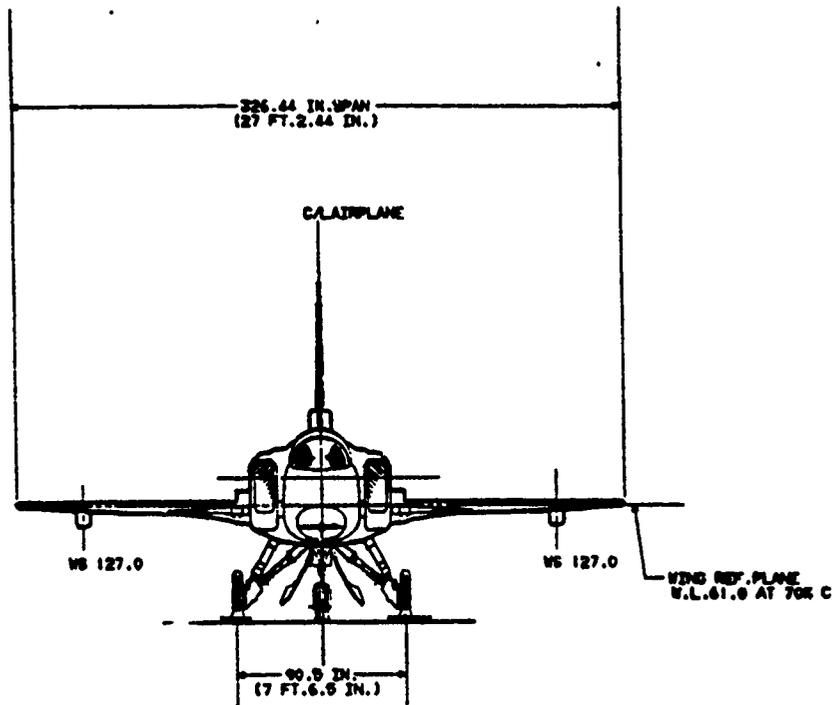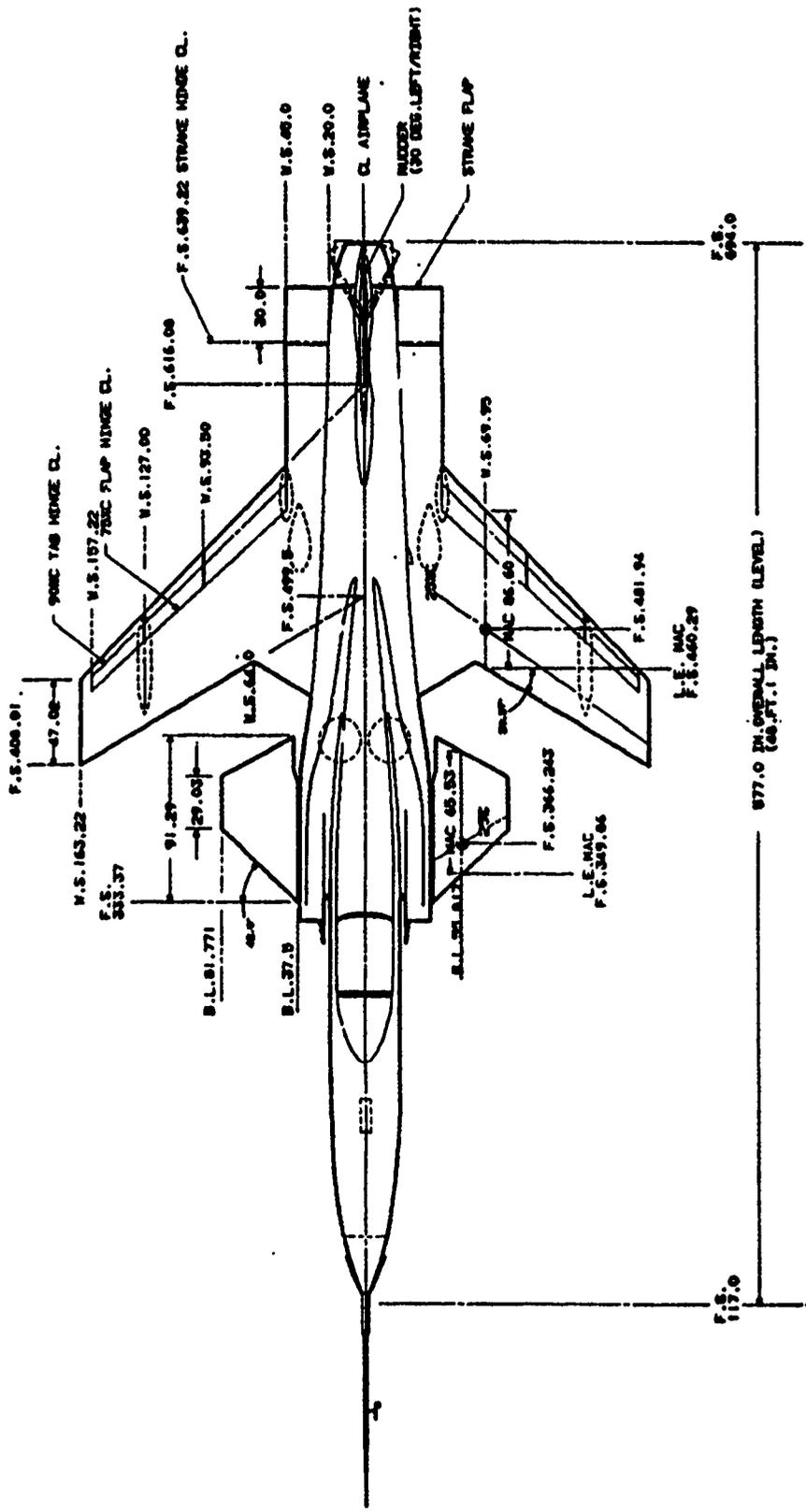
Figure A7   X-29 Aircraft Schematic   (Concluded)

91

Figure A8   X-29 Sign Convention

APPENDIX B
TEST DATA

This page intentionally left blank.

X-29 USAF S/N 820049
FLIGHT 1G INITIAL TRIM
MIL POWER   XCG=449in
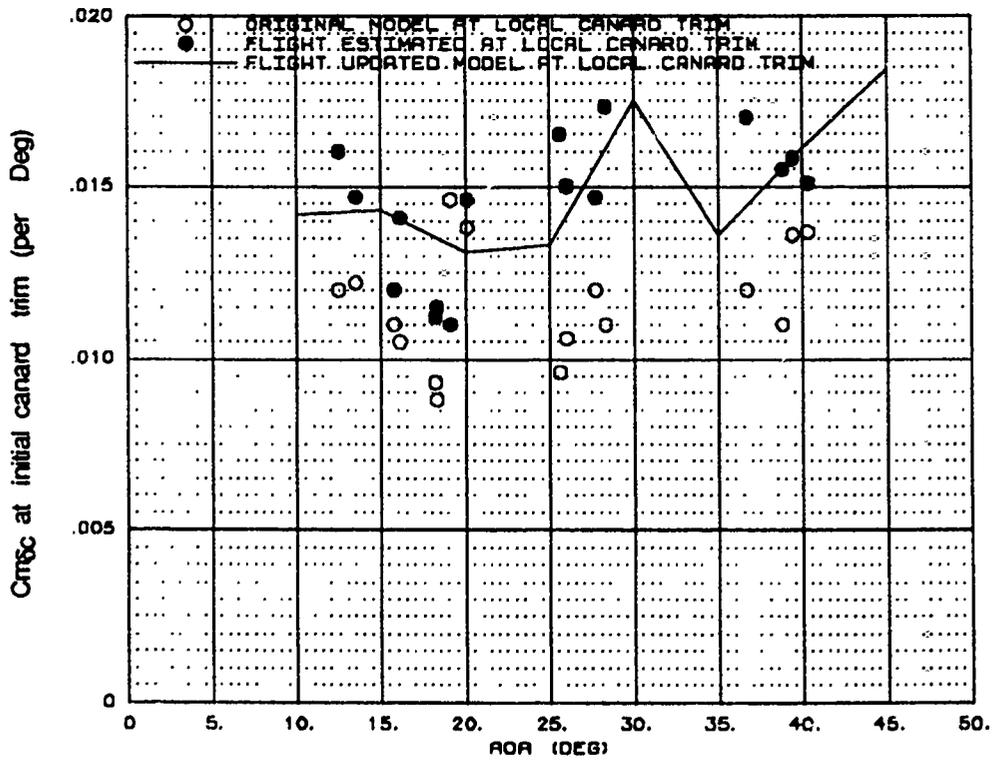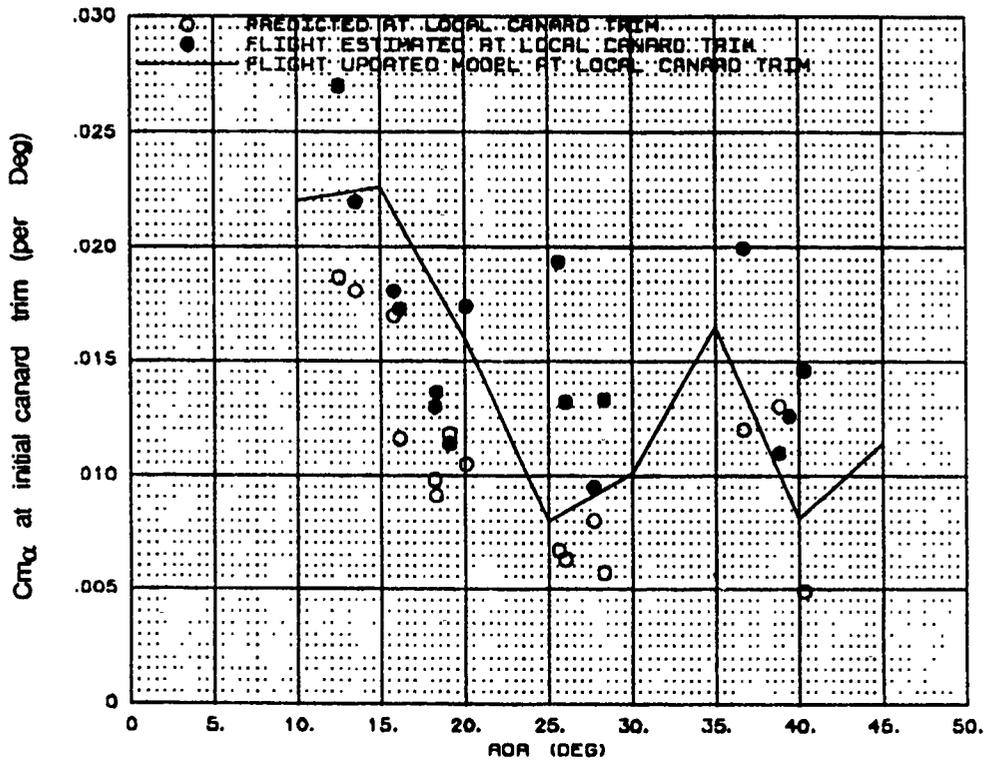
Figure B1   Longitudinal Parameter Estimation Data

X-29 USAF S/N 820049
POWER OFF
CANARD= -57 deg   SYM FLAP= 21.5deg   STRAKE= 30deg

AERO MODEL COMPARISON
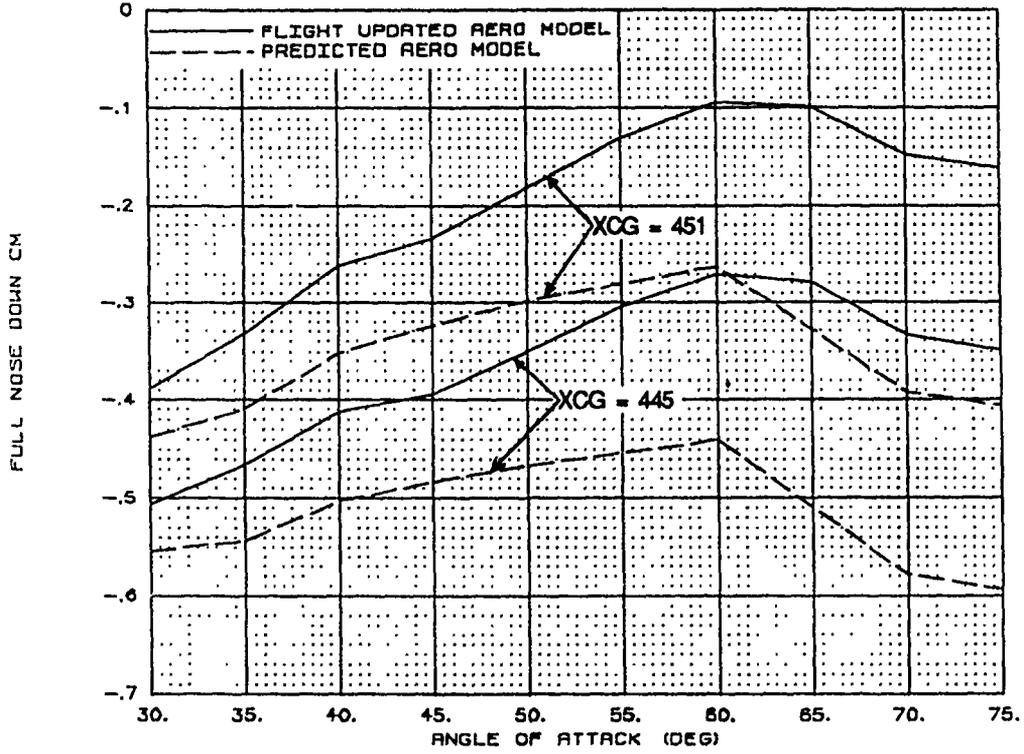
Figure B2   Full Nose Down Pitching Moment Comparison

96

X-29 USAF S/N 820049
1 G ACC TRIM   XCG=449 in
AOA=10 deg   MACH=0.3   ALT=30K ft
AERO MODEL COMPARISONS
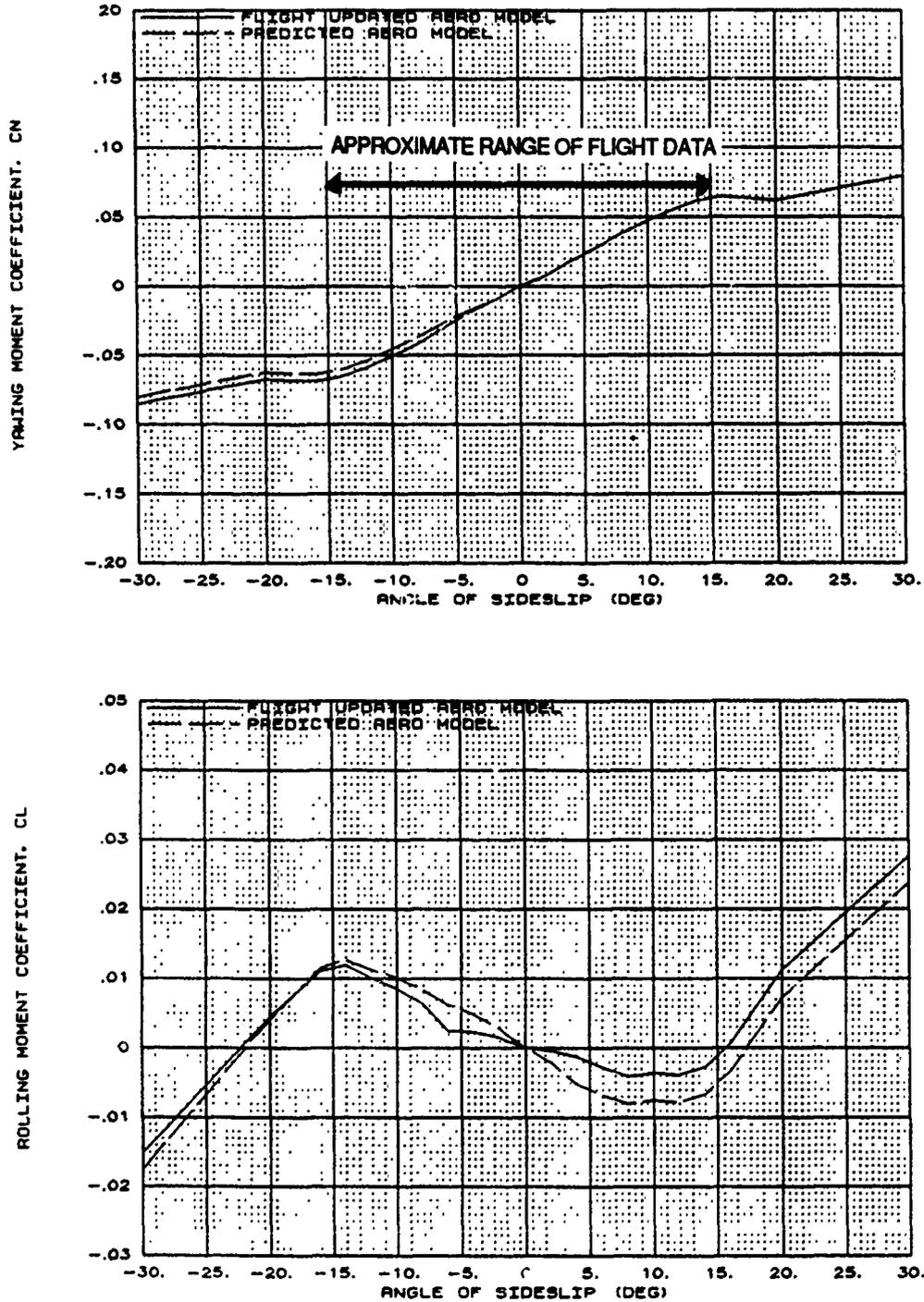
Figure B3 Updated Lateral-Directional Aerodynamics at 10 Degrees AOA

97
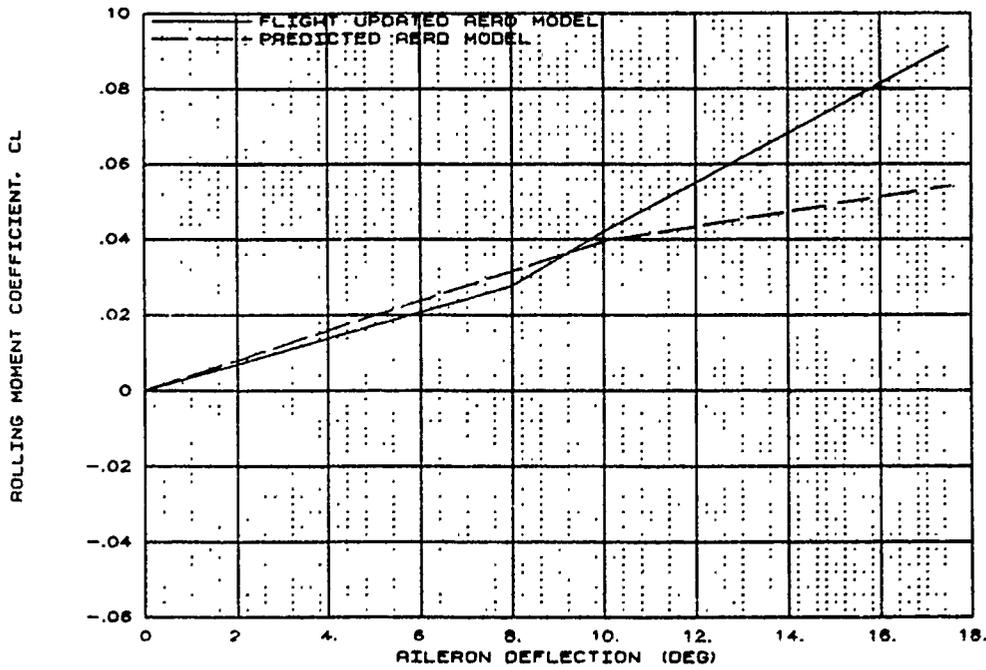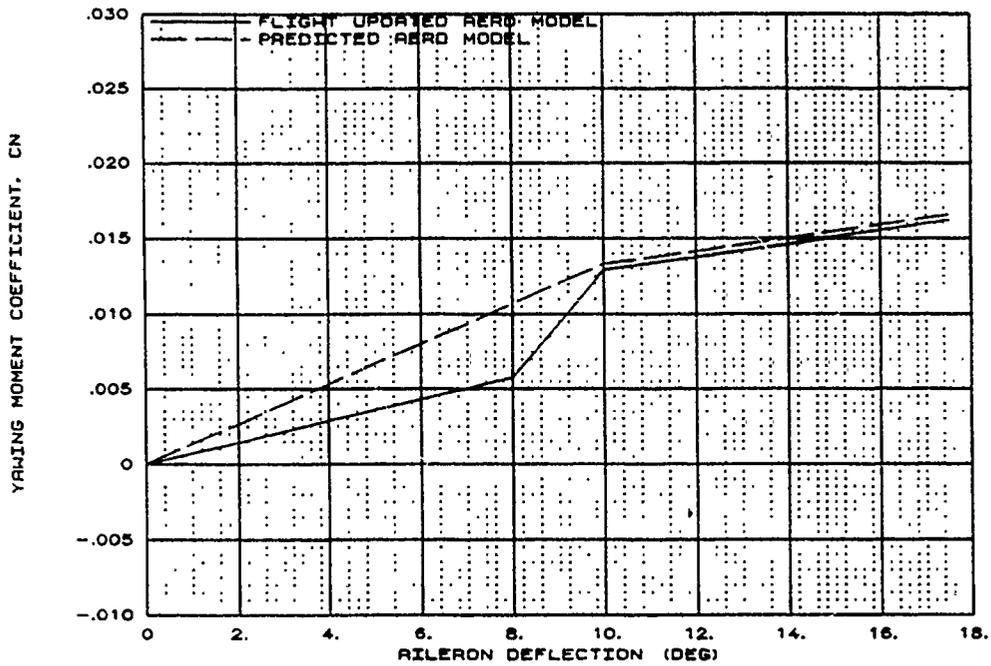
**Figure B3 Updated Lateral-Directional Aerodynamics
at 10 Degrees AOA (Continued)**

98
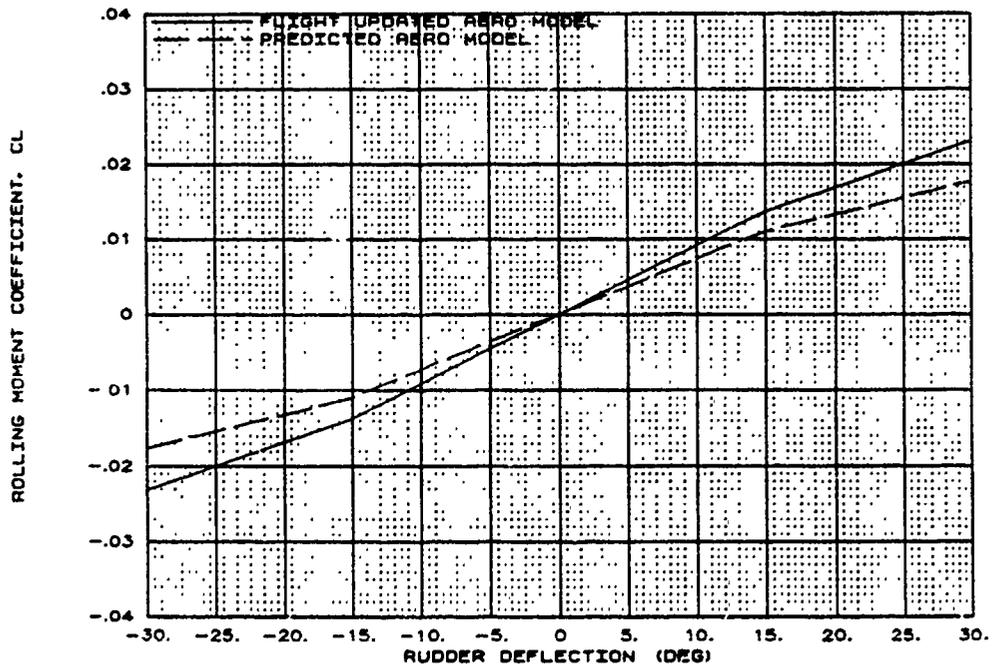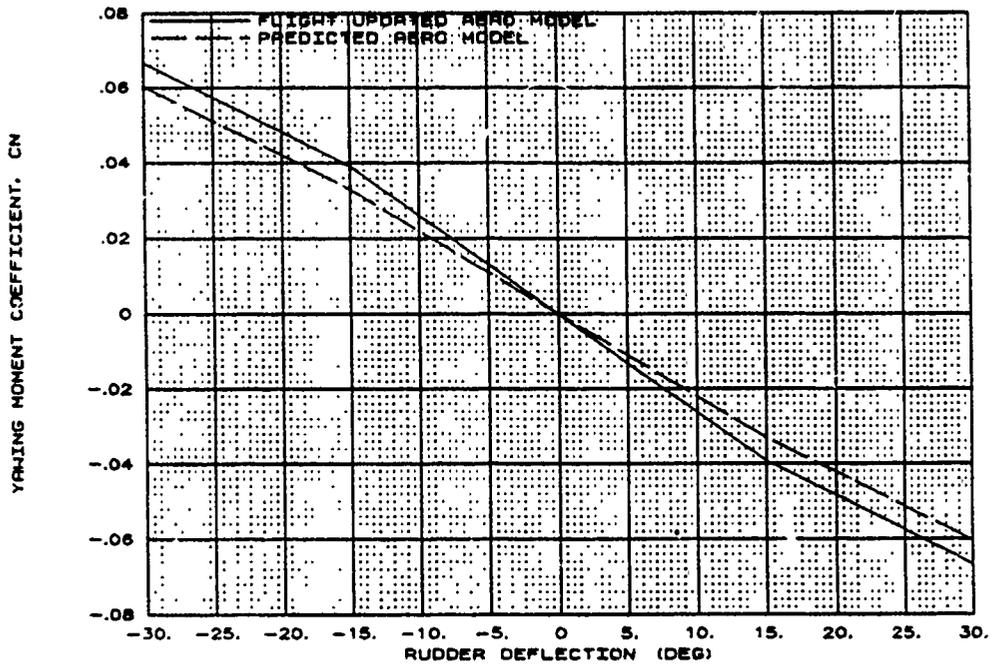
**Figure B3 Updated Lateral-Directional Aerodynamics
at 10 Degrees AOA (Concluded)**

X-29 USAF S/N 820049
1 G ACC TRIM   XCG=449 in
AOA=15 deg   MACH=0.3   ALT=30K ft
AERO MODEL COMPARISONS

APPROXIMATE RANGE OF FLIGHT DATA

Legend: FLIGHT UPDATED AERO MODEL / PREDICTED AERO MODEL

Y-axis: YAWING MOMENT COEFFICIENT, CN
X-axis: ANGLE OF SIDESLIP (DEG)

Legend: FLIGHT UPDATED AERO MODEL / PREDICTED AERO MODEL

Y-axis: ROLLING MOMENT COEFFICIENT, CL
X-axis: ANGLE OF SIDESLIP (DEG)
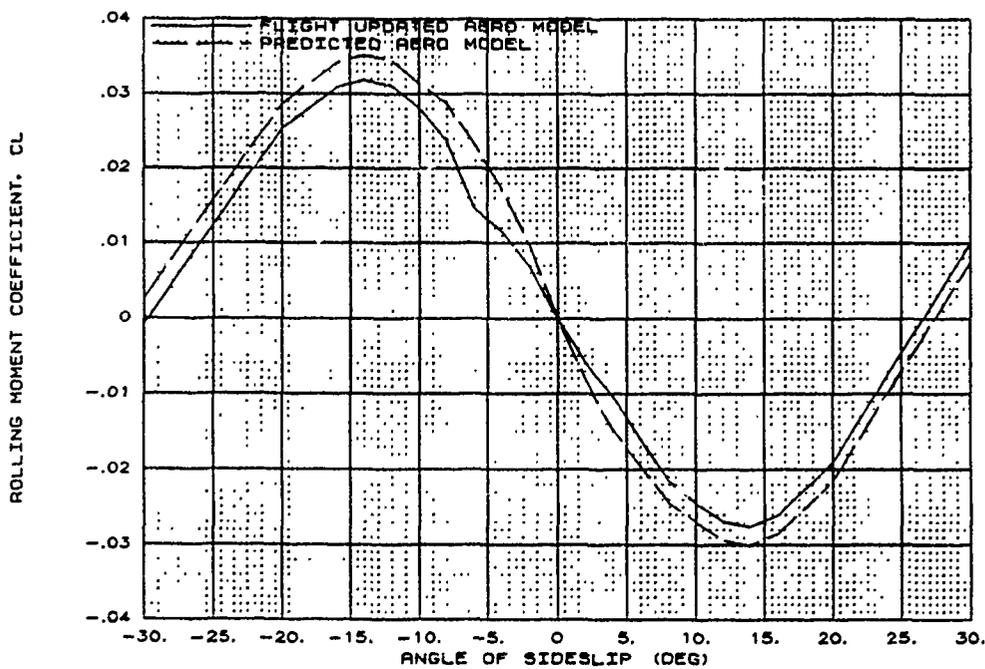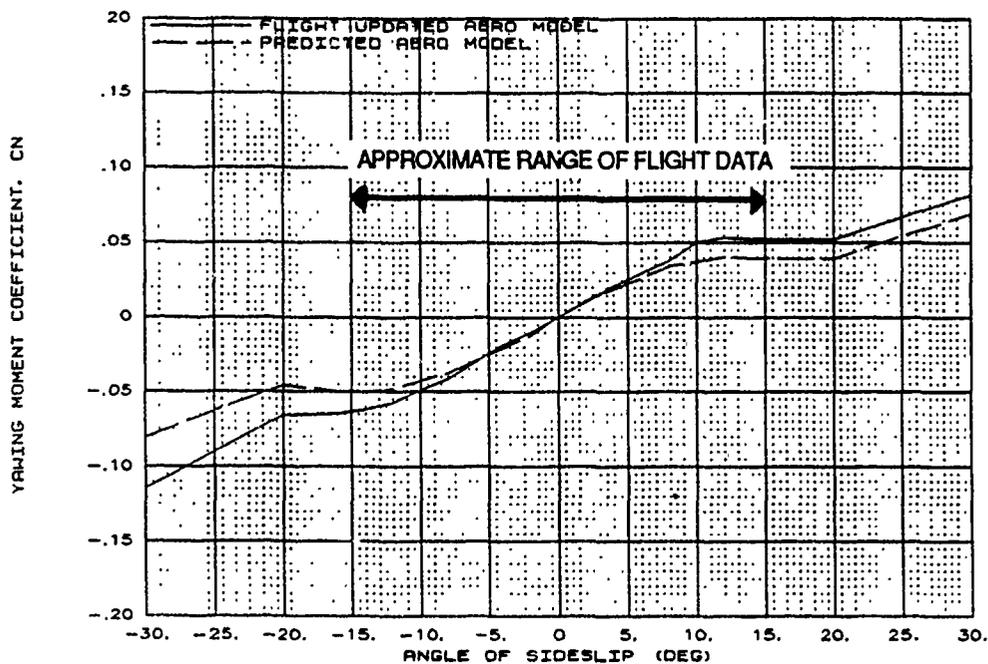
Figure B4   Updated Lateral-Directional Aerodynamics at 15 Degrees AOA
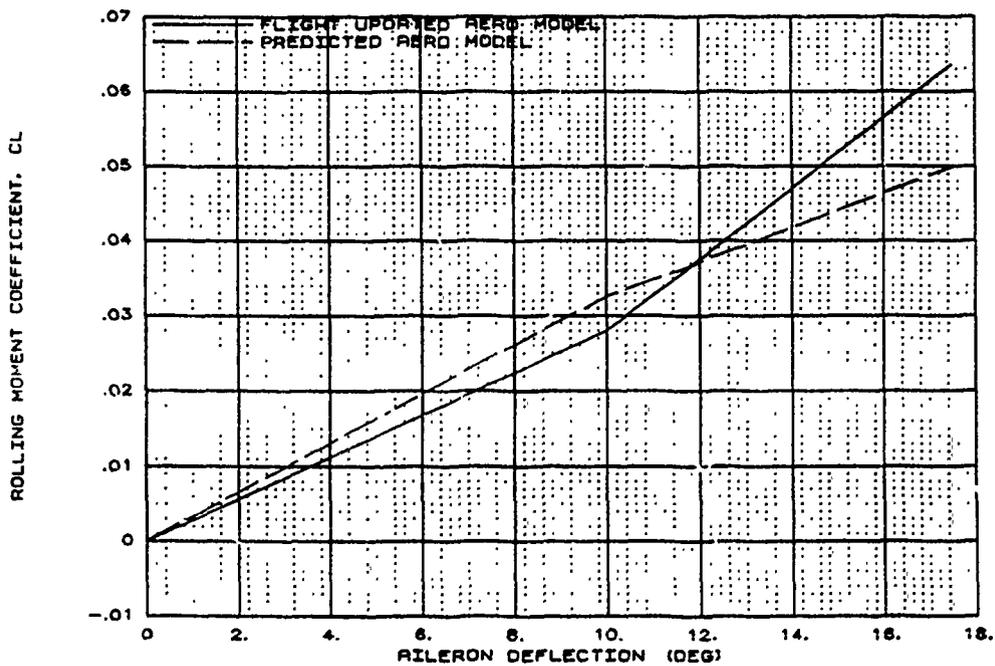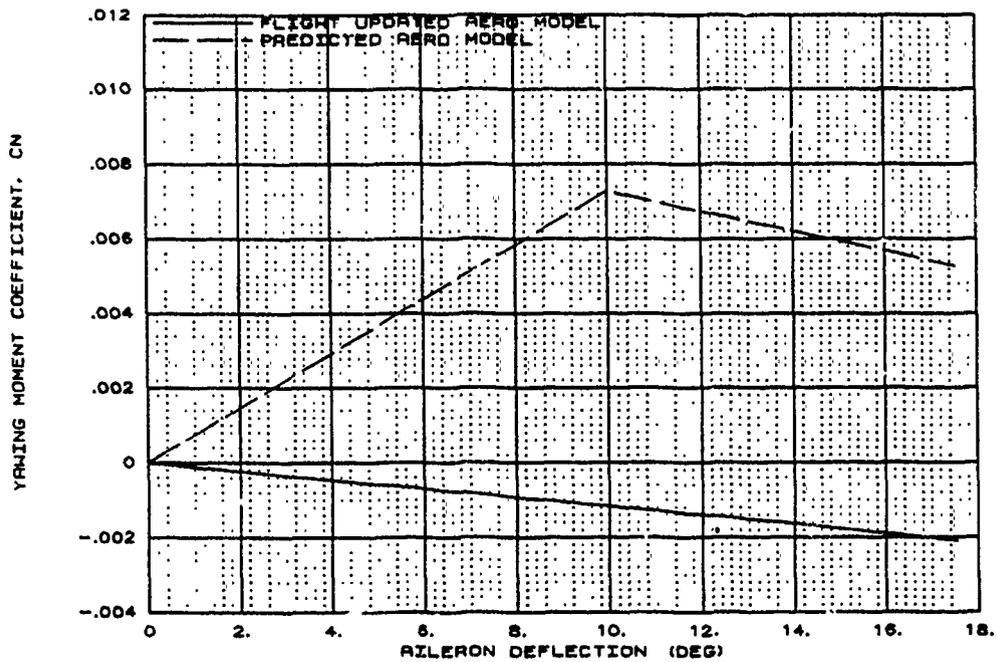
Figure B4 Updated Lateral-Directional Aerodynamics at 15 Degrees AOA (Continued)

101
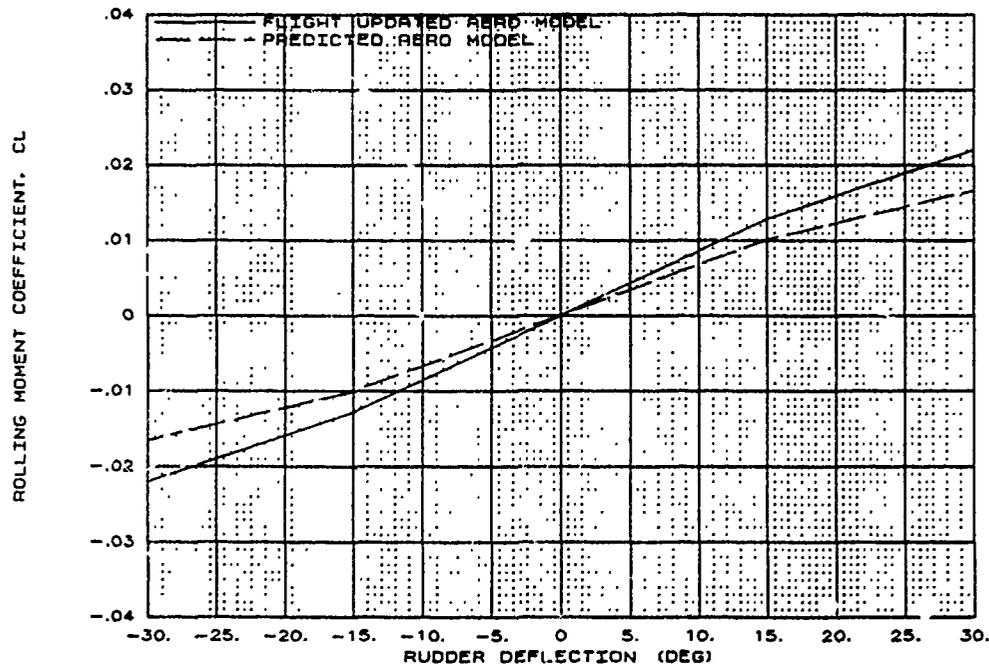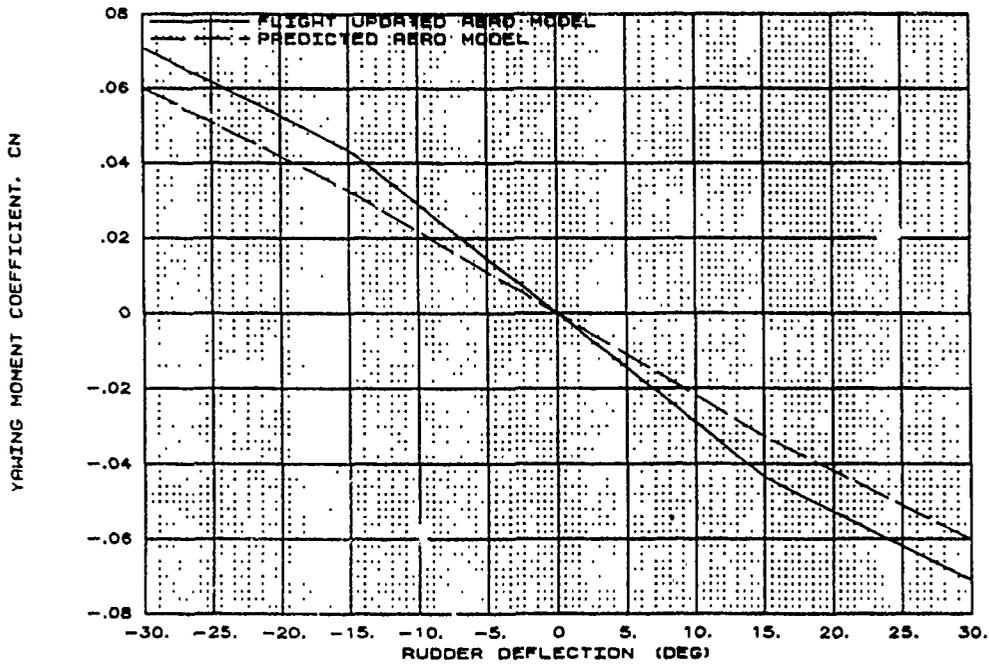
**Figure B4 Updated Lateral-Directional Aerodynamics
at 15 Degrees AOA (Concluded)**

X-29 USAF S/N 82004
1 G ACC TRIM   XCG=449 in
AOA=20 deg   MACH=0.3   ALT=30K ft
AERO MODEL COMPARISONS
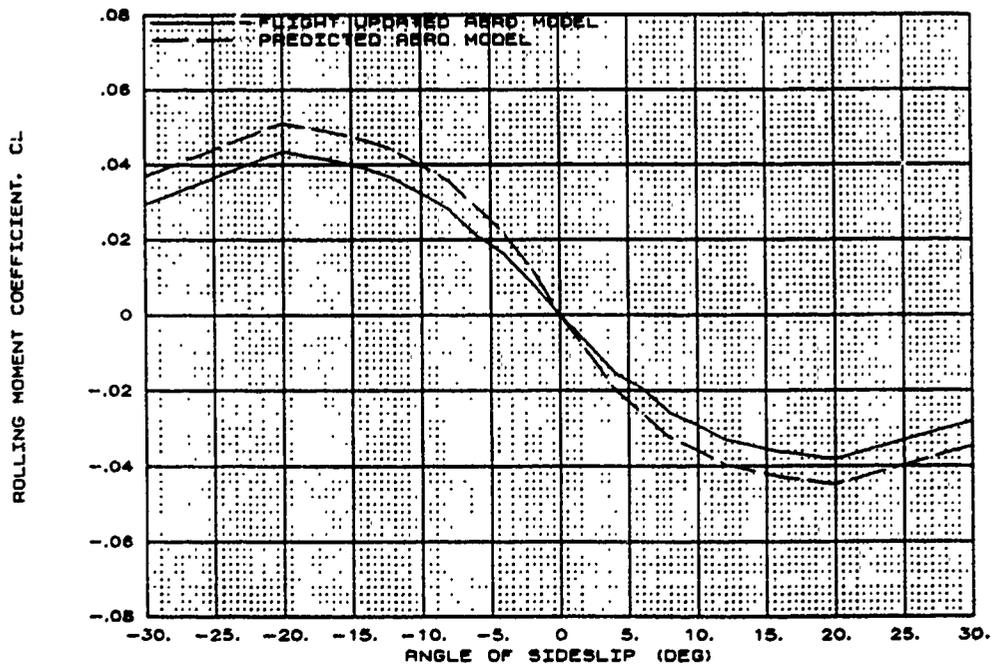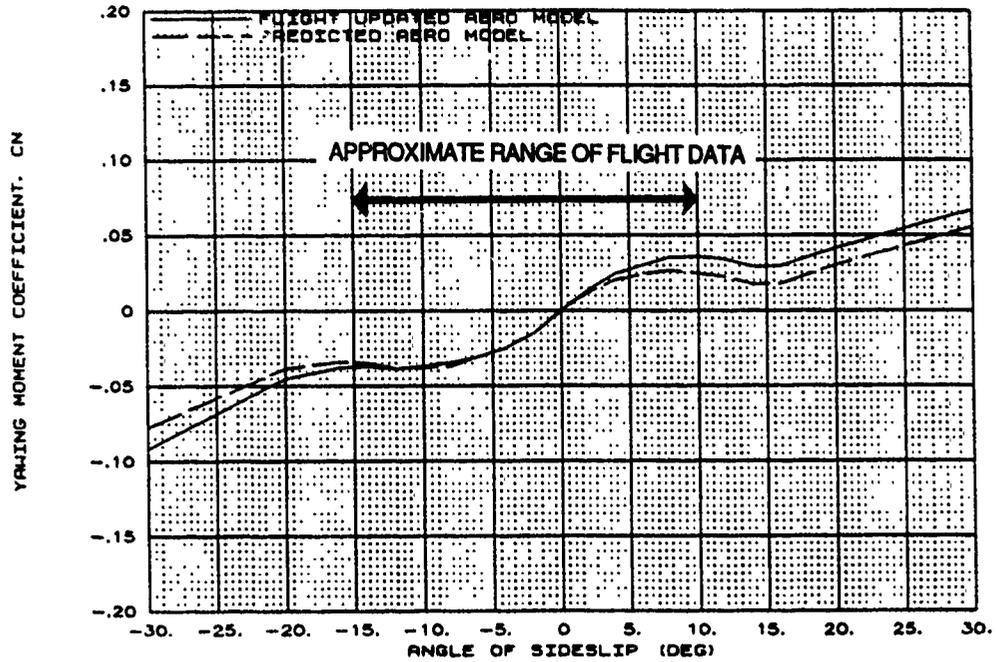
Figure B5 Updated Lateral-Directional Aerodynamics at 20 Degrees AOA
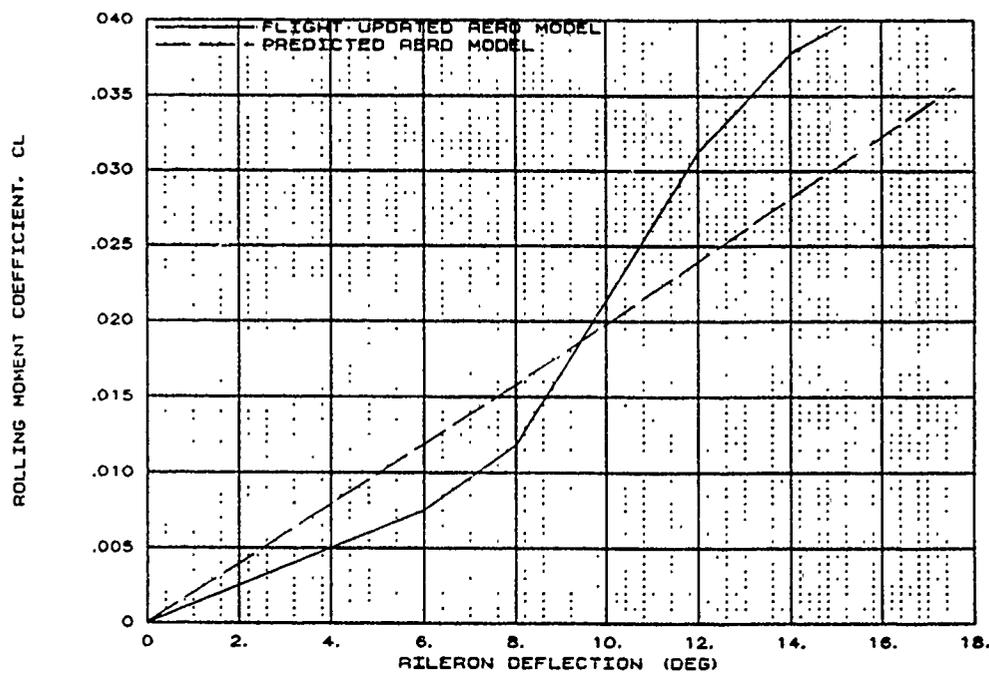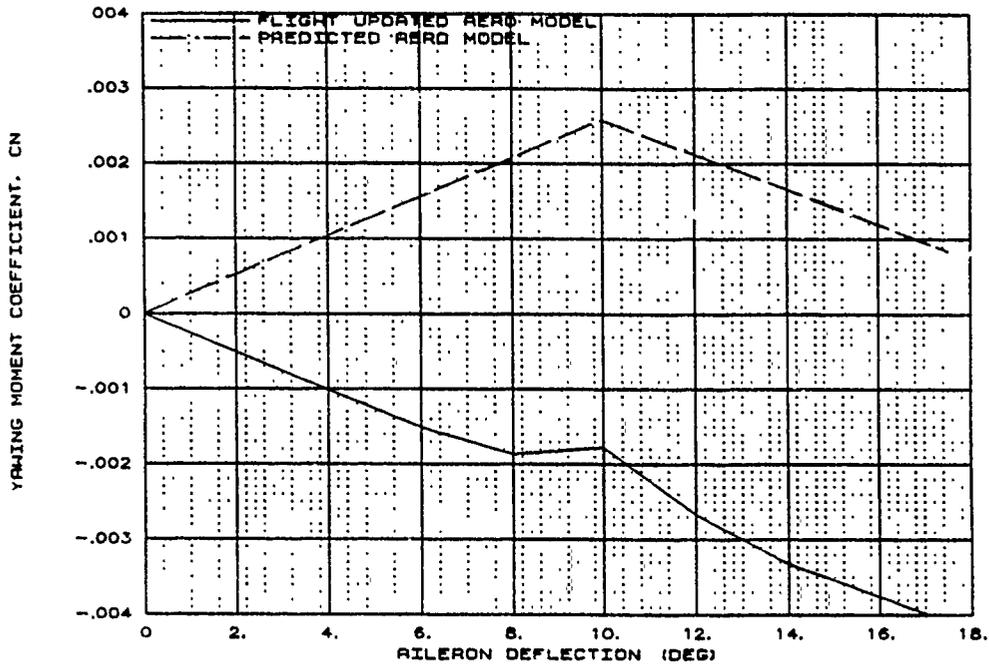
**Figure B5 Updated Lateral-Directional Aerodynamics
at 20 Degrees AOA (Continued)**

104
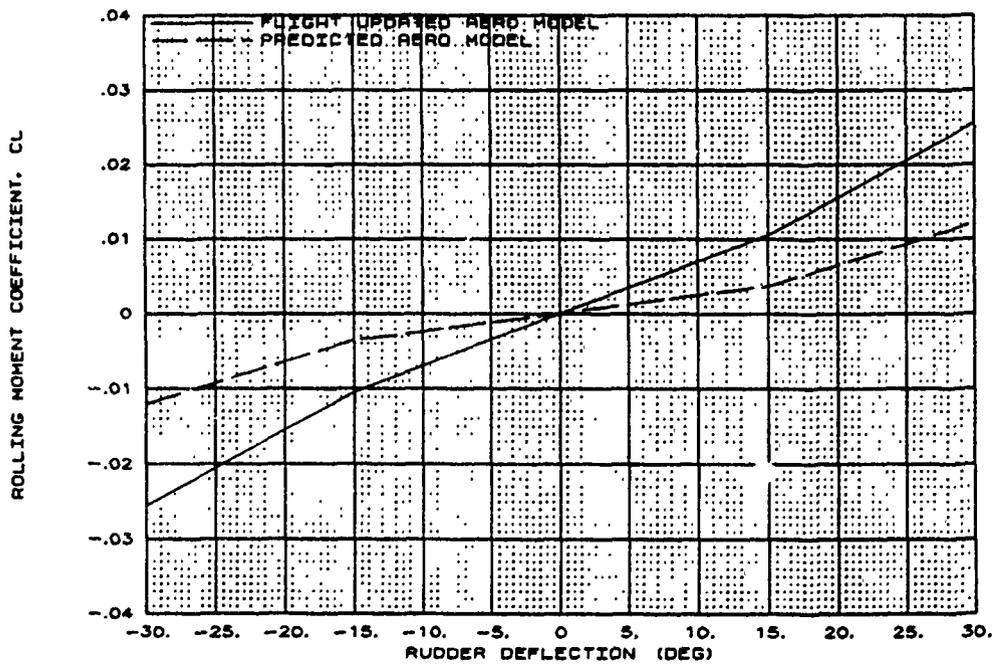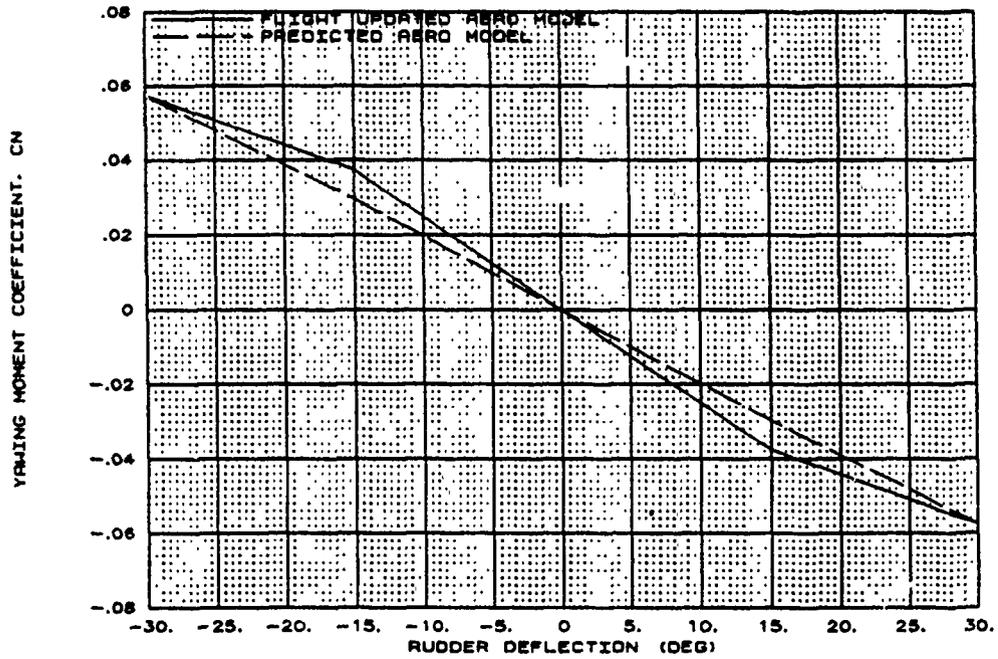
**Figure B5 Updated Lateral-Directional Aerodynamics
at 20 Degrees AOA (Concluded)**

105

X-29 USAF S/N 82004
1 G ACC TRIM   XCG=449 In
AOA=25 deg   MACH=0.3   ALT=30K ft
AERO MODEL COMPARISONS
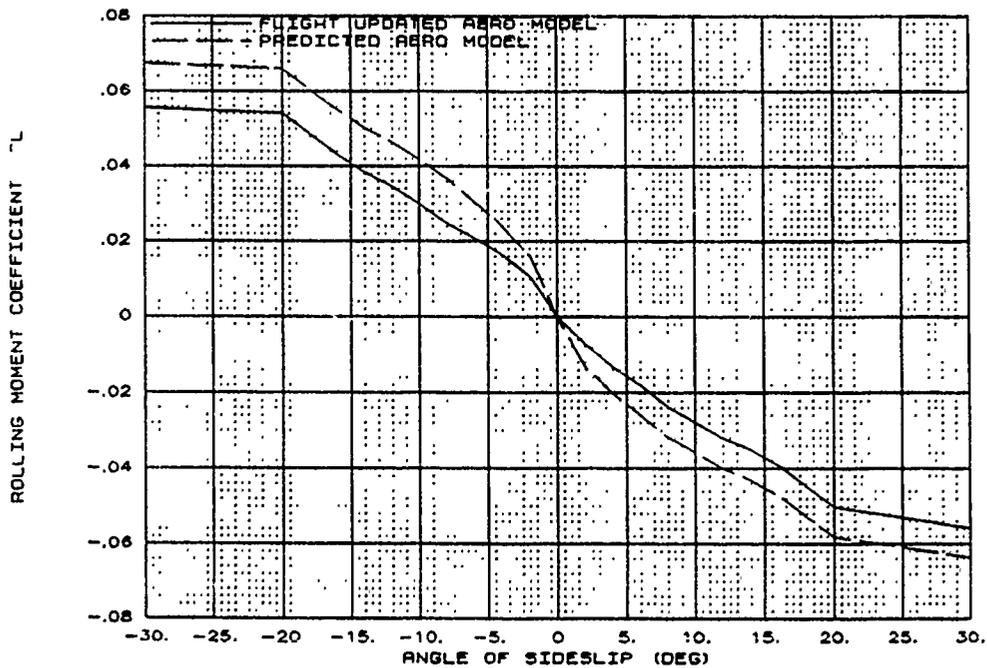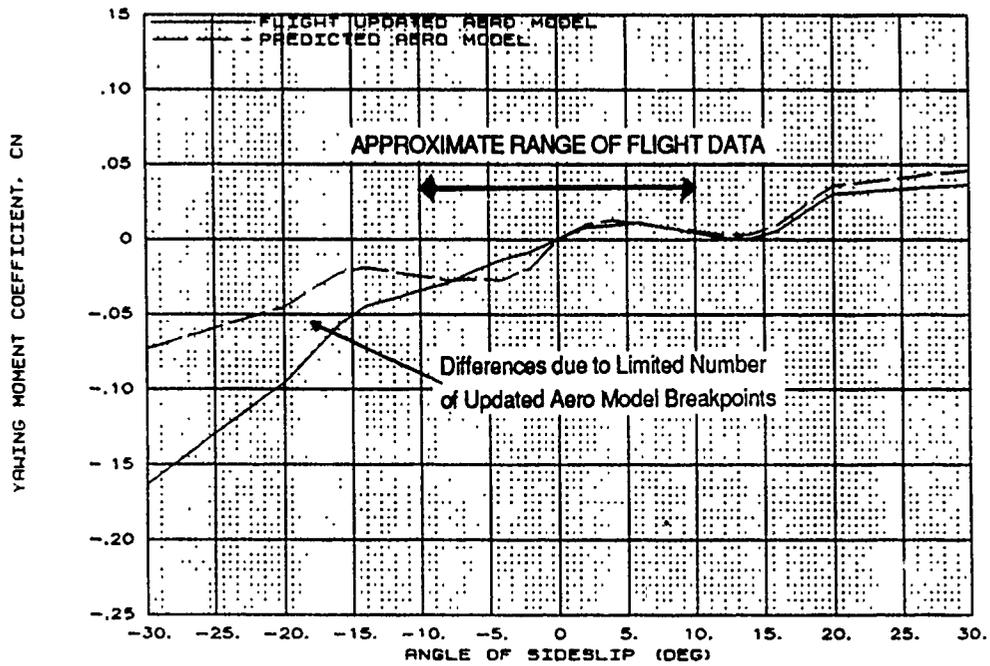
Figure B6 Updated Lateral-Directional Aerodynamics at 25 Degrees AOA
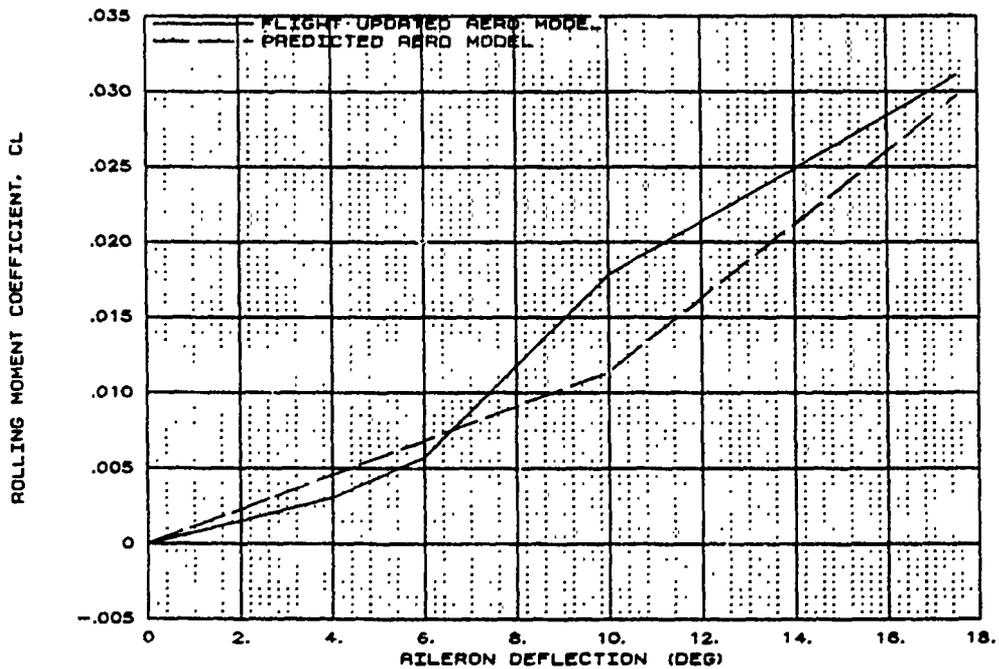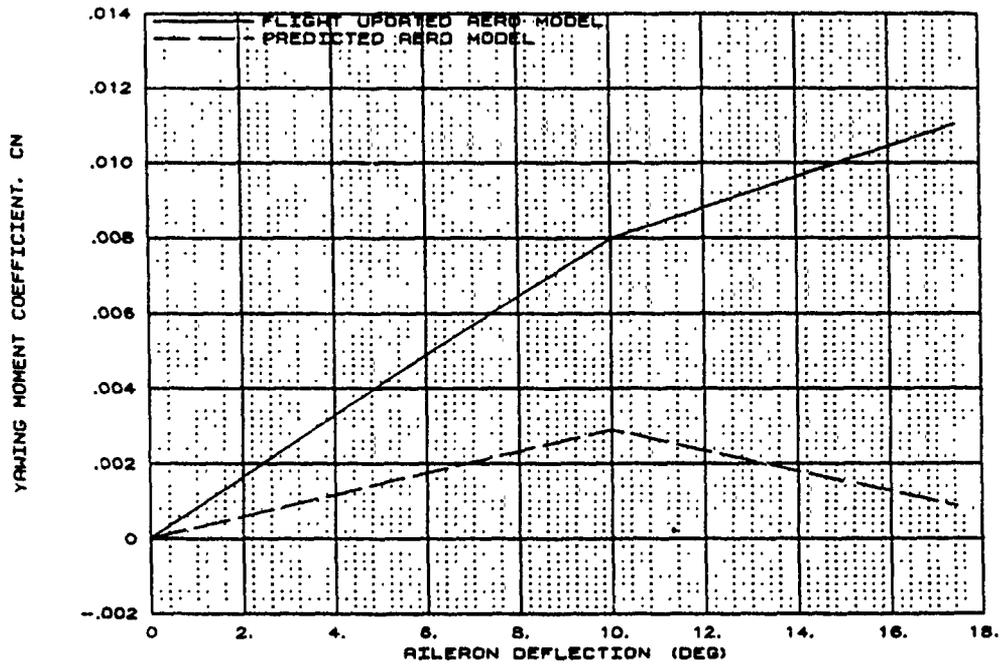
Figure B6 Updated Lateral-Directional Aerodynamics
at 25 Degrees AOA (Continued)
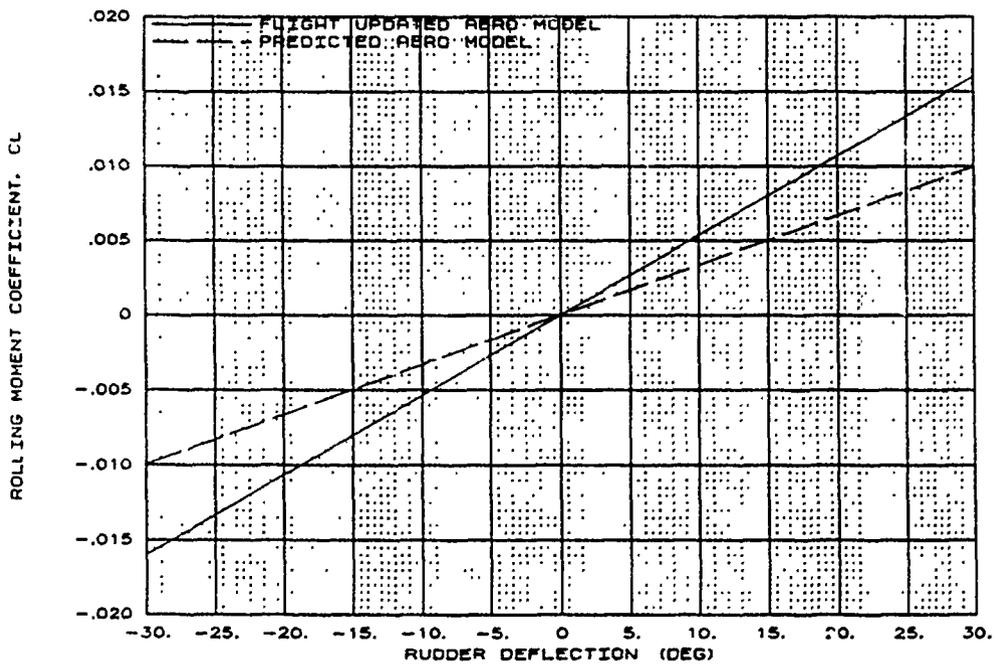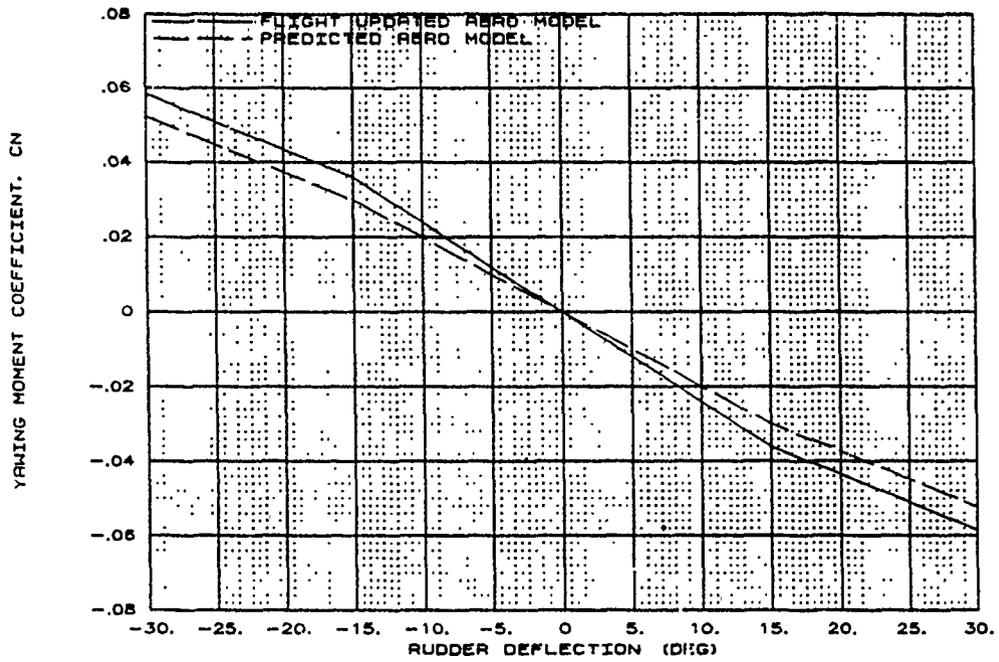
Figure B6 Updated Lateral-Directional Aerodynamics
at 25 Degrees AOA (Concluded)

X-29 USAF S/N 82004
1 G ACC TRIM   XCG=449 in
AOA=30 deg   MACH=0.3   ALT=30K ft
AERO MODEL COMPARISONS
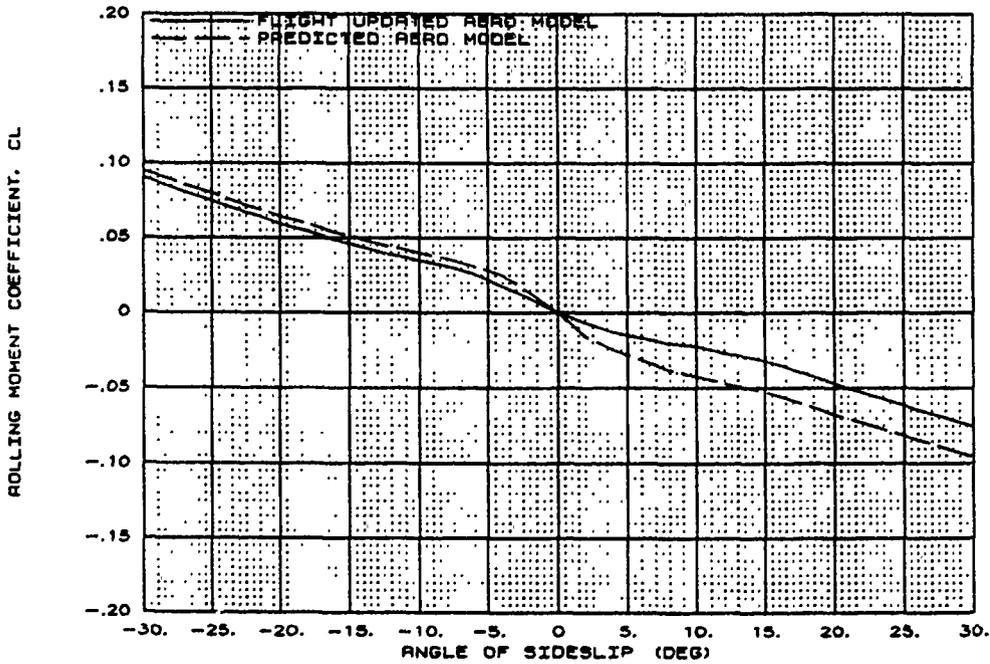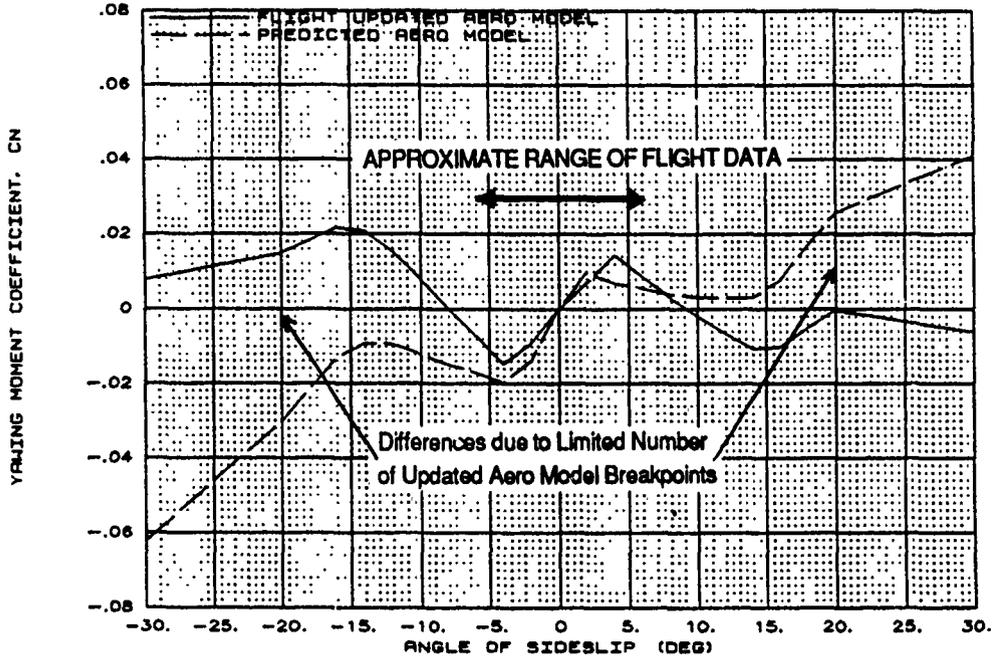
Figure B7 Updated Lateral-Directional Aerodynamics at 30 Degrees AOA
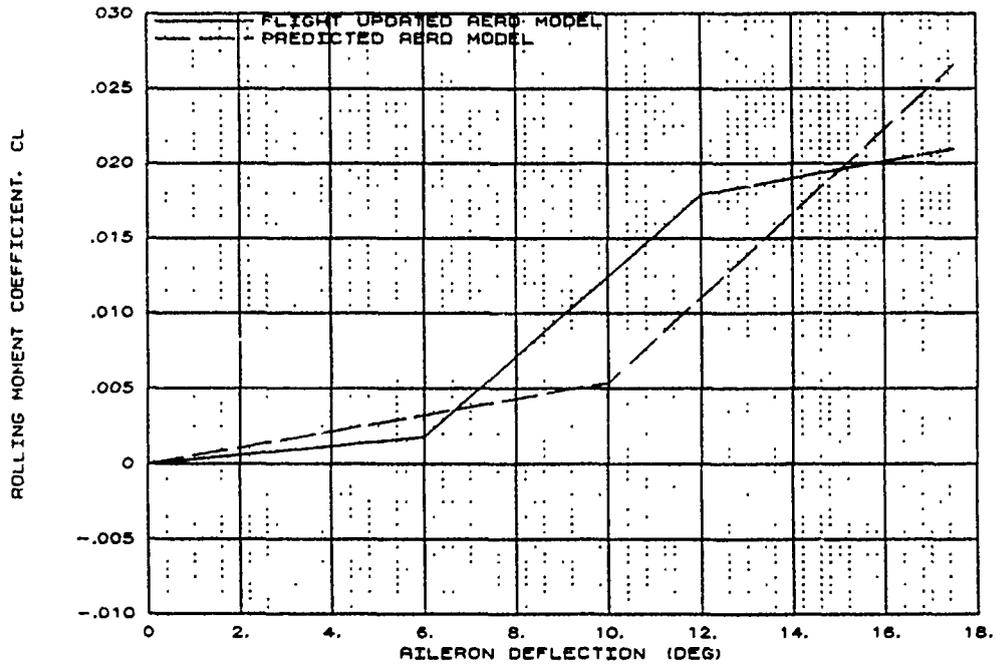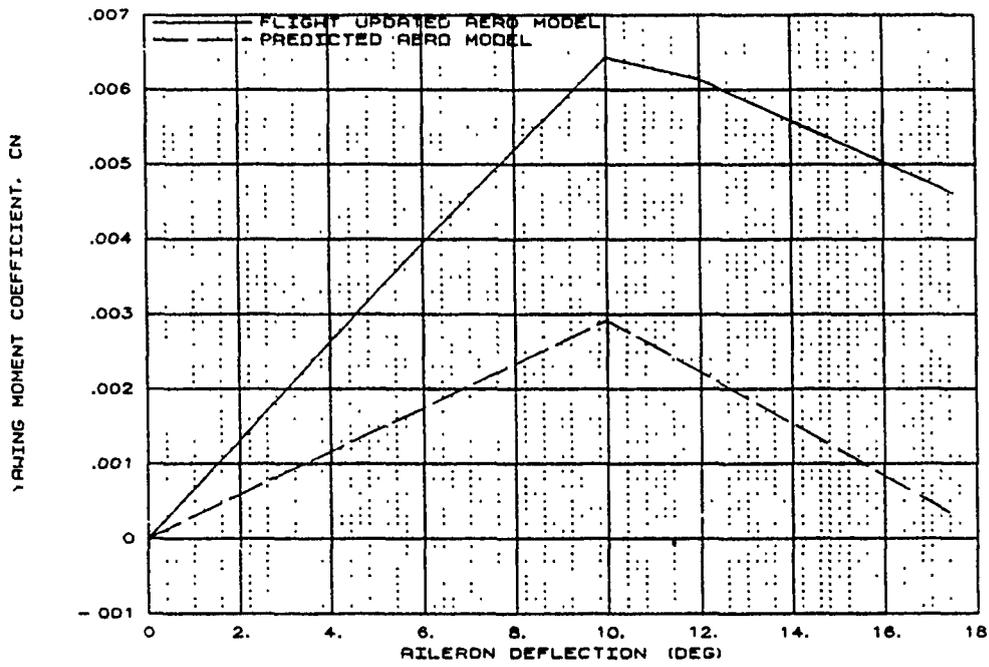
Figure B7 Updated Lateral-Directional Aerodynamics
at 30 Degrees AOA (Continued)
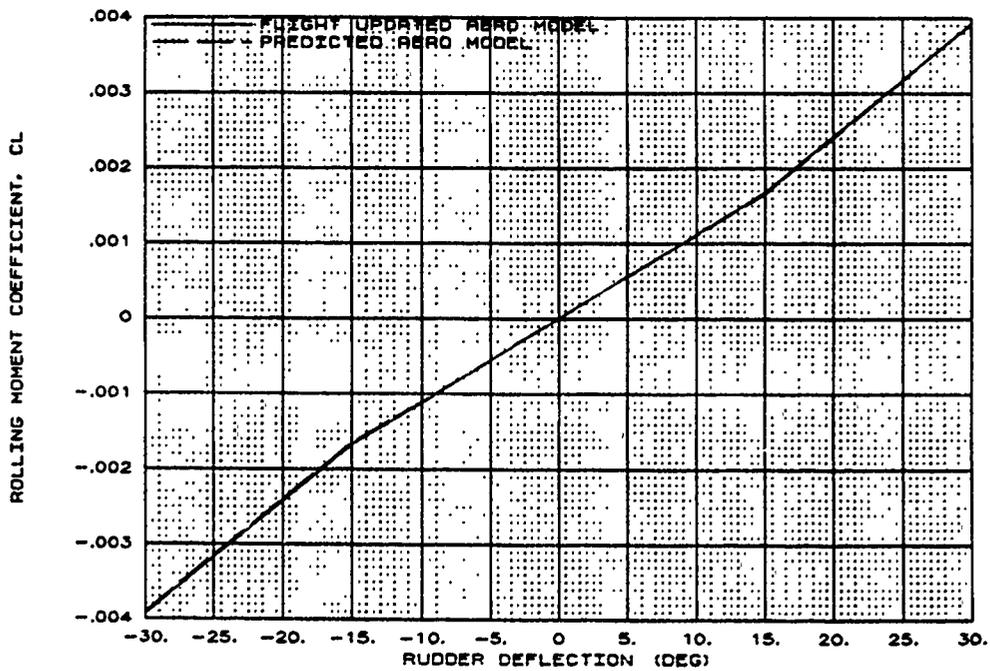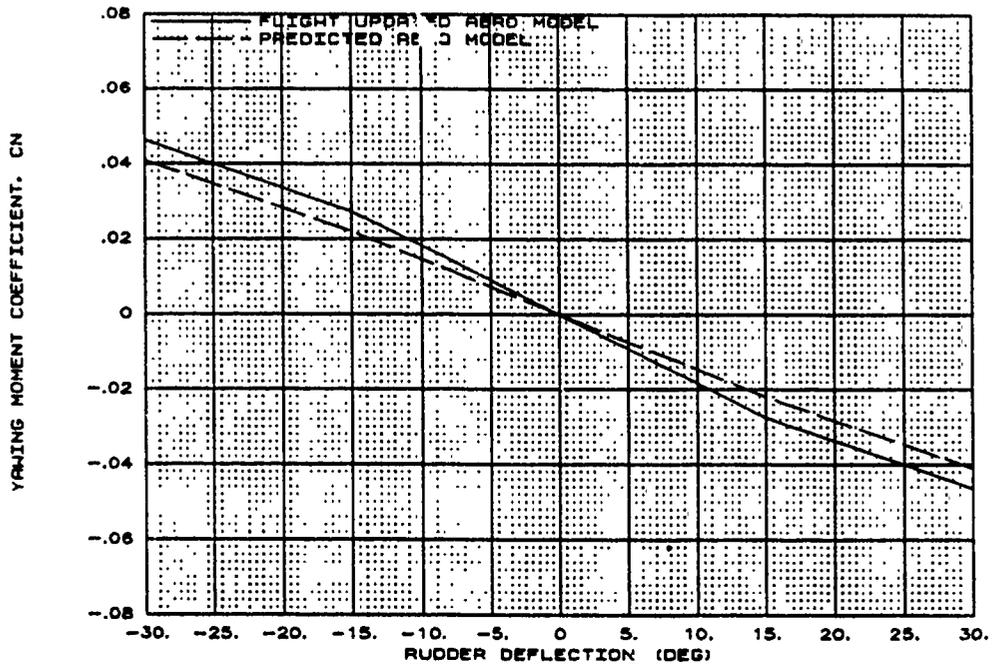
110

**Figure B7 Updated Lateral-Directional Aerodynamics
at 30 Degrees AOA (Concluded)**

X-29 USAF S/N 82004
1 G ACC TRIM   XCG=449 in
AOA=35 deg   MACH=0.3   ALT=30K ft
AERO MODEL COMPARISONS
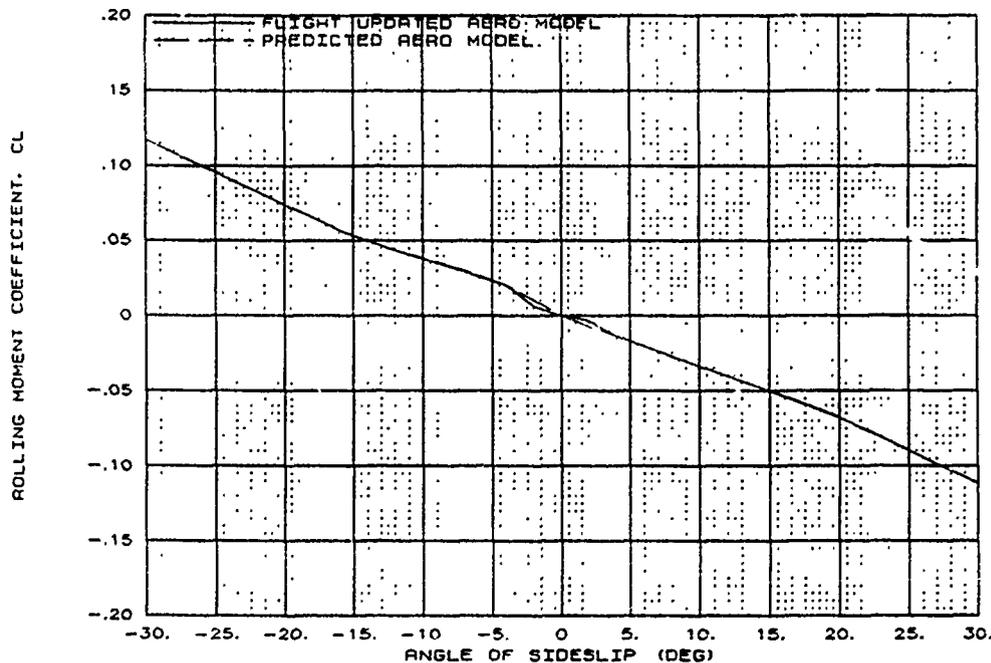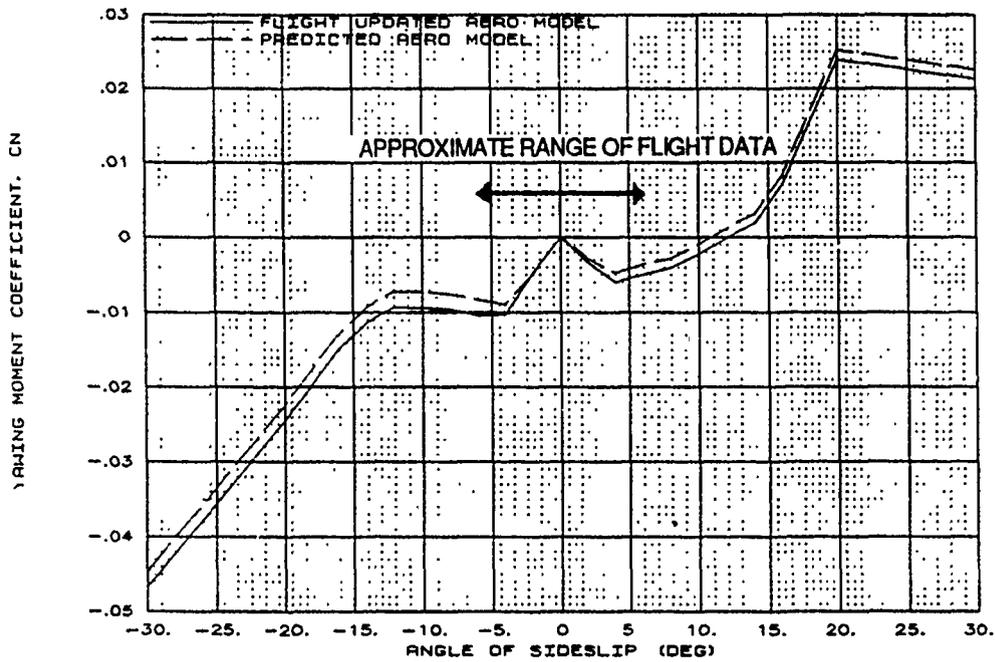
Figure B8 Updated Lateral-Directional Aerodynamics at 35 Degrees AOA
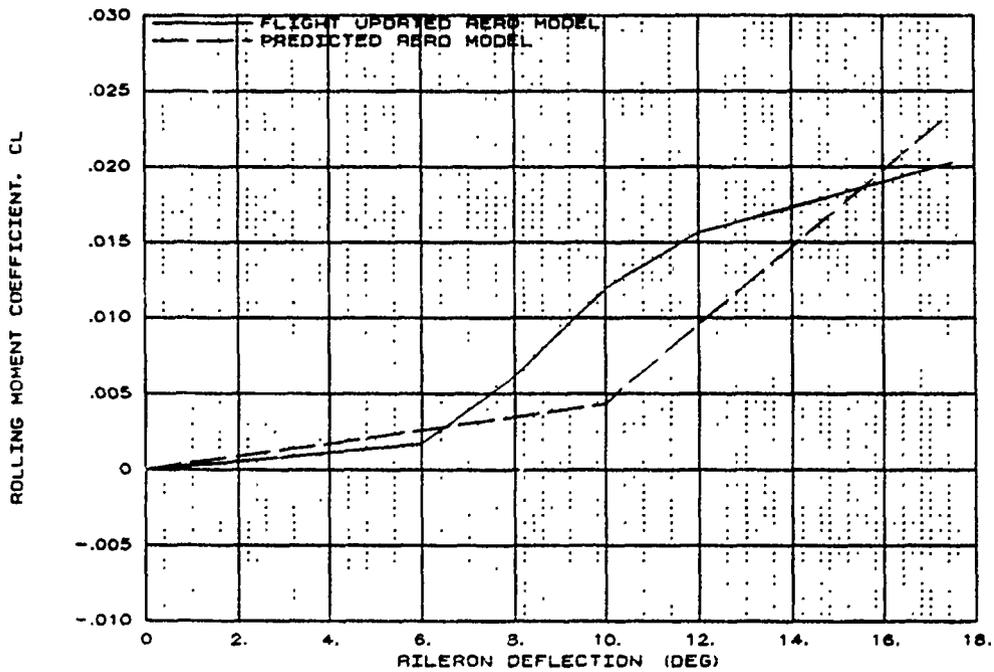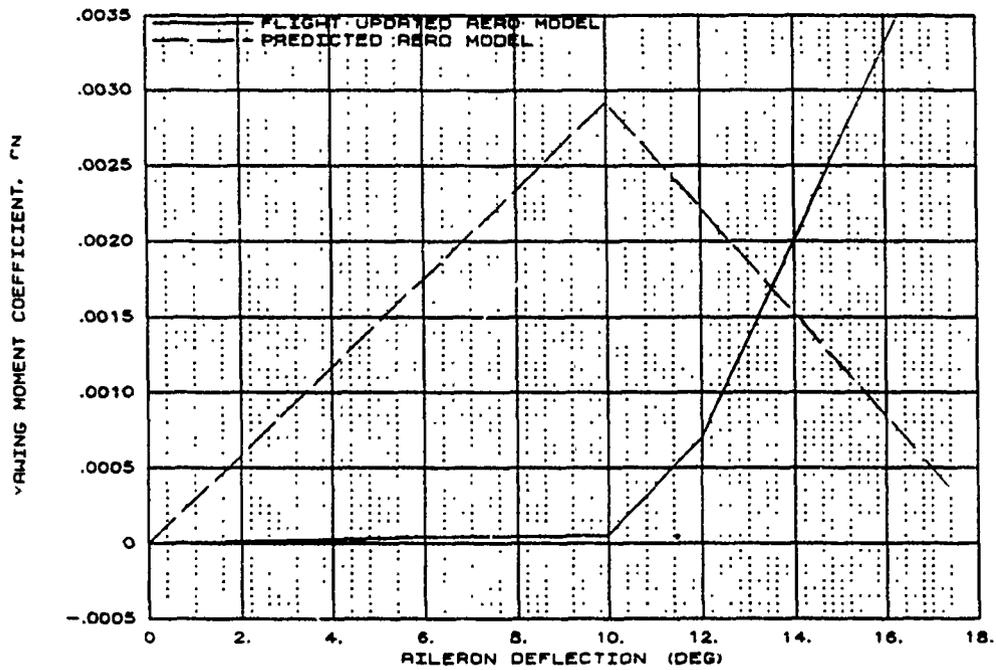
112

**Figure B8 Updated Lateral-Directional Aerodynamics
at 35 Degrees AOA (Continued)**

113

**Figure B8 Updated Lateral-Directional Aerodynamics
at 35 Degrees AOA (Concluded)**

114
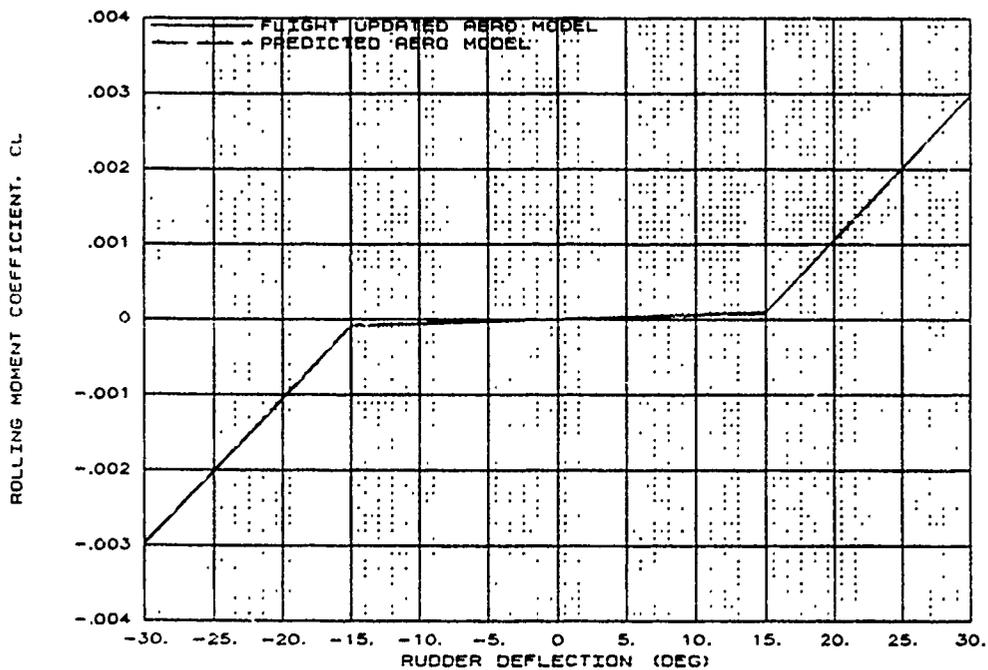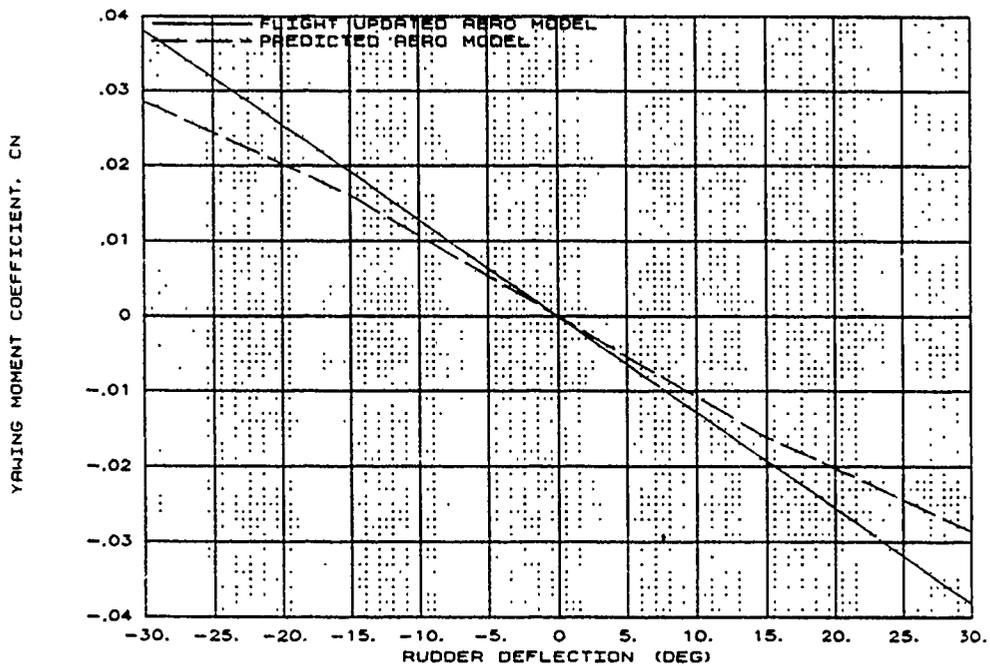
X-29 USAF S/N 820049
1 G ACC TRIM   XCG=449 in
AOA=40 deg   MACH=0.3   ALT=30K ft
AERO MODEL COMPARISONS
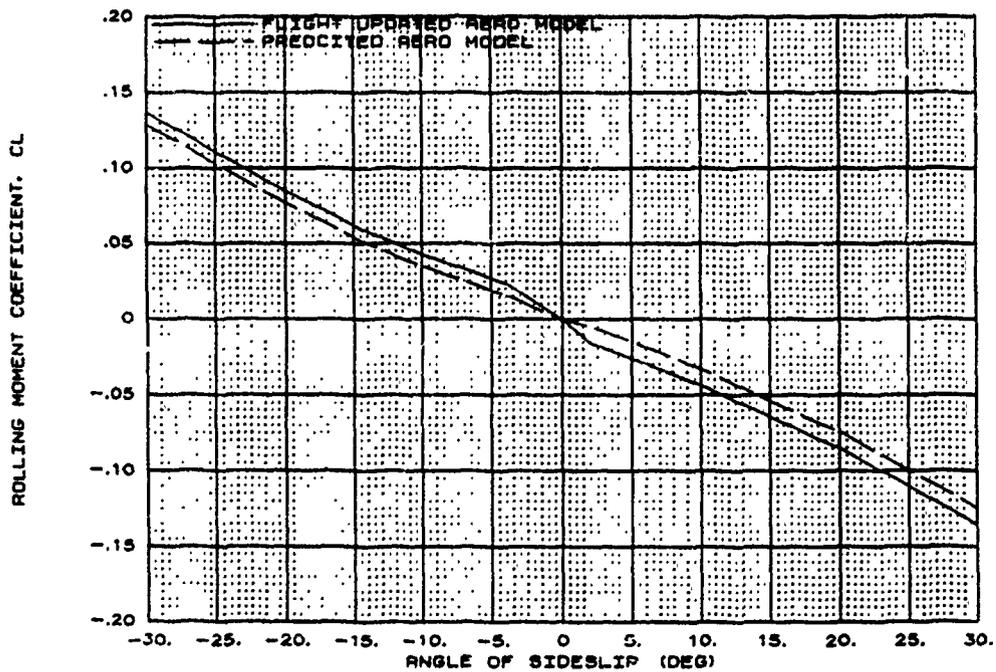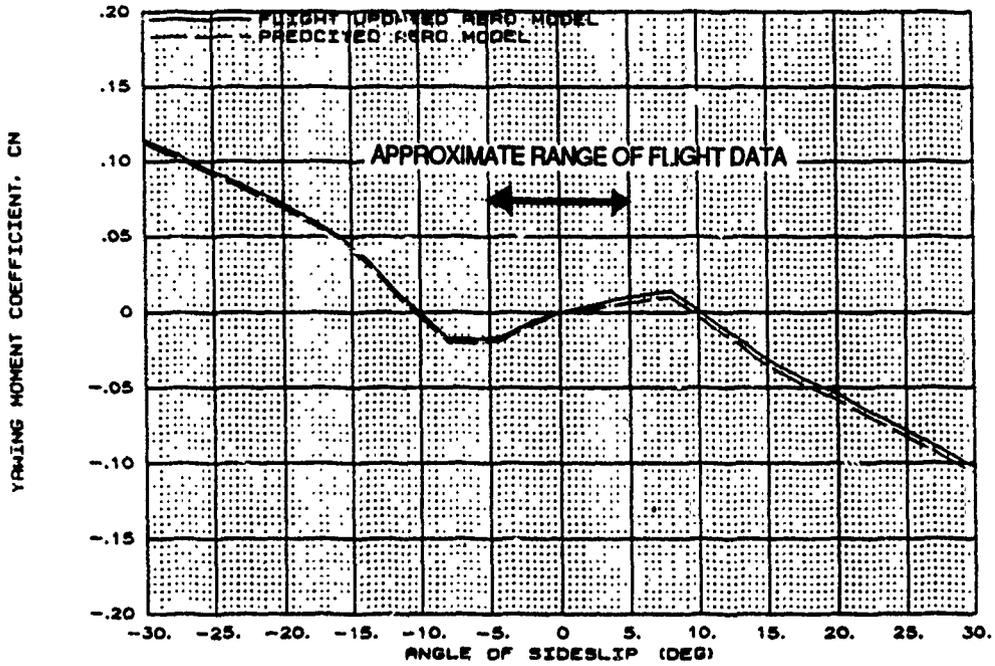
Figure B9 Updated Lateral-Directional Aerodynamics at 40 Degrees AOA
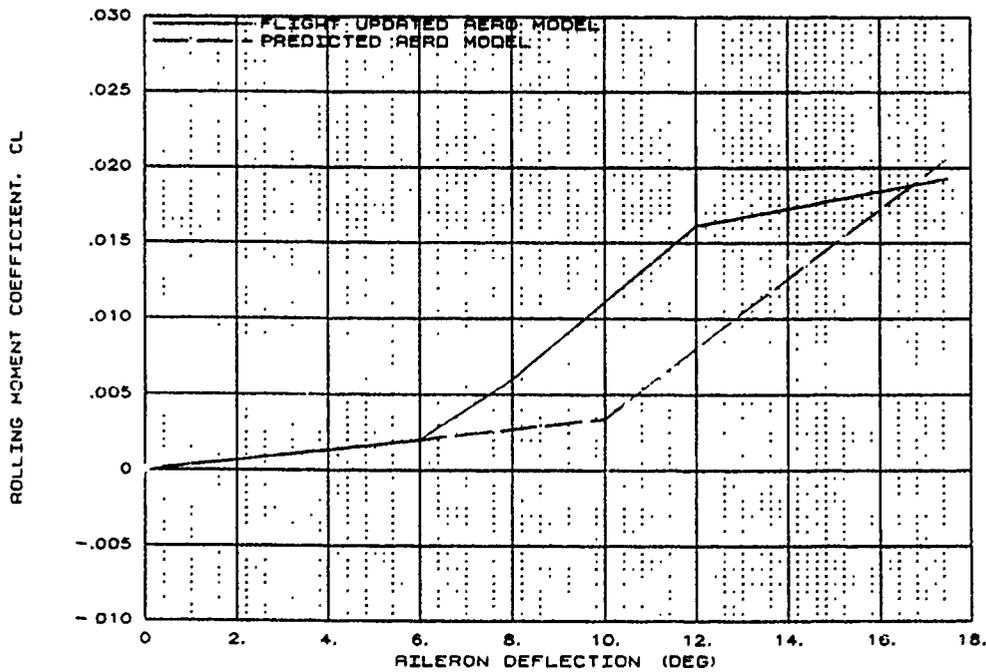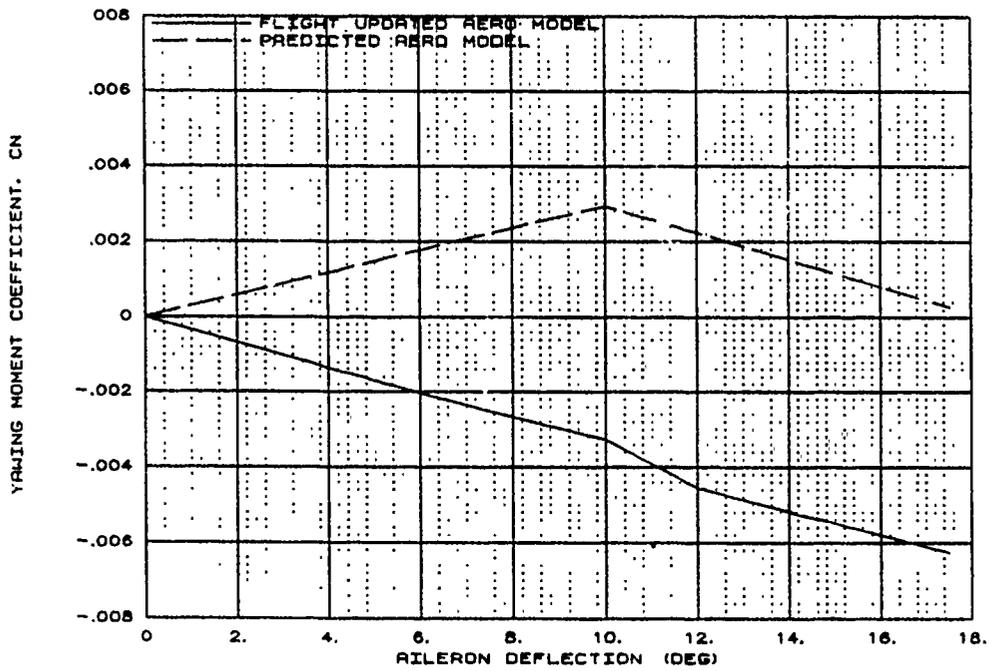
Figure B9 Updated Lateral-Directional Aerodynamics at 40 Degrees AOA (Continued)

116
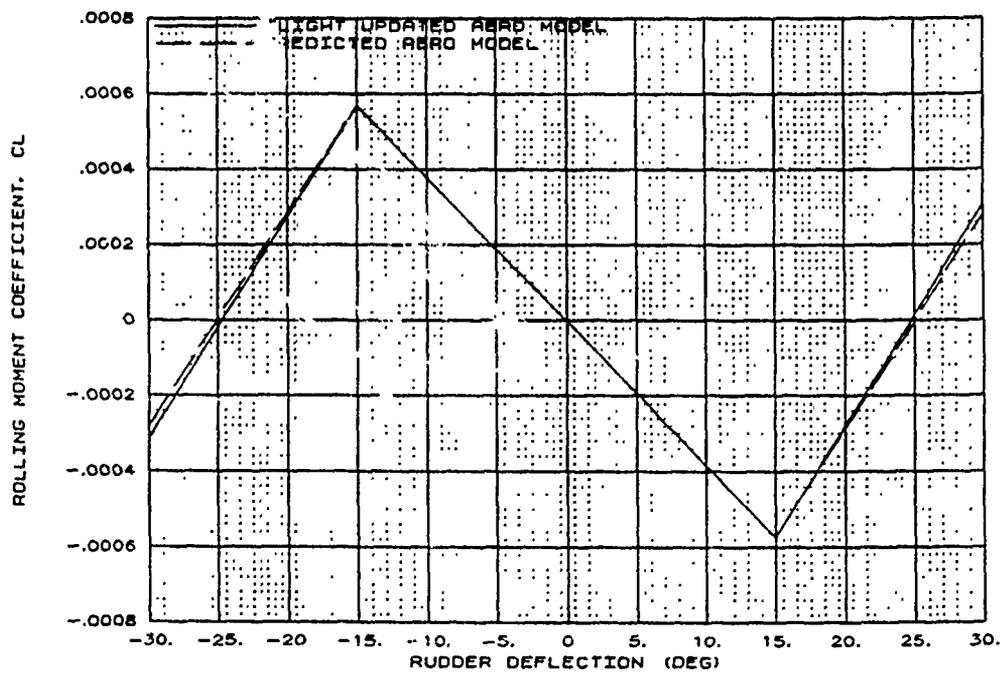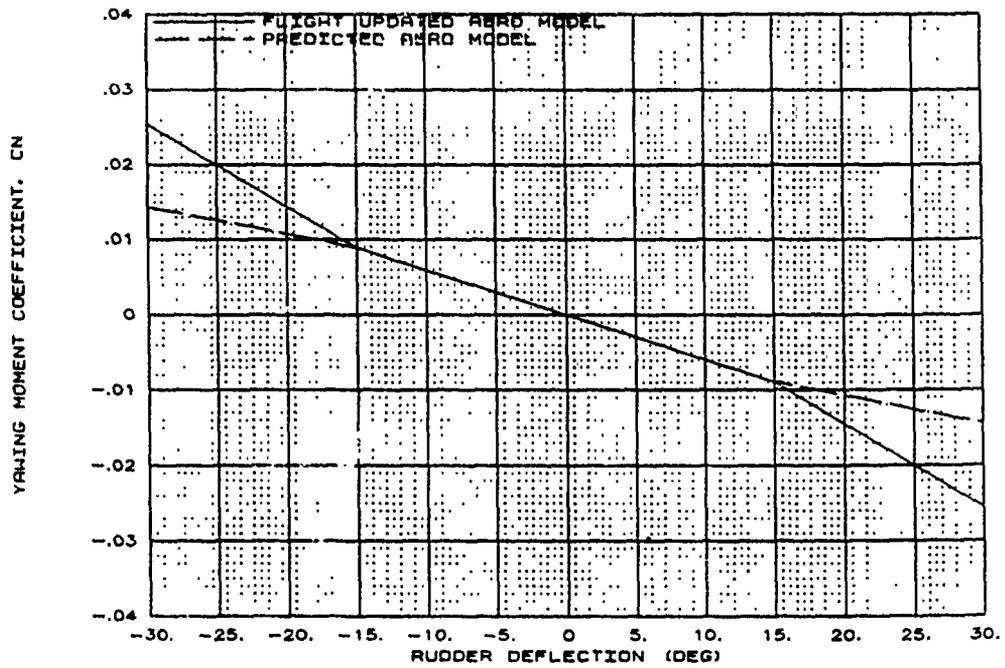
**Figure B9 Updated Lateral-Directional Aerodynamics
at 40 Degrees AOA (Concluded)**

117

X-29 USAF S/N 820049
1 G ACC TRIM   XCG=449 in
AOA=45 deg   MACH=0.3   ALT=30K ft
AERO MODEL COMPARISONS
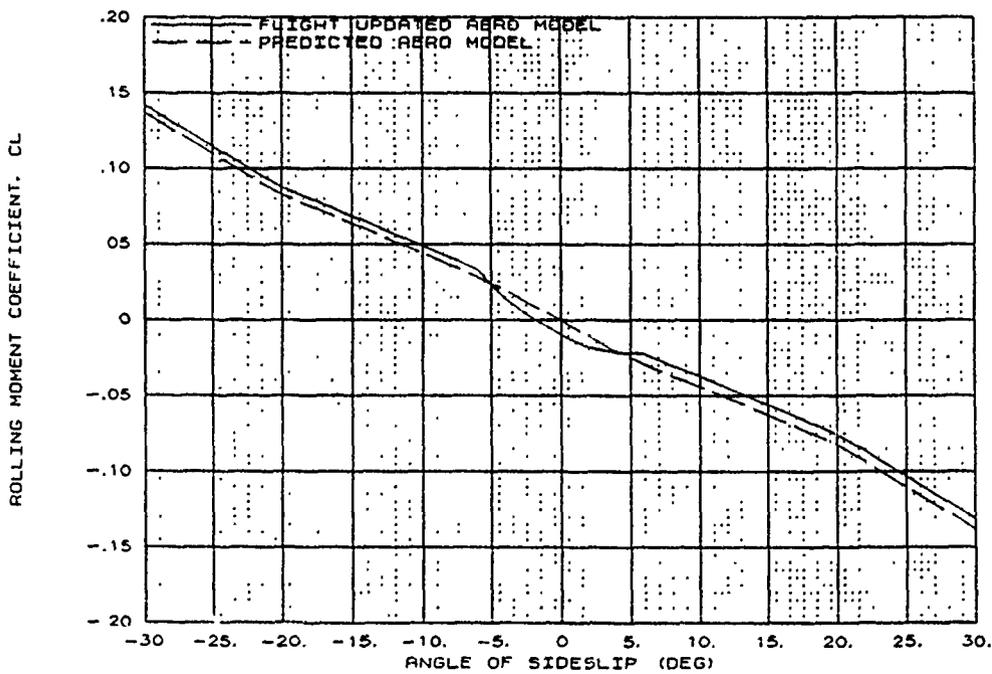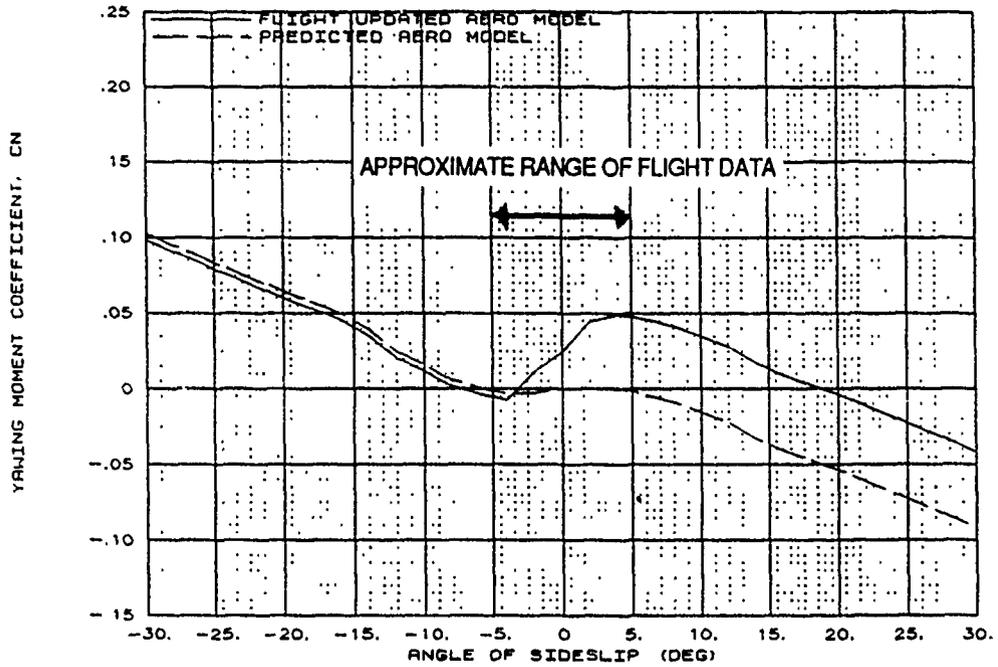
Figure B10 Updated Lateral-Directional Aerodynamics at 45 Degrees AOA
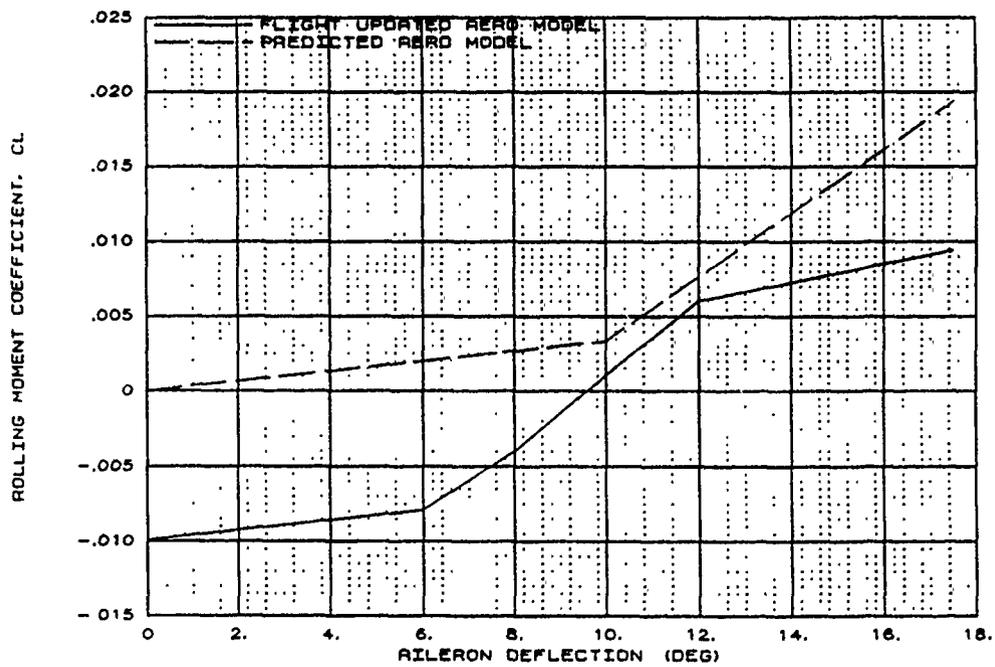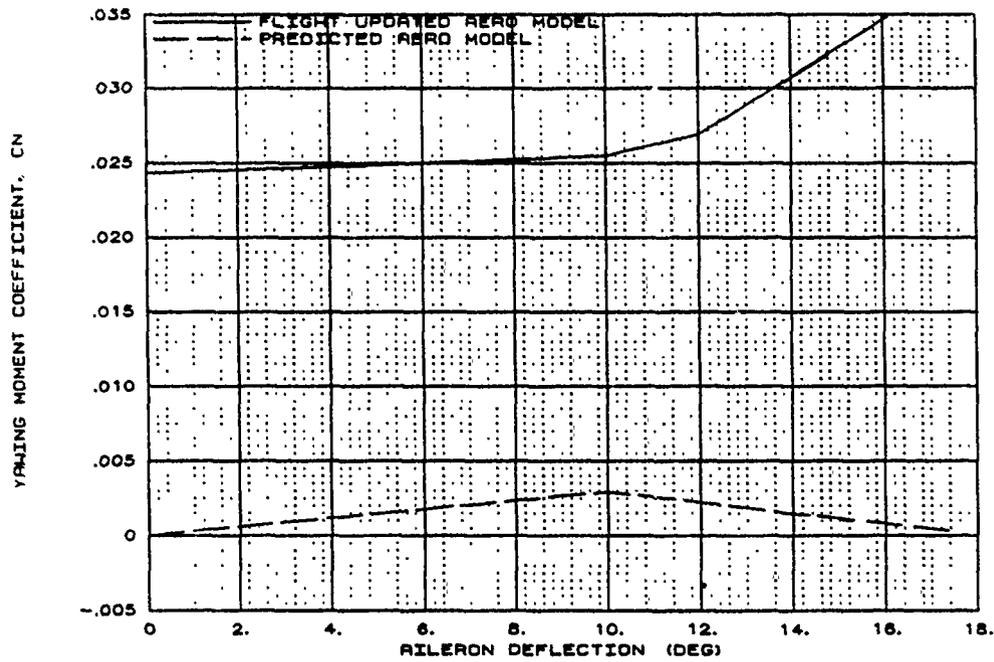
118

Figure B10 Updated Lateral-Directional Aerodynamics
at 45 Degrees AOA (Continued)

119
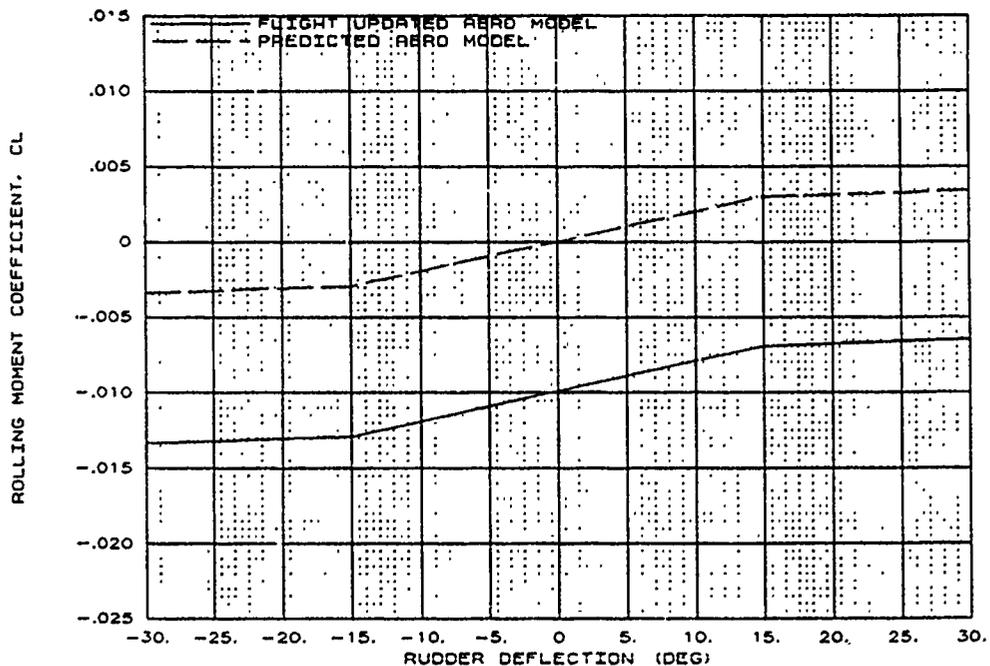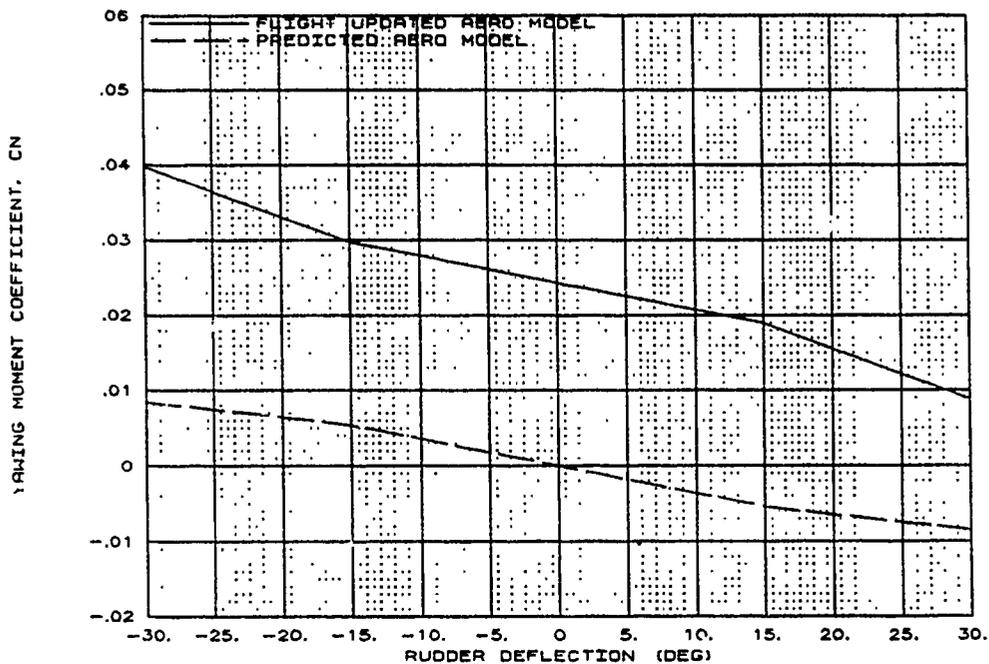
Figure B10 Updated Lateral-Directional Aerodynamics at 45 Degrees AOA (Concluded)

X-29 USAF S/N 820049
1 G ACC TRIM XCG=449 in
AOA=50 deg MACH=0.3 ALT=30K ft
AERO MODEL COMPARISONS
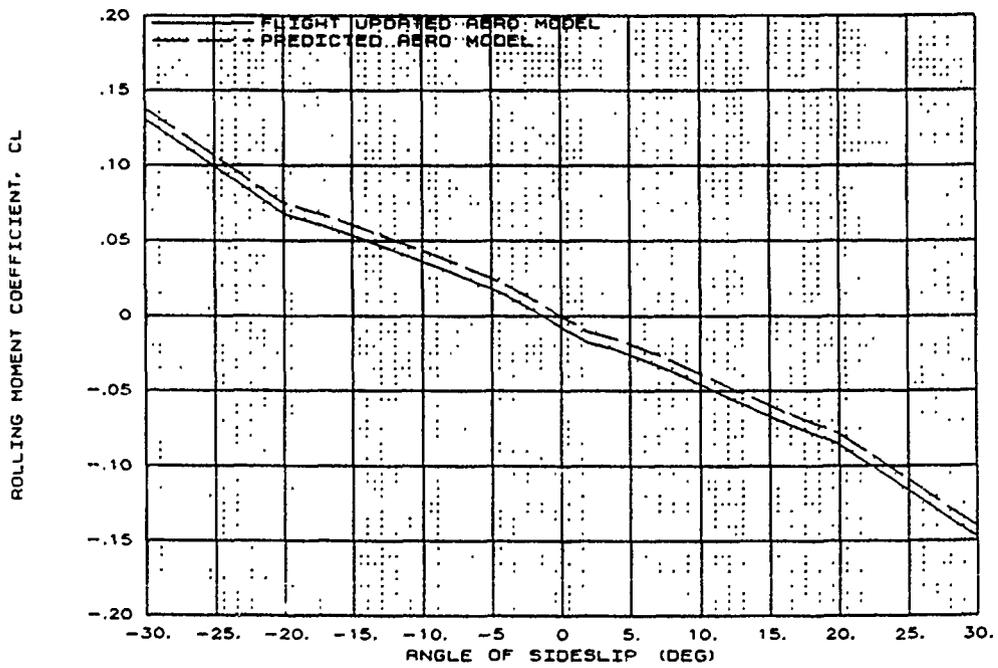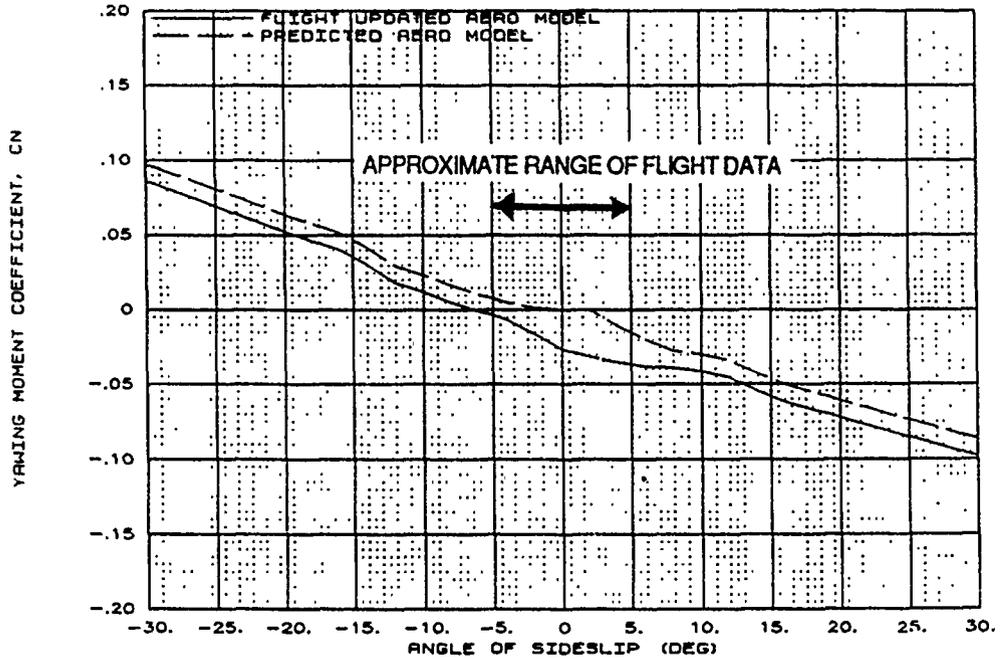
Figure B11 Updated Lateral-Directional Aerodynamics at 50 Degrees AOA
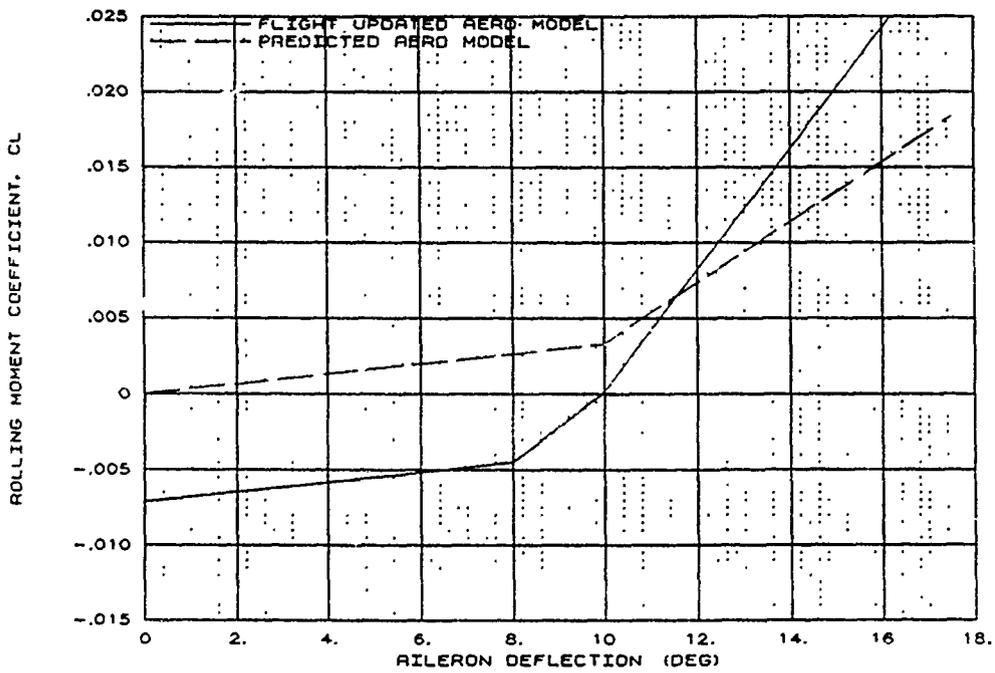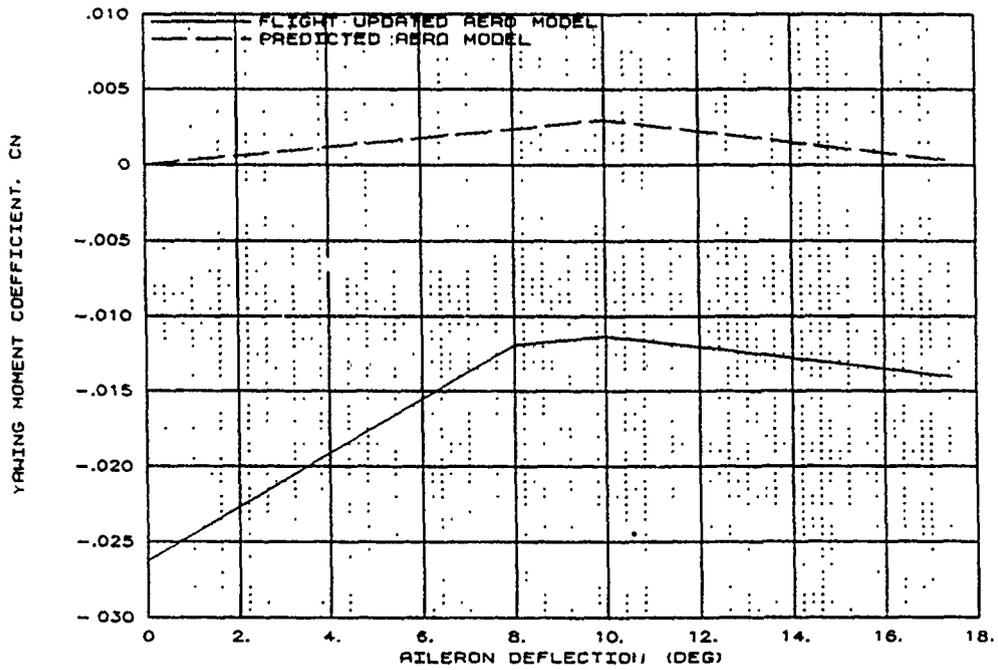
**Figure B11 Updated Lateral-Directional Aerodynamics
at 50 Degrees AOA (Continued)**
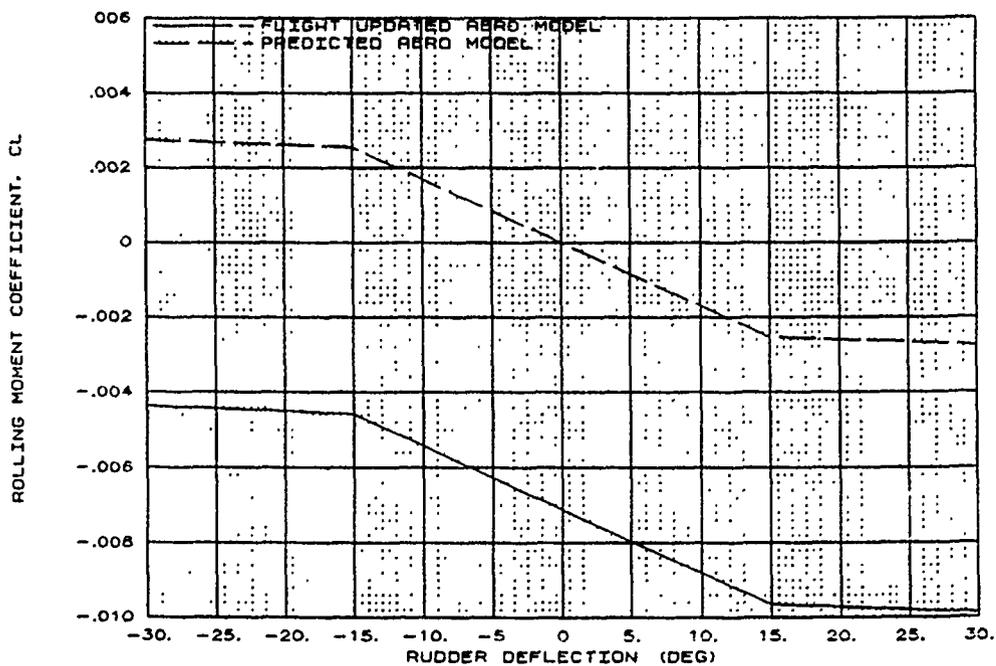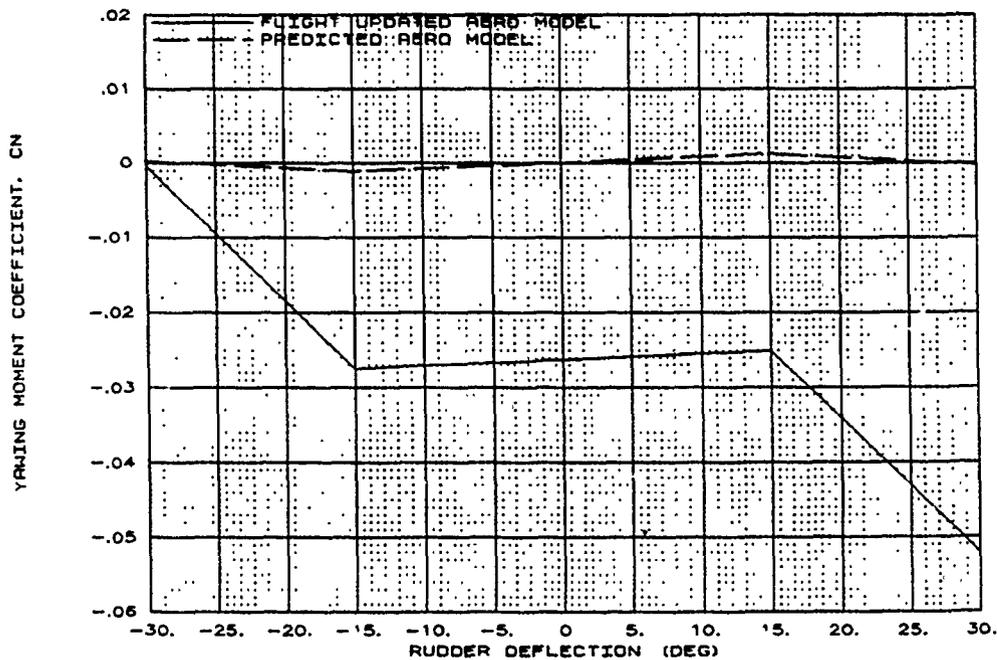
122

**Figure B11 Updated Lateral-Directional Aerodynamics
at 50 Degrees AOA (Concluded)**

123

X-29 USAF S/N 820049
1 G ACC TRIM
MIL POWER   XCG=447 in
ALT=38K TO 25K ft
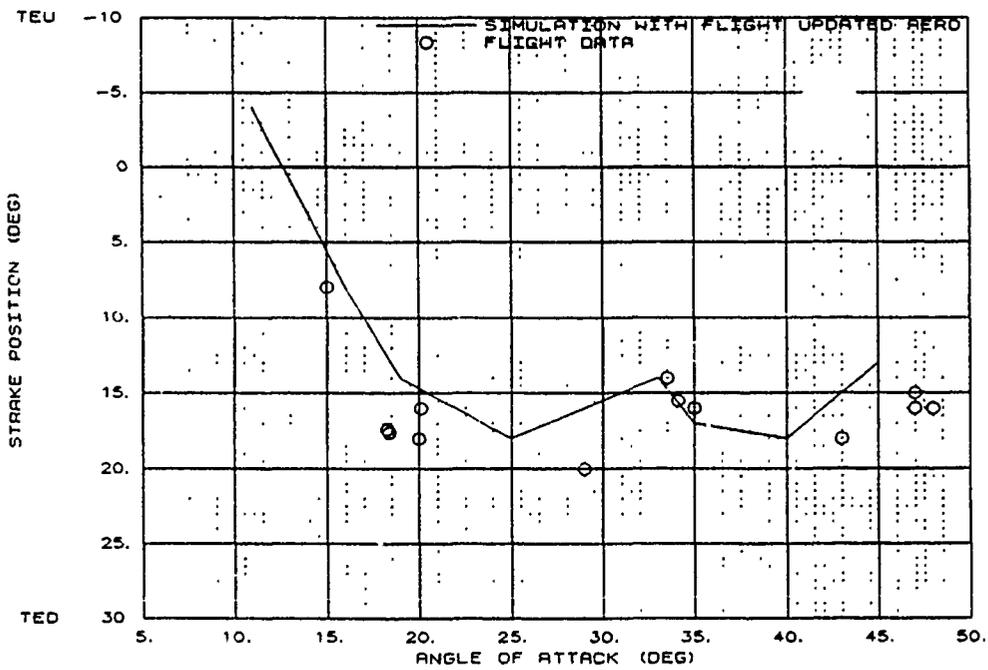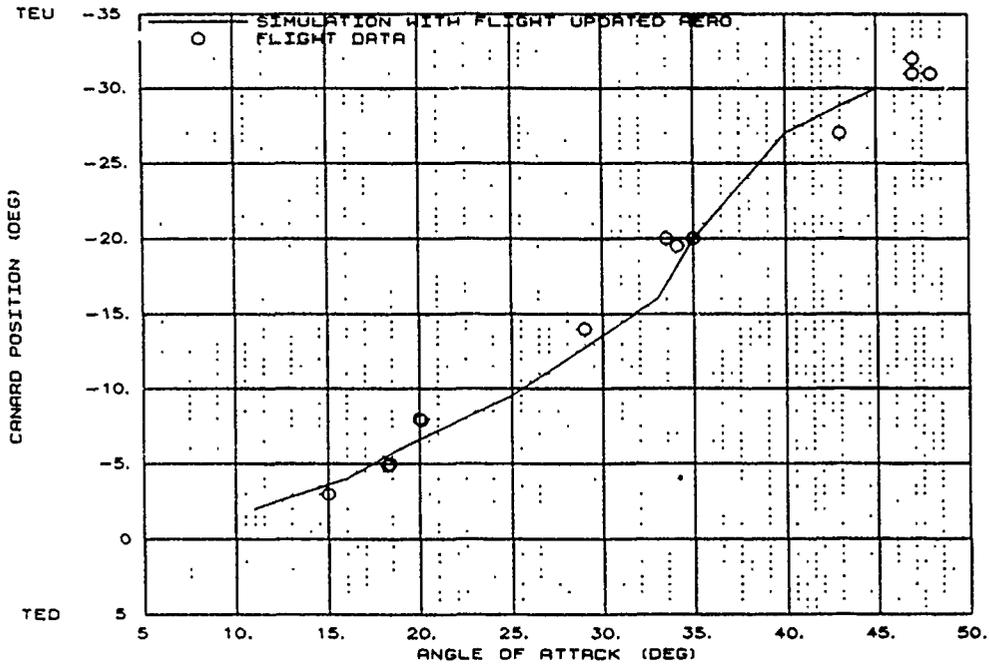
Figure B12 One-G ACC Trim at 447 Inches Center of Gravity

X-29 USAF S/N 820049
1-G ACC TRIM
MIL POWER   XCG=450 in
ALT=38K TO 25K ft
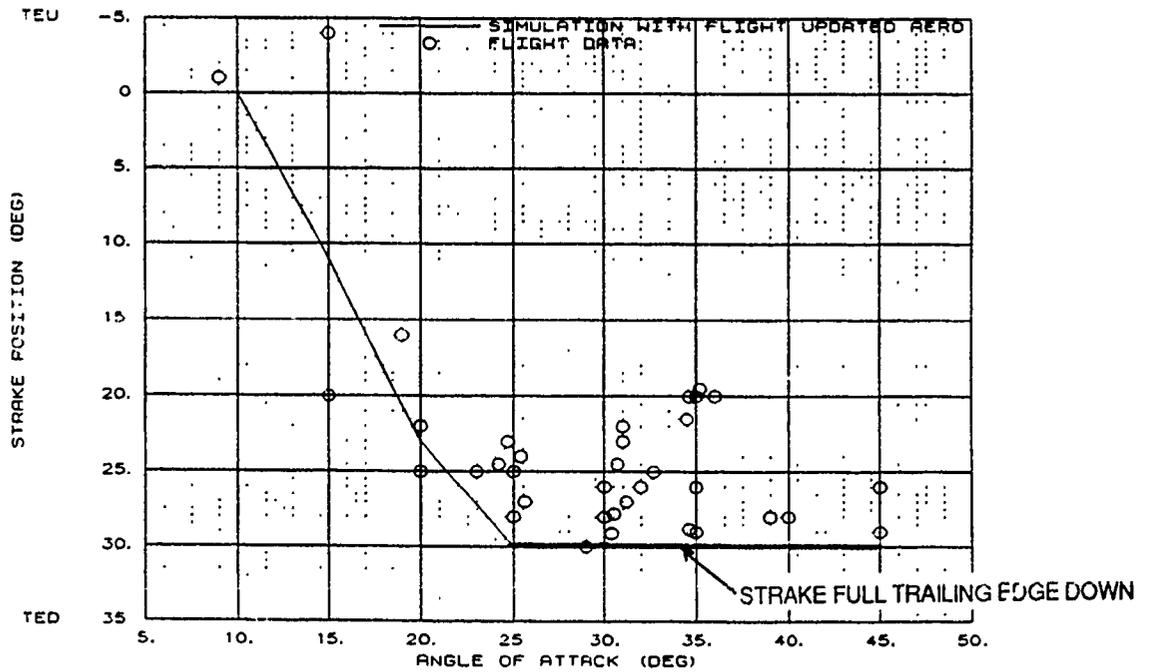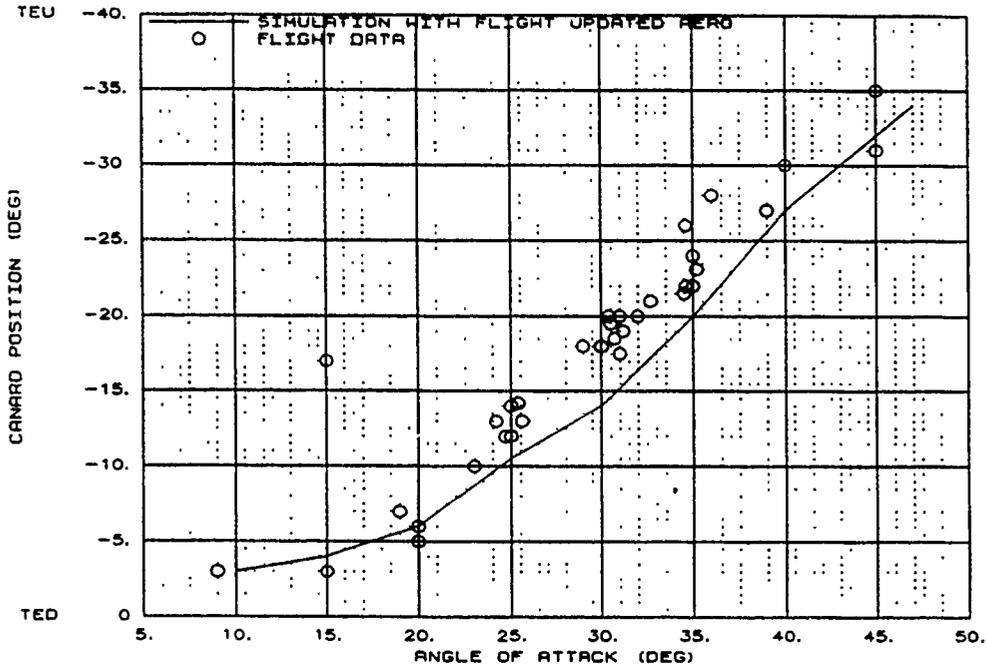
Figure B13 One-G ACC Trim at 450 Inches Center of Gravity

X-29 USAF S/N 820049
MAX POWER   XCG=449 in
200 KCAS ENTRY   ALT=20K ft
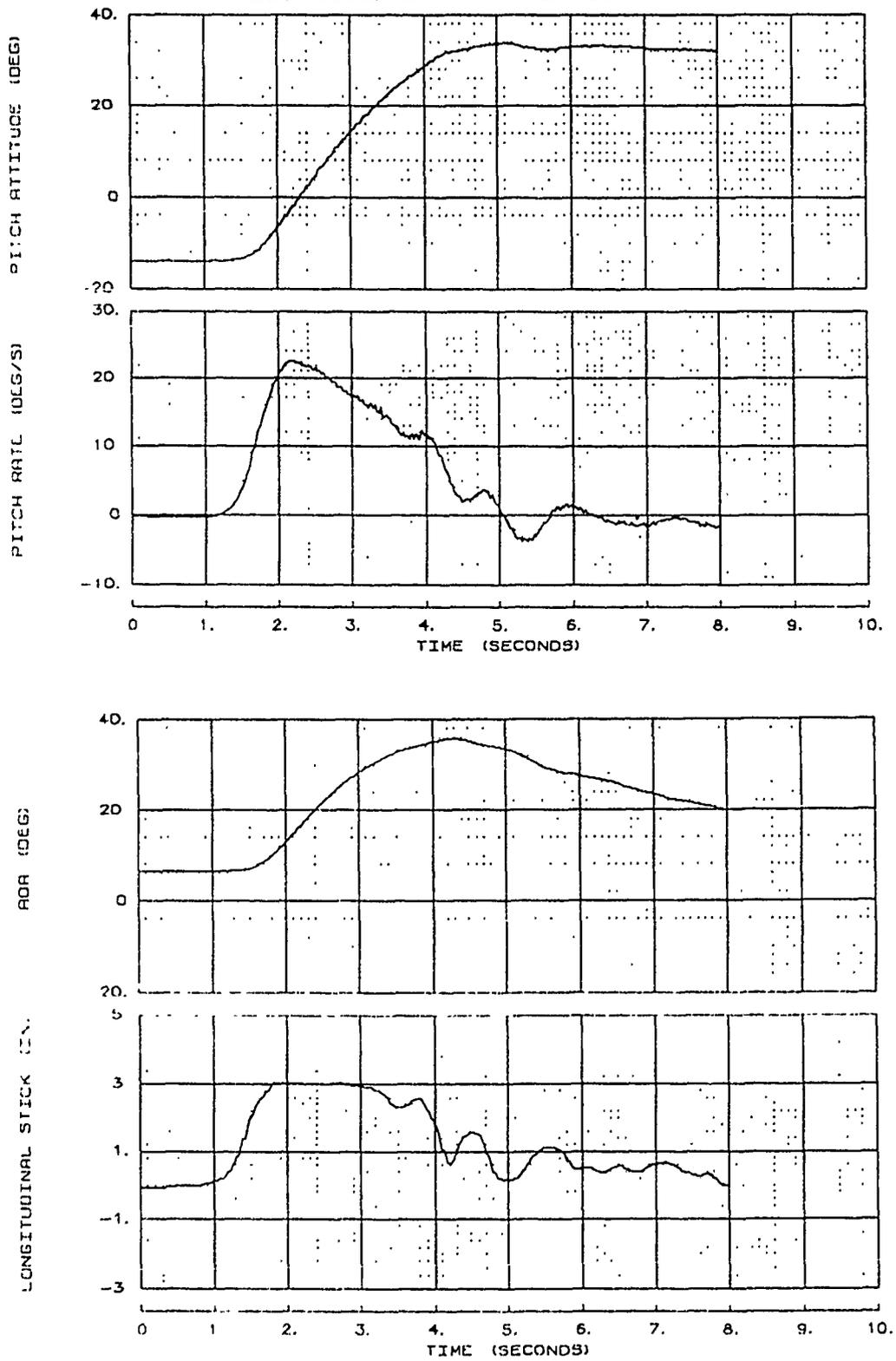
Figure B14 Pitch Attitude Capture Entered From 200 KCAS

126

X-29 USAF S/N 820049
1 G TRIM
MIL POWER   XCG=448 in
ALT=25K TO 17K ft
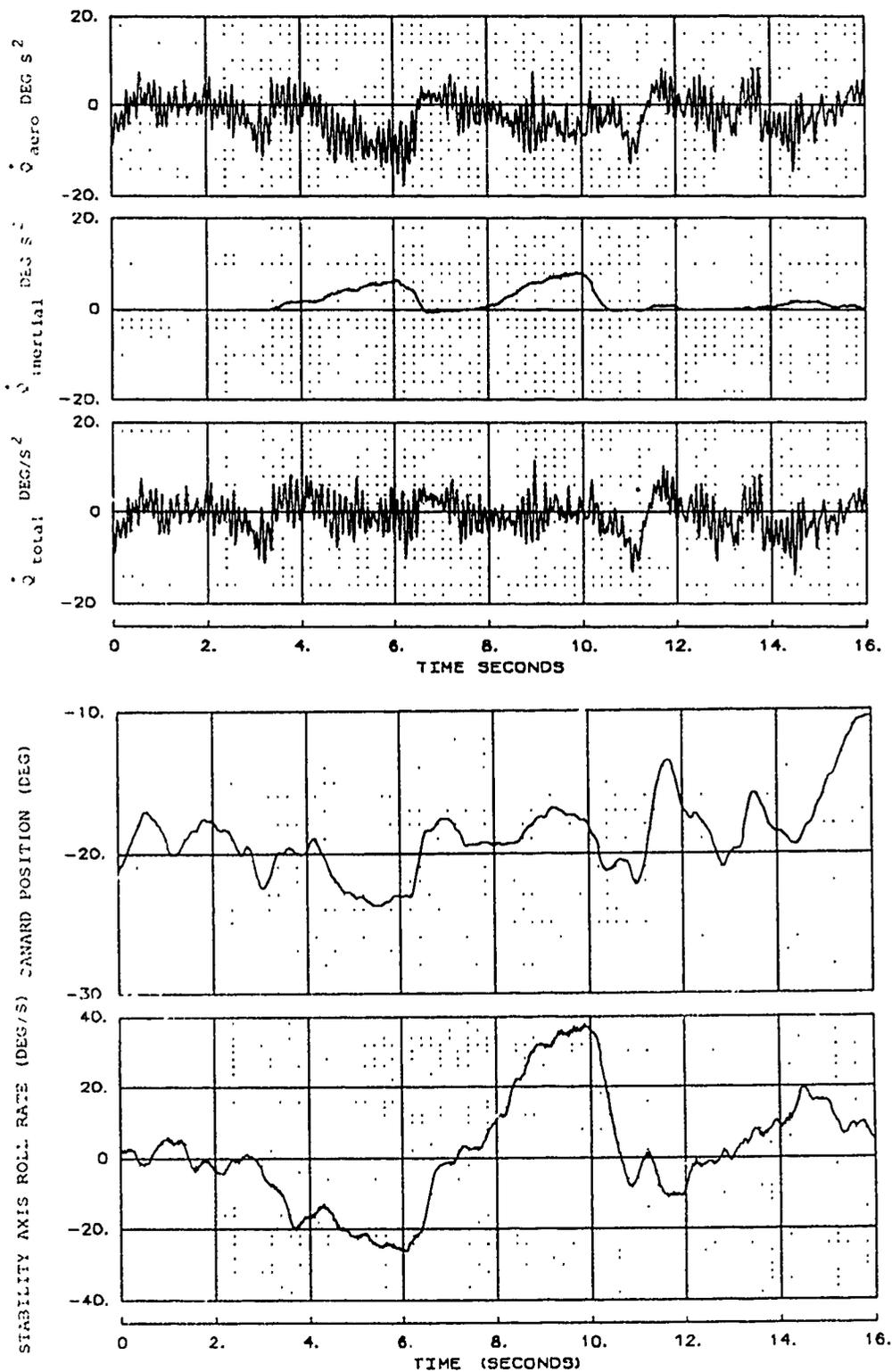
Figure B15 Canard Control of Inertial Coupling During a 1-G Roll

127
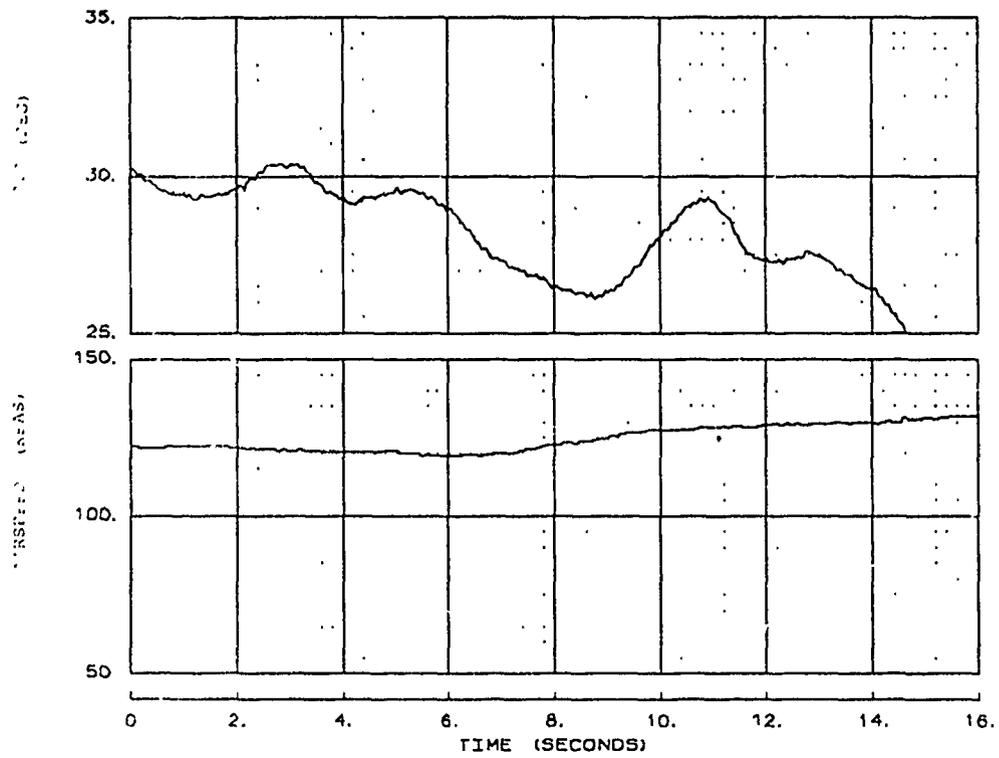
Figure B15 Canard Control of Inertial Coupling During a 1-G Roll (Concluded)

128

Figure B16 One-G Pull-up From 40 to 67 Degrees AOA

129

Figure B16 One-G Pull-up From 40 to 67 Degrees AOA (Continued)

130

Figure B16 One-G Pull-up From 40 to 67 Degrees AOA (Continued)

131

Figure B16 One-G Pull-up From 40 to 67 Degrees AOA (Continued)

132

Figure B16 One-G Pull-up From 40 to 67 Degrees AOA (Continued)

133

Figure B16 One-G Pull-up From 40 to 67 Degrees AOA (Continued)

134

X-29 USAF S/N 820049

XCG=445.4 IN.   IXX=4564   IYY=53200   IZZ=58300   IXZ=2570
1-G TO 67 DEG   BLK IX-AA01

Figure B16 One-G Pull-up From 40 to 67 Degrees AOA (Continued)

Lon Stick
Position
(in)

Pitch Rate
(deg/sec)

Canard Position
(deg)

Flap Position
(deg)

Strake Position
(deg)

ELAPSED TIME (SEC)

135

X-29 USAF S/N 820049
XCG=445.4 IN.   IXX=4564   IYY=53200 IZZ=58300   IXZ=2570
1-G TO 67 DEG   BLK IX-AA01

Figure B16 One-G Pull-up From 40 to 67 Degrees AOA (Continued)

X-29 USAF S/N 82C049

XCG=445.4 IN. IXX=4564 IYY=53200 IZZ=58300 IXZ=2570
1-G TO 67 DEG BLK IX-AA01

Figure B16 One-G Pull-up From 40 to 67 Degrees AOA (Continued)

137

Figure B16 One-G Pull-up From 40 to 67 Degrees AOA (Continued)

138

X-29 USAF S/N 820049

XCG=445.4 IN.   IXX=4564   IYY=53200   IZZ=58300   IXZ=2570

1-G TO 67 DEG   BLK IX-AA01

Figure B16 One-G Pull-up From 40 to 67 Degrees AOA (Continued)

139

Figure B16 One-G Pull-up From 40 to 67 Degrees AOA (Continued)

140

Figure B16 One-G Pull-up From 40 to 67 Degrees AOA (Concluded)

Figure B17 One-G Pull-up From 40 to 55 Degrees AOA

Figure B17 One-G Pull-up From 40 to 55 Degrees AOA (Continued)

143

Figure B17 One-G Pull-up From 40 to 55 Degrees AOA (Continued)

144

Figure B17 One-G Pull-up From 40 to 55 Degrees AOA (Continued)

Figure B17 One-G Pull-up From 40 to 55 Degrees AOA (Continued)

146

X-29 USAF S/N 820049

XCG=447.1 IN.

IXX=4564 IYY=52610 IZZ=57770 IXZ=2584

1-G TO 55 DEG BLK IX-AA01

Figure B17 One-G Pull-up From 40 to 55 Degrees AOA (Continued)

147

Figure B17 One-G Pull-up From 40 to 55 Degrees AOA (Continued)

148

X-29 USAF S/N 820049

XCG=447.1 IN.   IXX=4564   IYY=52610   IZZ=57770   IXZ=2594
1-G TO 55 DEG   BLK IX-AA01

Figure B17 One-G Pull-up From 40 to 55 Degrees AOA (Continued)

149

Figure B17 One-G Pull-up From 40 to 55 Degrees AOA (Continued)

150

Figure B17 One-G Pull-up From 40 to 55 Degrees AOA (Continued)

151

X-29 USAF S/N 820049

XCG=447.1 IN. IXX=4564 IYY=52610 IZZ=57770 IXZ=2594
1-G TO 55 DEG BLK IX-AA01

Figure B17 One-G Pull-up From 40 to 55 Degrees AOA (Continued)

152

Figure B17 One-G Pull-up From 40 to 55 Degrees AOA (Continued)

153

Figure B17 One-G Pull-up From 40 to 55 Degrees AOA (Concluded)

154

X-29 USAF S/N 820049
MIL POWER   XCG=452 in   1 G ACC TRIM
AOA=10 deg   ALT=38K TO 25K ft

PREDICTED AERO DATA AT ZERO
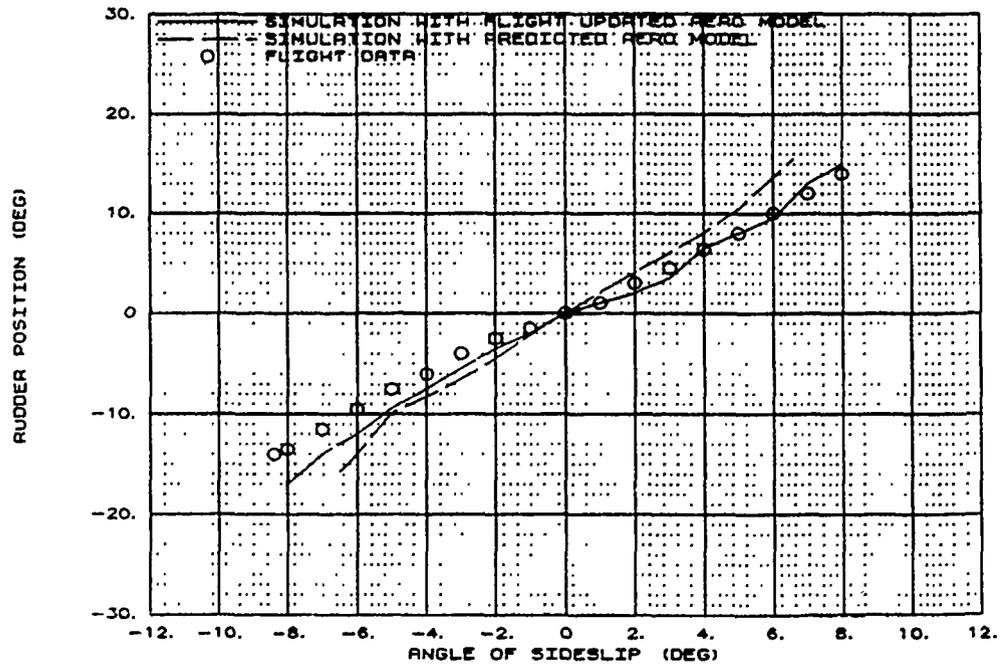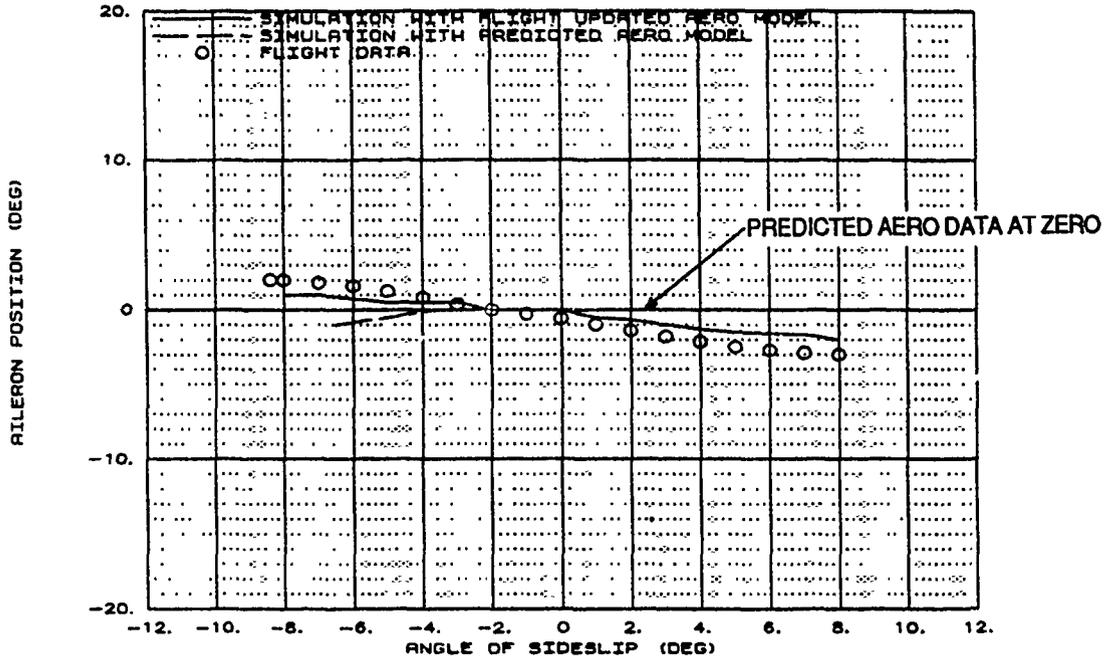
Figure B18   Wings–Level Sideslip at 10 Degrees AOA

155

X-29 USAF S/N 820049
MIL POWER   XCG=446 in   1 G ACC TRIM
AOA=15 deg   ALT=38K TO 25K ft
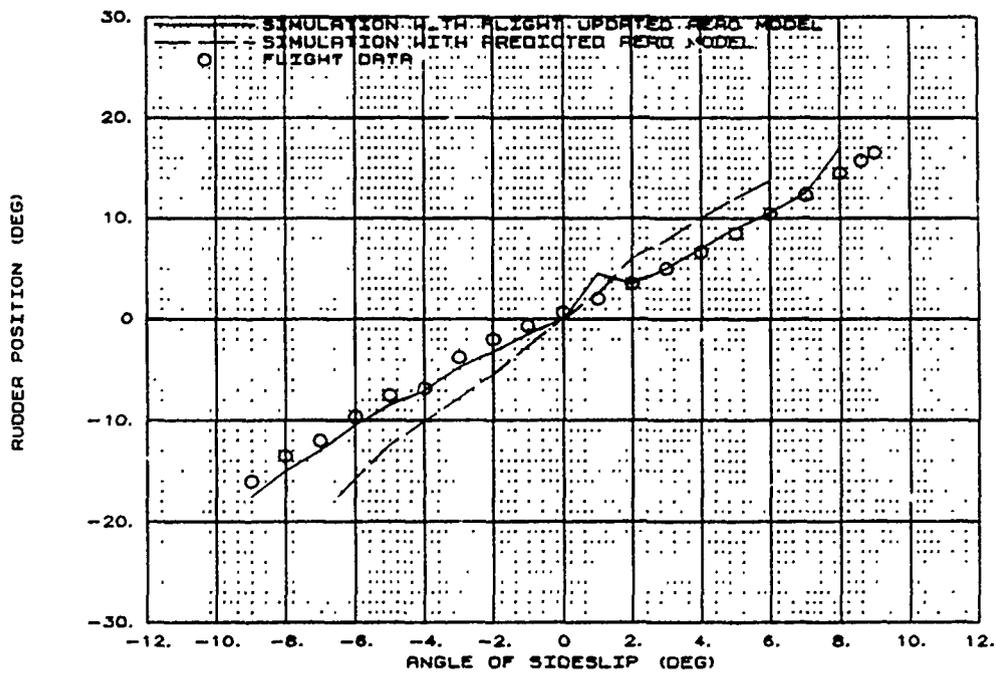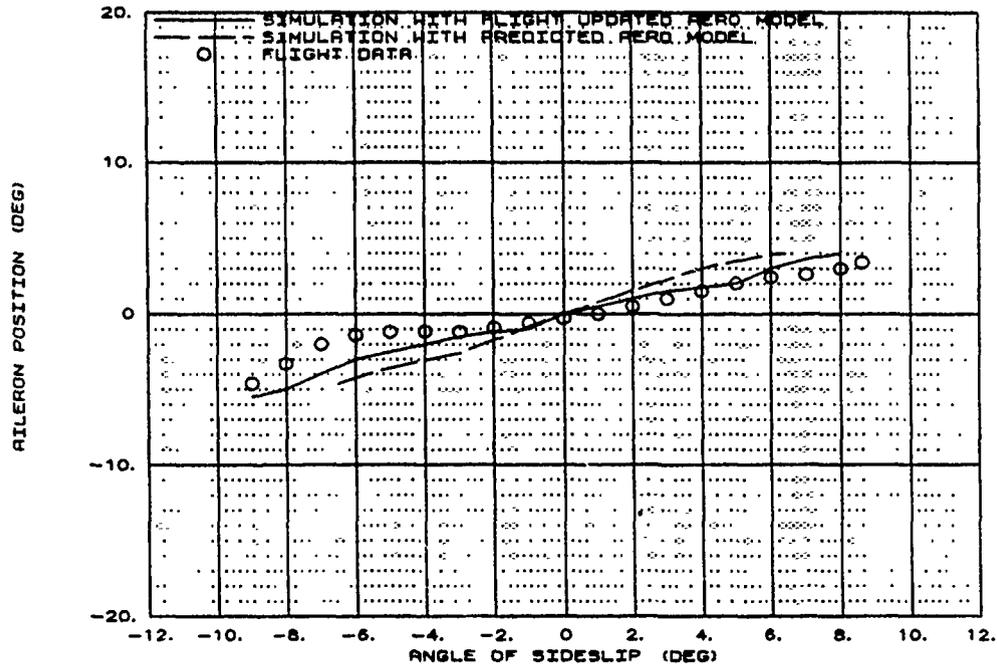
Figure B19   Wings-Level Sideslip at 15 Degrees AOA

156

MIL POWER   XCG=448 in   1 G ACC TRIM
AOA=20 deg   ALT=38K TO 25K ft
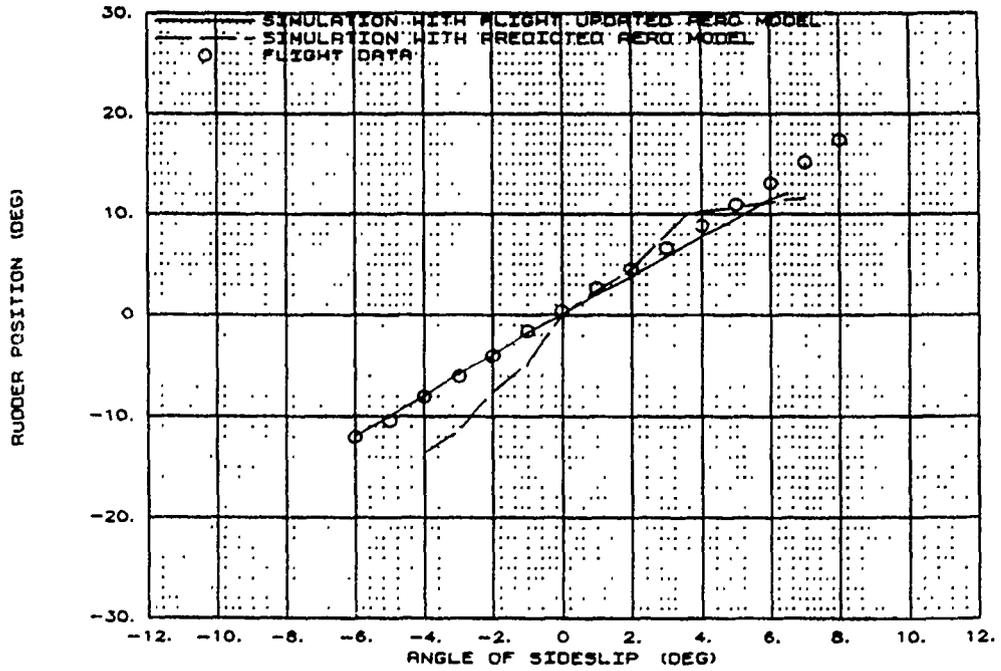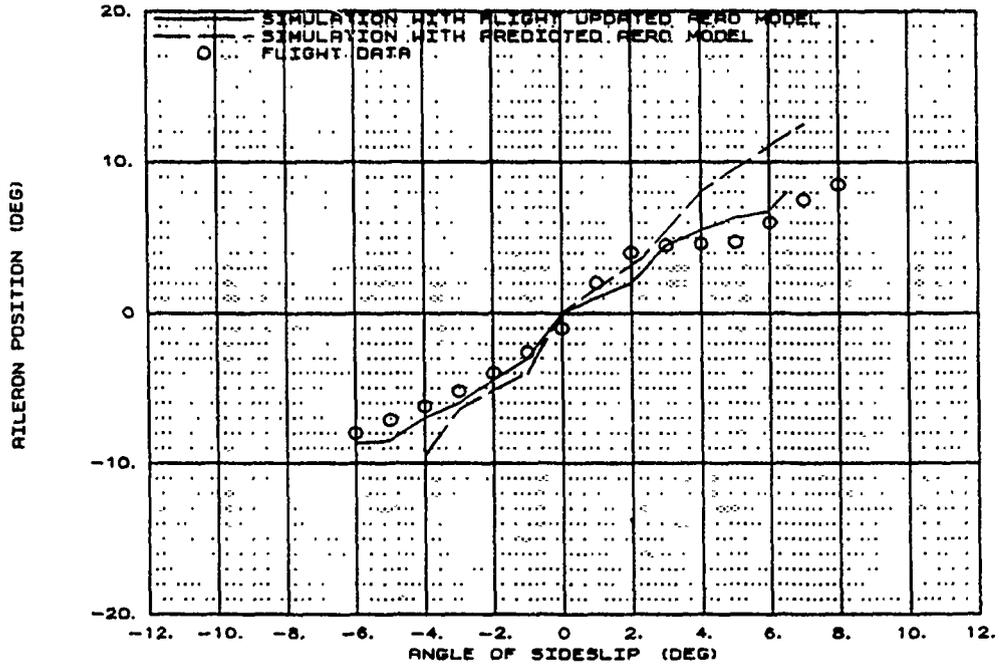
Figure B20   Wings-Level Sideslip at 20 Degrees AOA

X-29 USAF S/N 820049
MIL POWER   XCG=450 in   1 G ACC TRIM
AOA=25 deg   ALT=38K TO 25K ft
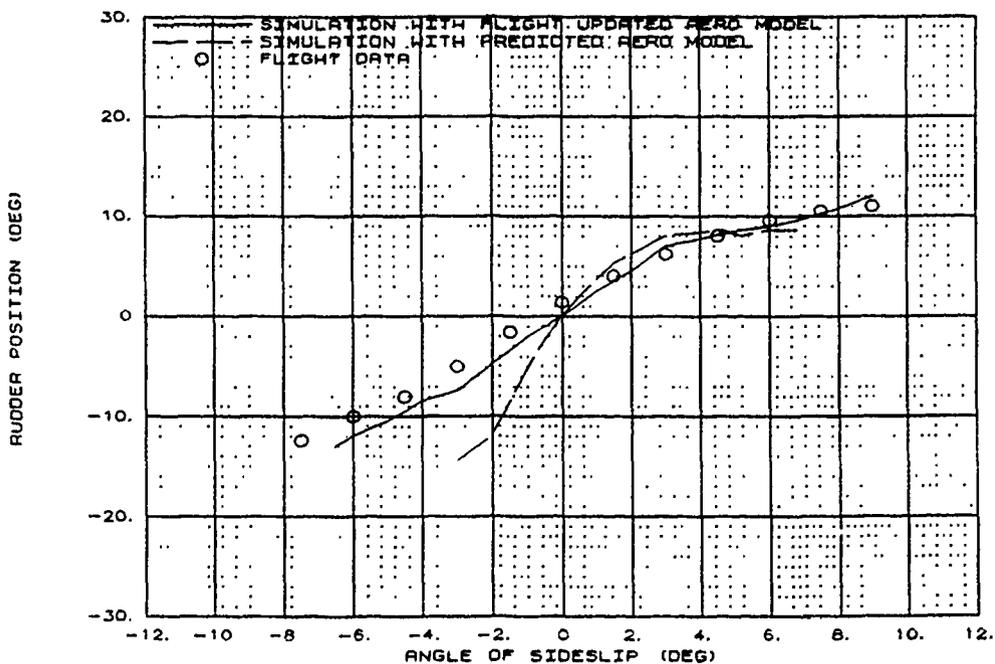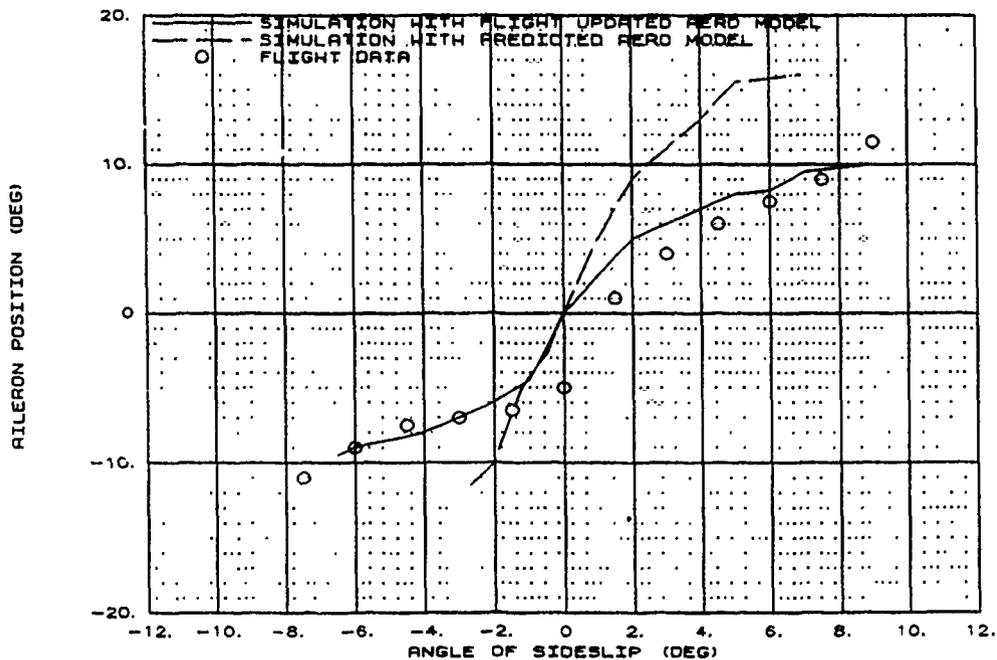
Figure B21   Wings-Level Sideslip at 25 Degrees AOA

X-29 USAF S/N 820049
MIL POWER   XCG=448 in   1 G ACC TRIM
AOA=30 deg   ALT=38K TO 25K ft
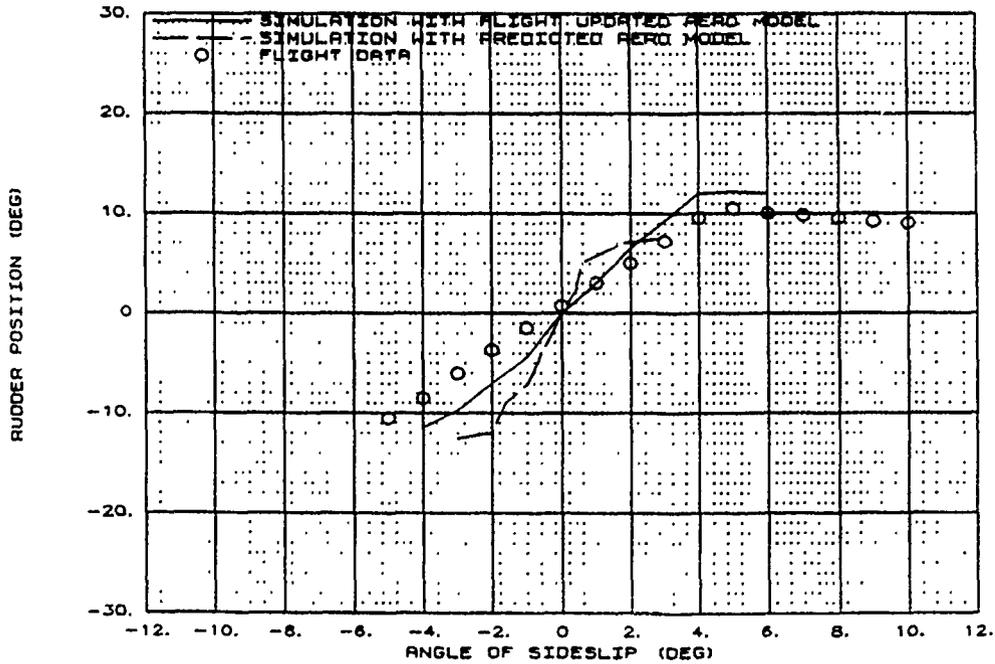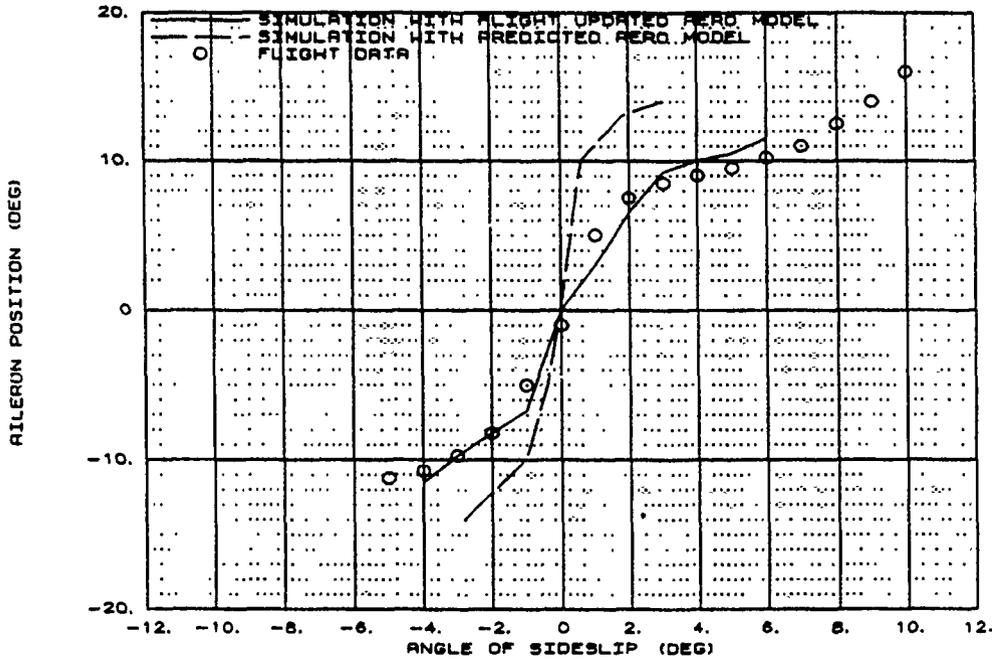
Figure B22   Wings-Level Sideslip at 30 Degrees AOA

159

X-29 USAF S/N 820049
MIL POWER   XCG=449 in   1 G ACC TRIM
AOA=35 deg   ALT=39K TO 25K ft
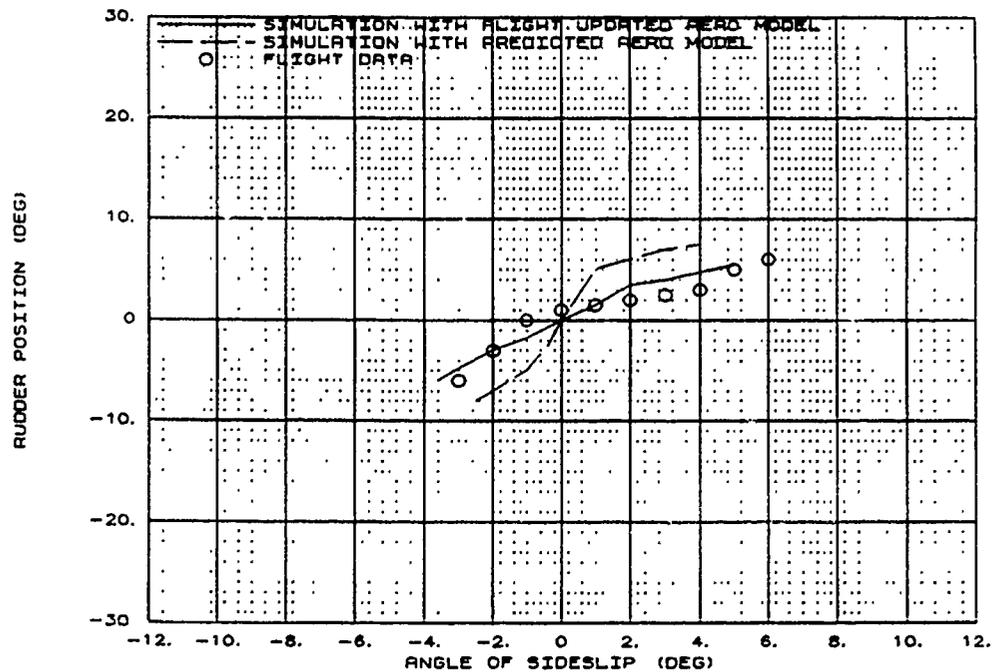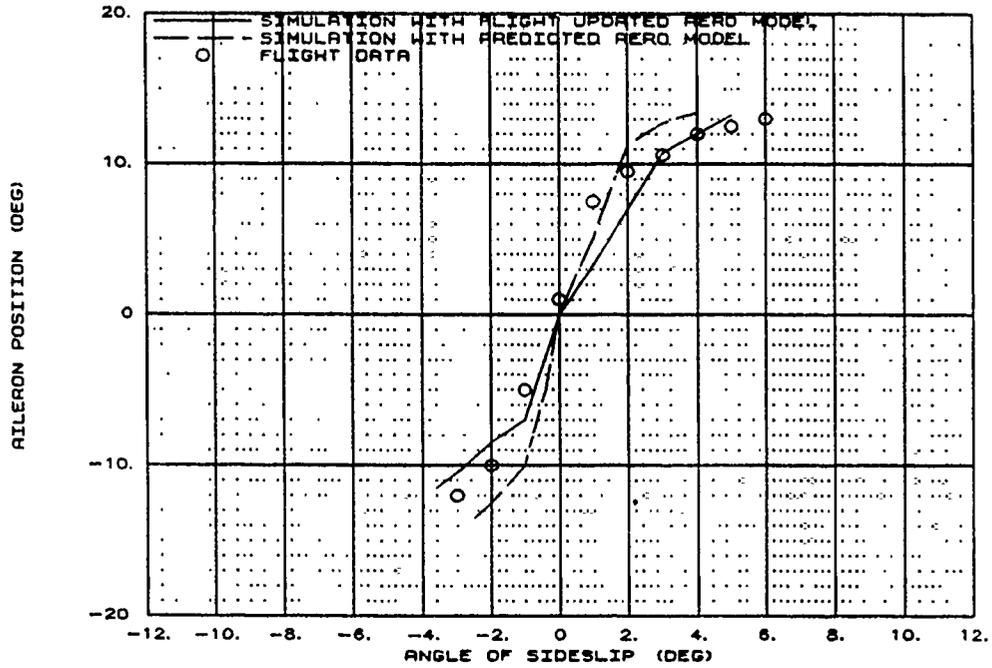
Figure B23   Wings-Level Sideslip at 35 Degrees AOA

160

X-29 USAF S/N 820049
MIL POWER   XCG=451 in   1 G ACC TRIM
AOA=40 deg   ALT=38K TO 25K ft
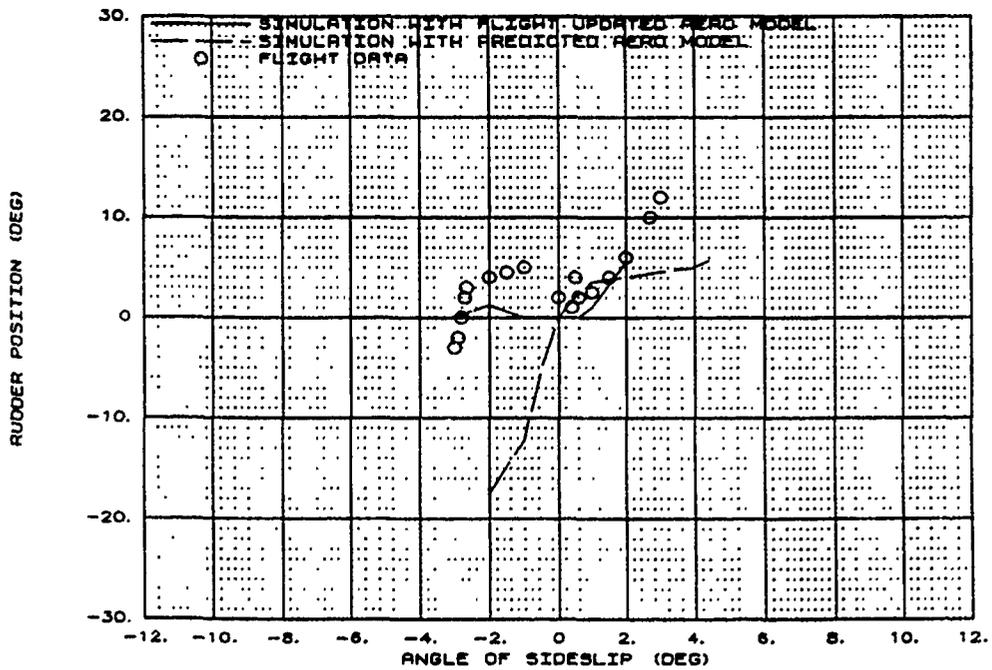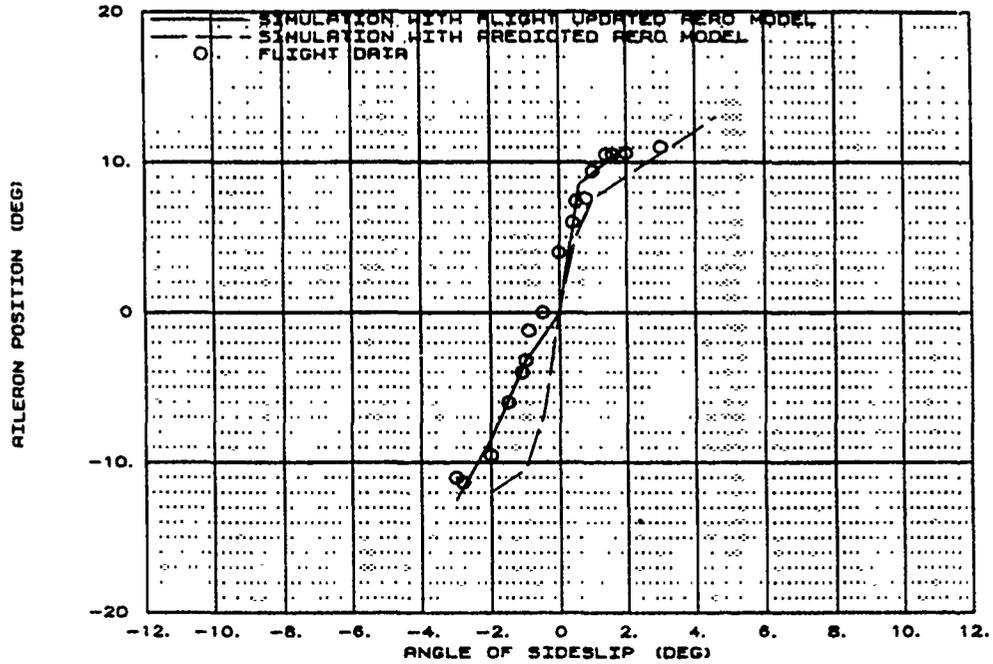
Figure B24   Wings-Level Sideslip at 40 Degrees AOA

161

X-29 USAF S/N 820049
MIL POWER   ALT=38K TO 25K ft
BLOCKIX-AA01 CONTROL LAWS
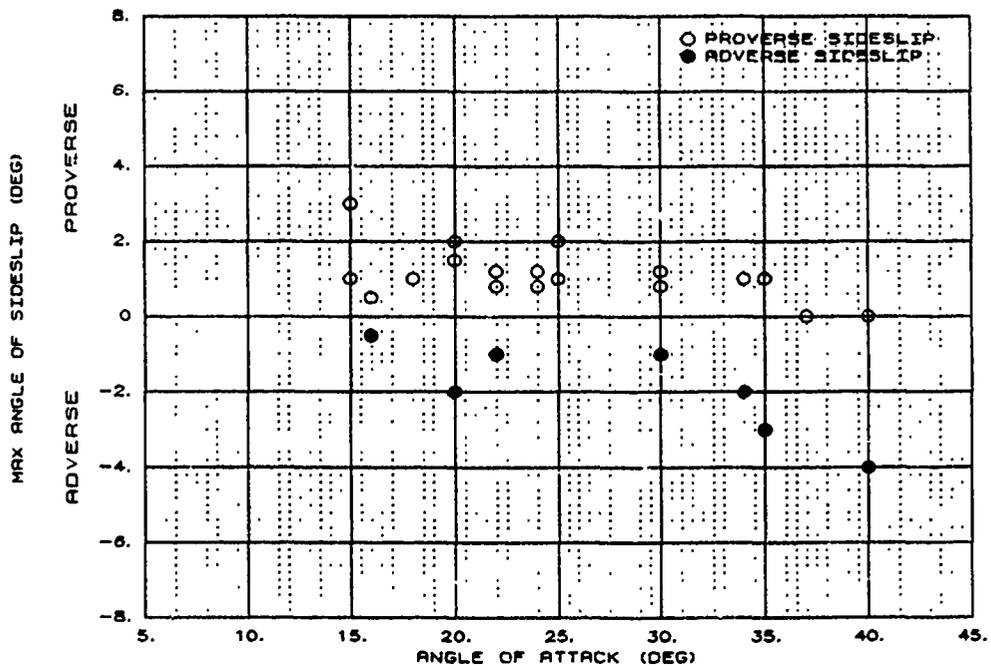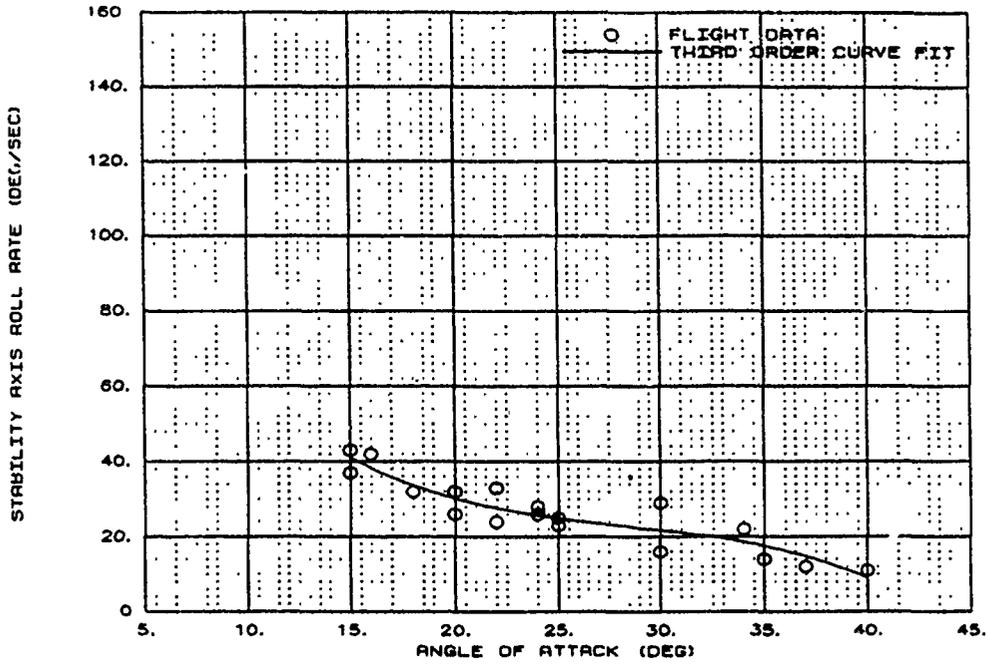
Figure B25 BLOCKIX-AA01 1-G Roll Performance

X-29 USAF S/N 820049
## MIL POWER   ALT=38K TO 25K ft
BLOCKIX-AA01 CONTROL LAWS
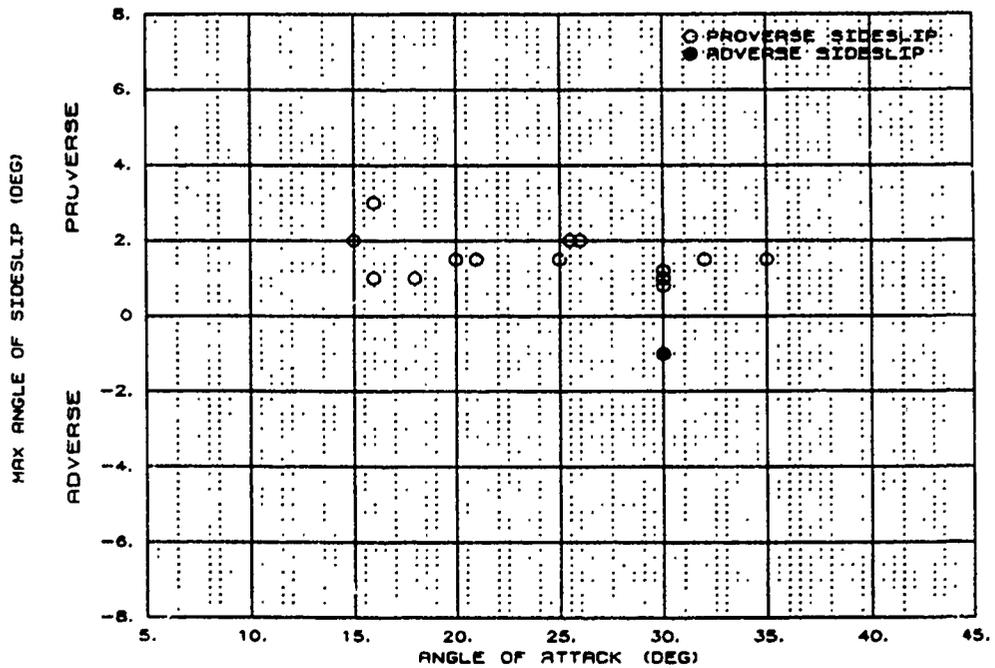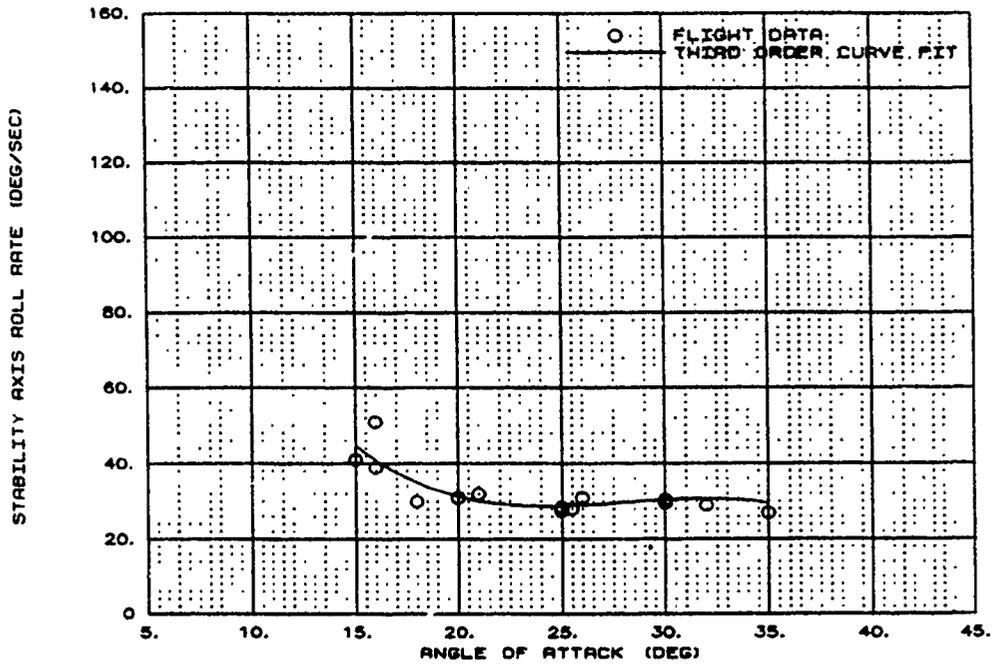
Figure B26   BLOCKIX-AA01 160 KCAS Roll Performance

X-29 USAF S/N 820049
MIL POWER   ALT=38K TO 25K ft
BLOCKIX-AA01 CONTROL LAWS
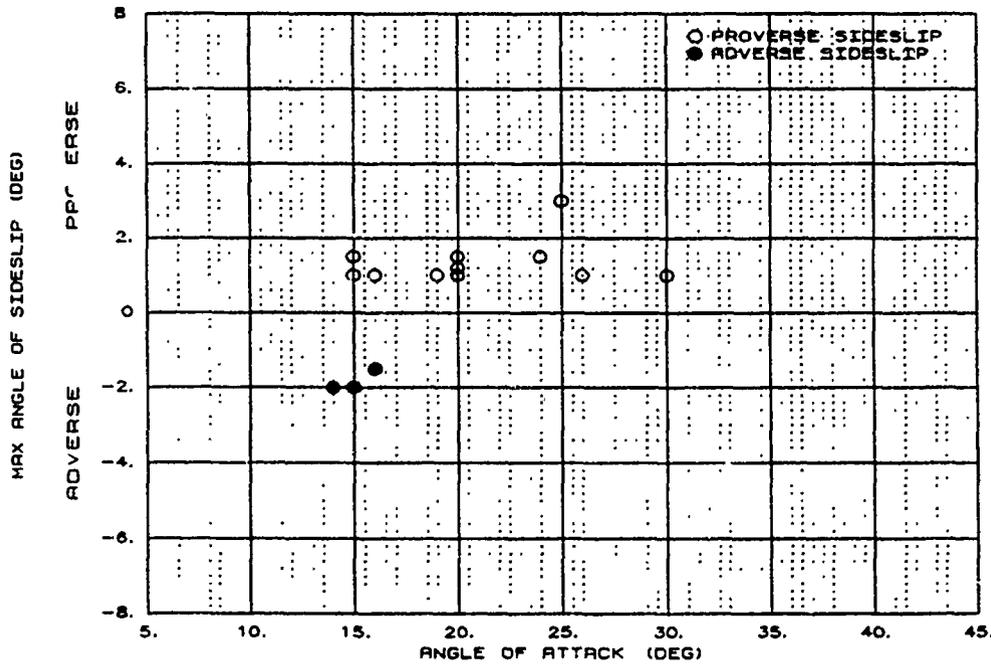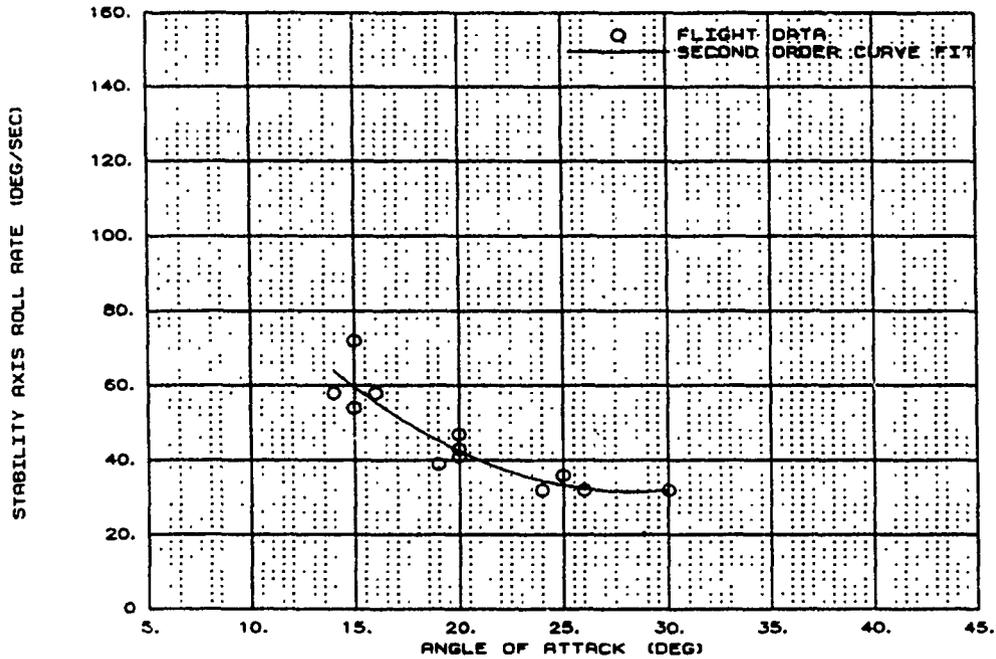

Figure B27   BLOCKIX-AA01 200 KCAs Roll Performance

X-29 USAF S/N 820049
# MIL POWER ALT=25K TO 17K ft
BLOCKIX-AAO2 CONTROL LAWS
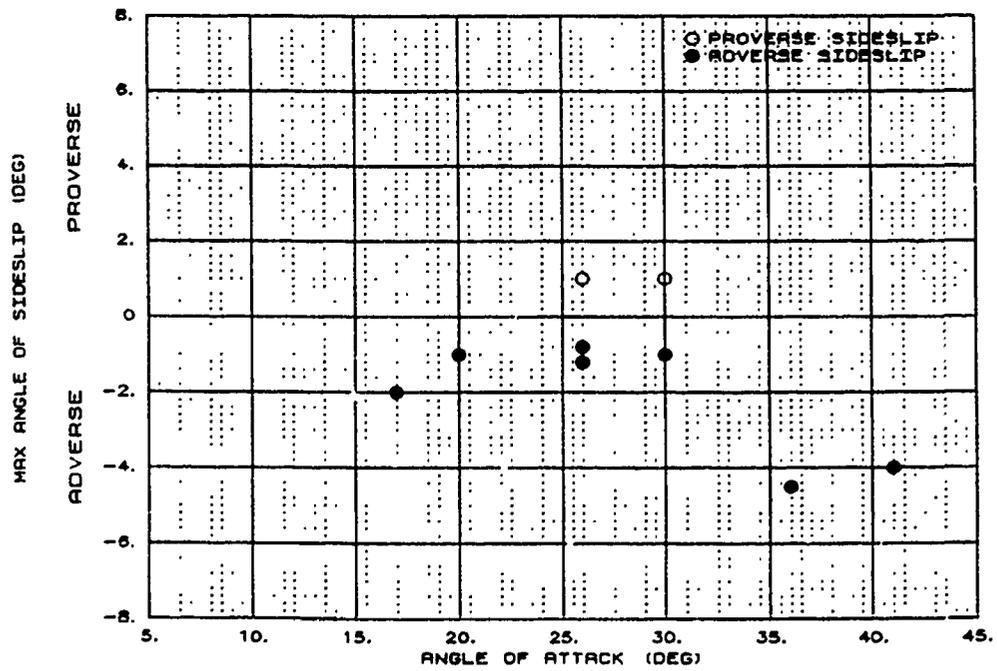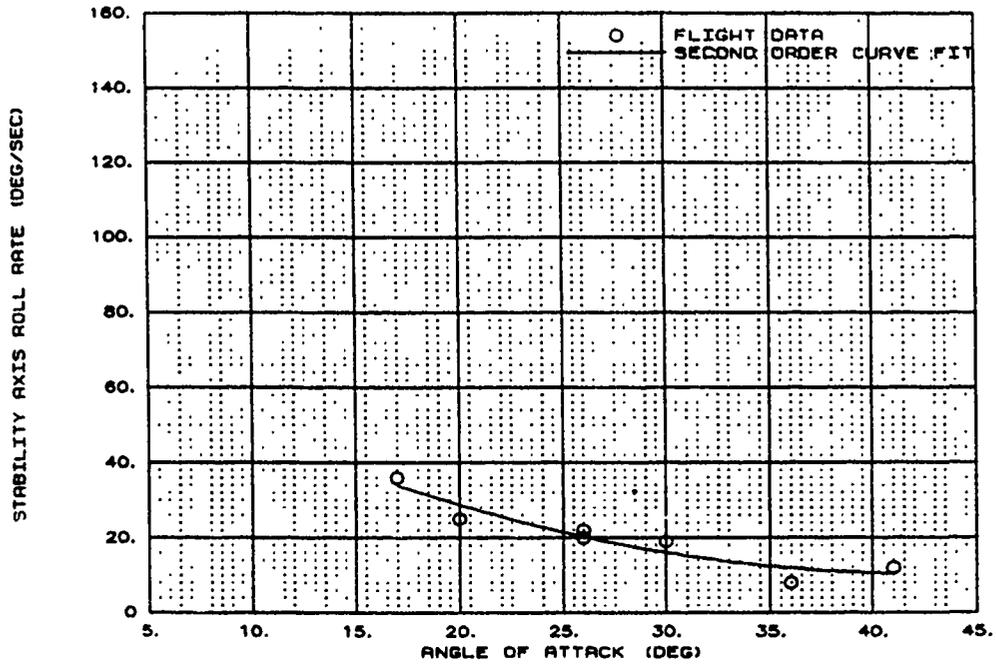
Figure B28 BLOCKIX-AA02 1-G Roll Performance

X-29 USAF S/N 820049
MIL POWER ALT=25K TO 17K ft
BLOCKIX-AAO2 CONTROL LAWS
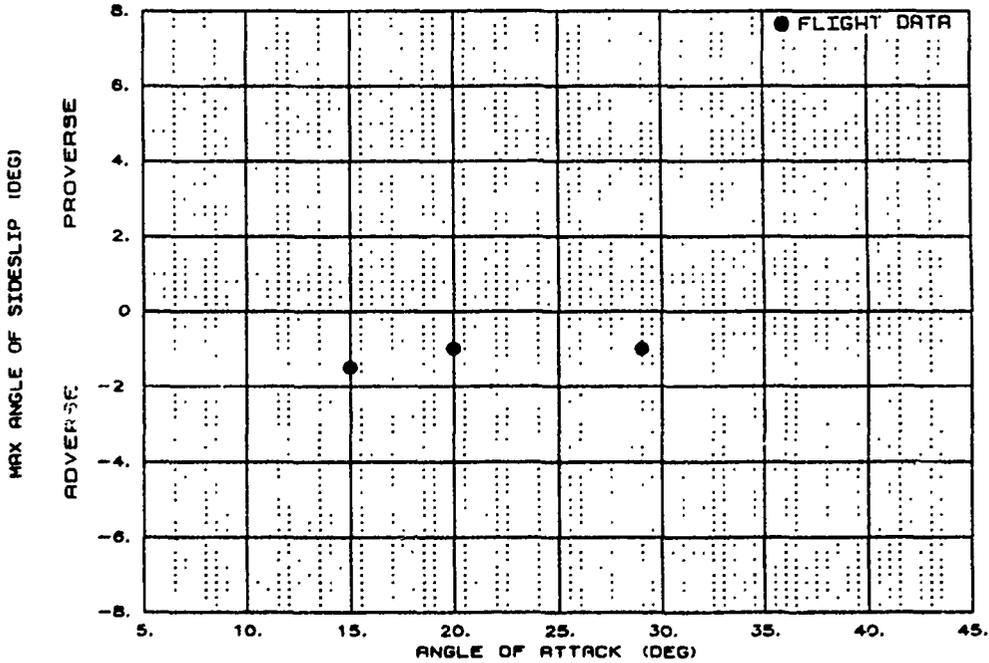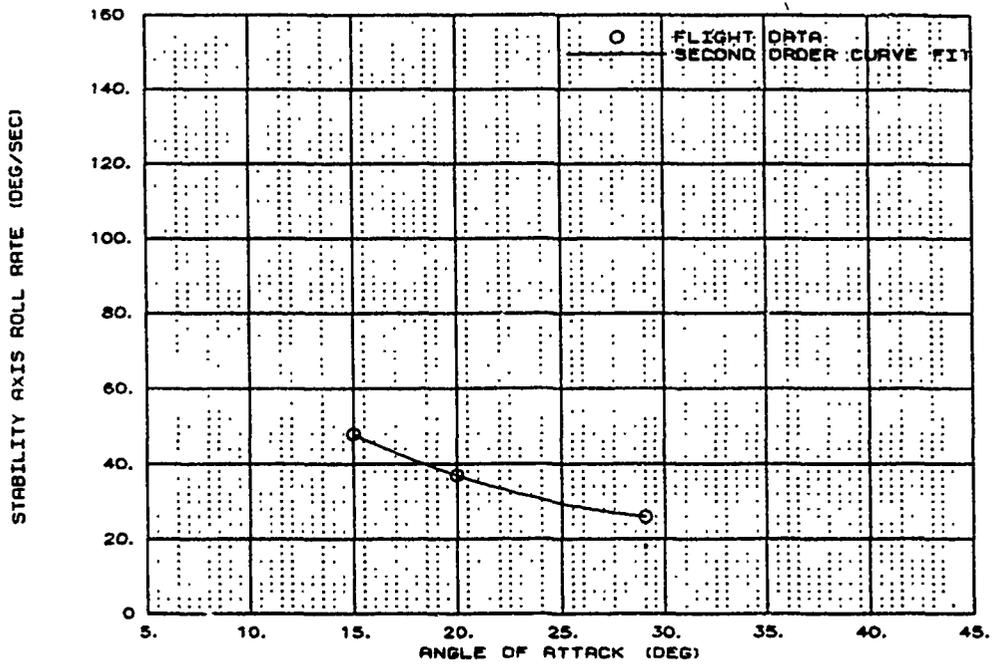
Figure B29   BLOCKIX-AAO2 160 V.CAS Roll Performance

X-29 USAF S/N 820049
MIL POWER   ALT=25K TO 17K ft
BLOCKIX-AAO2 CONTROL LAWS
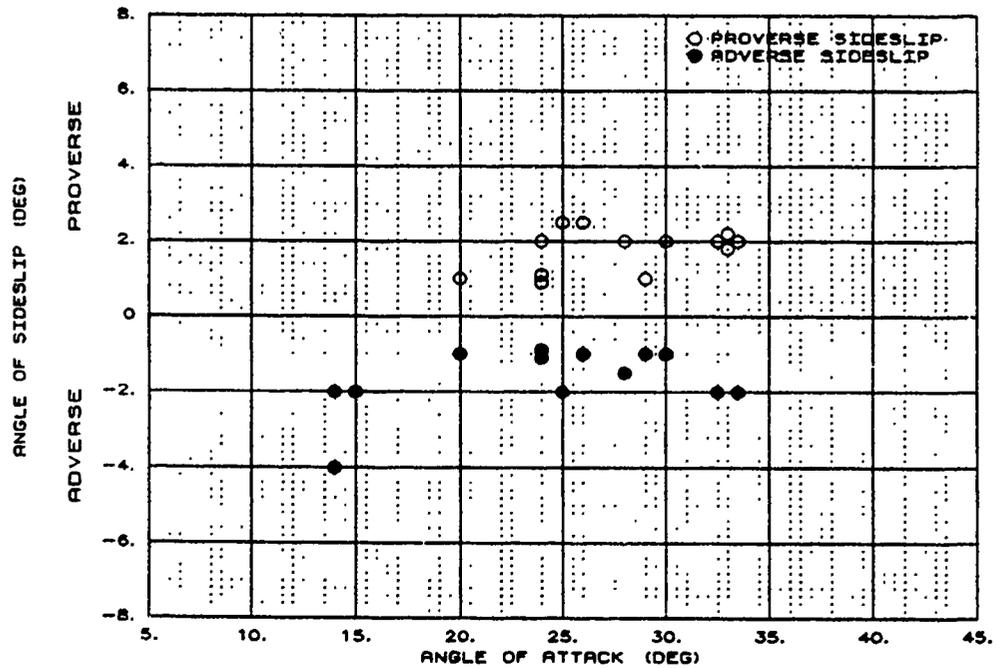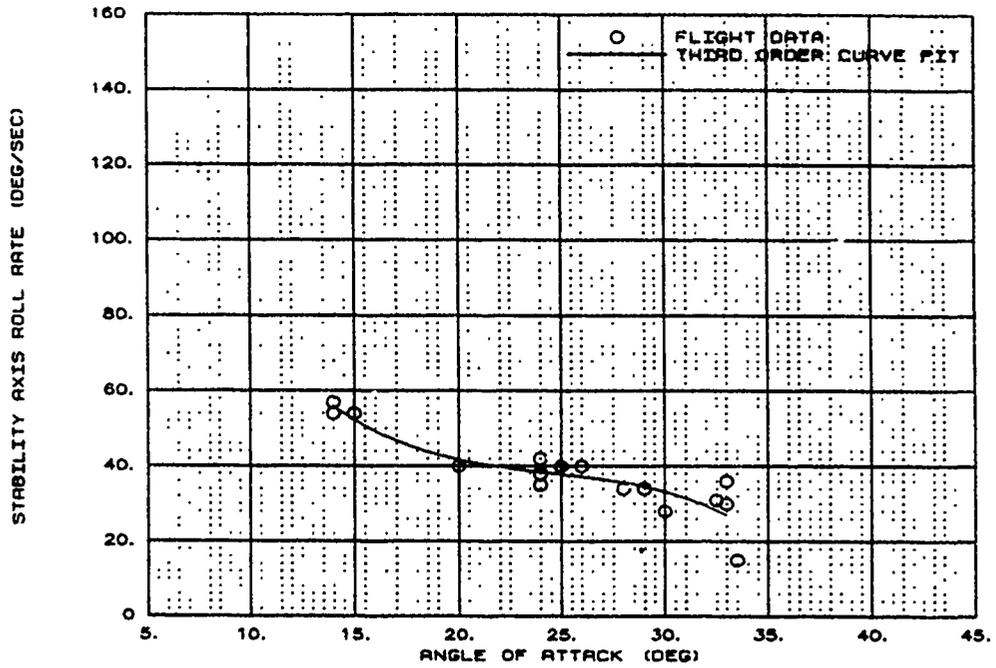
Figure B30   BLOCKIX-AAO2 200 KCAS Roll Performance

X-29 USAF S/N 820049
MIL POWER ALT=25K TO 17K ft
BLOCKIX-AAO2 CONTROL LAWS
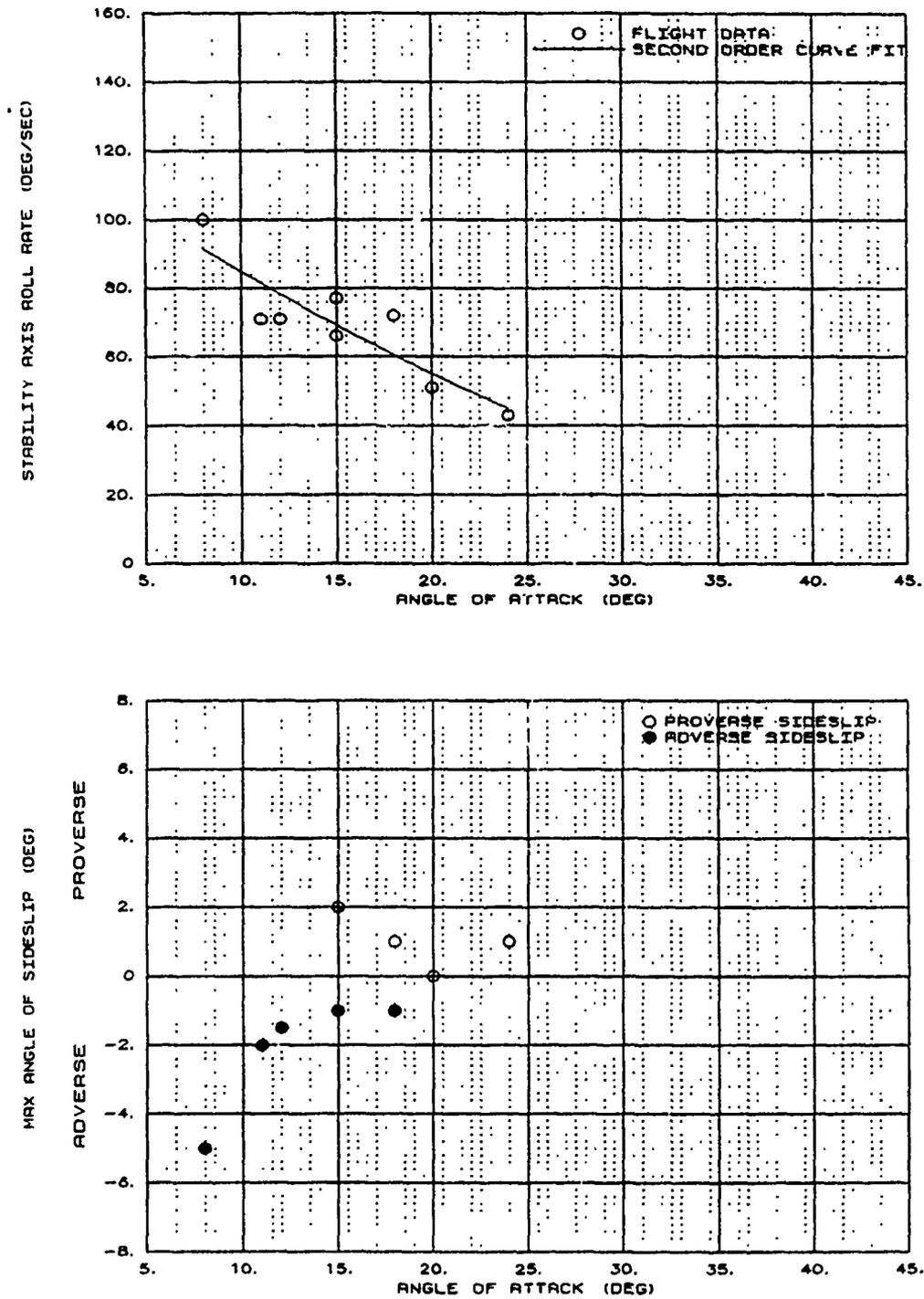
Figure B31   BLOCKIX-AAO2 250 XCAS Roll Performance

168

X-29 USAF S/N 820049
MIL POWER   ALT=25K TO 17K ft
BLOCKIX-AAO2 CONTROL LAWS
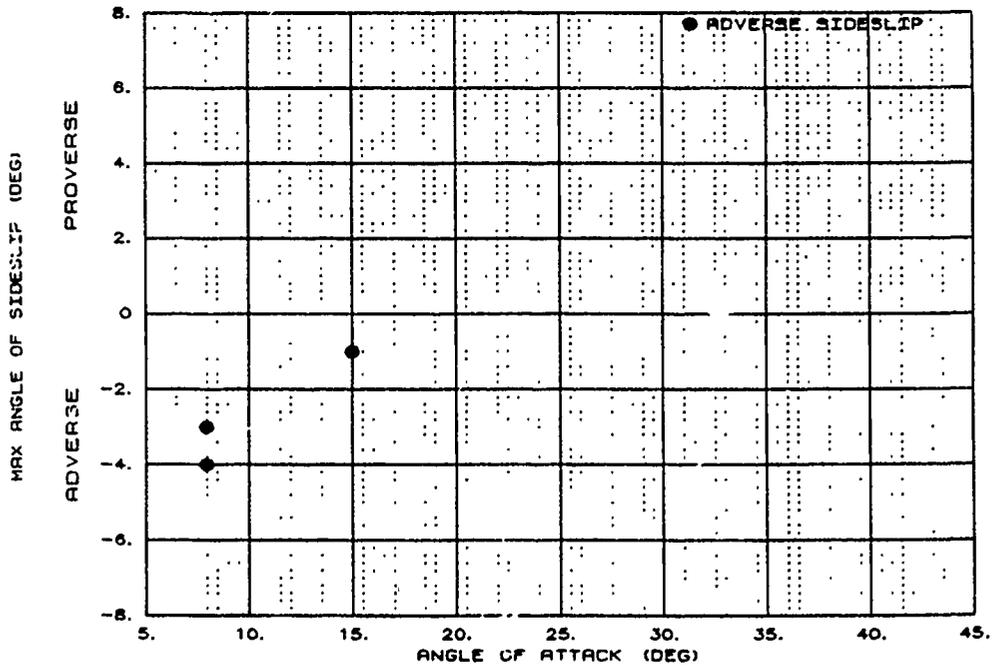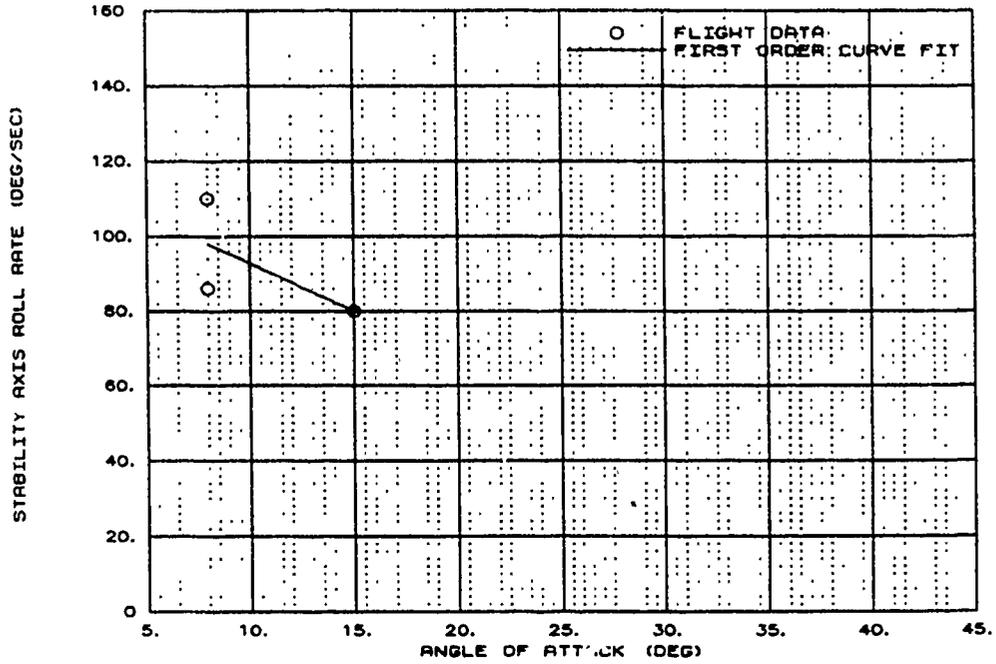
Figure B32   BLOCKIX-AAO2 300 KCAS Roll Performance

X-29 USAF S/N 820049
MIL POWER   ALT=25K TO 17K ft
BLOCKIX-AAO2   TW47   CONTROL LAWS
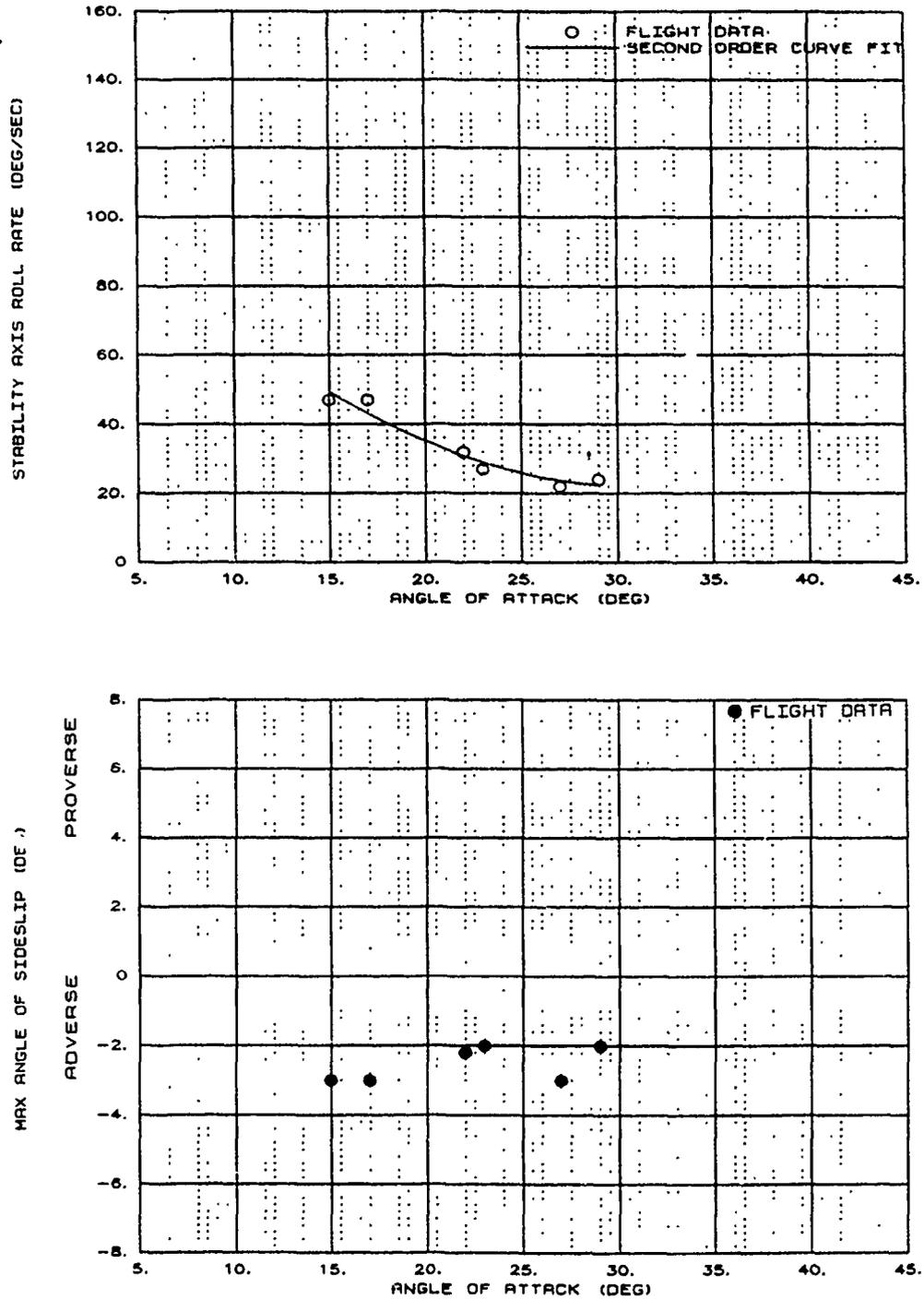
Figure B33 BLOCKIX-AA02 TW47 1-G Roll Performance

X-29 USAF S/N 820049
MIL POWER ALT=25K TO 17K ft
BLOCKIX-AAO2 TW47 CONTROL LAWS
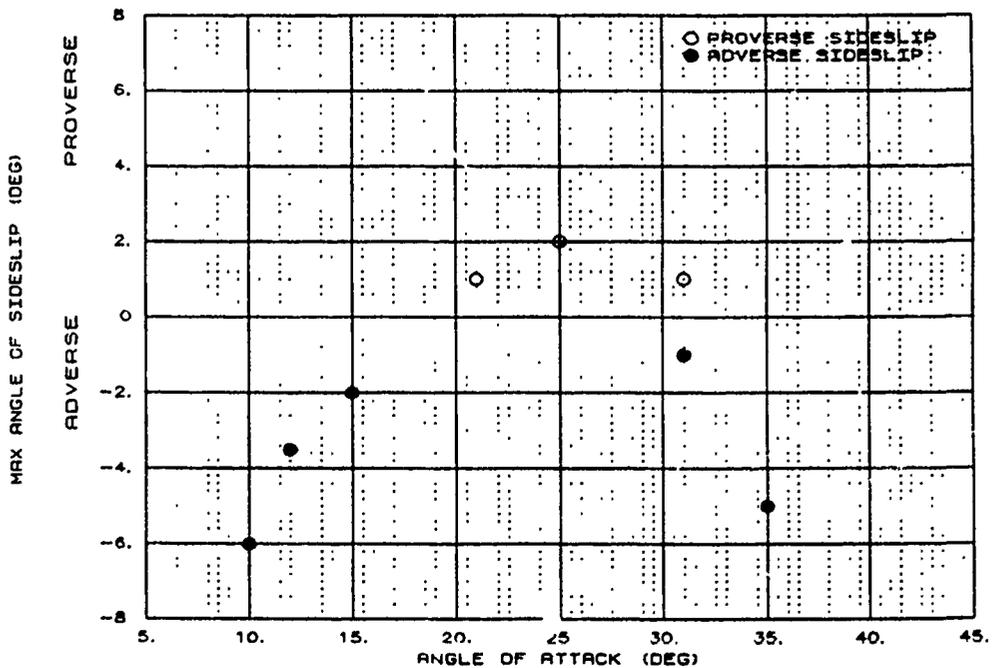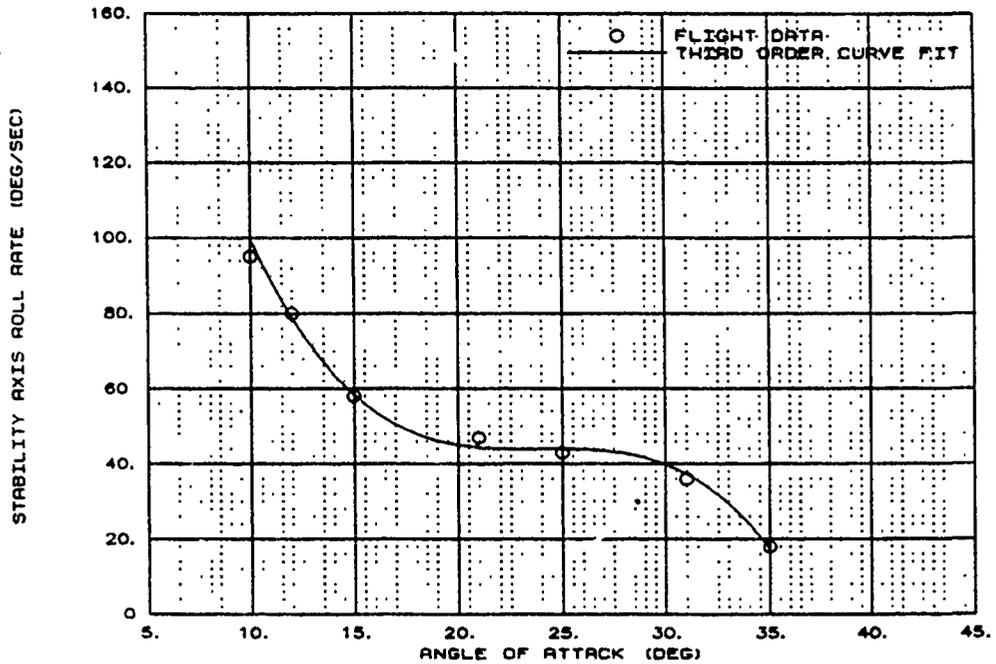
Figure B34   BLOCKIX-AAO2 TW47 160 KCAS Roll Performance

X-29 USAF S/N 820049
MIL POWER   ALT=25K TO 17K ft
BLOCKIX-AAO2 TW47   CONTROL LAWS
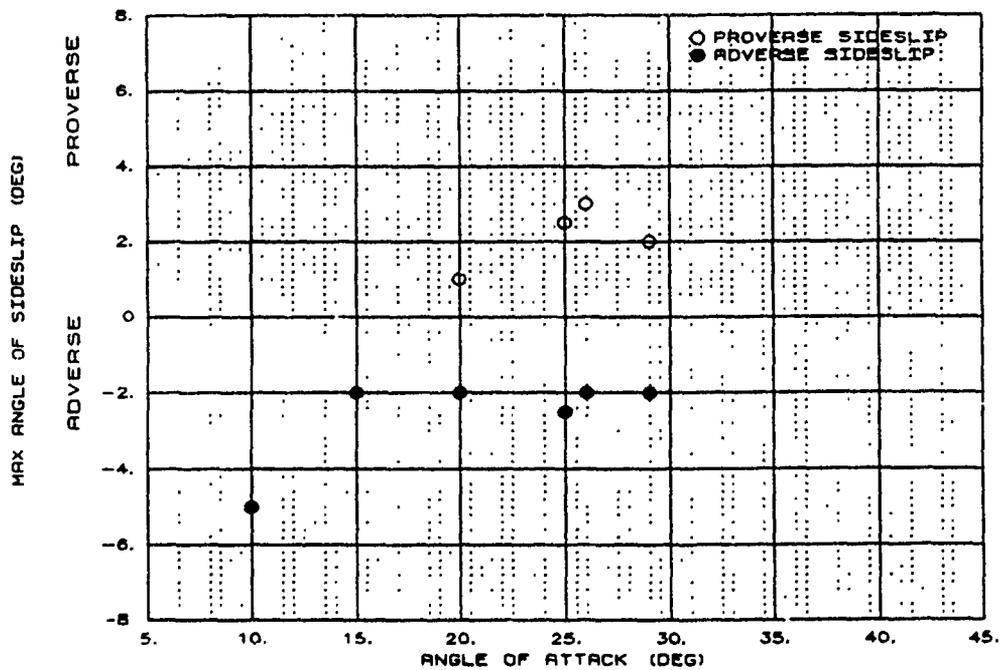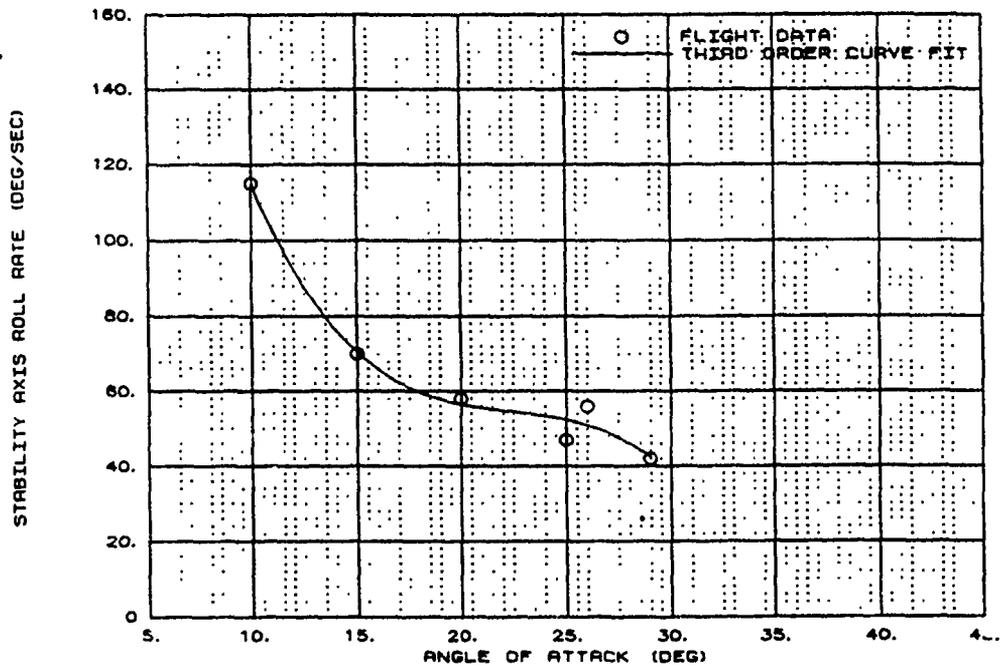
Figure B35   BLOCKIX-AAO2 TW47 200 KCAS Roll Performance

172

X-29 USAF S/N 820049
MIL POWER ALT=25K TO 17K ft
BLOCKIX-AAO2 TW47 CONTROL LAWS
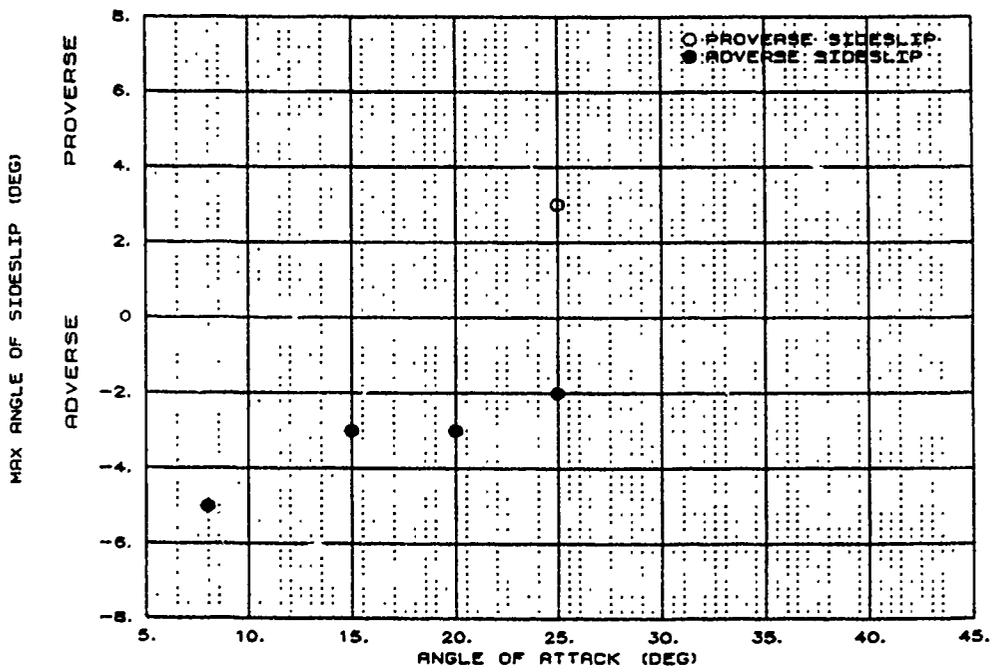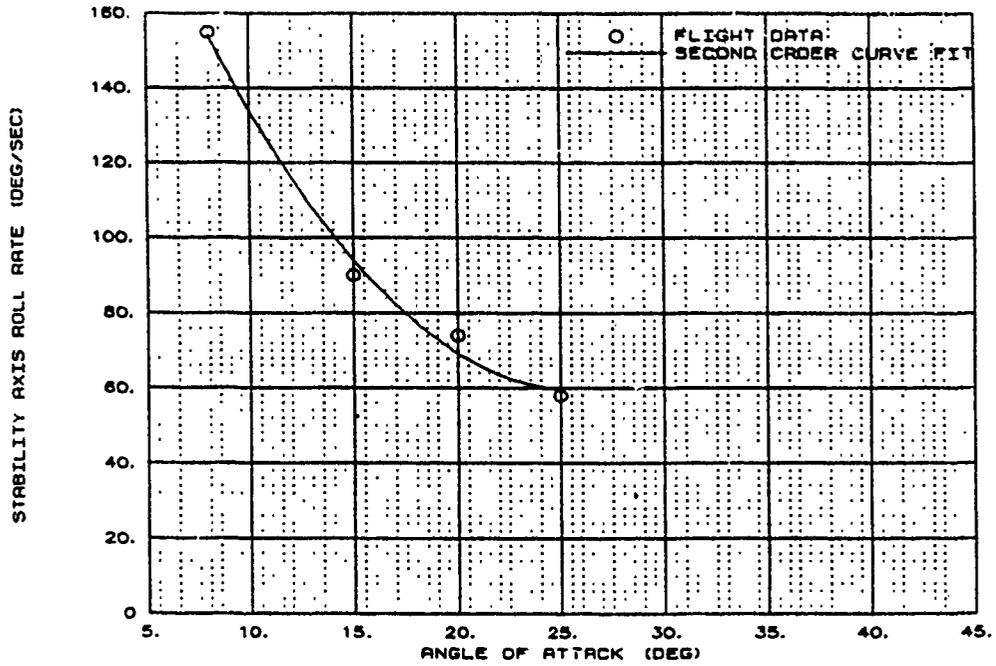
Figure B36 BLOCKIX-AAO2 TW47 250 KCAS Roll Performance

173

X-29 USAF S/N 820049
MIL POWER ALT=25K TO 17K ft
BLOCKIX-AAO2 TW53 CONTROL LAWS
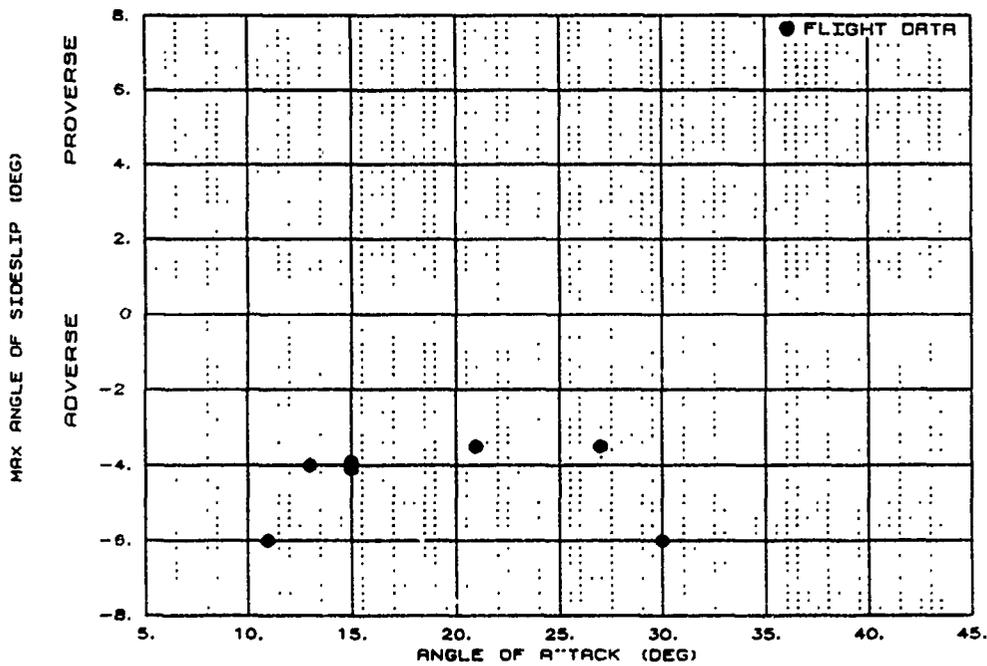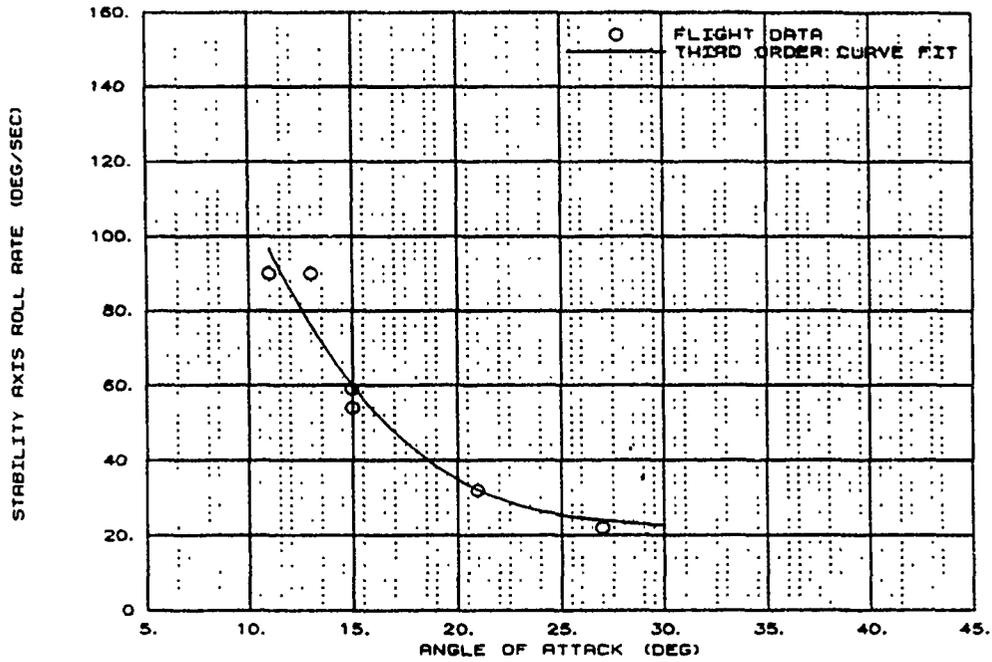
Figure B37 BLOCKIX-AA02 TW53 1-G Roll Performance

X-29 USAF S/N 820049
MIL POWER ALT=25K TO 17K ft
BLOCKIX-AAO2 TW53 CONTROL LAWS
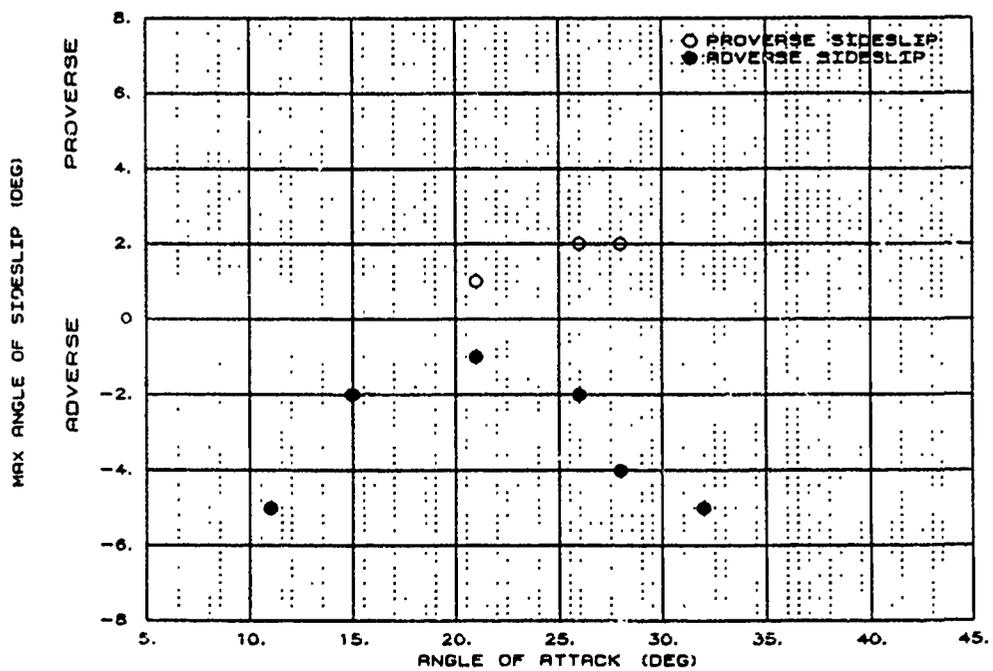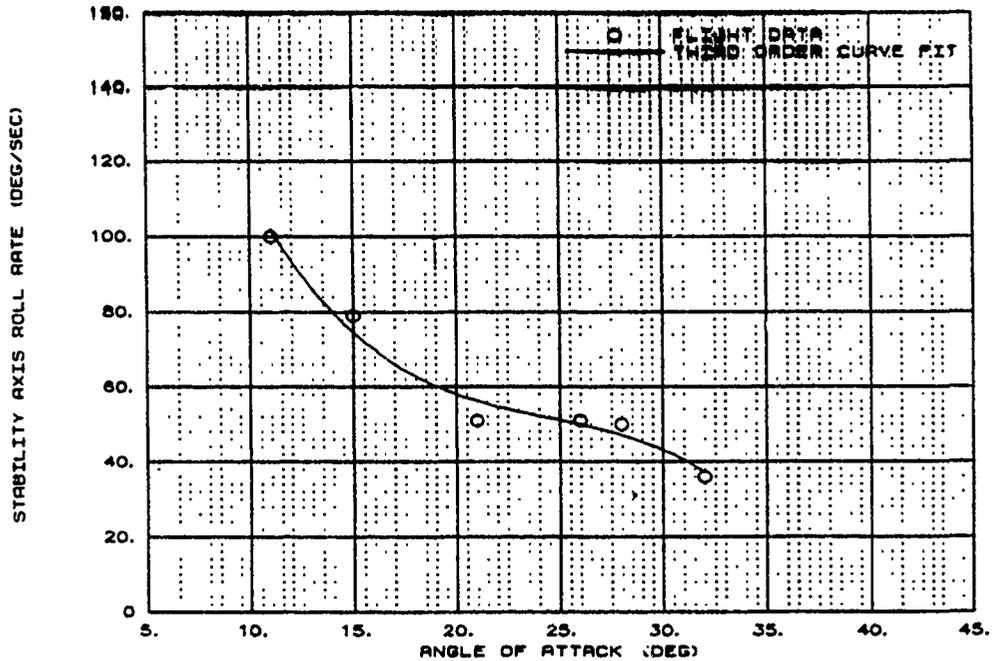
Figure B38 BLOCKIX-AAO2 TW53 160 KCAS Roll Performance

175

X-29 USAF S/N 820049
MIL POWER   ALT=25K TO 17K ft
BLOCKIX-AAO2   TW53   CONTROL LAWS
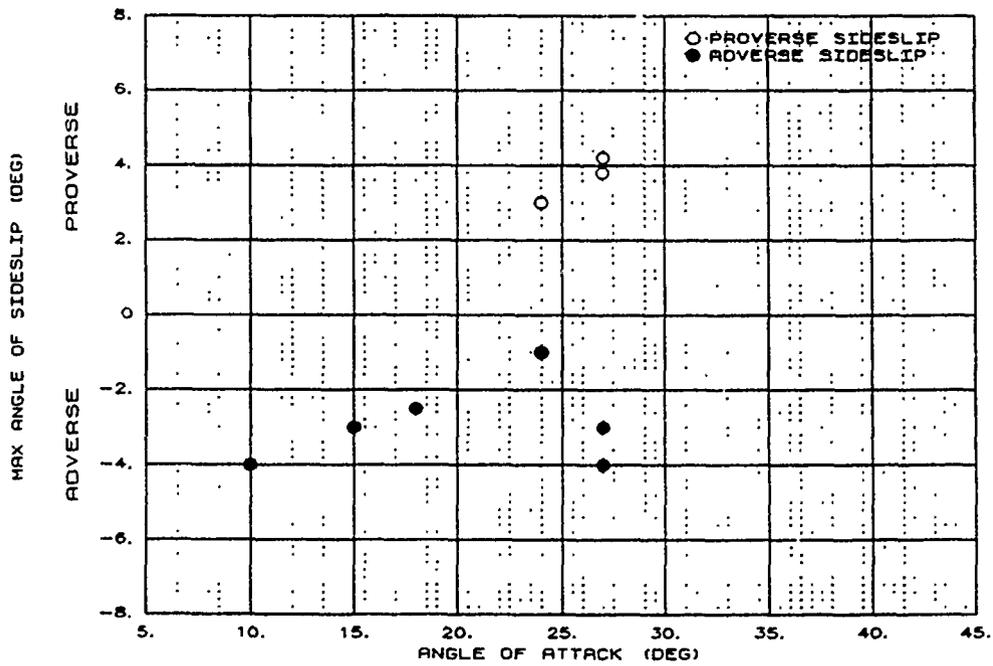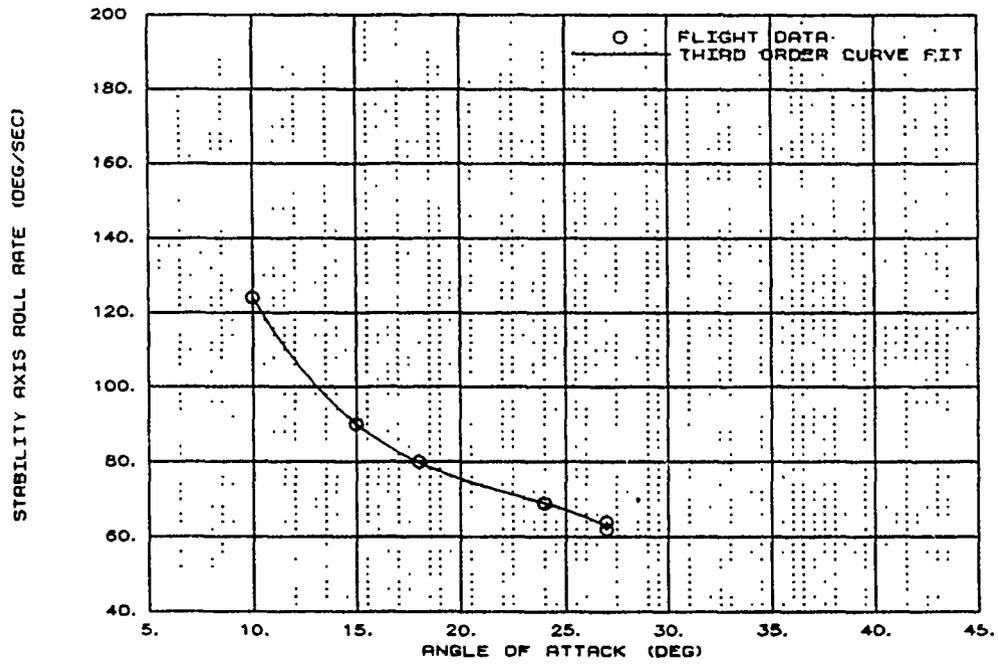
Figure B39   BLOCKIX-AAO2 TW53 200 KCAS Roll Performance

X-29 USAF S/N 820049
MIL POWER   ALT=25K TO 17K ft
BLOCKIX-AAO2 TW53 CONTROL LAWS
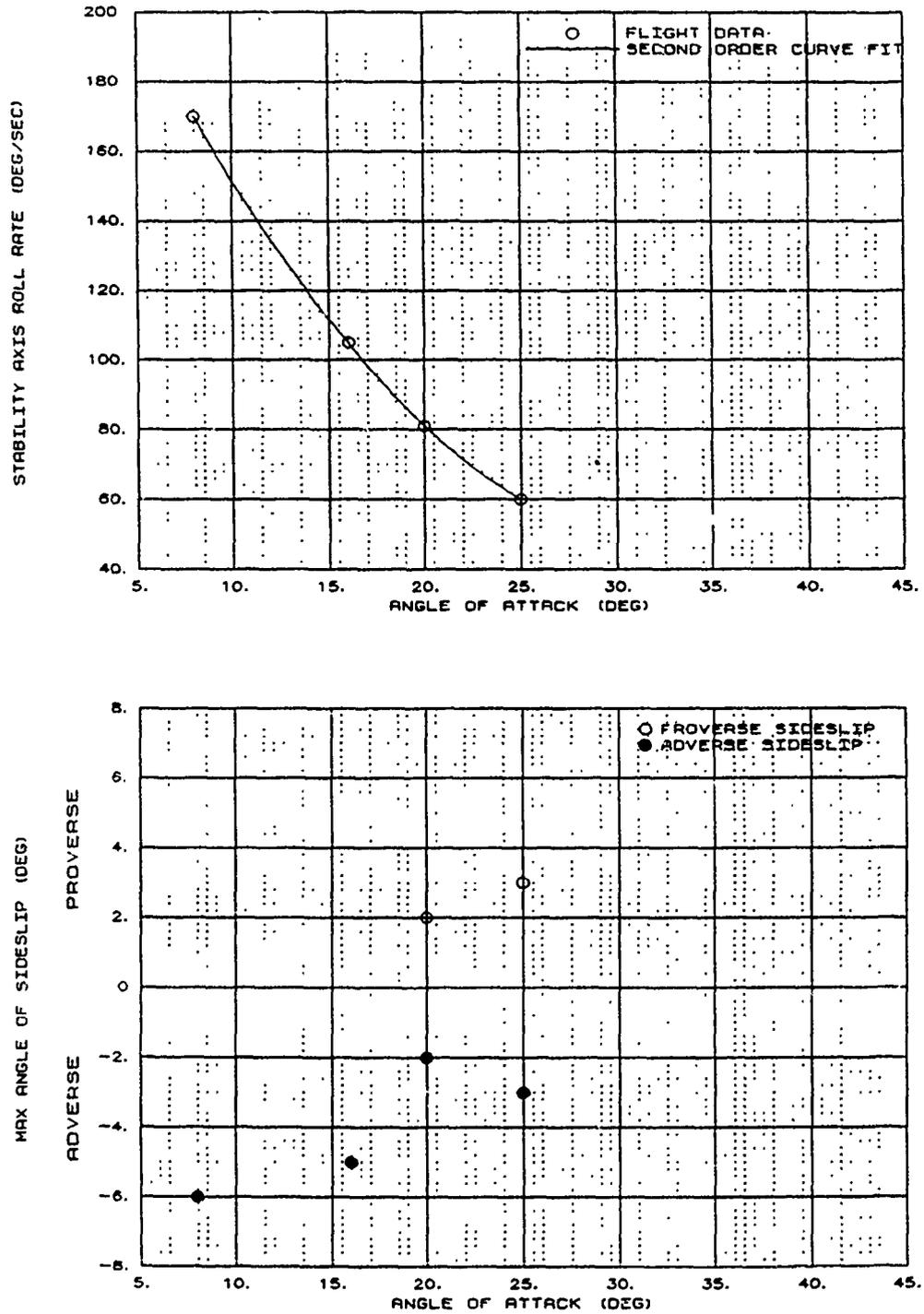
Figure B40   BLOCKIX-AAO2 TW53 250 KCAS Roll Performance

177

Figure B41 One-G Roll With BLOCKIX-AA01 at 25 Degrees AOA

178

Figure B41 One-G Roll With BLOCKIX-AA01 at 25 Degrees AOA   (Continued)

179

Figure B41 One-G Roll With BLOCKIX-AA01 at 25 Degrees AOA   (Continued)

180

X-29 USAF S/N 820049

XCG=448.7 IN.   IXX=4571   IYY=52178   IZZ=57335   IXZ=2577

1-G 360 DEG ROLL   25 DEG   BLK IX-AA01

Strake Position (deg)	Flap Position (deg)	Canard Position (deg)	Pitch Rate (deg/sec)	Lon Stick Position (in)

ELAPSED TIME (SEC)

Figure B41   One-G Roll With BLOCKIX-AA01 at 25 Degrees AOA   (Continued)

Figure B41   One-G Roll With BLOCKIX-AA01 at 25 Degrees AOA   (Continued)

Figure B41 One-G Roll With BLOCKIX-AA01 at 25 Degrees AOA   (Concluded)

183

Figure B42 200 KCAS Roll With BLOCKIX-AA01 at 25 Degrees AOA

184

Figure B42 200 KCAS Roll With BLOCKIX-AA01 at 25 Degrees AOA   (Continued)

185

Figure B42 200 KCAS Roll With BLOCKIX-AA01 at 25 Degrees AOA   (Continued)

186

Figure B42 200 KCAS Roll With BLOCKIX-AA01 at 25 Degrees AOA   (Continued)

187

Figure B42   200 KCAS Roll With BLOCKIX-AA01 at 25 Degrees AOA   (Continued)

188

Figure B42 200 KCAS Roll With BLOCKIX-AA01 at 25 Degrees AOA (Concluded)

Figure B43 160 KCAS Roll With BLOCKIX-AA02 at 35 Degrees AOA

Figure B43 160 KCAS Roll With BLOCKIX-AA02 at 35 Degrees AOA   (Continued)

191

Figure B43 160 KCAS Roll With BLOCKIX-AA02 at 35 Degrees AOA   (Continued)

192

Figure B43 160 KCAS Roll With BLOCKIX-AA02 at 35 Degrees AOA   (Continued)

Figure B43   160 KCAS Roll With BLOCKIX-AA02 at 35 Degrees AOA   (Continued)

194

Figure B43 160 KCAS Roll With BLOCKIX-AA02 at 35 Degrees AOA (Concluded)

Figure B44 200 KCAS Roll With BLOCKIX-AA02 at 30 Degrees AOA

196

Figure B44 200 KCAS Roll With BLOCKIX-AA02 at 30 Degrees AOA   (Continued)

Figure B44   200 KCAS Roll With BLOCKIX-AA02 at 30 Degrees AOA   (Continued)

198

Figure B44 200 KCAS Roll With BLOCKIX-AA02 at 30 Degrees AOA   (Continued)

199

X-29 USAF S/N 820049

XCG=448.1 IN.   IXX=4569   IYY=53850   IZZ=59110   IXZ=2565
200 KCAS ENTRY ROLL   35 DEG   BLK IX-AA02

Figure B44 200 KCAS Roll With BLOCKIX-AA02 at 30 Degrees AOA   (Continued)

ELAPSED TIME (SEC)

Lon Stick Position (in)
Pitch Rate (deg/sec)
Canard Position (deg)
Flap Position (deg)
Strake Position (deg)

200

Figure B44 200 KCAS Roll With BLOCKIX-AA02 at 30 Degrees AOA   (Concluded)

201

Figure B45 One-G Roll With BLOCKIX-AA02 TW47 at 30 Degrees AOA

202

Figure B45 One-G Roll With BLOCKIX-AA02 TW47 at 30 Degrees AOA   (Continued)

203

Figure B45   One-G Roll With BLOCKIX-AA02 TW47 at 30 Degrees AOA   (Continued)

204

Figure B45   One-G Roll With BLOCKIX-AA02 TW47 at 30 Degrees AOA   (Continued)

Figure B45   One-G Roll With BLOCKIX-AA02 TW47 at 30 Degrees AOA   (Continued)

206

X-29 USAF S/N 820049

XCG=447.6 IN.   IXX=4565   IYY=54080   IZZ=58245   IXZ=2595

1-G BANK-TO-BANK   BLK IX-AA02   TW47

Figure B45 One-G Roll With BLOCKIX-AA02 TW47 at 30 Degrees AOA   (Concluded)

207

Figure B46   One-G Roll With BLOCKIX-AA02 TW47 at 35 Degrees AOA

208

Figure B46   One-G Roll With BLOCKIX-AA02 TW47 at 35 Degrees AOA   (Continued)

209

Figure B46   One-G Roll With BLOCKIX-AA02 TW47 at 35 Degrees AOA   (Continued)

210

Figure B46 One-G Roll With BLOCKIX-AA02 TW47 at 35 Degrees AOA   (Continued)

211

Figure B46 One-G Roll With BLOCKIX-AA02 TW47 at 35 Degrees AOA   (Continued)

Figure B46 One-G Roll With BLOCKIX-AA02 TW47 at 35 Degrees AOA (Concluded)

213

Figure B47 200 KCAS Roll With BLOCKIX-AA02 TW47 at 25 Degrees AOA

214

Figure B47   200 KCAS Roll With BLOCKIX-AA02 TW47 at 25 Degrees AOA   (Continued)

215

Figure B47 200 KCAS Roll With BLOCKIX-AA02 TW47 at 25 Degrees AOA (Continued)

216

X-29 USAF S/N 820049

XCG=450.1 IN.   IXX=4546   IYY=51850   IZZ=57030   IXZ=2540
200 KCAS BANK-TO-BANK   BLK IX-AA02   TW47

Figure B47   200 KCAS Roll With BLOCKIX-AA02 TW47 at 25 Degrees AOA   (Continued)

217

Figure B47 200 KCAS Roll With BLOCKIX-AA02 TW47 at 25 Degrees AOA (Continued)

218

X-29 USAF S/N 820049

XCG=450.1 IN.   IXX=4546   IYY=51850 IZZ=57030   IXZ=2540

200 KCAS BANK-TO-BANK   BLK IX-AA02   TW47

Lateral Stick Position (in)

Rudder Pedal Position (in)

Aileron Position (deg)

Rudder Position (deg)

ELAPSED TIME (SEC)

Figure B47 200 KCAS Roll With BLOCKIX-AA02 TW47 at 25 Degrees AOA   (Concluded)

Figure B48 One-G Roll With BLOCKIX-AA02 TW53 at 35 Degrees AOA

220

Figure B48 One-G Roll With BLOCKIX-AA02 TW53 at 35 Degrees AOA   (Continued)

221

Figure B48   One-G Roll With BLOCKIX-AA02 TW53 at 35 Degrees AOA   (Continued)

222

Figure B48 One-G Roll With BLOCKIX-AA02 TW53 at 35 Degrees AOA   (Continued)

223

Figure B48 One-G Roll With BLOCKIX-AA02 TW53 at 35 Degrees AOA   (Continued)

224

Figure B48 One-G Roll With BLOCKIX-AA02 TW53 at 35 Degrees AOA   (Concluded)

225

Figure B49 160 KCAS Roll With BLOCKIX-AA02 TW53 at 35 Degrees AOA

226

Figure B49 160 KCAS Roll With BLOCKIX-AA02 TW53 at 35 Degrees AOA   (Continued)

227

Figure B49   160 KCAS Roll With BLOCKIX-AA02 TW53 at 35 Degrees AOA   (Continued)

228

Figure B49   160 KCAS Roll With BLOCKIX-AA02 TW53 at 35 Degrees AOA   (Continued)

229

Figure B49 160 KCAS Roll With BLOCKIX-AA02 TW53 at 35 Degrees AOA   (Continued)

230

Figure B49 160 KCAS Roll With BLOCKIX-AA02 TW53 at 35 Degrees AOA   (Concluded)

231

Figure B50 Rudder Roll

232

Figure B50 Rudder Roll (Continued)

233

X-29 USAF S/N 820049

IXX=4562 IYY=51800 IZZ=57060 IXZ=2510

XCG=449.5 i l. RUDDER ROLL 30 DEG BLK IX-AA01
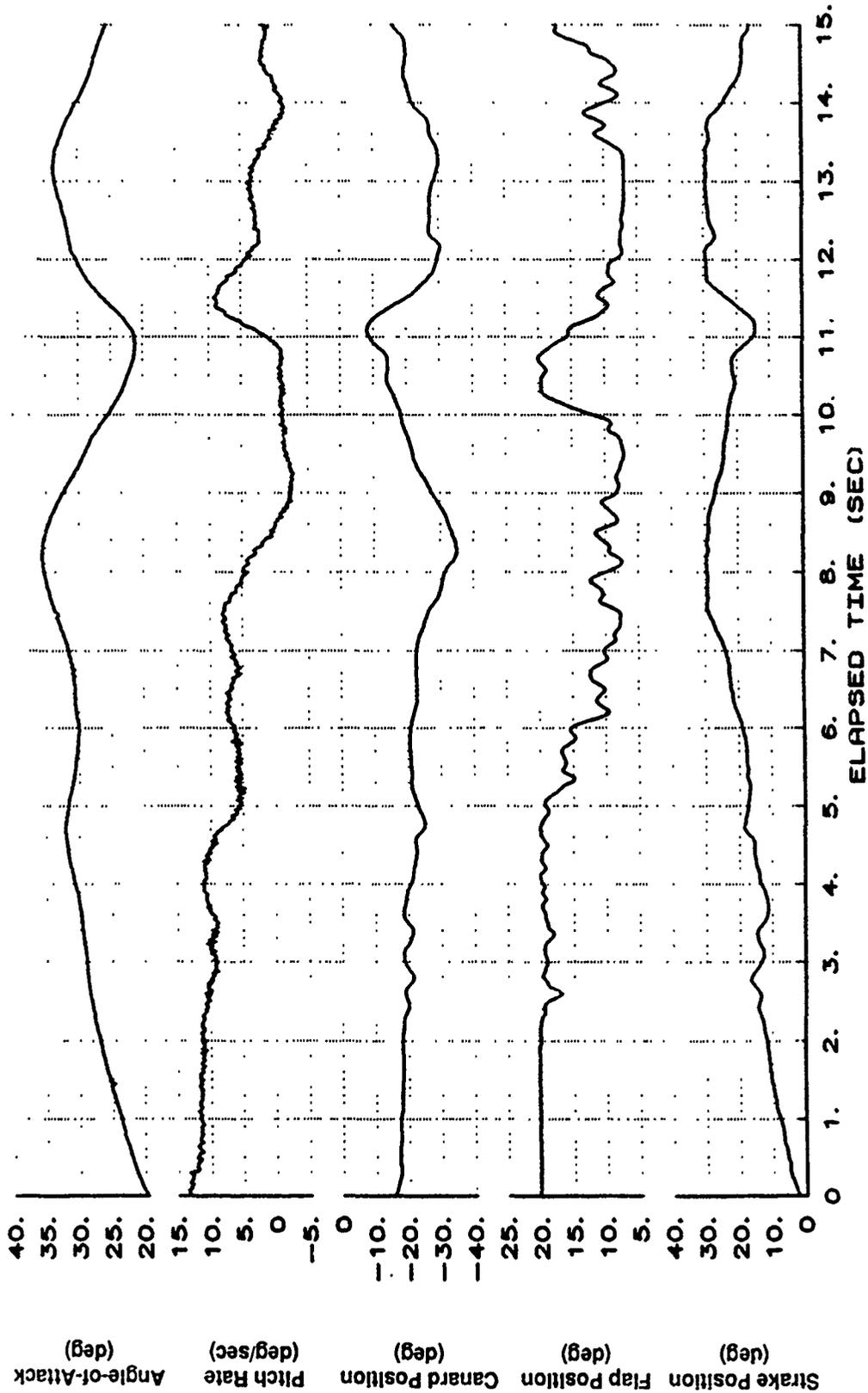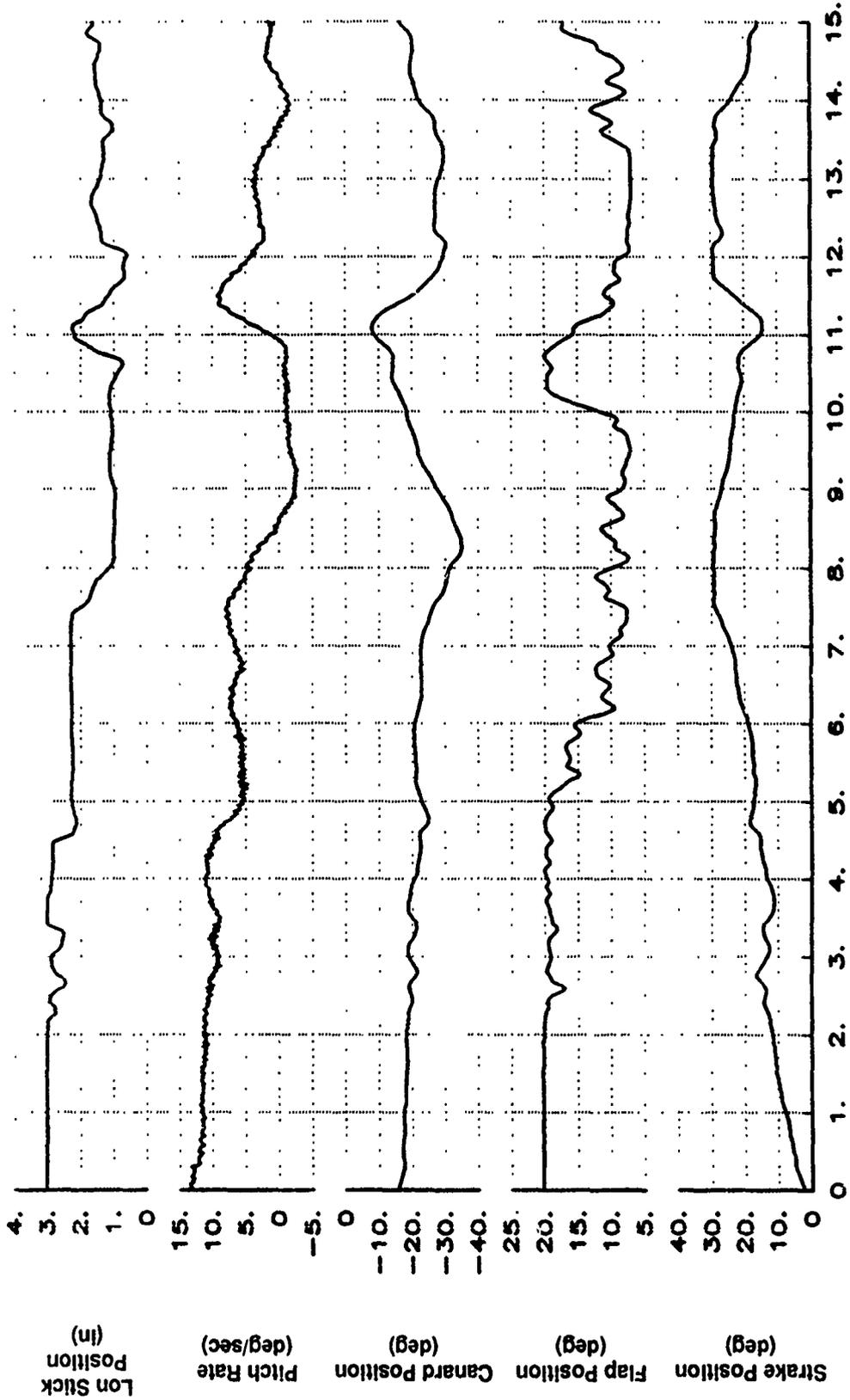
200 KCAS

Figure B50 Rudder Roll (Continued)

234

Figure B50 Rudder Roll (Continued)

235

Figure B50 Rudder Roll (Continued)

236

X-29 USAF S/N 820049
IXX=4562 IYY=51900 IZZ=57060 IXZ=2510
XCG=449.5 IN. RUDDER ROLL
200 KCAS 30 DEG BLK IX-AA01

Figure B50 Rudder Roll (Concluded)

237

Figure B51 Wing Rock at 40 to 45 Degrees AOA

238

Figure B51 Wing Rock at 40 to 45 Degrees AOA (Continued)

239

Figure B51   Wing Rock at 40 to 45 Degrees AOA   (Continued)

240
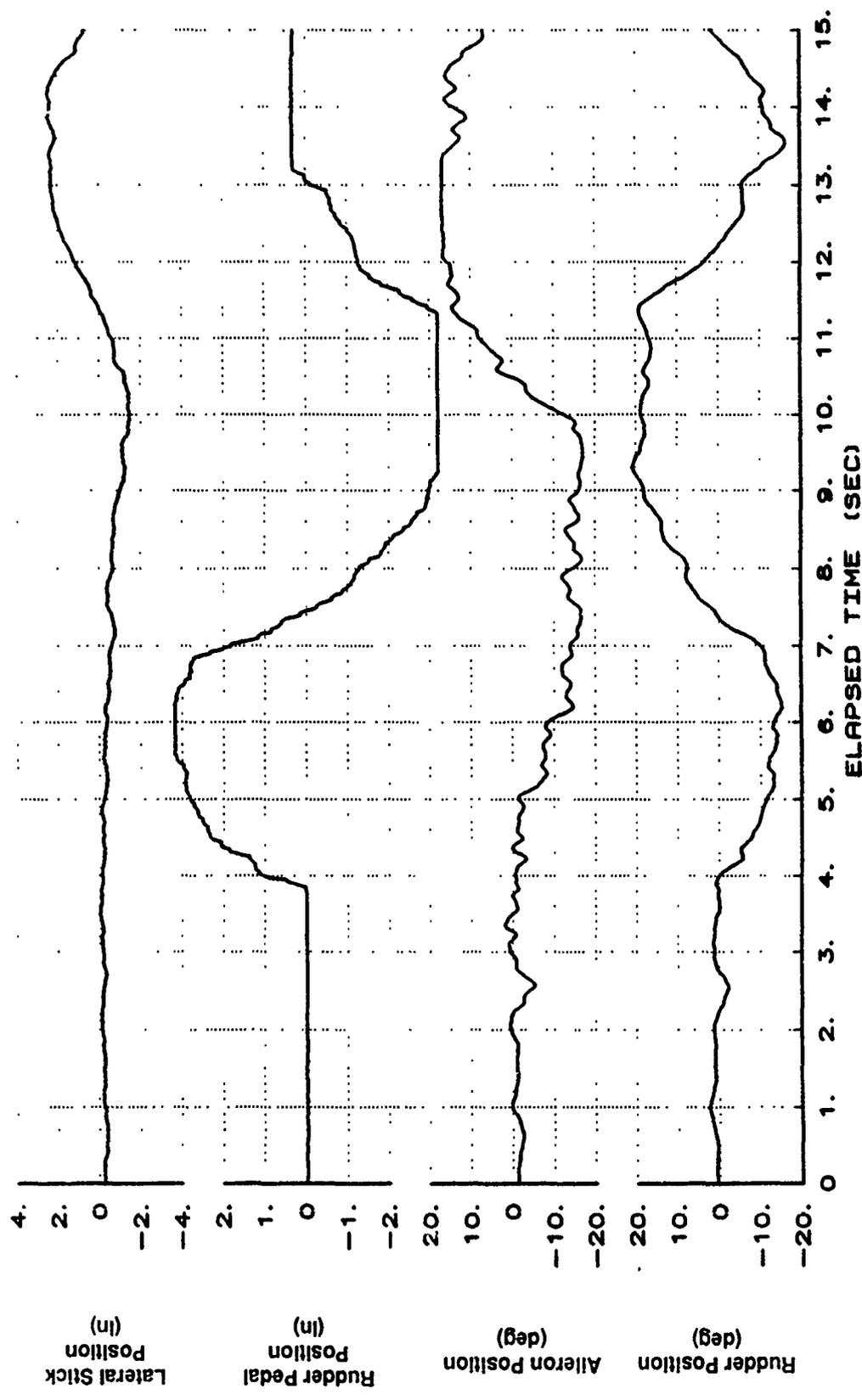
X-29 USAF S/N 820049

XCG=445.3 IN. IXX=4565 IYY=53055 IZZ=58220 IXZ=2571

1-G WING ROCK BLK IX-AA01

Figure B51 Wing Rock at 40 to 45 Degrees AOA (Continued)

241

Figure B51 Wing Rock at 40 to 45 Degrees AOA (Concluded)

242

X-29 USAF S/N 820049
XCG=447.5 IN.   IXX=4568   IYY=52920   IZZ=58060   IXZ=2597
1-G TO 50 DEG   BLK IX-AA01

Figure B52   Pull-Up to 50 Degrees AOA

243

X-29 USAF S/N 820049

XCG=447.5 IN. IXX=4568 IYY=52920 IZZ=58060 IXZ=2597

1-G TO 50 DEG BLK IX-AA01

Figure B52 Pull-Up to 50 Degrees AOA (Continued)

244

Figure B52 Pull-Up to 50 Degrees AOA (Continued)

245

X-29 USAF S/N 820049

XCG=447.5 IN.   IXX=4568   IYY=52920   IZZ=58060   IXZ=2597
                 1-G TO 50 DEG   BLK IX-AA01

ELAPSED TIME (SEC)

Dynamic Pressure
(psf)

True Airspeed
(ft/sec)

Figure B52 Pull-Up to 50 Degrees AOA   (Continued)

X-29 USAF S/N 820049

XCG=447.5 IN.   IXX=4568   IYY=52920   IZZ=58060   IXZ=2597

1-G TO 50 DEG   BLK IX-AA01

Figure B52 Pull-Up to 50 Degrees AOA   (Continued)

247

Figure B52   Pull-Up to 50 Degrees AOA   (Continued)

248

Figure B52 Pull-Up to 50 Degrees AOA (Continued)

249

Figure B52 Pull-Up to 50 Degrees AOA (Continued)

250

Figure B52 Pull-Up to 50 Degrees AOA   (Continued)

251

Figure B52 Pull-Up to 50 Degrees AOA   (Continued)

252

Figure B52 Pull-Up to 50 Degrees AOA   (Continued)

253

Figure B52 Pull-Up to 50 Degrees AOA   (Continued)

254

Figure B52 Pull-Up to 50 Degrees AOA   (Concluded)

255

Figure B53   Asymmetry Control Between 40 and 50 Degrees AOA

256

X-29 USAF S/N 820049

XCG=449.8 IN.   IXX=4554   IYY=51880 IZZ=57050   IXZ=?532
1-G   40 TO 50 DEG AOA   BLK IX-AA01

Figure B53   Asymmetry Control Between 40 and 50 Degrees AOA   (Continued)

Figure B53 Asymmetry Control Between 40 and 50 Degrees AOA   (Continued)

Figure B53 Asymmetry Control Between 40 and 50 Degrees AOA   (Continued)

259

X-29 USAF S/N 820049

XCG=449.8 IN.   IXX=4554   IYY=51880   IZZ=57050   IXZ=2532
1-G   40 TO 50 DEG AOA   BLK IX-AA01

Figure B53   Asymmetry Control Between 40 and 50 Degrees AOA   (Continued)

260

Figure B53 Asymmetry Control Between 40 and 50 Degrees AOA   (Continued)

Figure B53 Asymmetry Control Between 40 and 50 Degrees AOA (Continued)

262

Figure B53 Asymmetry Control Between 40 and 50 Degrees AOA   (Continued)

Figure B53   Asymmetry Control Between 40 and 50 Degrees AOA   (Continued)

264

Figure B53 Asymmetry Control Between 40 and 50 Degrees AOA   (Continued)

265

Figure B53   Asymmetry Control Between 40 and 50 Degrees AOA   (Continued)

Figure B53 Asymmetry Control Between 40 and 5U Degrees AOA (Continued)

267

Figure B53 Asymmetry Control Between 40 and 50 Degrees AOA (Concluded)

268

X-29 USAF S/N 820049

XCG=450.4 IN.   IXX=4550   IYY=51820   IZZ=56980   IXZ=2545
1-G   40 TO 50 DEG AOA   BLK IX-AA01

Figure B54 Asymmetry Control Between 40 and 50 Degrees AOA

269

Figure B54 Asymmetry Control Between 40 and 50 Degrees AOA   (Continued)

270

Figure B54 Asymmetry Control Between 40 and 50 Degrees AOA (Continued)

Figure B54   Asymmetry Control Between 40 and 50 Degrees AOA   (Continued)

272

Figure B54 Asymmetry Control Between 40 and 50 Degrees AOA   (Continued)

273

Figure B54 Asymmetry Control Between 40 and 50 Degrees AOA   (Continued)

Figure B54 Asymmetry Control Between 40 and 50 Degrees AOA   (Continued)

275

Figure B54   Asymmetry Control Between 40 and 50 Degrees AOA   (Continued)

276

Figure B54 Asymmetry Control Between 40 and 50 Degrees AOA (Continued)

277

Figure B54   Asymmetry Control Between 40 and 50 Degrees AOA   (Continued)

278

Figure B54 Asymmetry Control Between 40 and grees AOA   (Continued);

Figure B54 Asymmetry Control Between 40 and 50 Degrees AOA (Continued)

280

X-29 USAF S/N 820049

XCG=450.4 IN.   IXX=4550   IYY=51820 IZZ=56990 IXZ=2545
1-G   40 TO 50 DEG AOA   BLK IX-AA01
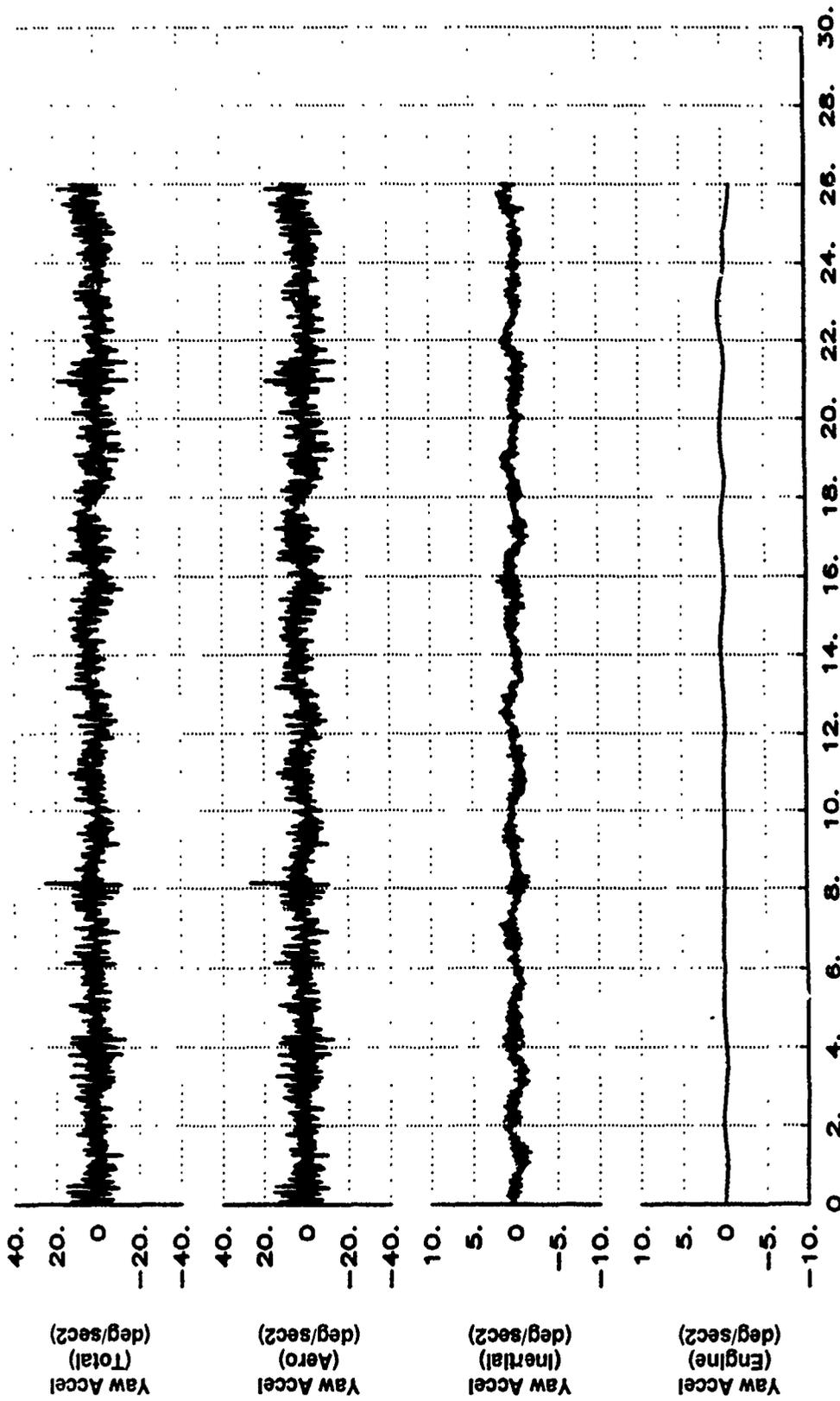
Figure B54   Asymmetry Control Between 40 and 50 Degrees AOA   (Concluded)

281

This page intentionally left blank.

APPENDIX C

AERODYNAMIC MODEL UPDATE

PROCESS AND VALIDATION

This page intentionally left blank.

AERODYNAMIC MODEL UPDATE PROCESS AND VALIDATION

INTRODUCTION

The X-29 high angle-of-attack (AOA) predicted aerodynamic mathematical model, AERO9B, contained the integrated results from eight static wind tunnel tests plus forced oscillation and rotary balance tests. The integration of this wind tunnel data into a FORTRAN mathematical model was completed in two parts. Grumman developed the longitudinal portion and NASA Langley developed the lateral-directional portion. The longitudinal and lateral-directional portions were integrated by Grumman into a single model which was labeled AERO9B. This was the version used to support the high AOA envelope expansion and served as the basis for all of the flight-based aerodynamic updates. The range of validity of the AERO9B model is shown in Table C1. See Reference 6 for details of the AERO9B model and the updates.

A method to update the nonlinear predicted model with flight data was developed. A point by point update of the predicted model was not practical due to the size and complexity of the AERO9B model. The method developed used the addition of flight derived aerodynamic increments (deltas) to the predicted total force and moment coefficients.

The update deltas, which were functions of Mach number, AOA, and surface position were applied in a piece-wise linear fashion by using multiple breakpoints. Breakpoints were functions of angle of attack, angle of sideslip, and surface position. This method allowed the basic nonlinearities of the predicted data base to be preserved.

The predicted nonlinear model was used to determine the predicted aerodynamics at the flight test conditions (Mach number, pressure altitude, dynamic pressure, cg, AOA, sideslip, surface positions, etc.). Plots of predicted total coefficients at flight test conditions served as the starting point for calculating the deltas between the predicted and flight aerodynamics. The final model was updated to the limits of the flight data. Beyond this point predicted trends in the predicted model were followed. See Reference 6 for a complete listing of the FORTRAN code and for the final values of the aero deltas.

The longitudinal and lateral-directional update models had different formats. The basic format of each

model and a brief description of the validation process are discussed separately in the following sections.

LONGITUDINAL UPDATES

General:

Two problems were encountered while updating the predicted longitudinal data base. First, the simultaneous movement of all three pitch control surfaces made it impossible to obtain separate surface derivatives. Second, locally linearized derivatives determined from flight data had to be converted into total delta pitching moments in order to be applied to the update model. The process required a trial and error approach.

During the initial envelope expansion, only pitching moment variations with AOA were modeled. This allowed the flight trimmed surface positions to be matched. Later, these pitching moment deltas were expanded to obtain a better balance between control power, basic pitching moment and static instability ($Cm\delta c$, Cm_0, and $Cm\alpha$, respectively).

Model Format:

The format of the longitudinal update model is shown in Figure C1. The update was applied after the predicted aerodynamics were computed at the wind tunnel reference cg of 454 inches.

Data Analysis:

A FORTRAN program was developed which computed the total predicted force and moment coefficients by driving the predicted aerodynamic model with appropriate flight measured inputs (Mach number, AOA, sideslip, surface positions etc.). The resultant predicted data were compared to the flight computed total force and moment coefficients (see Appendix E) to determine regions of major difference. A simplified engine model was used to subtract thrust and ram drag effects from the flight data. The pitching moment due to ram drag was large at high angles of attack and could not be ignored (see Figure C2). The total coefficient matching method along with tracking trimmed surface positions were the primary

longitudinal aerodynamic analysis tools used to expand the flight envelope.

Additional analysis of both slow and fast pitch doublets and stick pulses resulted in local linear (about trim) longitudinal static stability and canard power. The strake and flap control powers were assumed to be equal to their predicted values and the control power delta was attributed to the canard.

Update Process:

The procedure used to update the longitudinal aerodynamic model is outlined below. See Figure C3 for a flowchart of the longitudinal update process.

A linearization routine used measured flight conditions and surface positions to determine predicted values of Cm_α and $Cm\delta c$ about trim. The total coefficient matching method and pEst (Reference 7), a parameter estimation program which utilized a Modified Maximum Likelihood technique, were used to analyze flight data and estimate local values of Cm_α and $Cm\delta c$ which were then compared to the predicted values (see Figures C4 and C5).

The variation in total pitching moment coefficient with AOA term ($\Delta Cm[M,\alpha]$) in the update model had breakpoints at every 5 degrees angle of attack. A value of ΔCm_α was chosen midway between the breakpoints (see Figure C4) and was applied to the 5-degree AOA interval in order to evaluate a total change in pitching moment coefficient (ΔCm) at the next breakpoint. An example of the results are shown in Figure C6.

The $\Delta CM\delta c(M,\alpha,\delta c)$ in the update model had breakpoints at every 5 degrees AOA and also had separate tables for each canard breakpoint (-60, -40, -20, zero degrees). This complicated determining a ΔCm for the canard breakpoints. Local linear data were usually derived at trim conditions which were well away from the canard breakpoints. The longitudinal parameters were also nonlinear with canard position. For a given AOA, the $\Delta Cm\delta c$ was applied at the trim canard position on a total Cm versus δc plot, and the slope was extrapolated to the nearest canard breakpoints. The total ΔCm was the difference between the new Cm and the predicted value at the canard breakpoints (see Figure C7). The large gap between the canard breakpoints and nonlinearities introduced errors from extrapolating over large canard ranges.

Both ΔCm_α and $\Delta Cm\delta c$ had to be manipulated simultaneously. Since changing $\Delta Cm\delta c$ (which was a function of M, α, and δc) would also effect the local Cm_α results, an iterative process involving comparison of local linearized derivatives, total moment overplots, and 1-g surface trims was used to define a solution The process was concluded when an acceptable match with flight data was obtained from all three sources.

Limitations and Deficiencies:

The large intervals between canard position breakpoints required extrapolating measured control power deltas over ranges beyond their validity. This made fine tuning of the model difficult and resulted in having to sacrifice good values at off trim conditions, in order to model the trim points accurately. Inaccuracies occurred when the canard moved substantially away from its trimmed position.

The normal force coefficient was not updated. Pitching moment variations were included in the model as pure delta pitching moments. The moment increment when transferring across a cg range used the predicted normal force. Moment variations due to differences between predicted and flight normal force were not accounted for. The model included lift and drag coefficient updates which were not transferred to normal or axial force coefficients. The model could be improved by the addition of the appropriate normal and axial force coefficient deltas.

LATERAL-DIRECTIONAL UPDATES

General:

Piece-wise linear deltas between flight and prediction were used to update the nonlinear lateral-directional model. The deltas were functions of Mach number, angle of attack, angle of sideslip, aileron deflection, and rudder deflection. Appropriate breakpoints for each independent variable were required to add the deltas in a piece-wise linear fashion.

An early version of the update model used deltas which were functions of Mach number, angle of attack, and surface position with two fixed breakpoints for sideslip and aileron deflection and one fixed breakpoint for rudder deflection. Additional breakpoints for sideslip and aileron deflection at every

5 degrees AOA were added later to model the high degree of nonlinearity. The sideslip breakpoints were expanded into positive and negative values to account for the asymmetries in both in the predicted model and in the flight test results. Breakpoints were also added so that the total roll and yaw moment coefficients (Cl and Cn, respectively) would have separate sets of sideslip breakpoints.

Model Format:

The final format for updating the Cl and Cn equations involved table lookups with four sideslip breakpoints (two for positive and two for negative sideslip) each. This allowed application of a six slope correction to predicted values of Cn and Cl with sideslip at a given angle of attack. Two aileron position breakpoints allowed a three slope correction at a given angle of attack. The nonlinearity of rudder control power with deflection was not strong and a single rudder position breakpoint was sufficient.

Early versions of the update model only used AOA and Mach number as breakpoints for the roll damping update (ΔClp). The update model was later modified to include three sideslip values for ΔClp at each AOA. This was required for modeling wing rock and dynamic maneuvers.

The final format for the lateral-directional update model is shown in Figure C8.

Data Analysis:

Total coefficient, linear pEst results, and hand computation methods were used to determine control power derivatives from lateral stick and rudder pedal pulses for both small and large amplitude inputs. Hand computations of total moment coefficients with surface deflection aided in determining the nonlinear control power with deflection. Linear pEst results would only give an average control power over the deflection range. Hand computations provided a total moment produced by a given deflection.

Initial stability derivatives ($Cn\beta$, $Cl\beta$, and Clp) were determined from lateral-directional doublets using linear results from pEst. Lateral-directional stability and control derivatives were obtained to approximately 45 degrees AOA using pEst and other methods. The quality of the data reduced above 35 degrees AOA as dynamic pressure became low. The

reduced quality often required multiple repeats of the maneuvers to obtain reasonable data.

The linear derivative data were used to define an initial nonlinear update. The update was generated to match the results to the limits of the linear flight data. The trend indicated by the flight data was extrapolated to larger sideslips and surface deflections beyond the predicted trends with the independent variable in question. The extrapolated nonlinear update was modified as more flight data became available from larger amplitude maneuvers, which involved time history matching of wings level sideslips, aileron, and rudder rolls through batch simulations using both the predicted and flight updated aerodynamic models.

Update Process:

The processes used to update each separate coefficient were similar. An explanation of how Cn was modified with sideslip will be used to detail the updated process.

Analysis using pEst produced linearized flight values of $Cn\beta$ about zero sideslip. These values were compared to the predicted data in order to evaluate the differences and develop deltas ($\Delta Cn\beta$). Figure C9 illustrates the determination of $\Delta Cn\beta$. The local $\Delta Cn\beta$ was applied to the total predicted Cn versus sideslip plot at zero sideslip and extrapolated to higher sideslips by following the predicted trends. The ΔCn between predicted and the updated model was then plotted versus sideslip. The $\Delta Cn\beta$ and sideslip breakpoints were determined from this plot as shown in Figure C10. The updated model was then evaluated against flight maneuvers run through a batch simulation. Comparison of the simulated and actual flight dynamics was used to refine the model in an iterative process.

Several versions of the batch simulation were used to accomplish the matching:

Version 1:

full 6 degrees-of-freedom (DOF)

nonlinear aerodynamic model

closed loop, flight control system (FCS) in the loop

Version 2:

variable DOF (lateral or directional or lateral-directional)

nonlinear aerodynamic model

open loop, FCS out of the loop

flight values in longitudinal axis

flight values in appropriate lateral-directional axis

biases added to integrated values (p, r, β)

Version 3:

3 DOF lateral-directional simulation (p, r, β)

nonlinear aerodynamic model

closed loop, lateral-directional FCS in the loop

flight values in longitudinal axis

The full 6 DOF simulation (Version 1) was rarely used because the simulation would not remain on condition long enough to extract any useful information. Version 2 allowed the true airframe lateral-directional axis to be analyzed without the FCS in the loop. However, above 20 degrees AOA, the unstable roll damping required the stabilizing influence of the control system to prevent divergences. The Version 3 simulation solved this problem by including the lateral-directional FCS in the loop but used flight measured longitudinal states for the equations of motion. The addition of the FCS in the loop added the surface positions as matching states.

Variations to other lateral-directional parameters were made in a similar fashion and incorporated into the updated model. Time history matching of larger amplitude maneuvers using the Version 3 simulation was then used to modify the update model to obtain acceptable matches. As a final step, quantitative and qualitative data were obtained in the real time simulator with the updated aero model.

Limitations and Deficiencies:

The major drawback with early versions of the lateral-directional update model was the lack of sufficient breakpoints to correctly model the nonlinearities and asymmetries. This resulted in distortions of the nonlinearity of the predicted model and was solved by increasing the number of breakpoints for parameter updates. The need for multiple breakpoints and piece-wise linear update of the nonlinear model is demonstrated in Figure C11. The predicted and final updated values for total Cn versus sideslip at 30 degrees AOA using multiple ΔCnβ and sideslip breakpoints are compared to the result where a single ΔCnβ was used in the update model. The single linear ΔCnβ provided erroneous results. The initial low sideslip ΔCnβ was correct, but the deltas changed with sideslip and, using the single value, no longer provided acceptable simulated flight dynamics time history matches. The number of breakpoints required was proportional to the degree of nonlinearity in both the predicted and flight updated models.

AEROMODEL VALIDATION

Longitudinal Aerodynamics:

The updated longitudinal aerodynamics were validated through three primary methods:

1. Comparisons of the trimmed surface positions from the real time simulator using both the updated and predicted aerodynamic models with trim values from flight. A comparison of flight and updated simulation trim surface positions can be found in Appendix B (Figures B12 and B13) and the Test and Evaluation section (Figure 11).

2. Comparison of linearized coefficients about trim conditions using updated aerodynamic model and the flight determined values from pEst linear parameter estimation. Plots of the linear model and flight estimated derivatives can be found in Appendix B (Figure B1).

3. Total moment coefficient overplots between the flight values and the updated model. Figures C12 through C14 show some of these results for various pitch doublets, a windup turn, and a 1-g pitch-up to 55 degrees AOA.

The surface trims, linear coefficient comparisons, and the total moment matches using the updated longitudinal model generally matched flight better than the original model below 40 degrees AOA. Above 40 degrees AOA, the model was not conservative since it has a greater nosedown recovery capability than was

288

encountered in flight, but was usually closer to flight than the predicted model. The fidelity of the flight updated model could have been improved by increasing the number of canard breakpoints and more in depth balancing of $Cm\alpha$ and $Cm\delta c$.

Lateral-Directional Aerodynamics:

The updated lateral-directional aerodynamics were validated through two primary methods:

1. Real time simulator response characteristics of sideslips and wing rock. Steady-state sideslip comparisons between flight and the simulation using the updated aerodynamic model are shown in Appendix B (Figures B18 through B24).

2. Version 3 lateral-directional batch simulation flight dynamics comparisons between flight data, predicted and updated aerodynamics. Examples of representative time history overplots comparing flight to predicted and updated simulation are shown in Figures C15 through C21. Included are stabilized points, aileron and rudder rolls, and wings level sideslips at various angles of attack and airspeeds.

The real time and batch simulation results showed that the updated lateral-directional model matched flight results better than when the predicted aerodynamics were used.

A matching problem between the batch and updated real-time simulation was encountered when trying to match wing rock characteristics. Roll damping derivatives generated to match batch simulation wing rock did not provide acceptable real-time simulation characteristics. The real-time simulation wing rock had a larger magnitude than both flight or the batch simulation. Roll damping derivatives were adjusted to provide the best real-time simulation matches following initial development with the batch simulation. Time delays with the real-time simulation were credited with the difference although full tests to verify this were not accomplished.

Conclusion:

The updated aerodynamics produced responses that were more characteristic of the observed flight responses than did the predicted aero-model. This was supported by several analysis methods including a large number of batch simulation overplots and real-time simulation studies using the updated aero and covering the range of angle of attack, sideslip, and airspeed tested.

Table C1 AERO9B Validity Range

	Mach Number Region		
	0.0 - 0.6M	0.6 - 0.9M	0.9 - 2.0M
Angle of Attack Range	-50° to 90°	-4° to 40°	-4° to 24°
Angle of Sideslip Range	-30° to 30°	-20° to 20°	-16° to 16°
Canard Range	-60° to 30°	-30° to 20°	-30° to 20°
Flaperon Range	-10° to 25°	-10° to 25°	-10° to 25°
Strake Range	-30° to 30°	-30° to 30°	-30° to 30°
Aileron Range	-17.5° to 17.5°	-17.5° to 17.5°	-17.5° to 17.5°
Rudder Range	-30° to 30°	-30° to 30°	-30° to 30°

```
Cj = Cjpredicted + ΔCj(M,α) + ΔCj(M,α,δc) + ΔCj(M,α,δf) +

        ΔCj(M,α,δs) + ΔCj(M,α)qc/2Vt

for Cj = Cm, CL, CD

range for the ΔCj:  0 < α < 90   Δ = 5 degrees

          M = 0.0, 0.6, 0.8, 0.9

breakpoints:

        δc: -60, -40, -20, 0

        δf: -10, 0, 10, 20, 30

        δs: -30, 0, 30
```

Figure C1   Longitudinal Update Model Format

PREDICTED AERO MODEL
MIL POWER   1 G ACC TRIM
MACH=0.3   ALT=30K FT   XCG=451 IN

(Y-axis: PITCHING MOMENT DUE TO RAMDRAG)
(X-axis: ANGLE OF ATTACK (DEG))
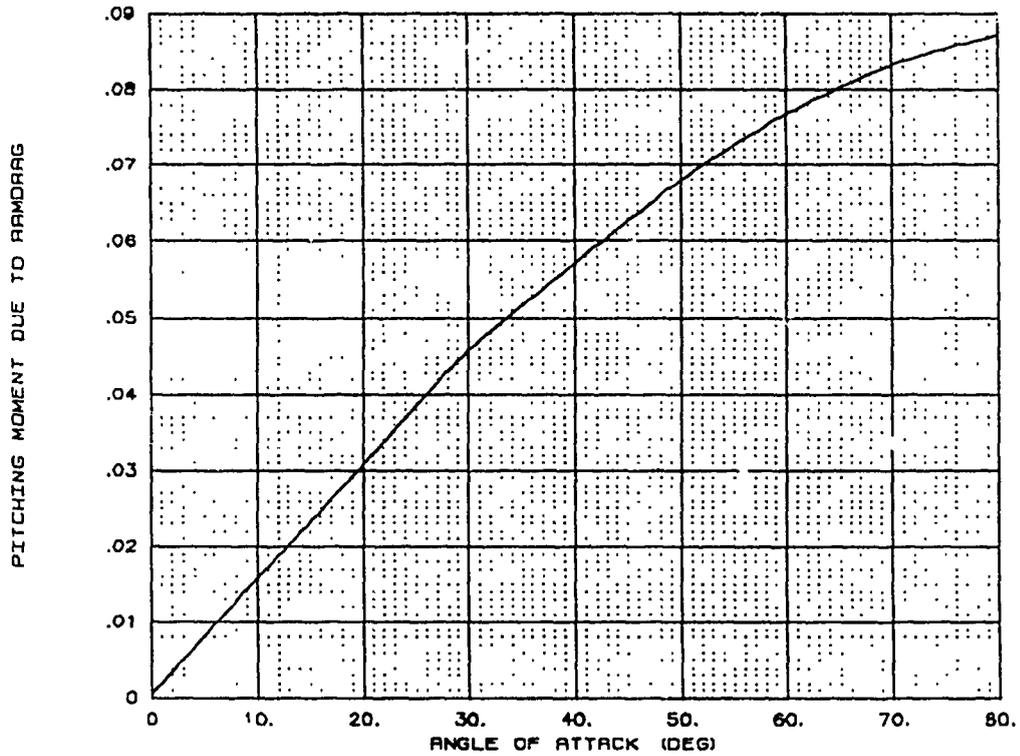
Figure C2 Ram Drag Effects

291
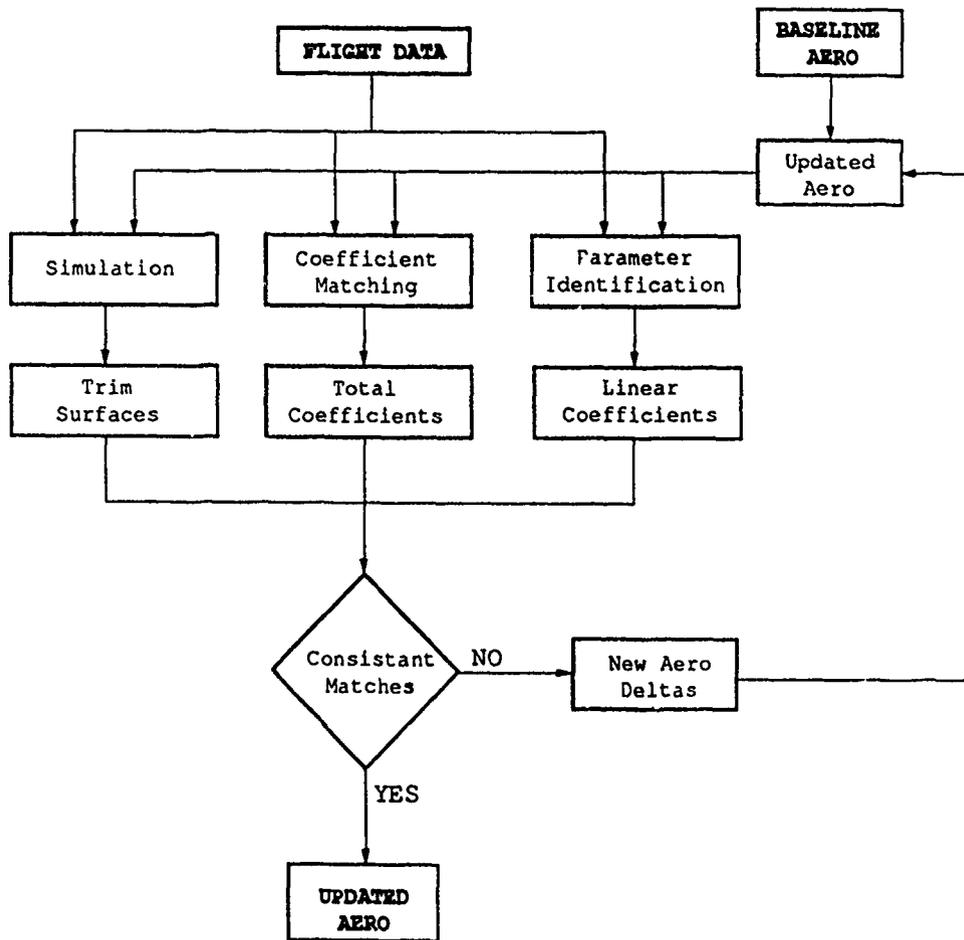
Figure C3   Longitudinal Aero Model Update Process
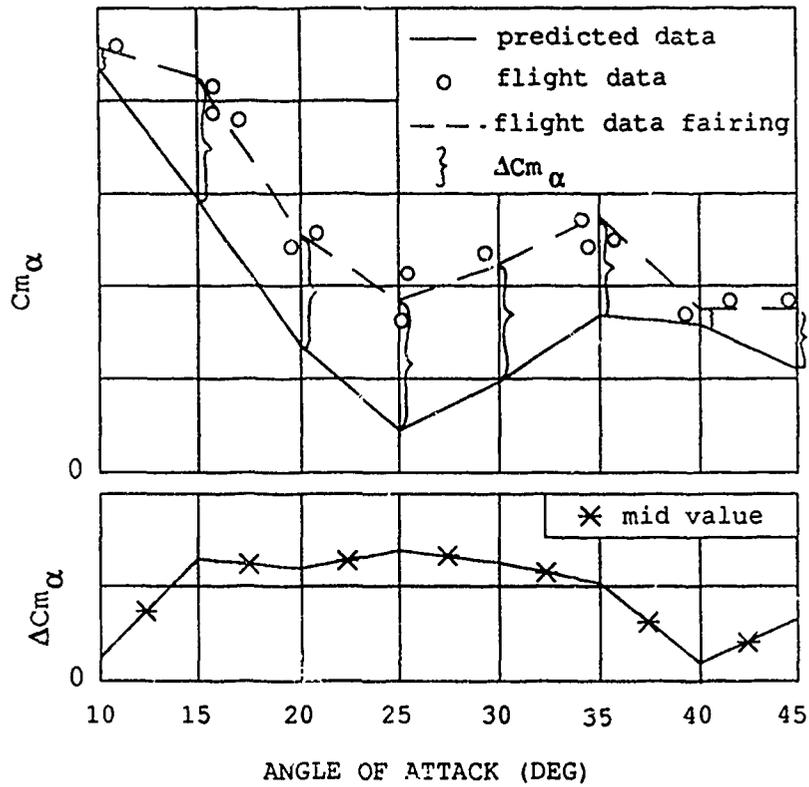
Figure C4 Comparison of Flight to Predicted Data to Determine the Change in Static Longitudinal Stability

293
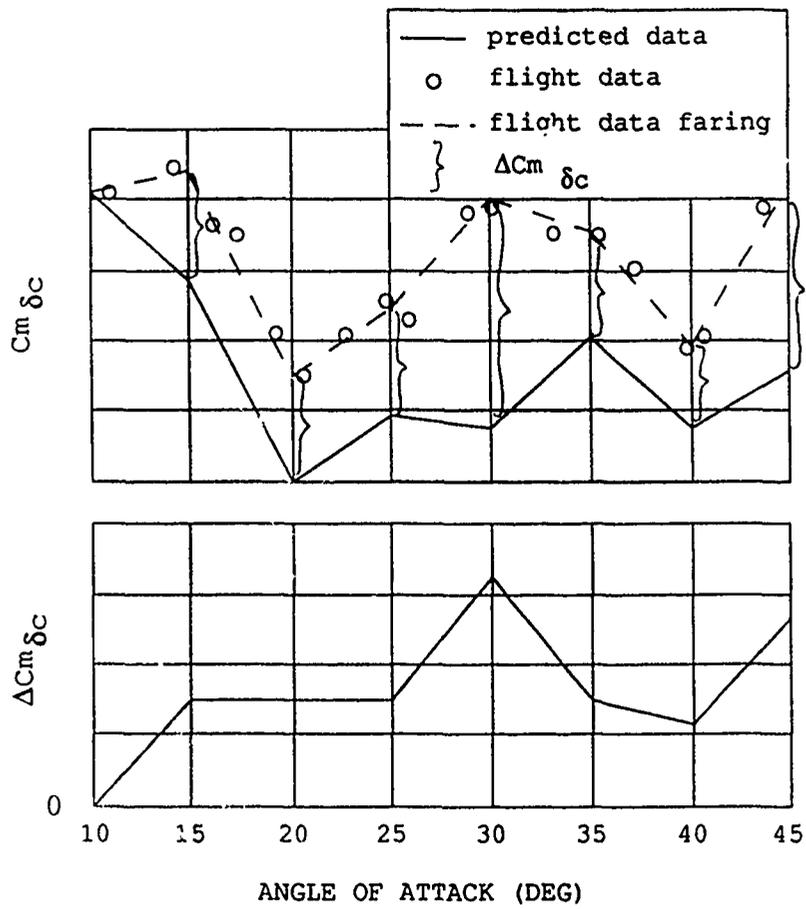
Figure C5 Comparison of Flight to Predicted Data to Determine the Change in Longitudinal Control Power

294
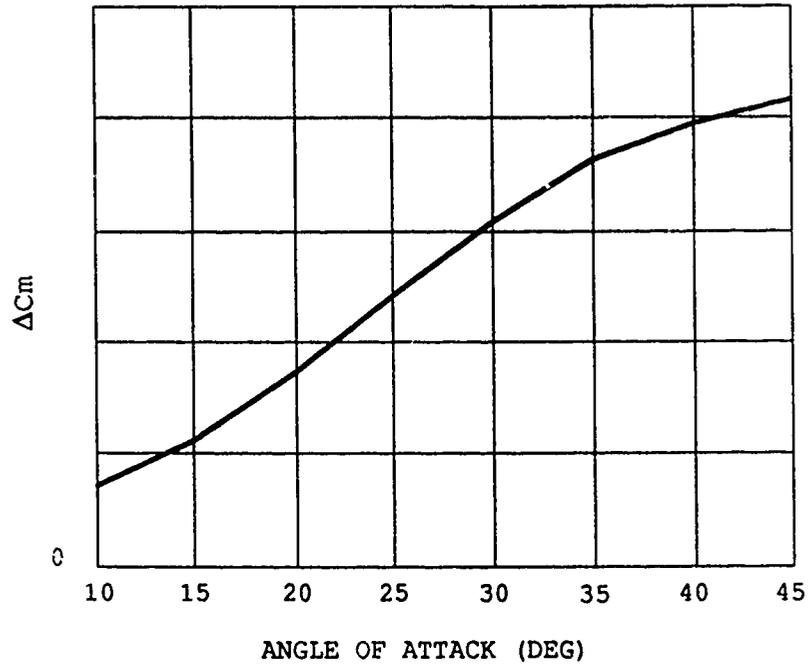
**Figure C6 Results From Converting Delta Pitching Moment
Slopes Into Total Delta Pitching Moments**

For a given angle of attack:

$\triangle$ Predicted Cm at trim canard

O   Predicted Cm at canard break pts

□   Updated Cm at canard break pts

CANARD POSITION (DEG)
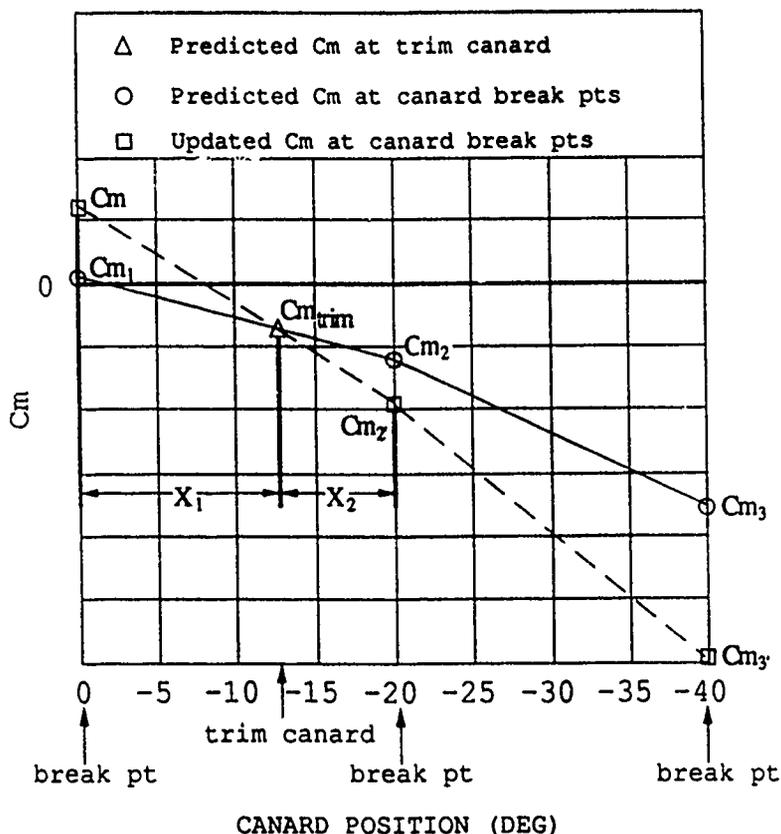
The updated Cm values were calculated as follows:

$$Cm_{1'} = Cm_{trim} - \left[\frac{Cm_2 - Cm_1}{20} - \Delta Cm_{\delta c} \right] * X_1$$

$$Cm_{2'} = Cm_{trim} + \left[\frac{Cm_2 - Cm_1}{20} - \Delta Cm_{\delta c} \right] * X_2$$

$$Cm_{3'} = Cm_{2'} + \left[\frac{Cm_3 - Cm_2}{20} - \Delta Cm_{\delta c} \right] * 20$$

And the ΔCm values were the difference between the updated and the predicted coefficients:

$$\Delta Cm_1 = Cm_{1'} - Cm_1 \qquad \Delta Cm_2 = Cm_{2'} - Cm_2 \qquad \Delta Cm_3 = Cm_{3'} - Cm_3$$

**Figure C7 Conversion of Canard Power Deltas
Into Total Moment Coefficients**

296

$$Cj = Cj_{bas} + \Delta Cj_o(M,\alpha) + \Delta Cj(M,\alpha,\beta) + \Delta Cj(M,\alpha,\delta a) +$$

$$\Delta Cj(M,\alpha,\delta r) + \Delta Cj_p(M,\alpha,\beta)\, Pb/2V_t + \Delta Cj_r(M,\alpha)\, rb/2V_t$$

where $Cj = Cl,\ Cn,\ Cy$

and $\Delta Cj(M,\alpha,\beta) = [\Delta Cj_{\beta_1} * \beta_{B_1} + \Delta Cj_{\beta_2} * (\beta_{B_2} - \beta_{B_1}) +$

$$\Delta Cj_{\beta_3} * (\,{}^{\beta}\!. - \beta_{B_2})] * \text{sign } \beta$$

for breakpoints β_{B_1}, β_{B_2}, and β_{B_3}

$\Delta Cj(M,\alpha,\delta a)$ and $\Delta Cj(M,\alpha,\delta r)$ were similar but used their respective breakpoints.

range for the ΔCj : $0 < \alpha < 90$ $\Delta = 5$ degrees

$$M = 0.0,\ 0.6,\ 0.8,\ 0.9$$

sideslip breakpoints:

Cn and Cy: $\beta_{B_{1R}}(\alpha)$, $\beta_{B_{2R}}(\alpha)$, $\beta_{B_{1L}}(\alpha)$, $\beta_{B_{2L}}(\alpha)$

Cl: $\beta_{B_{1R}}(\alpha)$, $\beta_{B_{2R}}(\alpha)$, $\beta_{B_{1L}}(\alpha)$, $\beta_{B_{2L}}(\alpha)$

Clp: $\beta_{B_1} = 0$, $\beta_{B_2} = 2$, $\beta_{B_3} = 10$

where R is right or positive and

L is left or negative

$0 < \alpha < 90$ $\Delta = 5$ degrees

aileron breakpoints : $\delta a_1(\alpha)$, $\delta a_2(\alpha)$

where $0 < \alpha < 90$ $\Delta = 5$ degrees

rudder breakpoint   : $\delta r = 15$ degrees

Figure C8   Lateral-Directional Model Update Format
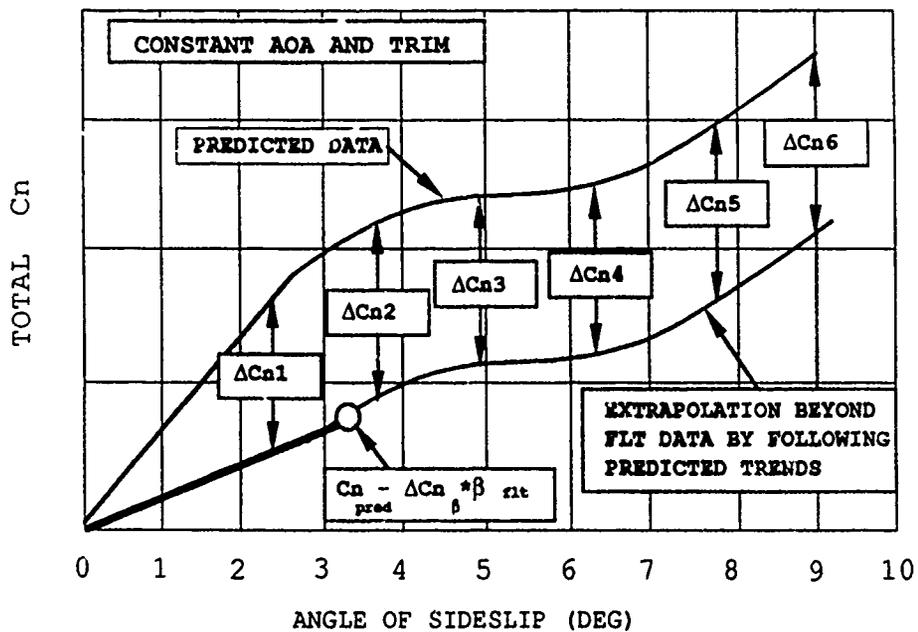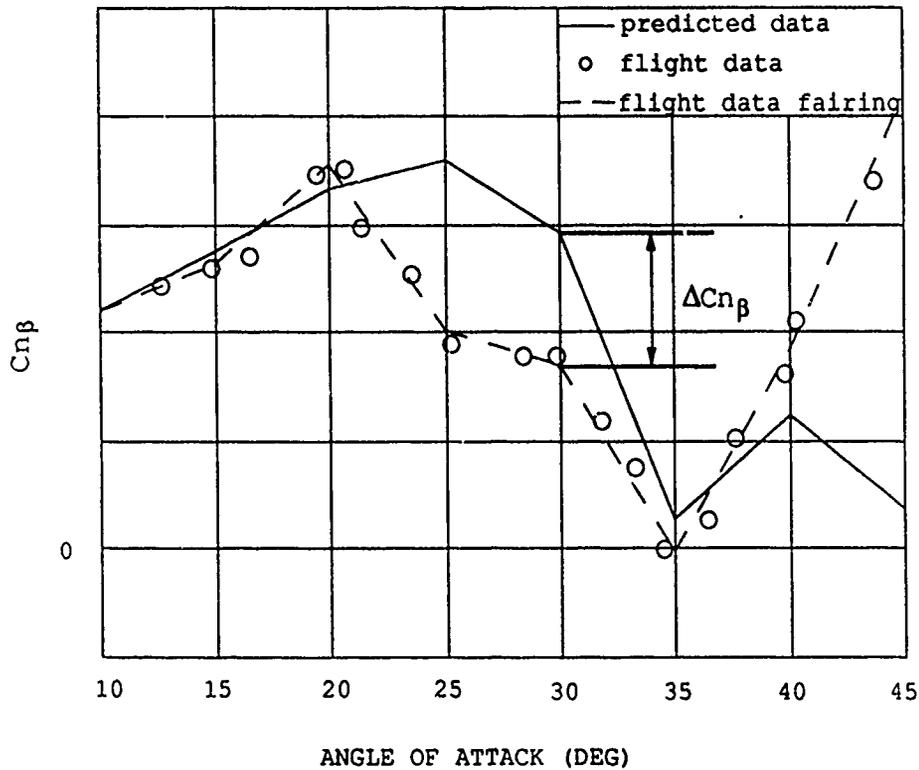
Figure C9   Determining the Change in Static Directional Stability
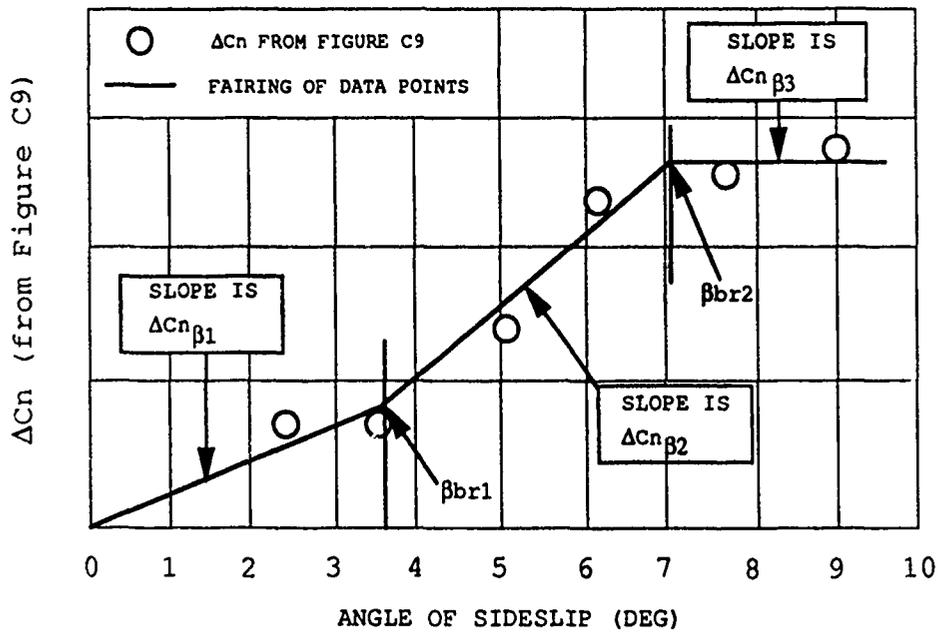
Figure C10 Determining the Piece-wise Linear Static Directional Stability and Appropriate Breakpoints

299
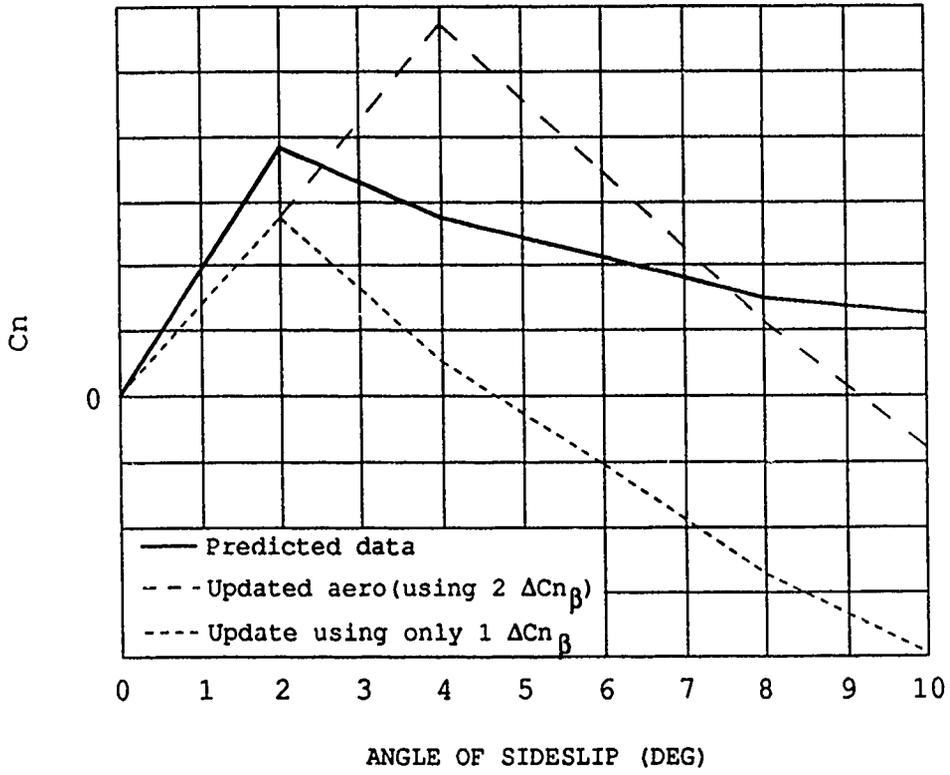
Figure C11   Example of the Effects of Insufficient Breakpoints

300
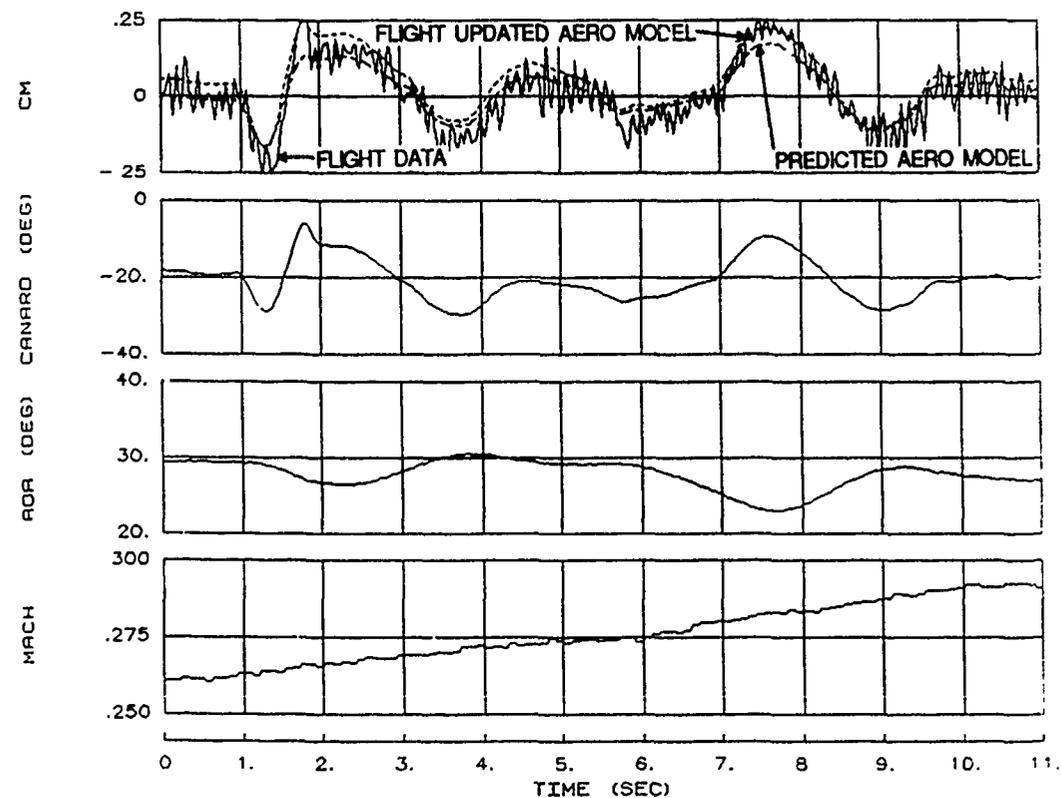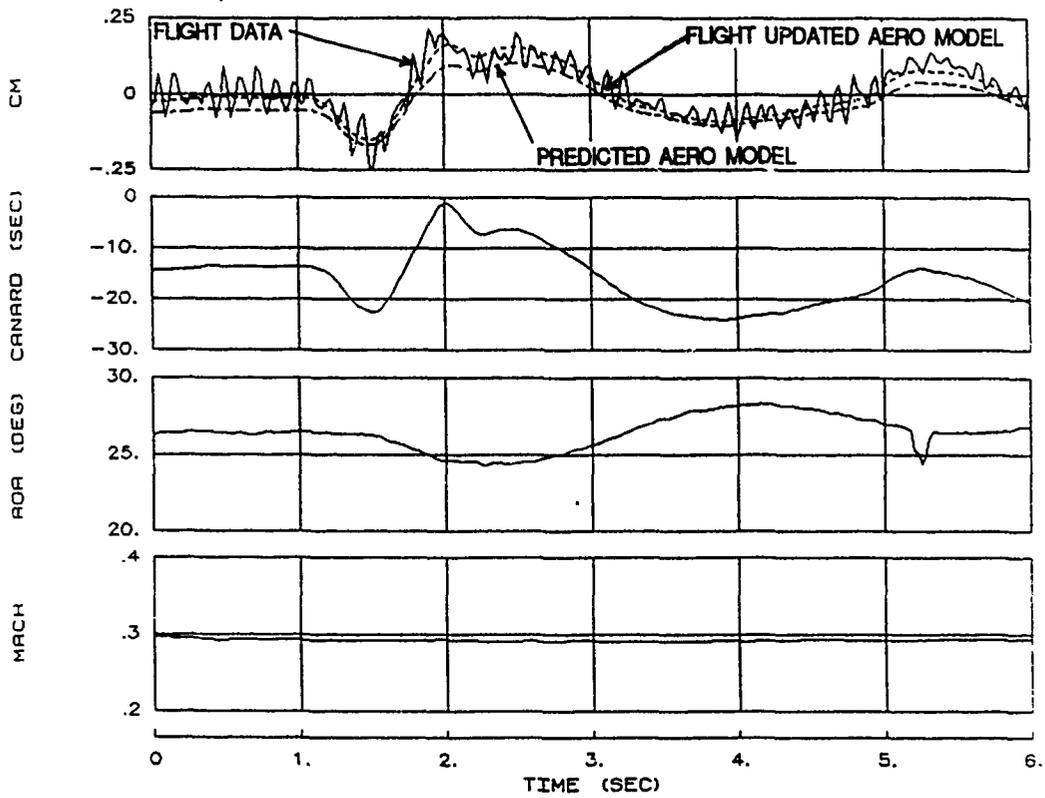
**Figure C12 Comparison of Total Pitching Moment
Coefficient During 1-G Pitch Doublets**

301
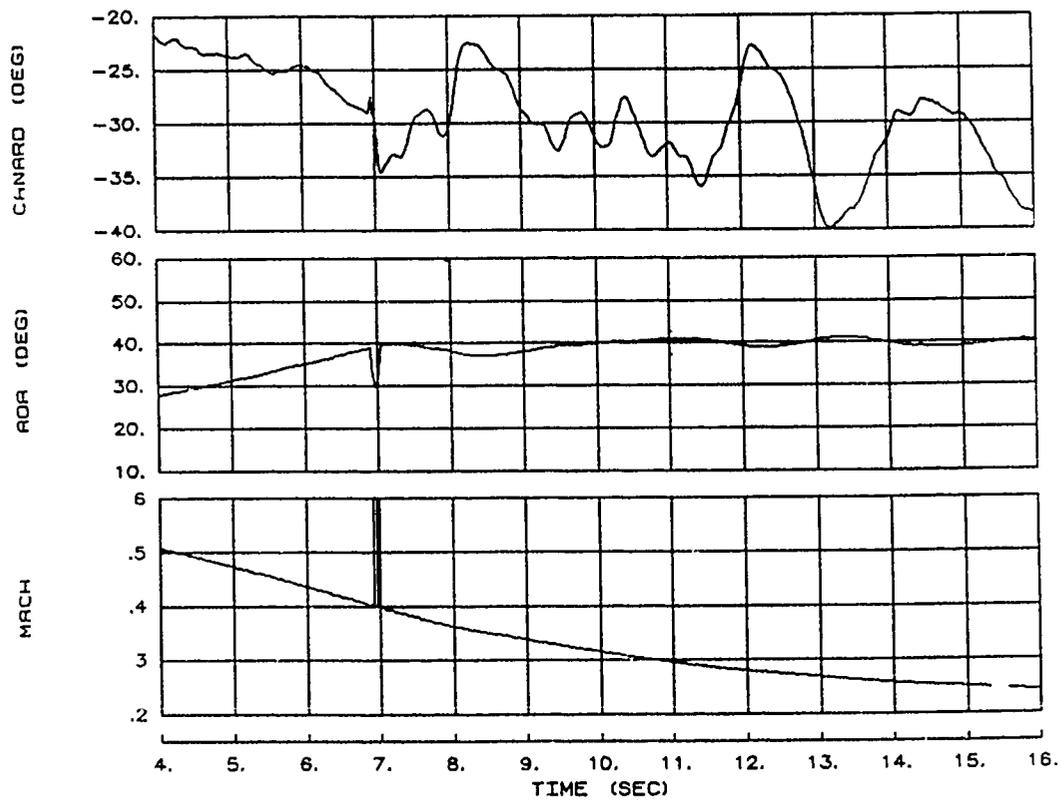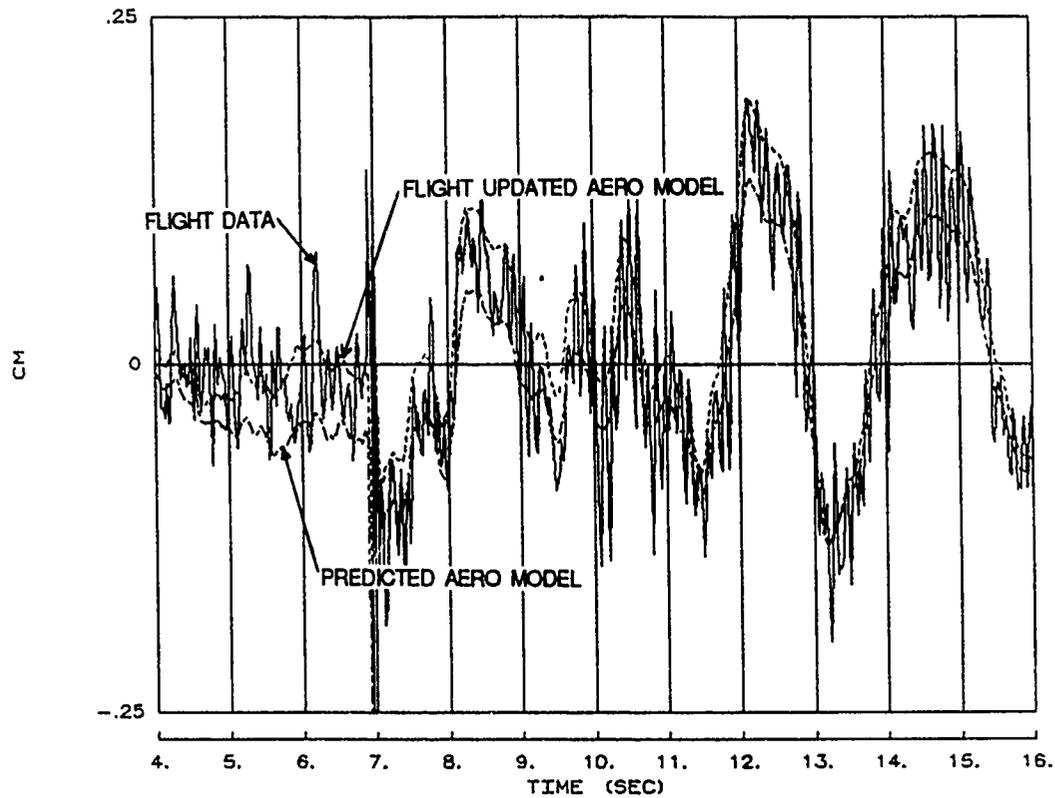
Figure C13 Comparison of Total Pitching Moment Coefficient During a Windup Turn to 40 Degrees AOA

302
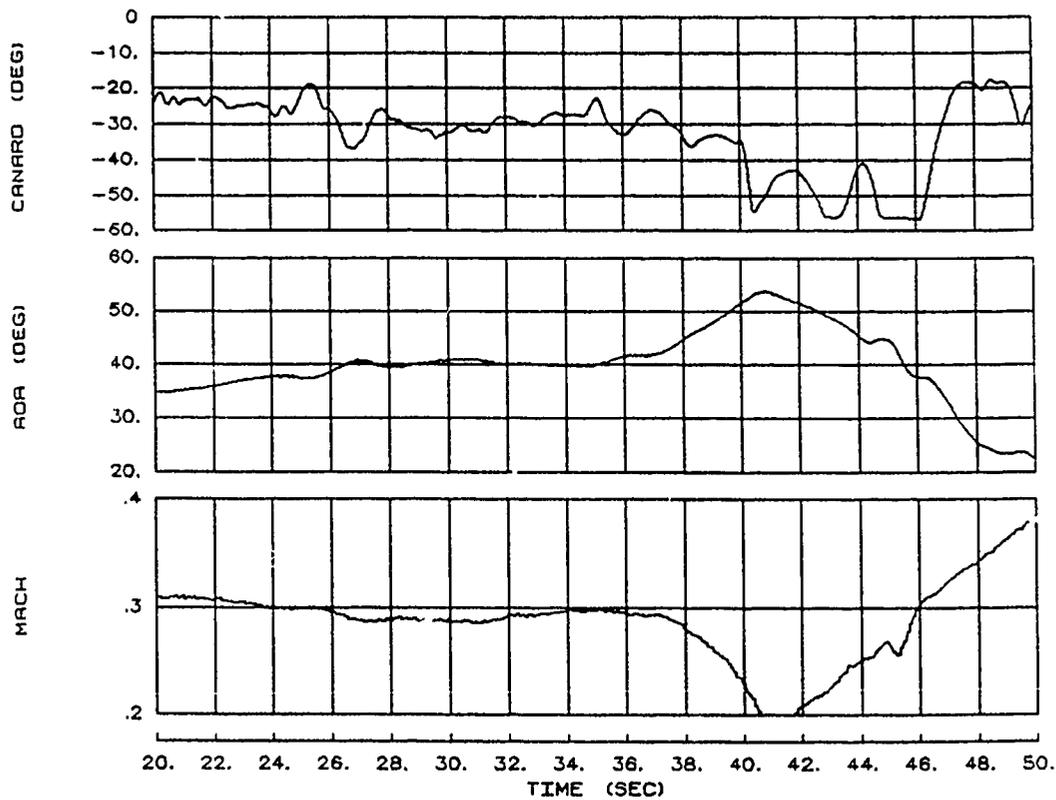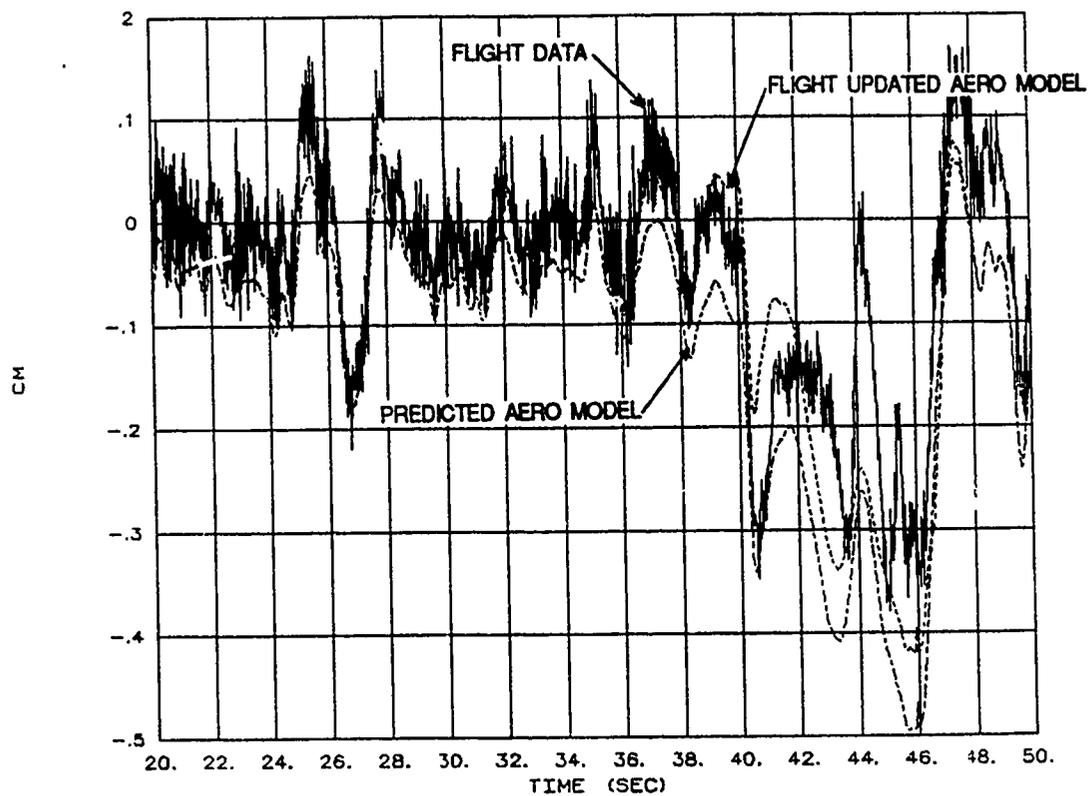
**Figure C14 Comparison of Total Pitching Moment
Coefficient During a Pull-Up to 55 Degrees AOA**

**Figure C15   Batch Simulation Comparison of a 1-G,
45 Degree AOA Stabilized Point**

Figure C15   Batch Simulation Comparison of a 1-G,
45 Degree AOA Stabilized Point (Continued)
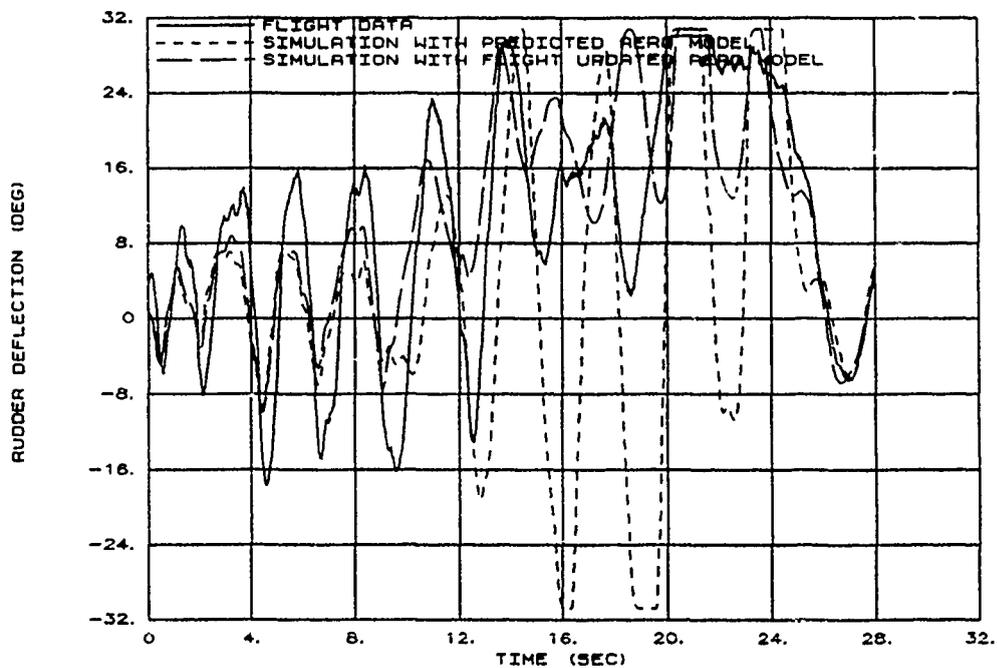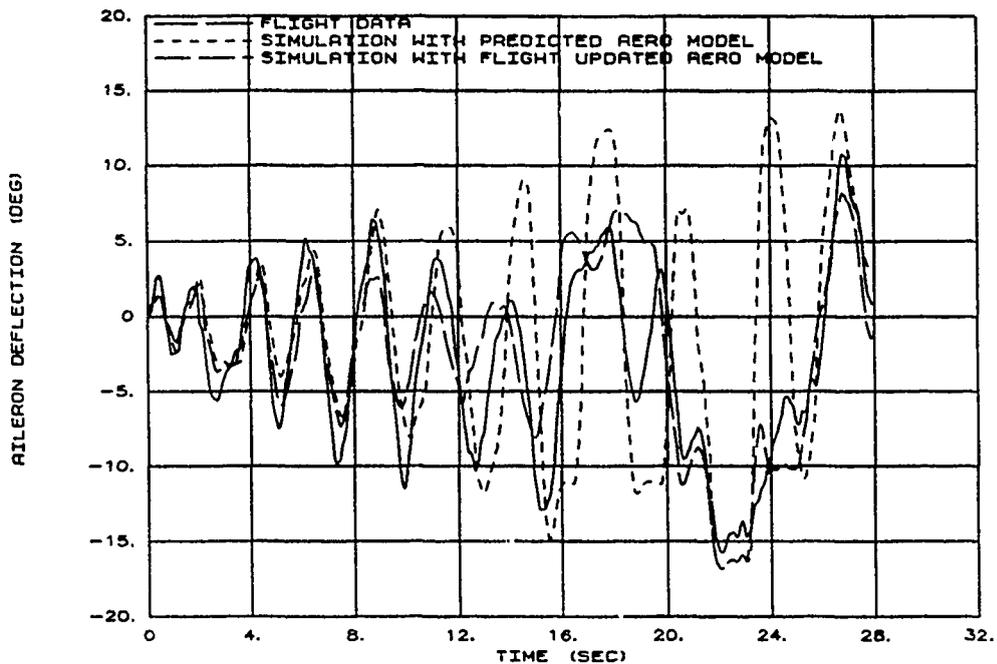
Figure C15 Batch Simulation Comparison of a 1-G,
45 Degree AOA Stabilized Point (Concluded)

Figure C16 Batch Simulation Comparison of a 1-G,
40 Degree AOA Full Stick Aileron Roll

**Figure C16   Batch Simulation Comparison of a 1-G, 40 Degree
AOA Full Stick Aileron Roll   (Continued)**
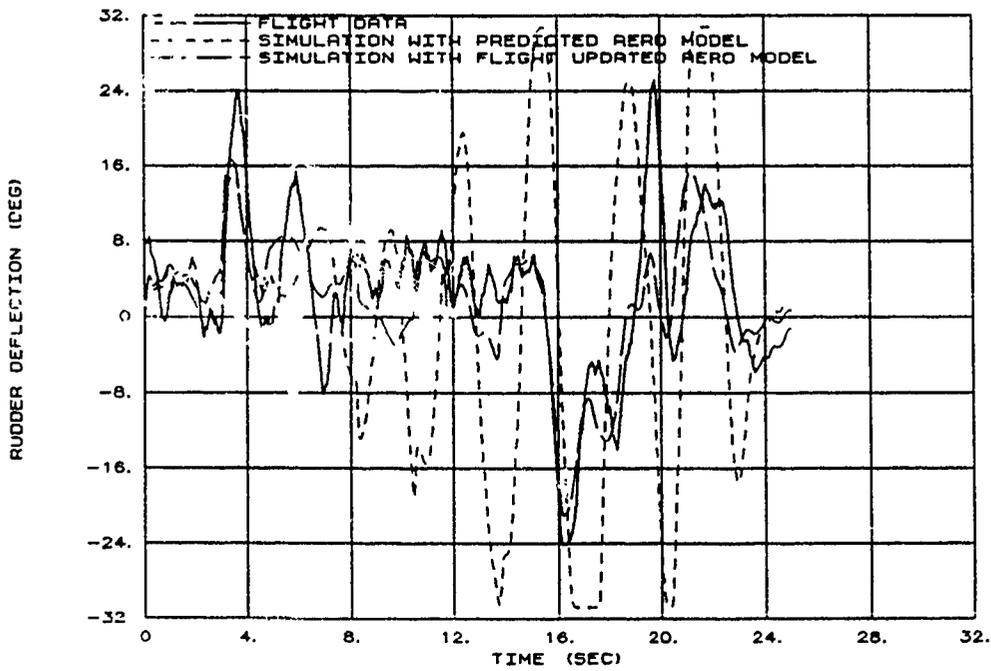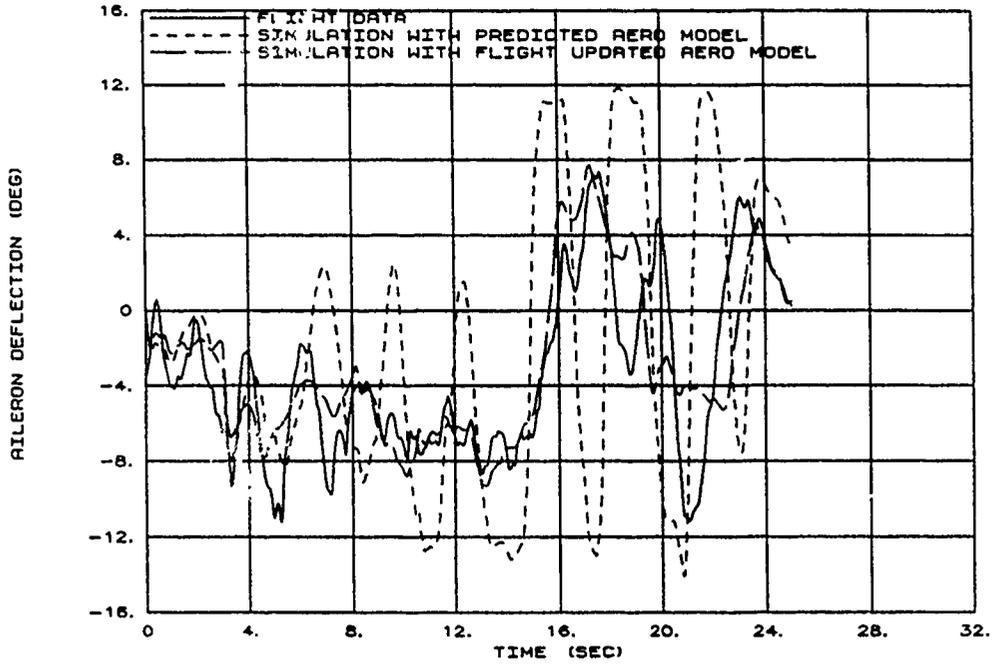
Figure C16   Batch Simulation Comparison of a 1-G, 40 Degree AOA Full Stick Aileron Roll   (Concluded)
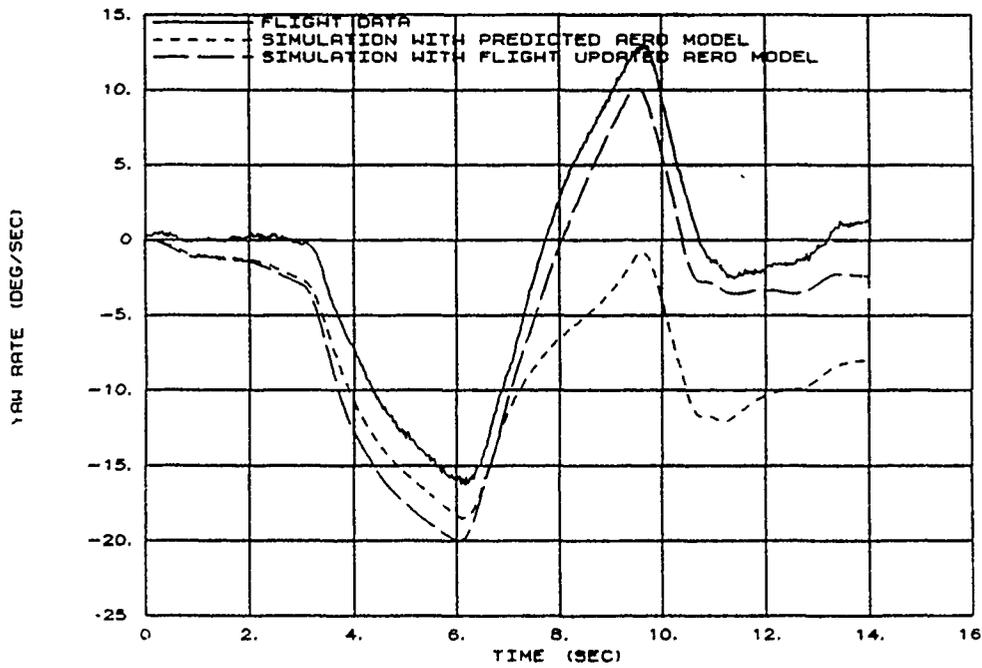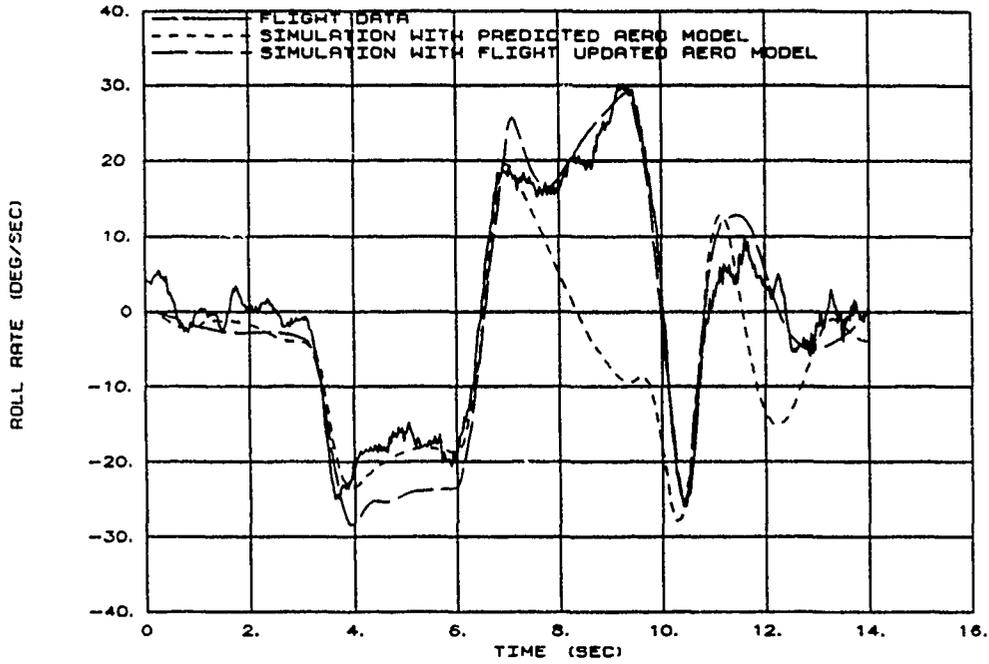
Figure C17   Batch Simulation Comparison of a 1-G, 25 Degree AOA Full Stick Aileron Roll with TW 53

Figure C17   Batch Simulation Comparison of a 1-G,
25 Degree AOA Full Stick Aileron Roll
with TW 53 (Continued)

Figure C17   Batch Simulation Comparison of a 1-G,
25 Degree AOA Full Stick Aileron Roll
with TW 53   (Concluded)

Figure C18   Batch Simulation Comparison of a 1-G, 35 Degree
AOA Full Stick Aileron Roll with TW 53

313

Figure C18   Batch Simulation Comparison of a 1-G, 35 Degree AOA Full Stick Aileron Roll with TW 53 (Continued)
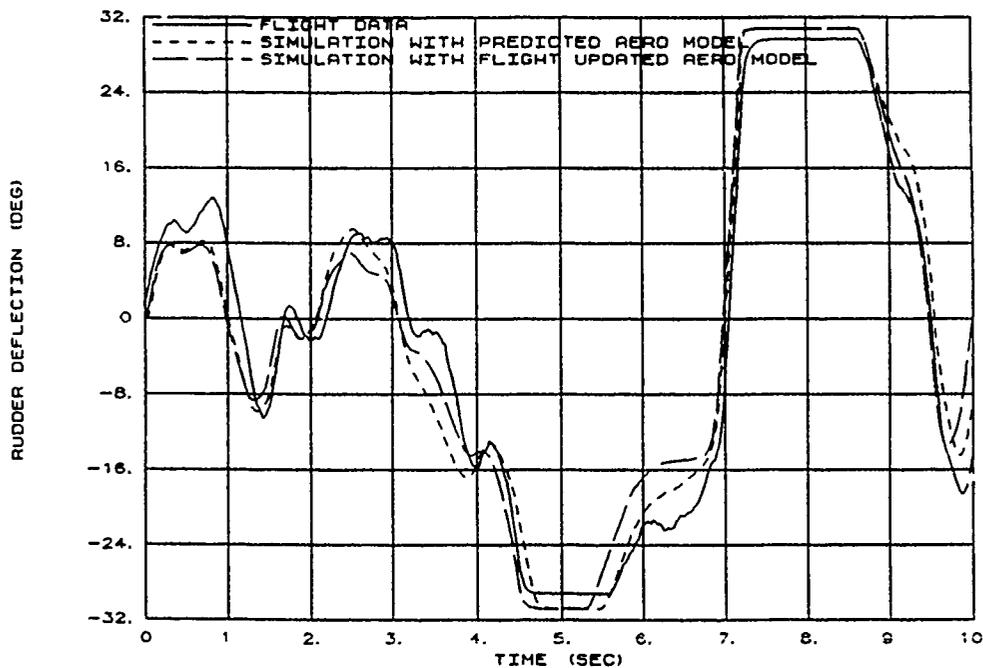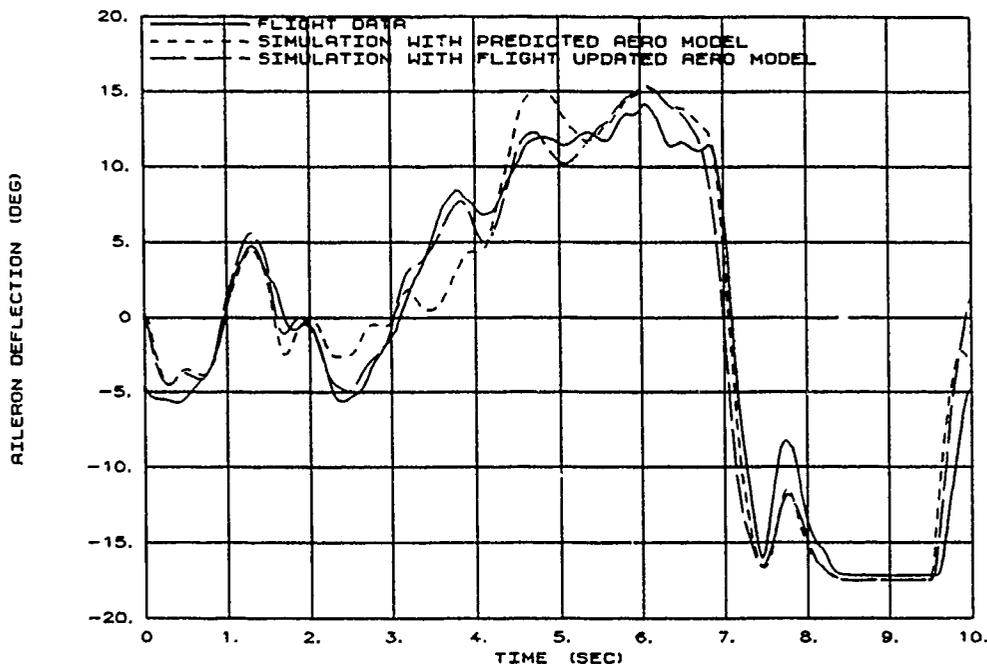
X-29 USAF S/N 820049

Figure C18   Batch Simulation Comparison of a 1~G,
35 Degree AOA Full Stick Aileron Roll
with TW 53 (Concluded)

Figure C19   Batch Simulation Comparison of a 1-G,
            30 Degree AOA Full Pedal Rudder Roll

**Figure C19   Batch Simulation Comparison of a 1-G, 30 Degree
AOA Full Pedal Rudder Roll   (Continued)**

317

Figure C19   Batch Simulation Comparison of a 1-G, 30 Degree
AOA Full Pedal Rudder Roll   (Concluded)

318

Figure C20   Batch Simulation Comparison of a 160 KCAS,
25 Degree AOA Full Pedal Rudder Roll

Figure C20   Batch Simulation Comparison of a 160 KCAS, 25 Degree
AOA Full Pedal Rudder Roll (Continued)

320

Figure C20 Batch Simulation Comparison of a 160 KCAS, 25 Degree AOA Full Pedal Rudder Roll (Concluded)

Figure C21   Batch Simulation Comparison of a 1-G,
30 Degree AOA Wings-Level Sideslip

Figure C21   Batch Simulation Comparison of a 1-G, 30 Degree
AOA Wings Level Sideslip (Continued)
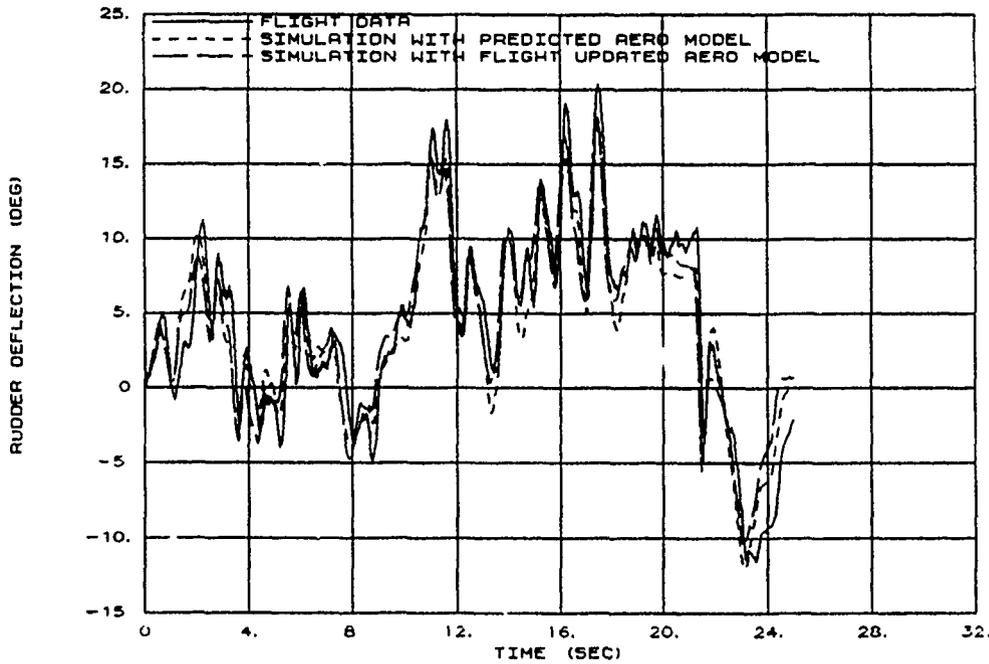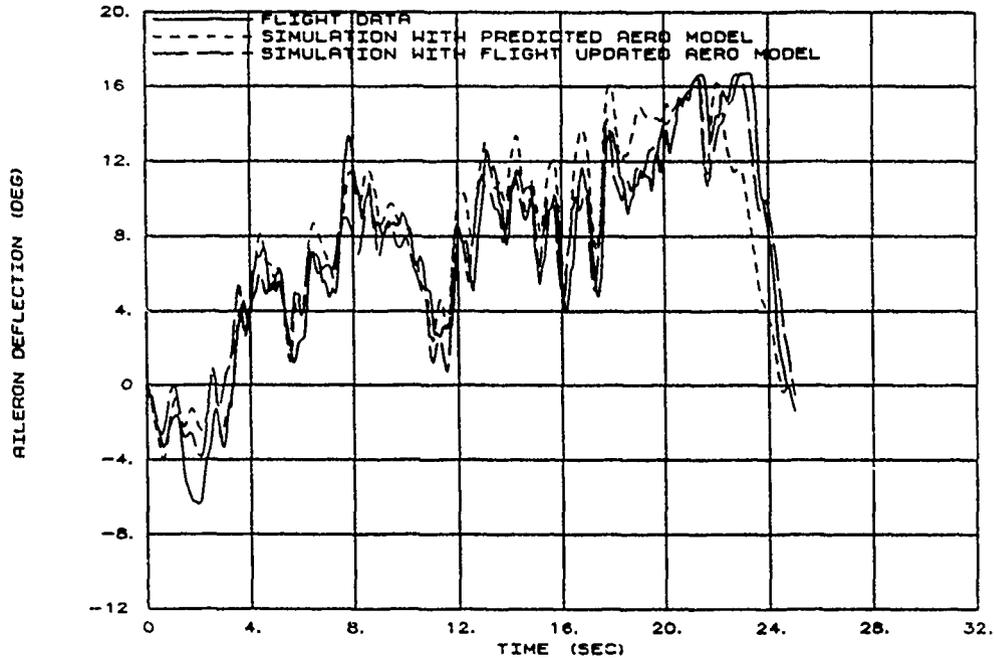
Figure C21 Batch Simulation Comparison of a 1-G, 30 Degree AOA Wings Level Sideslip (Concluded)

APPENDIX D
FLIGHT CONTROL SYSTEM DESCRIPTION

This page intentionally left blank.

FLIGHT CONTROL SYSTEM DESCRIPTION

GENERAL

This section covers modifications to the X-29 flight control system (FCS) for high angle-of-attack (AOA) research. Software and limited hardware modifications were made prior to flight test and during the program. This is a functional overview of the high AOA system and is not intended as complete documentation. Reference 3 contains the high AOA software and gain descriptions in detail and Reference 2 contains a full functional overview of the general low AOA control system flown to 20 degrees AOA.

The modifications described pertain to BLOCKIX-AA, BLOCKIX-AA01 and BLOCKIX-AA02 software releases for high AOA research with the X-29 USAF S/N 820049 aircraft. The BLOCKIX software release series used the low AOA BLOCKVIII-AD release as a baseline for modification. The original BLOCKIX-AA software release was validated and verified (V and V) to 0.6 Mach number up to the full AOA capability of the aircraft. The BLOCKIX-AA01 release contained a full 8-g longitudinal command capability and was implemented as a result of flight test results. The BLOCKIX-AA02 release contained lowered roll rate feedback gains, a roll notch filter, and modified variable gain ("dial-a-gain") for increasing lateral and aileron-to-rudder interconnect (ARI) command gains for research. The release also contained an analog roll axis simple notch filter, and Redundancy Management modifications. The BLOCKIX-AA02 release was V and V to 0.8 Mach number and the full AOA capability of the aircraft.

Early on in the FCS design phase a decision was made to maintain the basic "low AOA" control laws (-10 degrees) intact and to keep high AOA modifications to a minimum. This was specified in order to minimize design, envelope expansion, and V and V efforts. As a result, the high AOA control law modifications were faded in between 10 and 15 degrees AOA. The system remained essentially unchanged (with minor exceptions) from BLOCKVIII-AD below 10 degrees AOA. Above 15 degrees AOA, the high AOA control laws and modifications were functional.

FLIGHT CONTROL SYSTEM MODES

The two primary FCS modes were normal digital (ND) and analog reversion (AR). The ND mode was modified for high AOA flight research. The AR mode was not modified.

The ND mode was separated into several submodes:

1. Normal digital/automatic camber control (ND/ACC)

2. Normal digital/manual camber control (ND/MCC)

3. Normal digital/power approach (ND/PA)

The ND/ACC had an additional submode for high AOA operation called "NORMHI" which eliminated the surface reasonableness test. Both the ND/ACC and the ND/MCC modes contained high AOA control laws above 10 degrees AOA, although the ND/MCC mode was not V and V or tested at high AOA. The ND/PA mode was not modified from the BLOCKVIII-AD low AOA release.

The ND/ACC mode was the primary up-and-away (UA) flight mode. Basic stabilization and aircraft response were controlled by this mode. In addition a slow trimming feature, the automatic camber control (ACC), was incorporated which provided predetermined canard trim positions as a function of flight condition. For hig' AOA the canard trim was determined to maximize lift coefficient.

The ND/MCC mode was similar to ND/ACC with the exception that trim flaperon position was pilot selectable rather than automatically selected to position the canard trim position.

The AR mode was divided into two submodes:

1. Analog reversion/up and away (AR/UA)

2. Analog reversion/power approach (AR/PA)

The AR mode was a simple minimal sensor and gain system. The longitudinal forward loop gain was scheduled with impact pressure (qci) while all other gains remained fixed. The AR mode was designed as

a last resort "get home" back-up mode and was not modified for high AOA flight due to limited available space on the circuitry cards. The AR mode was considered unacceptable at high AOA and was not flight tested. The AR/PA mode was a fixed gain system minimal sensor system designed for take off and landing.

REDUNDANCY MANAGEMENT

General:

Redundancy management (RM) was provided by triplex sensor assemblies and the flight control computers (FCC). Mid-value selection signal voting and fault detection were used for the digital modes and pure mid-value selection was used for the analog modes. Failure detection was provided within the digital modes. The analog modes relied on midvalue selection of signals for failure detection. The digital modes were designed to be fail operational for initial failures and fail safe for additional failures. Multiple failures could result in automatic downmodes to the AR mode. Reference 3 contains a basic signal flow, fault detection and isolation description.

Several modifications were required in both the RM logic and associated sensor suites for high AOA flight. These modifications were made to account for increased FCS reliance on AOA, pitot probe accuracy at high AOA and for the single string Euler Angle data from the attitude heading reference system (AHRS). The modifications in RM and sensor capability include:

1. Addition of triplex noseboom AOA vanes

2. Triplex monitoring, signal selection and failure detection of AOA

3. Sole use of noseboom total and static pressure above 15 degrees AOA (Later modified to 40 degrees AOA for BLOCKIX-AA02)

4. Monitoring of noseboom analog and digital impact pressure for fault detection and backup gain selection above AOA for activation of single string noseboom air data (15 degrees for BLOCKIX-AA, AA01 and 40 degrees for BLOCKIX-AA02)

5. Deactivation of the surface reasonableness test for automatic downmode to AR (NORMH1)

6. Elimination of Euler Angle use above 15 degrees AOA

7. Deactivation of the Euler Angle analytic monitor above 20 degrees AOA

AOA Redundancy Management:

Additional vanes were added to the noseboom to provide adequate triplex redundancy in AOA. The original side fuselage mounted vanes had inadequate range and accuracy to provide signal selection or fault detection capability.

Midvalue selection of AOA was used when no failure states were detected. A trip level of 5 degrees was used to isolate faulty signals. After a single failure the average of the remaining signals was used. Detection of a second failure (miscompare of two remaining vanes) caused AOA to be ramped to zero at a rate of 10 degrees per second.

Provisions for upwash calibration were included. Corrections for induced angles due to pitch and roll rates were not included.

Air Data Redundancy Management:

The original air data fault reaction remained unchanged below 15 degrees AOA. The first two high AOA software releases (BLOCKIX-AA and BLOCKIX-AA01) modified the system to use only total and static pressure from the noseboom above 15 degrees AOA. A local monitor of analog and digital noseboom indicated q_{ci} was used to detect sensor failures. If a miscompare above 0.5 inch of mercury was detected, default values of total and static pressure were used. The default values for the first two software release corresponded to 0.4 Mach number at 30,000 feet pressure altitude.

The AOA for single string noseboom air data use was changed to 40 degrees AOA for the BLOCKIX-AA02 software release based on flight test results from the initial envelope expansion to 67 degrees AOA. In addition, the default air data total and static pressure values were modified to a 0.6 Mach number at 30,000 feet pressure altitude to handle the increased airspeed range for this release.

Normal signal selection and fault reaction using the fuselage mounted side pitot probes was disabled

328

above the activation AOA. The side mounted probes were considered to be potentially prone to early stall at high AOA. Subsequent flight testing indicated that the errors between the noseboom and side probes were well within trip levels to 40 degrees AOA and the appropriate modification to the software was made with the BLOCKIX-AA02 release.

Reasonableness Test Inhibit:

The X-29 control laws contained a digital surface command reasonableness test which compared surface rate commands with pre-established limits. If the command exceeded the limit it was held at the limit and if exceeded for more than 0.05 second, an automatic downmode to the AR occurred.

During the control law design phase, it was determined that the reasonable test could cause downmodes to AR during departures, spins, recoveries, or hard maneuvering. Downmode to AR was not desirable at high AOA, particularly during potential out of control conditions. A submode of ND/ACC known as "NORMHI" was defined which was identical to ND/ACC, but eliminated the automatic downmode to AR. The digital command rate limiting was maintained. The mode was pilot selectable through a FCS panel switch. The mode was entered prior to high AOA maneuver entry. The basic ND/ACC mode was left intact for use at low AOA.

AHRS Monitor Lockout:

The X-29 used a single string Litton LR-80 AHRS to provide roll and pitch Euler angles to the control laws. The signals were used in the longitudinal command path and the estimated sideslip rate to the rudder.

The AHRS monitor provided a degree of analytic redundancy through integration of body axis rates and subsequent comparisons to the AHRS information. The integration routines were approximations and operated only between ±60 degrees pitch attitude. The monitor was considered inaccurate during potentially large attitude changes and high rates at high AOA. Use of Euler angles for the control laws at high AOA was rejected due to the single string nature of the AHRS and the potential inaccurate analytic monitor. The monitor was subsequently bypassed (but still updated) above 15 degrees AOA where the Euler angles were no longer used in the control laws.

CONTROL LAWS

Architectural Fading:

Design requirements leaving the basic low AOA (10 degrees) control laws intact necessitated the design of logic to fade in the new architecture. This was accomplished by defining variables which fade from zero to 1 between 10 and 15 degrees AOA. Angle-of-attack gain scheduling at 10, 15 and 40 degrees AOA was also used. The break between 10 and 15 degrees was used to fade lateral gains K3, K4, K14 and K18 (stability axis yaw rate to aileron, lateral load factor [Ny] to aileron, rudder-to-aileron interconnect [RAI] gain and Ny to rudder, respectively) to zero.

The low AOA control laws contain a variable (BLEND) which blended in the full envelope architecture above 0.6 Mach number and 30,000 feet pressure altitude. The BLEND function was modified to add a 10 to 15 degree AOA band for activation (BLENDA). Two additional blending variables were defined:

a. HABLND=1.0-BLENDA

b. BLENDB which varies from zero to 1 between 15 and 20 degrees AOA

Longitudinal ND/ACC and NORMHI:

Figures D1 and D2 present the longitudinal control law block diagrams above 15 degrees AOA, after the fading process had been implemented. Reference 3 contains a full description of the fading process.

The X-29 longitudinal control laws were generally termed an incremental normal load factor command system, which was equivalent to a gravity vector compensated pitch rate command system. Commanded incremental normal load factor was converted to a pitch rate command which was summed with a combined normal load factor, pitch rate, and estimated pitch acceleration signal to produce an error signal. The error signal was passed through a proportional plus integral filter to generate the canard command signal. Symmetric flaperon and strake commands were generated with constant gains (-0.3 and -0.7, respectively) from the canard command. These provided the command and stabilization capability of the system.

329

A slow trimming mode ACC was incorporated to provide predetermined canard trim scheduling through integration of a canard trim error signal to the symmetric flaperon and strake. The integrated error signal commanded flaperon position until saturation (21.5 degrees trailing-edge-down for BLOCKIX releases) and then the integration was transferred to the strake. The high AOA canard schedule was designed to maximize trim lift coefficient. The mode was rate limited to 10 degrees per second and was fully implemented only during steady-state maneuvering or trims.

Minor modifications to the original longitudinal control laws from the BLOCKVII-AD design were required for high AOA:

1. Negative AOA limiting (AOA limit = -10.0 degrees)

2. Negative load factor limiting (Nz limit = -1.0 g)

3. Weak AOA feedback in place of speed stability

4. Elimination of Euler angle gravity vector compensation to the command path.

5. Change the symmetric flaperon saturation limit from 24.75 to 21.5 degrees trailing edge down (TED).

Gain scheduling with AOA was not required in the pitch axis.

Basic operation of the longitudinal control laws was the same as the low AOA system with the minor modifications noted. The largest modification was the change to a pure pitch rate command system above 15 degrees AOA. A pure pitch rate command system will provide varying normal load factor at a given flight and stick command condition as a function of aircraft attitude. The removal of gravity vector compensation provided the change fror incremental normal load factor to a pitch rate command system and also changed the Nz-Cos(theta) to a Nz-1.0 feedback.

Speed stability was blended to a weak AOA feedback with a constant gain between 10 and 15 degrees AOA. Angle of attack was processed through a first order low pass filter to prevent potential aeroservoelastic coupling.

Lateral-Directional ND/ACC and NORMHI:

The low AOA control laws commanded pure roll rate and rudder position. Nonlinear lateral stick gearing of stick position commanded roll rate which was then combined with roll rate, side force, and a washed-out estimated sideslip rate feedback to provide an error signal. The error signal was passed through a proportional plus integral filter to command aileron (differential full span flaperon). A RAI was incorporated into the lateral command to input aileron with rudder pedal input. Rudder input was commanded from rudder pedal position combined with an ARI signal from the lateral stick. The command was combined with a washed yaw rate (estimated sideslip rate above 0.6 Mach number or 30,000 feet pressure altitude) and sideforce to provide commanded rudder position.

Significant modifications to the lateral-directional control laws above 15 degrees AOA were required to provide adequate stability and control:

1. Linear lateral command gearing was substituted in place of nonlinear gearing

2. The lateral integrator was removed

3. Series gains with the same independent variables were collapsed to constants and a single varying gain

4. Feedback paths were simplified to minimal required signals

5. The RAI was eliminated

6. The washed-out sideslip rate was modified to a washed out stability axis yaw rate (R-0.8*P(α)) and added to the rudder at all airspeeds above 15 degrees AOA

7. A parallel washed-out path to the ARI was added in addition to a direct path

8. Euler angle compensation was eliminated

9. Gains were heavily scheduled with AOA

10. Spin prevention logic was provided

Figure D3 presents the architecture of the ND/ACC lateral directional control laws above 15 degrees AOA. Figure D4 shows the operation of the spin prevention logic.

The original nonlinear lateral gearing and command (PC2) was modified to a pure linear command gradient above 15 degrees AOA. Lateral command authority was directly proportional to stick displacement. A first order lag filter which was operational for the low speed portion of the low AOA control laws was extended to all AOAs above 15 degrees.

The low AOA lateral command gain maximum roll rate command (PMAX) was faded to a constant value of 180. The nonlinear portion of the low AOA command gain was faded to zero above 15 degrees. The lateral gearing gain (K13) was modified to use AOA break points of 10, 15 and 40 degrees.

The summed feedback signals and pilot command were passed through a constant gain (KP3) to produce the aileron command signal. The lateral integrator gain and its residual state were faded to zero above 15 degrees AOA. The proportional gain (KP3) was faded to a constant of 0.1 above 15 degrees AOA.

The integrator was removed to reduce aileron position saturation tendencies at high AOA. Saturation of the aileron via integration of a roll rate command error signal could produce severe roll coordination and potential spin entry problems.

Constant values of PMAX and KP3 were required to avoid problems with multiplying series table look up gains which were functions of the same independent variable. The total gain achieved through the multiplication was a linear combination only at common break points. Gain values between break points were a polynomial function of the independent variables. The order of the polynomial was equal to the number of series gains multiplied together. The phenomena resulted in gain values significantly different than those anticipated when at conditions in between break points. The solution was to collapse the series gains with common independent variables to a

single gain (K13), and fade the other gains (PMAX and KP3) to constants. The values of the constants were selected to minimize the magnitude of the change from the scheduled values.

The rudder command path remained unmodified. The RAI was removed between 10 and 15 degrees AOA. Large values of stable dihedral effect made the RAI loop unnecessary. The RAI provided aileron in the same direction as rudder pedal input to compensate for low dihedral effect at low AOA. This was an undesirable characteristic and not required at high AOA. The dihedral effect for AOA above 10 degrees was sufficient to provide rudder roll capability without aid of the ailerons. In addition, an RAI would fight recovery control inputs from an inadvertent departure or spin.

The ARI was modified with an additional washed-out parallel path. The parallel path applied double rudder commands at the initiation or termination of a step aileron input. The command was then washed-out to the direct path value. Simulation indicated that the required ARI gain to initially prevent adverse sideslip generation was higher than that required for steady velocity vector roll maneuvers due to propelling aerodynamic yaw and roll damping. The washed-out ARI gain also helped to overcome rotational inertia and to compensate for the high yaw to roll inertia ($I_{zz}/I_{xx}=10.0$) during roll reversals. Modification of the rudder requirements during steady-state velocity vector rolls could also be achieved with increasing the stability axis yaw rate gain (K17). This was an undesirable solution since high stability axis yaw rate feed back gains also increased autoroll susceptibility. The washed-out ARI parallel path solved the trade off and also provided increased coordination during rapid roll reversals.

Side force to both the aileron and rudder (K4 and K18) as well as washed-out stability axis yaw rate to the aileron (K3) were faded to zero above 15 degrees AOA. The feedbacks were not required and added unnecessary complexity to the system.

Roll rate feedback to the aileron (K2) was gain scheduled at 10, 15 and 40 degrees AOA. High gain values were required to stabilize the undamped aerodynamic wing rock. Analysis determined that a -0.6 deg/deg/s was the maximum allowable value for K2. Higher values could make the system susceptible to high frequency lateral limit cycles due to actuator nonlinearities. Table lookup values for K2 were

331

significantly higher than the limit. The table value of K2 was looked up and then limited in software to -0.6 if necessary. This method was used to maintain the highest possible slope of gain increase with AOA prior to reaching the limit. Simply placing the maximum allowable value in the 40 degree AOA table lowered the slope with AOA and made the aircraft susceptible to wing rock onset below 30 degrees AOA. The K2 gain was a factor of 10 higher in the tables than was necessary since it was subsequently multiplied by the constant KP3 gain of 0.1.

The low AOA control laws used a washed out sideslip rate estimator ([R-P(α) + ((g/v)* (Cos(theta) *Sin(phi)-Ny)])to the rudder above 0.6 Mach number or above 30,000 feet pressure altitude (see Reference 3) A modified feedback gain (R- 0.8*P(α)) without the gravity vector terms and with a scale factor on the roll rate term was defined for high AOA. The deletion of the gravity vector and sides force terms modified the feedback from a sideslip rate estimator to a stability axis yaw rate The 0.8 factor was added to approximate the Sin(α) term in the equations of motion. The gain (K17) was scheduled at 10, 15 and 40 degrees AOA. The feedback was removed above 55 degrees AOA (RFOUT). The rudder was ineffective in this region and the feedback interfered with spin prevention logic.

Spin prevention logic was added to provide full antispin inputs during an incipient spin. The logic was activated above 40 degrees AOA (later modified to 50 degrees with the BLOCKIX-AA02 software) and above 2 degrees per second yaw rate. The logic was activated at -25 degrees AOA for inverted spin entries. A time fader (GAINSP1) was activated upon the above conditions which slewed to the full value of 1.0 in 0.125 second. Lowering the AOA or yaw rate below the trigger value reversed the process. Once activated, the other parameters (XSPIN XSPINA=1.0- XSPIN) were computed as a function of the absolute value of yaw rate. These parameters were used to fade out the roll rate feedback to the aileron, the ARI, and to increase the pilot command authority. Roll rate feedback was removed to prevent prospin inputs and the ARI was removed to avoid interference with anti-spin pilot commands. The pilot command authority was sufficiently increased to completely override the automatic inputs and reverse to full prospin if desired.

The roll rate feedback and ARI fade out were accomplished by 10 degrees per second yaw rate. The automatic recovery commands to the aileron and rudder (XKRREC and XKYREC, respectively)

provided full surface authority inputs by 30 degrees per second yaw rate with neutral lateral stick or rudder pedal.

CONTROL LAW MODIFICATIONS DURING THE PROGRAM

General:

Two FCS upgrades from the original BLOCKIX-AA control law release were made during the test program. Modifications were made based on flight test results and to increase the airspeed envelope beyond 0.6 Mach number.

BLOCKIX-AA01 Release:

The BLOCKIX-AA01 release increased the longitudinal command gain maximum normal load factor command (GMAX) from a 6.4- to an 8-g incremental load factor command above approximately 350 KCAS and doubled the low speed (below approximately 200 KCAS) command to 2 g's. Modifications were made when it became apparent that the original commands were insufficient to provide adequate maneuvering capability beyond approximately 120 KCAS.

BLOCKIX-AA02 Release:

The BLOCKIX-AA02 release contained significant modifications to allow envelope expansion beyond 0.6 Mach number and to correct problems which were encountered during flight test.

Tail buffet produced a 16-hertz roll rate command signal to the ailerons. The high gain feedback amplified the high frequency noise and produced actuator RM trips. An analog 16-hertz simple notch filter was added to the roll rate feedback and the FCS simplified actuator model rate limits were upgraded to the correct value.

The addition of the notch filter added phase lag to the roll axis which increased the susceptibility to high frequency oscillation or limit cycles. Flight test results indicated that the high roll rate feedback gains could be reduced from the original values due to beneficial aerodynamic differences from predictions. The addition of the notch filter required significant reductions in the original roll rate feedback gains beyond approximately 200 KCAS to provide adequate high frequency stability margins. Roll feedback gains

were reduced 10 to 30 percent depending on AOA and airspeed. Lowering the roll rate feedback gains also increased the steady-state stability axis roll rates by a proportional amount.

Flight tests indicated that the side pitot-probe errors from the noseboom were well within tolerances up to 40 degrees AOA. The change to single string noseboom air data at 15 degrees AOA was expanded to 40 degrees AOA.

The spin prevention activation AOA was raised from 40 to 50 degrees AOA to prevent aileron and rudder transients during maneuvers between 40 and 45 degrees AOA. The beneficial aerodynamic differences allowed greater capability in this AOA region than was originally predicted.

All three AOA releases contained the capability to vary two gain combinations in flight (see Reference 3). The BLOCKIX-AA and BLOCKIX-AA01 releases allowed increased and decreased ARI, K27, and roll rate feedback K2, gains. The K2 decreases below 200 KCAS used in the BLOCKIX-AA02 software were flight tested prior to implementation using this feature with the BLOCKIX-AA01 software. The BLOCKIX-AA02 variable gains were modified to allow increases in the lateral command, K13, and ARI, K27, gains. Flight test results had indicated that significant roll rate increases over the original design may be possible and the variable gain combination was modified to allow quick evaluation of increased capability.
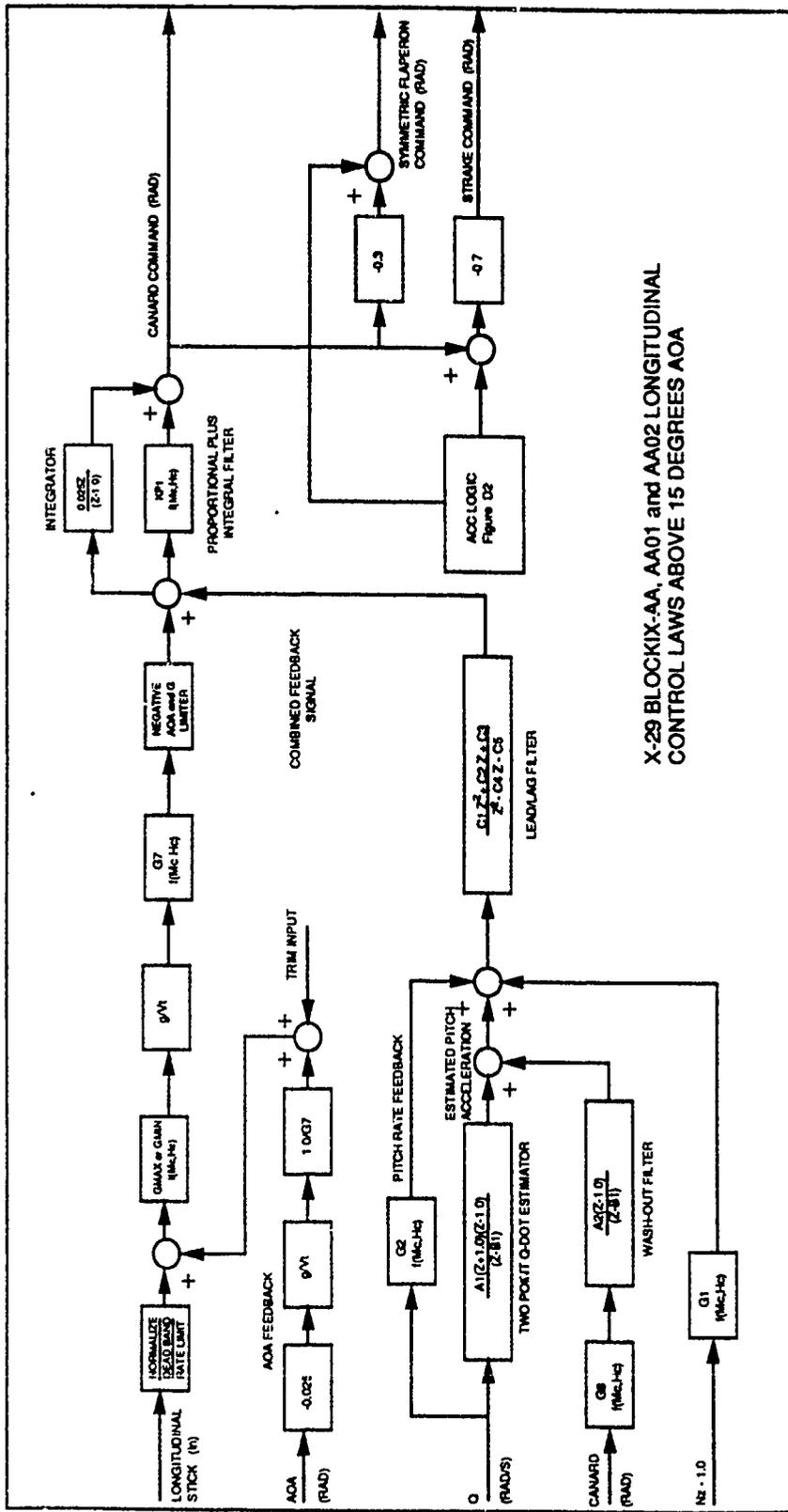
Figure D1 Longitudinal Control Law Block Diagram

334
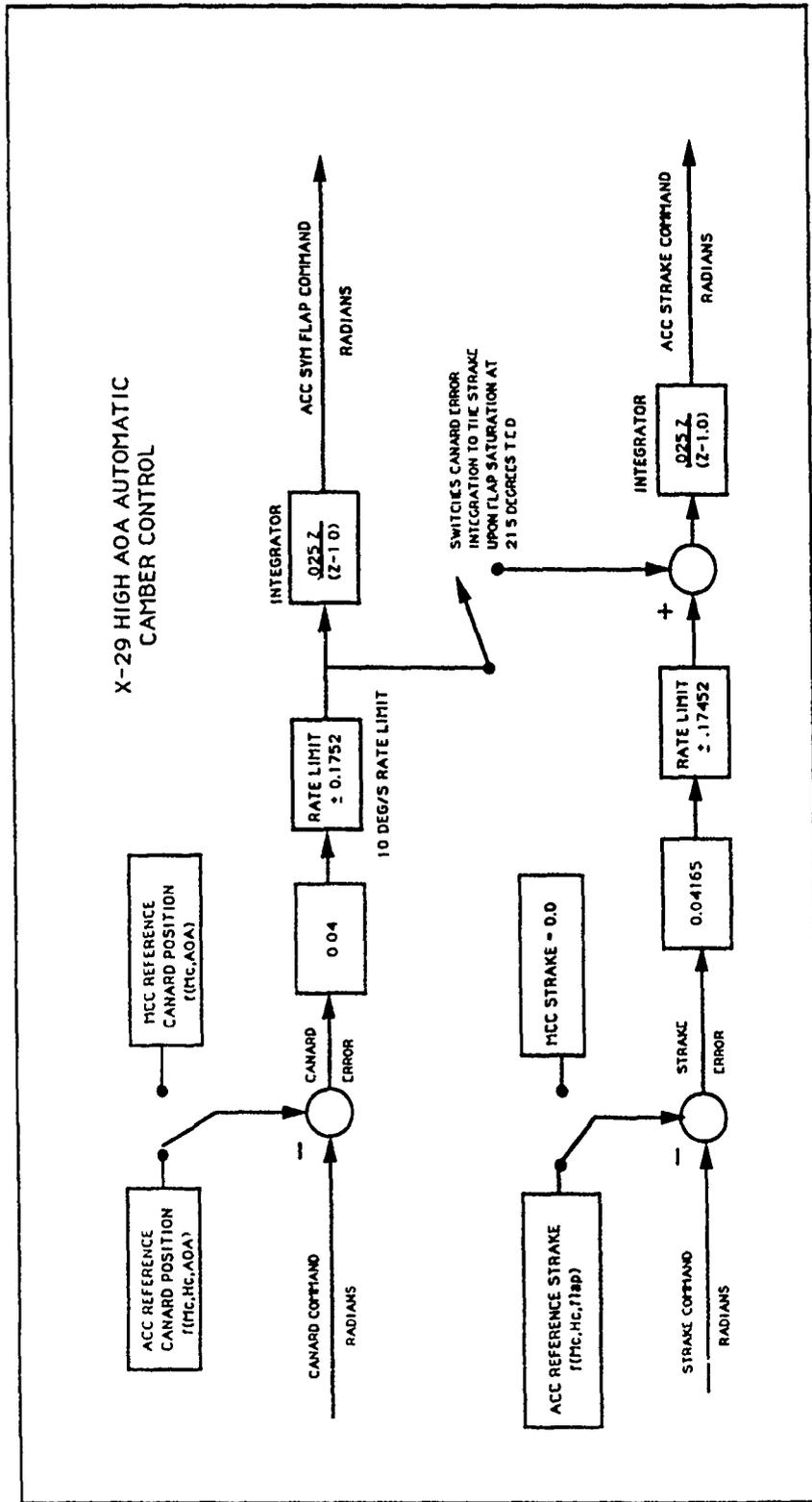
Figure D2 Automatic Camber Control Block Diagram
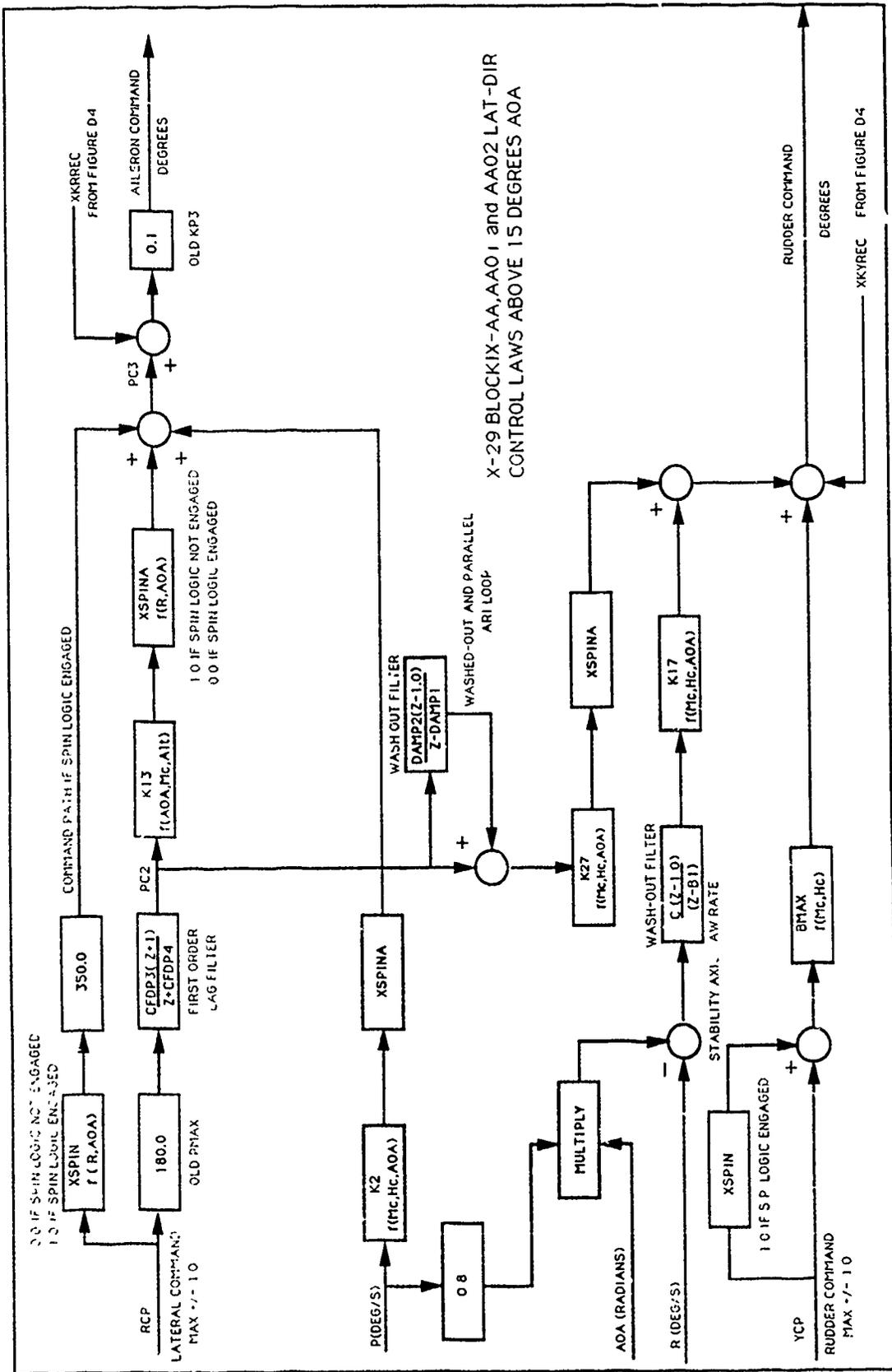
Figure D3 Lateral-Directional Control Law Block Diagram
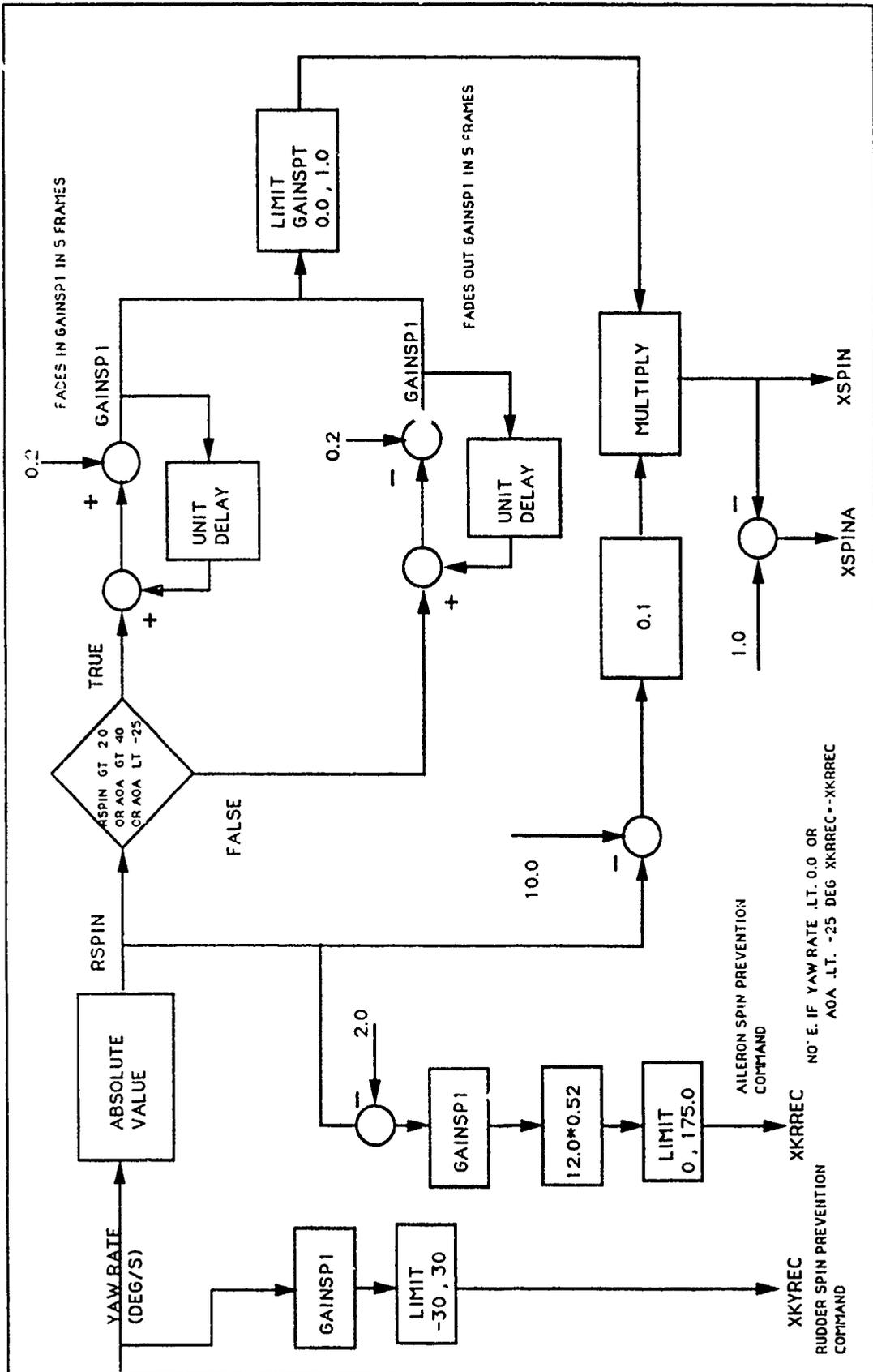
Figure D4 Spin Prevention Logic Operation

Spin Prevention Logic Surface Commands
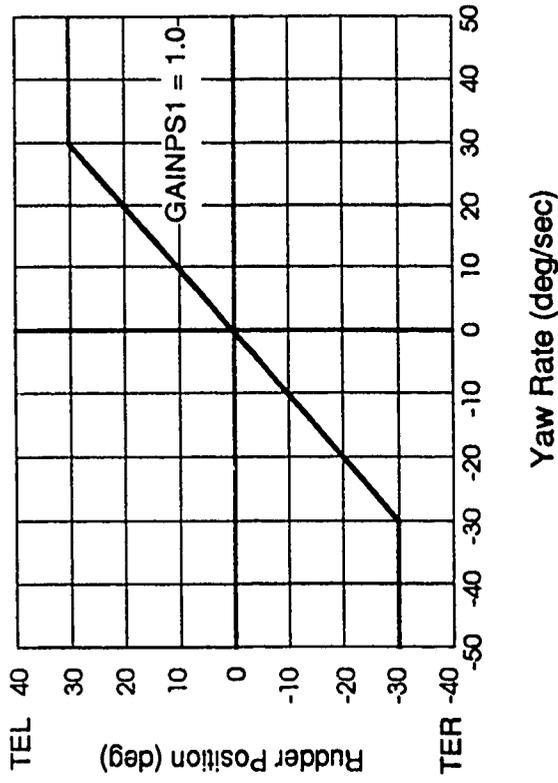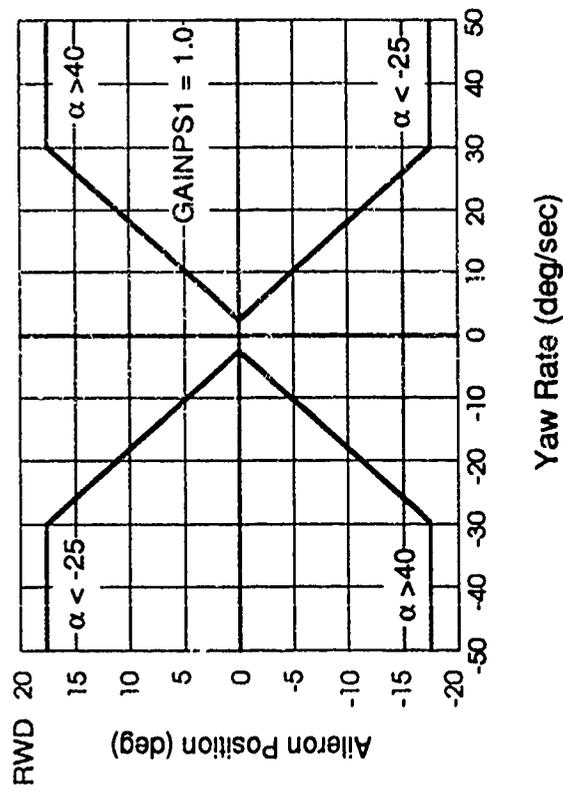
Figure D4 Spin Prevention Logic Operation (Concluded)

338

APPENDIX E
DATA ANALYSIS METHODS

This page intentionally left blank.

DATA ANALYSIS METHODS

AIR DATA

The X-29 noseboom had three angle-of-attack (AOA) vanes, a sideslip vane, a pitot probe, and a static pressure source (Figure E1). The forward AOA vane was used for postflight data analysis. The total temperature probe was located on the underside of the airplane just forward of the nosewheel.

Static position error, noseboom bending corrections, and low AOA vane upwash corrections were determined during the low AOA flight testing of X-29 USAF S/N 620003 (the first X-29). The same corrections were used during the X-29 high program using the USAF S/N 820049 aircraft. Reference 9 presents the corrections used.

The total pressure port on the noseboom pitot probe provided total pressure below 30 degrees AOA. Above 30 degrees AOA initial, the total pressure probe stall was noted. The total pressure probe was completely stalled by approximately 55 degrees AOA.

Data from the heated total temperature probe were also affected by stall at high AOA and caused it to lose validity above about 30 degrees AOA.

True angle of attack was determined by applying corrections to the nosebooms vane-indicated AOA for upwash, pitch rate, roll rate, and noseboom bending. Body-axis rate corrections to vane measured AOA and sideslip were functions of the rates, cg position, and true airspeed. The equations were solved iteratively as shown in Figure E2.

Above 30 degrees AOA true airspeed from the noseboom was lower than the actual true airspeed, which produced larger rate, corrections than were appropriate. To alleviate this, the true airspeed associated with an equivalent airspeed of 90 knots (approximate terminal airspeed for the X-29 above 45 degrees AOA) was computed and used as a minimum true airspeed in the rate correction equations. If the noseboom true airspeed was less than the minimum true airspeed, the minimum true airspeed was used.

INERTIAL NAVIGATION SYSTEM

The X-29 high AOA program employed a Litton LN-39 inertial navigation system (INS). The INS provided three components of ground-referenced velocity and the three aircraft Euler angles. The velocity and attitude data provided by the INS were used to compute AOA, sideslip, dynamic pressure, true airspeed, and Mach number. The INS was installed to provide more airspeed at high AOA while the noseboom pitot probe was stalled. Accurate dynamic pressure was needed to compute nondimensionalized force and moment coefficients and stability and control derivatives. The INS could also provided AOA and sideslip data, although the primary source for AOA and sideslip were the corrected vane values. Figure E3 presents the equations used to compute the air data from the INS.

The velocity components provided in the INS internal axis system were rotated through the wander angle to obtain the ground-referenced velocity vector in the North-East-Down (N-E-D) axis system. The wind velocity vector was computed in the N-E-D axis system and subtracted from the aircraft ground-referenced velocity vector to obtain the true airspeed vector. The true airspeed vector was rotated through the aircraft Euler angles to obtain the true airspeed vector in the body axes. The components were corrected for body-axis rates. Angle of attack and angle of sideslip were trigonometric functions of the three body axis true airspeed components. Mach number and dynamic pressure from the INS were computed using the position error corrected pressure altitude from the noseboom static port and tabled values of ambient temperature.

Wind was calculated while the X-29 was at low AOA (below 20 degrees) using the noseboom AOA and sideslip vanes and pitot-static system. Wind was determined by the equations indicated in Figure E3. Wind varied with altitude, time, and location. A typical X-29 high AOA maneuver would enter the high AOA region (above 20 degrees) at 40,000 feet and remain at high AOA while descending until recovery somewhere above 17,000 feet. The "Wind Calibration in Climb" (Reference 10) method was used to ensure that the wind vector used to compute the basic INS parameters was as accurate as possible. During the climb to the first high AOA maneuver of the flight, the wind vector was computed while below 20 degrees AOA and stored in a table as a function of pressure altitude. The wind vector was also computed prior to each high AOA maneuver. This updated wind vector was compared to

the table value from the initial wind calibration climb at the same altitude. The difference was applied as a constant correction to the original vector. The resulting wind vector (table values of the original winds corrected with the updated difference) was used for the computation of the INS parameters. The technique had the additional benefit of correcting for the accumulated INS error. Static temperature was also calibrated during initial climb and stored in a table as a function of altitude. An update was computed prior to each maneuver entry in a similar fashion to the wind corrections. The corrected table lookup values for ambient temperature (table values of the original ambient temperature with updates) were used for the computation of INS Mach number and dynamic pressure.

ANGULAR ACCELERATIONS - BODY AXIS

Flight instrumentation included a set of angular accelerometers. Aerodynamic components of angular acceleration were computed by subtracting the inertial and engine gyroscopic components from the measured angular accelerations. Flight values of inertia were used to compute moments. Figure E4 presents the computation of the inertial, engine, and aerodynamic contributions of the angular accelerations.

ACCELERATIONS - BODY AXIS

The measured body-axis accelerations were corrected from the fuselage location to the center of gravity. Fine-scale and coarse-scale accelerations were combined to produce the final output parameters. The fine-scale accelerations were used inside a predetermined threshold and the coarse measurements outside the threshold. Figure E5 presents the thresholds and correction equations for the body axis accelerometers.

ANGULAR RATES - STABILITY AXIS

Measured body axis angular rates were transformed to the stability axes with the equations presented in Figure E6.

ACCELERATIONS - FLIGHT PATH AXIS

Measured body axis accelerations were transformed to the flight path axis by the equations presented in Figure E6.

AERODYNAMIC FORCE AND MOMENT COEFFICIENTS

Body axis force and moment coefficients were computed by nondimensionalizing the body axis linear accelerations and the aerodynamic components of angular accelerations. Lift and drag coefficients were computed using thrust and ram drag corrected flight path accelerations. Two versions of each coefficient were computed. The noseboom version used the noseboom-indicated dynamic pressure, and the INS version used the INS-derived dynamic pressure. The force and moment coefficient equations are presented in Figure E7.

The pitching moment coefficient was corrected for predicted inlet and thrust effects using the simplified propulsion model. The correction equations are presented in Figure E7.

THRUST

Thrust was computed using the General Electric F404-GE-400 Engine Specification Model, GE Program Number 80031A(U), August 1981. The FORTRAN program was modified to read flight measured parameters to compute steady state engine performance parameters. Flight measured parameters input to the program were: power lever angle, Mach number, altitude, and ambient temperature. Parameters output from the program were: gross thrust, net thrust, ram drag, N1, N2, and air mass flow rate. The in-flight thrust model from X-29 performance program (Reference 9) was not used because internal engine parameters were not instrumented on the X-29 USAF S/N 820049 aircraft. The specification model used was estimated to be accurate within 15 percent.

SPECIFIC EXCESS POWER

Specific excess power was computed using flight path acceleration and true airspeed. The INS value of true airspeed was used above 30 degrees AOA. The specific excess energy was corrected to level flight using the equations shown in Figure E8.

TURN RATE AND TURN RADIUS

Turn rate and turn radius were computed using the standard computations which assume the airplane to be in a steady turn with small flight path angles. The equations used the flight path normal acceleration since large AOA was involved. The generally accepted use of body axis accelerations to compute turn rate and radius loses validity above 20 degrees AOA as small angle approximation assumptions are violated. The computations for turn rate and radius are presented in Figure E8.
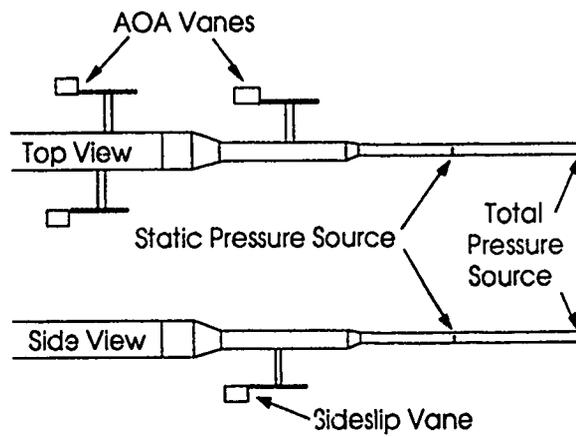
Figure E1   X-29 Noseboom

$$\alpha_t = \mathrm{Tan}^{-1}\left[\tan\alpha_v + \frac{Q\,L_{x\alpha}}{V_t\,\cos\alpha_t\,\cos\beta_t}\right] \qquad L_{x\alpha} = X_{cg} - X_{\alpha\,vane}$$

$$\beta_t = \mathrm{Sin}^{-1}\left[\tan\beta_v\,\cos\alpha_t\,\cos\beta_t + \frac{R\,L_{x\beta}}{V_t}\right] \qquad L_{x\beta} = X_{cg} - X_{\beta\,vane}$$

Figure E2   Rate Correction Equations

$$\begin{bmatrix} V_x \\ V_y \\ V_z \end{bmatrix} = \text{Ground-referenced velocity in internal INS axes}$$
$$(\text{WA} = \text{INS wander angle})$$

(A) $\quad \begin{bmatrix} V_{North} \\ V_{East} \\ V_{Down} \end{bmatrix} = \begin{bmatrix} V_x \cos WA - V_y \sin WA \\ -V_x \sin WA - V_y \cos WA \\ -V_z \end{bmatrix} = \vec{V}_{\text{Aircraft,gnd-ref, NED axes}}$

(B) $\quad \vec{V}_{\substack{\text{Aircraft,airmass-ref,}\\ \text{NED axes}}} = \vec{V}_{\substack{\text{Aircraft,gnd-ref,}\\ \text{NED axes}}} - \vec{V}_{\substack{\text{Wind,gnd-ref,}\\ \text{NED axes}}}$

(C) $\quad \vec{V}_{\substack{\text{Aircraft,airmass-ref,}\\ \text{Body axes}\\ \text{(Not Rate Corr.t'vd)}}} = \begin{bmatrix} Vx_{body} \\ Vy_{body} \\ Vz_{body} \end{bmatrix}_{\substack{\text{Not Rate}\\ \text{Corrected}}} = \begin{bmatrix} \text{3 by 3} \\ \text{Transformation} \\ \text{Matrix} \end{bmatrix} \vec{V}_{\substack{\text{Aircraft,airmass-ref,}\\ \text{NED axes}}}$

(D) $\quad \begin{bmatrix} Vx_{body} \\ Vy_{body} \\ Vz_{body} \end{bmatrix} = \begin{bmatrix} Vx_{body} \\ Vy_{body} \\ Vz_{body} \end{bmatrix}_{\substack{\text{Not Rate}\\ \text{Corrected}}} + \begin{bmatrix} Q\,zl + R\,yl \\ R\,xl - P\,zl \\ Q\,xl - P\,yl \end{bmatrix}$
$\qquad\qquad xl = X_{cg} - X_{INS\,mount}$
$\qquad\qquad yl = Y_{INS\,mount} - Y_{cg}$
$\qquad\qquad zl = Z_{INS\,mount} - Z_{cg}$

(E) $\quad \alpha_{INS} = \text{Tan}^{-1}\left(\dfrac{Vz_{body}}{Vx_{body}}\right) \quad \beta_{INS} = \text{Sin}^{-1}\left(\dfrac{Vy_{body}}{V_{t\text{-}INS}}\right) \quad V_{t\text{-}INS} = \sqrt{Vx_{body}^2 + Vy_{body}^2 + Vy_{body}^2}$

(F) $\quad M_{INS} = \dfrac{V_{t\text{-}INS}}{49.02\sqrt{T_{static}}} \qquad \left(T_{static} = {}^\circ R \,,\; V_t = {}^{ft}\!/_{sec}\right)$

$$\bar{q}_{INS} = 0.7\, P_s\, M_{INS}^2$$

INS Wind Computations:

$$\gamma = \Theta - \alpha_t \cos\Phi - \beta_t \sin\Phi \qquad \delta = \Psi + \beta_t \cos\Phi - \alpha_t \sin\Phi$$

$$\vec{V}_{\substack{\text{Wind,gnd-ref,}\\ \text{NED axes}}} = \begin{bmatrix} V_{North} \\ V_{East} \\ V_{Down} \end{bmatrix} + \begin{bmatrix} -V_{t\text{-noseboom}} \cos\gamma \cos\delta \\ -V_{t\text{-noseboom}} \cos\gamma \sin\delta \\ V_{t\text{-noseboom}} \sin\gamma \end{bmatrix}$$

Figure E3 INS Computations

345

$$\dot{P}_{inertial} = \frac{1}{I_{xx}}\left[(I_{yy} - I_{zz})QR + I_{xz}(\dot{R}+PQ) + I_{xy}(\dot{Q}-PR) + I_{yz}(Q^2-R^2)\right]$$

$$\dot{Q}_{inertial} = \frac{1}{I_{yy}}\left[(I_{zz} - I_{xx})PR + I_{xz}(R^2-P^2) + I_{xy}(\dot{P}+QR) + I_{yz}(\dot{R}-PQ)\right]$$

$$\dot{R}_{inertial} = \frac{1}{I_{zz}}\left[(I_{xx} - I_{yy})PQ + I_{xz}(\dot{P}-QR) + I_{xy}(R^2-Q^2) + I_{yz}(\dot{Q}-PR)\right]$$

$$\dot{Q}_{engine} = \frac{(0.105)(-R)}{I_{yy}}\left[I_{fan}N_{fan} + I_{core}N_{core}\right] \quad (N = RPM)$$

$$\dot{R}_{engine} = \frac{(0.105)(Q)}{I_{zz}}\left[I_{fan}N_{fan} + I_{core}N_{core}\right]$$

$$\dot{P}_{aero} = \dot{P}_{measured} - \dot{P}_{inertial}$$

$$\dot{Q}_{aero} = \dot{Q}_{measured} - \dot{Q}_{inertial} - \dot{Q}_{engine}$$

$$\dot{R}_{aero} = \dot{R}_{measured} - \dot{R}_{inertial} - \dot{R}_{engine}$$

Figure E4 Body Axis Angular Accelerations

$$\underline{\text{Parameter}} \quad \underline{\text{Threshold}}$$

Parameter	Threshold
Nx	+0.8 g
Ny	+0.8 g
Nz	-1.0 to +3.0 g

CG Correction Equations:

$$N_x = N_{x\text{-uncorr}} - \frac{1}{g_c}\left(-(Q^2+R^2)(X_{cg}-X_{mount}) + (PQ-\dot{R})(Y_{mount}-Y_{cg}) + (PR+\dot{Q})(Z_{cg}-Z_{mount})\right)$$

$$N_y = N_{y\text{-uncorr}} - \frac{1}{g_c}\left((PQ+\dot{R})(X_{cg}-X_{mount}) - (P^2+R^2)(Y_{mount}-Y_{cg}) + (QR-\dot{P})(Z_{cg}-Z_{mount})\right)$$

$$N_z = N_{z\text{-uncorr}} - \frac{1}{g_c}\left((PR-\dot{Q})(X_{cg}-X_{mount}) + (QR+\dot{P})(Y_{mount}-Y_{cg}) - (P^2+Q^2)(Z_{cg}-Z_{mount})\right)$$

Figure E5   Body Axis Accelerations

$$P_s = P\cos\alpha + R\sin\alpha$$
$$Q_s = Q$$
$$R_s = R\cos\alpha - P\sin\alpha$$

$$Nx_{fp} = (Nx\cos\alpha - Nz\sin\alpha)\cos\beta + Ny\sin\beta$$
$$Ny_{fp} = Ny\cos\beta - (Nx\cos\alpha - Nz\sin\alpha)\sin\beta$$
$$Nz_{fp} = Nz\cos\alpha + Nx\sin\alpha$$

Figure E6   Stability Axis and Flight Path Axis Conversion Equations

$$C_y = \frac{N_y}{\bar{q}\,S} \qquad\qquad C_L = \frac{\dot{P}_{aero}}{\bar{q}\,S\,b}$$

$$C_{Norm} = \frac{N_z}{\bar{q}\,S} \qquad\qquad C_M = \frac{\dot{Q}_{aero}}{\bar{q}\,S\,\bar{c}}$$

$$C_N = \frac{\dot{R}_{aero}}{\bar{q}\,S\,b}$$

Thrust corrections:

$$T_{net} = T_{gross}\cos\alpha - D_{ram}$$

$$\Delta M_{thrust} = T_{gross}\left(Z_{cg} - Z_{thrust\ line}\right)$$

$$L_x = \left(X_{cg} - X_{inlet}\right) \qquad L_Z = \left(Z_{inlet} - Z_{cg}\right)$$
$$\Delta M_{ram\ drag} = D_{ram}\left(L_x \sin\alpha + L_z \cos\alpha\right)$$

$$C_{M\ \substack{thrust\\corrected}} = C_M - \frac{\Delta M_{thrust} + \Delta M_{ram\ drag}}{\bar{q}\,S\,\bar{c}}$$

$$C_{lift} = \frac{N_{zfp}\,GW - T_{gross}\sin\alpha}{\bar{q}\,S}$$

$$C_{drag} = \frac{T_{gross}\cos\alpha - D_{ram} - N_{xfp}\,GW}{\bar{q}\,S}$$

Figure E7   Aerodynamic Coefficient Equations and Thrust Corrections

$$P_s = N_{xfp}V_t + \dot{H}$$

$$\text{Turn Rate} = \frac{\left(N_{zfp}^2 - 1\right)g}{V_t}$$

$$\text{Turn Radius} = \frac{V_t^2}{g\,\sqrt{\left(N_{zfp}^2 - 1\right)}}$$

Figure E8   Specific Excess Power, Turn Rate, and Turn Radius Equations

LIST OF ABBREVIATIONS AND SYMBOLS

Abbreviation or Symbol	Definition	Units
AB	afterburner	---
ACC	automatic camber control	---
A/D	analog-to-digital	---
ADFRF	Ames-Dryden Flight Research Facility	---
ADI	attitude director indicator	---
ADPO	Advanced Development Program Office	---
AFB	Air Force Base	---
AFFTC	Air Force Flight Test Center	---
AFR	Air Force Regulation	---
AFWL	Air Force Wright Laboratories	---
AHRS	attitude heading reference system	---
AMAD	aircraft mounted accessory drive	---
AOA	angle of attack	deg
AOS	angle of sideslip	deg
APU	abrupt pullup	---
AR	analog reversion	---
AR/PA	analog reversion/power approach	---
AR/UA	analog reversion/up-and-away	---
ARI	aileron to rudder interconnect	---
ASE	aeroservoelastic	---
ac	alternating current	---
amp	ampere(s)	---
BFM	basic fighter maneuver	---

LIST OF ABBREVIATIONS AND SYMBOLS (Continued)

Abbreviation or Symbol	Definition	Units
b	wingspan	in, ft
C	Centigrade	---
CA	axial force coefficient	dimension-less
CL	lift coefficient	---
Cl	rolling moment coefficient	dimension-less
ΔCl	incremental change in Cl	dimension-less
Cl_p	rolling moment coefficient due to roll rate	per rad
ΔCl_p	incremental change in Cl_p	per rad
Cl_r	rolling moment coefficient due to yaw rate	per rad
Cl_β	rolling moment coefficient due to angle of sideslip	per deg
ΔCl_β	incremental change in Cl_β	per deg
$Cl_{\delta a}$	rolling moment coefficient due to differential flaperon deflection	per deg
$\Delta Cl_{\delta a}$	incremental change in $Cl_{\delta a}$	---
$Cl_{\delta r}$	rolling moment coefficient due to rudder deflection	per deg
$\Delta Cl_{\delta r}$	incremental change in $Cl_{\delta r}$	per deg
Cm	pitching moment coefficient	dimension-less
ΔCm	increment in Cm	dimension-less
Cm_0	pitching moment coefficient at zero angle of attack	dimension-less
Cm_q	pitching moment coefficient due to pitch rate	per rad

350

LIST OF ABBREVIATIONS AND SYMBOLS (Continued)

Abbreviation or Symbol	Definition	Units
Cm_α	pitching moment coefficient due to angle of attack	per deg
ΔCm_α	increment in Cm_α	per deg
$Cm_{\delta c}$	pitching moment coefficient due to canard deflection	per deg
$\Delta Cm_{\delta c}$	increment in $Cm_{\delta c}$	per deg
$Cm_{\delta f}$	pitching moment coefficient due to symmetric flaperon deflection	per deg
$Cm_{\delta s}$	pitching moment coefficient due to strake flap deflection	per deg
CN	normal force coefficient	---
CN_q	normal force coefficient due to pitch rate	per rad
CN_α	normal force coefficient due to angle of attack	per deg
$CN_{\delta c}$	normal force coefficient due to canard deflection	per deg
$CN_{\delta f}$	normal force coefficient due to symmetric flaperon deflection	per deg
$CN_{\delta s}$	normal force coefficient due to strake flap deflection	per deg
Cn	yawing moment coefficient	dimension-less
ΔCn	incremental change in Cn	dimension-less
Cn_p	yawing moment coefficient due to roll rate	per rad
Cn_r	yawing moment coefficient due to yaw rate	per rad
Cn_β	yawing moment coefficient due to angle of sideslip	per deg
ΔCn_β	incremental change in Cn_β	per deg
$Cn_{\beta dyn}$	dynamic directional stability	per deg

LIST OF ABBREVIATIONS AND SYMBOLS (Continued)

Abbreviation or Symbol	Definition	Units
$Cn_{\delta a}$	yawing moment coefficient due to differential flaperon deflection	per deg
$\Delta Cn_{\delta a}$	incremental change in $Cn_{\delta a}$	per deg
$Cn_{\delta r}$	rolling moment coefficient due to rudder deflection	per deg
$\Delta Cn_{\delta r}$	incremental change in $Cn_{\delta r}$	per deg
Cy_{β}	side force coefficient due to angle of sideslip	per deg
$Cy_{\delta a}$	side force coefficient due to differential flaperon deflection	per deg
$Cy_{\delta r}$	side force coefficient due to rudder deflection	per deg
c	mean aerodynamic chord	in, ft
cg	center of gravity	in, ft, pct MAC
cos, Cos	cosine	---
D/A	digital-to-analog	---
DB	data bus	---
DC	canard position	deg
DDP	directional divergence parameter	---
DEG, deg	degree(s)	---
DEL	direct electrical link	---
DOD	Department of Defense	---
DOF	degree of freedom	---
DS	strake flap position	deg
dB, DB	decibel(s)	---
dc	direct current	---

LIST OF ABBREVIATIONS AND SYMBOLS (Continued)

Abbreviation or Symbol	Definition	Units
dps, deg/s	degrees per second	---
EAS	equivalent airspeed	knots
ECS	environmental control system	---
EMI	electromagnetic interference	---
EPU	emergency power unit	---
F	Fahrenheit	---
FCC	flight control computers	---
FCF	functional check flight	---
FCS	flight control system	---
FLT	flight	---
FS, F.S.	fuselage station	---
FSW	forward swept wing	---
FT., ft	foot, feet	---
FWD	forward	---
F_{lat}	lateral control stick force	lb
F_{lon}	longitudinal control stick force	lb
fps	feet per second	---
F_{rp}	rudder pedal force	lb
GAC	Grumman Aircraft Corporation	---
GASD	Grumman Aircraft Systems Division	---
GE	General Electric	---
GMAX	maximum normal load factor command	g
GMIN	minimum normal load factor command	g

LIST OF ABBREVIATIONS AND SYMBOLS (Continued)

Abbreviation or Symbol	Definition	Units
GW	gross weight	lb
GW/CG	gross weight/center of gravity	---
g, G	acceleration due to gravity	32.2 fps^2
gpm	gallons per minute	---
HADS	high accuracy digital sensor	---
H_c	pressure altitude	ft
HORIZ REF	horizontal reference	---
HQ	handling qualities	---
HQDT	handling qualities during tracking	---
HUD	head-up display	---
IAS	integrated servo activators	---
IBIT	initiated built-in-test	---
ID	identification	---
IDG	integrated drive generator	---
IN, in	inch(es)	---
INS	inertial navigation system	---
ISA	integrated servo actuator(s)	---
ITB	integrated test blocks	---
I_{xx}	rolling moment of inertia	slug-ft^2
I_{xz}	rolling-yawing product of inertia	slug-ft^2
I_{yy}	pitching moment of inertia	slug-ft^2
I_{zz}	yawing moment of inertia	slug-ft^2
KCAS	knots calibrated airspeed	---

Abbreviation or Symbol	Definition	Units
KEAS	knots equivalent airspeed	---
KIAS	knots indicated airspeed	---
KTAS	knots true airspeed	---
K13	lateral command gain	---
K27	ARI gain	---
kt	knot(s)	---
kVA	kilovoltamperes	---
L	left	---
LAT	lateral	---
LB, lb	pound(s)	---
LE	leading edge	---
L/H	lefthand	---
LVDT	linear variable differential transformer	---
LWD	left wing down	---
M	total pitching moment	ft-lbs
ΔM	increment in total pitching moment	ft-lbs
MAC	mean aerodynamic chord	in, ft
MAX	maximum	---
MCC	manual camber control	---
MIL	military	---
MIL SPEC	military specification	---
MMLE	modified maximum likelihood estimation	---
MVL	mean value logic	---

LIST OF ABBREVIATIONS AND SYMBOLS   (Continued)

Abbreviation or Symbol	Definition	Units
M_C	Mach number	dimension-less
mils	milliradians	---
NACA	National Advisory Committee for Aeronautics	---
NASA	National Aeronautics and Space Administration	---
ND	normal digital	---
ND/ACC	normal digital/automatic camber control	---
ND/MCC	normal digital/manual camber control	---
ND/PA	normal digital/power approach	---
na	not available	---
n/a	not applicable	---
No.	number	---
N_y, n_y	lateral load factor	g
N_z, n_z	normal load factor	g
PA	power approach	---
PID	parameter identification	---
PIO	pilot induced oscillation	---
PLA	power lever angle	deg
PMAX	maximum roll rate command	dps
PMD	program management directive	---
PSTAB	stability axis roll rate	deg/s
PTO	power takeoff	---
PTO	participating test organization	---
"pEst"	parameter estimation program	---

LIST OF ABBREVIATIONS AND SYMBOLS   (Continued)

Abbreviation or Symbol	Definition	Units
P_S	static pressure	psi, psf
psf	pounds per square foot	---
psi	pounds per square inch	---
P_t	total pressure	psi, psf
QBAR, qbar	dynamic pressure	psi, psf
Qc, qc	impact pressure	psi, psf
q	dynamic pressure	psf
q, Q	pitch rate	dps
q, Q	pitch acceleration	dps2
RAD, Rad	radians	---
RAI	rudder-to-aileron interconnect	---
RAV	remotely augmented vehicle	---
REF	reference	---
R/H	righthand	---
RM	redundancy management	---
RWD	right wing down	---
r, R	yaw rate	dps
rad	radian(s)	---
S	reference wing area	ft2
S&C	stability and control	---
SFO	simulated flame-out	---
S/N	serial number	---
SYM	symmetric	---

357

LIST OF ABBREVIATIONS AND SYMBOLS   (Continued)

Abbreviation or Symbol	Definition	Units
sec	second(s)	---
sin, Sin	sine	---
sps	samples per second	---
TE	trailing edge	---
TED	trailing edge down	---
TEL	trailing edge left	---
TER	trailing edge right	---
TEU	trailing edge up	---
TR	transformer rectifier	---
TW	thumbwheel	---
T_t	total temperature	deg F
UA	up-and-away	---
USAF	United States Air Force	---
V&V, V and V	verification and validation	---
Vt	true airspeed	fps
WL, W.L.	aircraft water line	in
WOW	weight-on-wheels	---
WS	wing station	in
WUT	windup turn	---
x_{cg}, XCG	longitudinal cg position	in, ft, pct MAC
y_{cg}, YCG	lateral cg position	in, ft,
z_{cg}, ZCG	vertical cg position	in, ft,
Δ	increment or change	---

LIST OF ABBREVIATIONS AND SYMBOLS (Concluded)

Abbreviation or Symbol	Definition	Units
α	angle of attack	deg
β	angle of sideslip	deg
β	angle of sideslip rate	dps
β_{est}	estimate of angle of sideslip rate	dps
δ_a	differential flaperon position	deg
δ_c	canard position	deg
δ_f	symmetric flaperon position	deg
δ_{lat}	lateral control stick position	in
δ_{lon}	longitudinal control stick position	in
δ_r	rudder position	deg
δ_{rp}	rudder pedal position	in
δ_s	strake flap position	deg
ϕ	bank angle	deg
θ	pitch attitude	deg

This page intentionally left blank.

Distribution List

Onsite Distribution	Number of Copies

Colonel John Hoffman
Air Force Flight Test Center
AFFTC/CV
Edwards AFB, CA 93523   1

Roger Crane
Air Force Flight Test Center
6510TW/DOE
Edwards AFB, CA 93523   1

Bob Evans
Air Force Flight Test Center
6510TW/DOR
Edwards AFB, CA 93523   1

Lt Col Greg Lewis
Air Force Flight Test Center
6510TW/DOR
Edwards AFB, CA 93523   1

Paul Kirsten
Air Force Flight Test Center
6510TW/DOEF
Edwards AFB, CA 93523   1

Bob Lee
Air Force Flight Test Center
6510TW/DOEF
Edwards AFB, CA 93523   1

Tom Twisdale
Air Force Flight Test Center
6510TW/DOEF
Edwards AFB, CA 93523   1

Major Dana Purifoy
Air Force Flight Test Center
6510TW/DORN
Edwards AFB, CA 93523   1

Fred Webster
Air Force Flight Test Center
6510TW/DORX
Edwards AFB, CA 93523   25

Distribution List (Continued)

Onsite Distribution	Number of Copies

Dave VanHoy
Air Force Flight Test Center
6510TW/DORX
Edwards AFB, CA 93523   1

Captain David Rajczewski
Air Force Flight Test Center
6510TW/DORX
Edwards AFB, CA 93523   1

Steve Smith
Air Force Flight Test Center
6510TW/DORM
Edwards AFB, CA 93523   1

Captain Al Lawless
Air Force Flight Test Center
6510TW/DORM
Edwards AFB, CA 93523   1

Paul Phillips
Air Force Flight Test Center
6510TW/DORH
Edwards AFB, CA 93523   1

Major Paul Brown
USAF Test Pilot School
USAFTPS/ST
Edwards AFB, CA 93523   1

Major Regis Hancock
USAF Test Pilot School
USAFTPS/ST
Edwards AFB, CA 93523   1

Captain Dennis Sager
Air Force Flight Test Center
6516TS/DO
Edwards AFB, CA 93523   1

Lt Howard Plevyak
Air Force Flight Test Center
6516TS/EN
Edwards AFB, CA 93523   1

Distribution List (Continued)

Onsite Distribution	Number of Copies
Research Projects Division Air Force Flight Test Center 6510TW/DOR Edwards AFB, CA 93523	10
Engineering Division Air Force Flight Test Center 6510TW/DOE Edwards AFB, CA 93523	5
USAF Test Pilot School Air Force Flight Test Center USAFTPS/ST Edwards AFB, CA 93523	2
Technical Library Air Force Flight Test Center 6510TW/TSTL Edwards AFB, CA 93523	3
History Office Air Force Flight Test Center AFFTC/HO Edwards AFB, CA 93523	1

Offsite Distribution

Colonel Ted Wierzbanowski Experimental Vehicle Planning Directorate AFSC/NAX Wright-Patterson AFB, OH 45433-6503	1
Lt Col Ken Griffen Experimental Vehicle Planning Directorate AFSC/NAX Wright-Patterson AFB, OH 45433-6503	1
Captain Tom Huckabone Air Force Institute of Technology AFIT/ Wright-Patterson AFB, OH 45433-5000	1
Tom Black Aeronautical Systems Division ASD/ENFTC Wright-Patterson AFB, OH 45433-6503	1

Distribution List (Continued)

Offsite Distribution	Number of Copies

Bob Mentzer
Aeronautical Systems Division
ASD/YPFT
Wright-Patterson AFB, OH 45433-6503   1

Major Jim Martin
Aeronautical Systems Division
ASD/VFTE
Wright-Patterson AFB, OH 45433-6503   1

Director, Design Analysis
Aeronautical Systems Division
ASD/XR
Wright-Patterson AFB, OH 45433-5000   1

Aeronautical Systems Division
ASD/ENF
Wright-Patterson AFB, OH 45433-5000   1

Aeronautical Systems Division
ASD/ENS
Wright-Patterson AFB, OH 45433-5000   1

Flight Technology Division
Aeronautical Systems Division
ASD/ENFT
Wright-Patterson AFB, OH 45433-5000   1

Raymond Haas
Aeronautical Systems Division
ASD/XRM
Wright-Patterson AFB, OH 45433-6553   1

Colonel Richard Borowski
Wright Laboratory
WL/FI
Wright-Patterson AFB, OH 45433-5000   1

Dr Richard Olsen
Wright Laboratory
WL/CA-F
Wright-Patterson AFB, OH 45433-5000   1

Captain Wade Smith
Wright Laboratory
WL/FIMT
Wright-Patterson AFB, OH 45433-5000   1

Distribution List (Continued)

Offsite Distribution	Number of Copies
Captain Daniel Wegman Wright Laboratory WL/TE Wright-Patterson AFB, OH 45433-5000	1
Lt John Cannon Wright Laboratory WL/FIMG Wright-Patterson AFB, OH 45433	1
Tom Cord Wright Laboratory WL/FIGCB Wright-Patterson AFB, OH 45433	1
Dr Thomas Weeks Wright Laboratory WDRC/FIMN Wright-Patterson AFB, OH 45433-6523	1
X-29A Advanced Development Program Office Wright Laboratory WL/FIMT Wright-Patterson AFB, OH 45433-6523	10
Aero Mechanics Division Wright Laboratory WL/FIM Wright-Patterson AFB, OH 45433-6523	1
Flight Control Division Wright Laboratory WL/FIG Wright-Patterson AFB. OH 45433-6523	1
Structures Division Wright Laboratory WL/FIB Wright-Patterson AFB, OH 45433-6523	1
Equipment Division Wright Laboratory WL/FIV Wright-Patterson AFB. OH 45433-6523	1

Distribution List (Continued)

Offsite Distribution	Number of Copies

Technology Exploitation Directorate
Wright Laboratory
WL/TXA
Wright-Patterson AFB, OH 45433-6523   1

Technology Exploitation Directorate
Wright Laboratory
WL/TXD
Wright-Patterson AFB, OH 45433-6523   1

Technical Library
Wright Laboratory
WL/IST
Wright-Patterson AFB, OH 45433-6523   1

Headquarters Systems Command
HQ AFSC/XR/XT/XTTA
Andrews AFB, MD 20334-5000   3

Technical Library
AFSC/TL
Andrews AFB, Washington, DC 20331   1

Aaron Brinson
AFATL/FXV
Eglin AFB, FL 32542-5434   1

3246 Test Wing/CC
Eglin AFB, FL 32542-5000   1

Technical Library
AD/AFATL/DOIL
Eglin AFB, FL 32542-5000   1

Headquarters Tactical Air Command
HQ TAC/DRB
Langley AFB, VA 23665-5000   1

Headquarters Tactical Air Command
HQ TAC/DRF
Langley AFB, VA 23665-5000   1

Colonel Michael Smith
USAF Academy
USAFA/DFAN
USAFA, CO 80840-5831   1

Distribution List (Continued)

Offsite Distribution	Number of Copies

Lt Col Jeff Ashworth
USAF Academy
USAFA/DFAN
USAFA, CO 80840-5831 — 1

Library
USAF Academy
USAFA/DFSEL-D
USAFA, CO 80840-5721 — 1

Technical Library
Arnold Engineering and Development Center
Arnold AFS, TN 37389-5000 — 1

AUL/LSE
Maxwell AFB, AL 36112-5000 — 1

Headquarters United States Air Force
HQ USAF/RD
Washington, DC 20330-5000 — 1

SAF/AL
Washington, DC 20330-5430 — 1

SAF/AQQU
Washington, DC 20330-1000 — 1

Bernie Kneeland
Naval Air Test Center/SA60
Patuxent River NAS, MD 20670-5000 — 1

Tom Santangelo
Naval Air Test Cente/SA60
Patuxent River NAS, MD 20670-5000 — 1

Captain Bob Trombadore
Naval Air Test Center/SA60
Patuxent River NAS, MD 20670-5000 — 1

Bill McNamara
Naval Air Test Center
PO Box 443
Patuxent River NAS, MD 20670-5000 — 1

Distribution List (Continued)

Offsite Distribution	Number of Copies
Commander Naval Air Test Center SA40 Patuxent River NAS, MD 20670-5000	1
USN Test Pilot School Naval Air Test Center SA40 Patuxent River NAS, MD 20670-5000	1
Central Library Naval Air Test Center Building 407 Patuxent River NAS, MD 20670	1
Carmen Mazza Naval Air Development Center Code 6053 Warminster, PA 18974	1
Technical Library Naval Air Development Center Warninster, PA 18974	1
Thomas Momiyama Naval Air Systems Command Code 931 Washington, DC 23061-9310	1
Director, Air Vehicle Division Naval Air Systems Command Washington, DC 23061-9310	1
Lt Col John Nix Defense Advanced Research Projects Agency DARPA/ASTO 1400 Wilson Boulevard Arlington, VA 22209-2308	1
Defense Technical Information Center DTIC/FCA Cameron Station Alexandria, VA 22304-6145	2
Joe Gera NASA Ames-Dryden Flight Research Facility NASA ADFRF/OF Edwards AFB, CA 93523-5000	1

Distribution List (Continued)

Offsite Distribution	Number of Copies

Joe Wilson
NASA Ames-Dryden Flight Research Facility
NASA ADFRF/OFV
Edwards AFB, CA 93523-5000   1

X-29A Project Office
NASA Ames-Dryden Flight Research Facility
NASA ADFRF/OP
Edwards AFB, CA 93523-5000   1

F-18 HARV Project Office
NASA Ames-Dryden Flight Research Facility
NASA ADFRF/OP
Edwards AFB, CA 93523-5000   1

PilotsU Office
NASA Ames-Dryden Flight Research Facility
NASA ADFRF/ODF
Edwards AFB, CA 93523-5000   1

Technical Library
NASA Ames-Dryden Flight Research Facility
NASA ADFRF
Edwards AFB, CA 93523-5000   1

Technical Library
NASA Ames Research Center
Moffett Field, CA 94035   1

Joe Chambers
NASA Langley Research Center
Mail Stop 246A
Hampton, VA 23665   1

Bill Gilbert
NASA Langley Research Center
Mail Stop 246A
Hampton, VA 23665   1

Luat Nguyen
NASA Langley Research Center
Mail Stop 355
Hampton, VA 23665   1

Patrick Murphy
NASA Langley Research Center
Mail Stop 498
Hampton, VA 23665   1

Distribution List (Continued)

Offsite Distribution	Number of Copies
Technical Library NASA Langley Research Center Hampton, VA 23665	1
Technical Library NASA Lewis Research Center Cleveland, OH 44135	1
Mr Ralph A'Harra NASA HDQ/Code RX 600 Independence Avenue SW Washington DC 20546	1
Robert Ryan Grumman Aircraft Systems Division Building 4839 Edwards AFB, CA 93523-5000	1
Joe Krumenacker Grumman Aircraft Systems Division Building 4839 Edwards AFB, CA 93523-5000	1
Paul Pellicano Grumman Aircraft Systems Division Building 4839 Edwards AFB, CA 93523-5000	1
Rod Womer Grumman Aircraft Systems Division Pacific Missle Test Center PO Box 42232, Plant 48 Pt Mugu, CA 93042	1
Joe Rivera Grumman Aircraft Systems Division PO Box 817 Port Huenme, CA 93044-0817	1
Kurt Schroeder Grumman Aircraft Systems Division Mail Stop B19-007 Calverton, NY 11933	1
Glenn Spacht Grumman Aircraft Systems Division Mail Stop C31-05 Bethpage, NY 11714	1

Distribution List (Continued)

Offsite Distribution	Number of Copies

William Mebes
Grumman Aerospace Corporation
Mail Stop C62-005
Bethpage, NY 11714   1

Technical Library
Grumman Aircraft Systems Division
Bethpage, NY 11714   1

Technical Library
Honeywell Incorporated
3660 Technology Drive
Minneapolis, MN 55418   1

Technical Library
Moog Aircraft Controls Division
Proner Airport
Seneca at Jamison Street
East Aurora, NY 14052   1

Tony Chamay
General Electric Company
Mail Drop 34016
100 Weston Avenue
Lynn, MA 01910-50001   1

Technical Library
General Electric Company
Post Office Box 5000
Binghamton, NY 13902   1

Juri Kalviste
Northrop Corporation
3836/82
1 Northrop Avenue
Hawthorne, CA 90250   1

Haig Asdurian
Northrop Corporation
1 Northrop Avenue
Hawthorne, CA 90250   1

Jerry Lockenour
Northrop Corporation
1 Northrop Avenue
Hawthorne, CA 90250   1

Distribution List (Continued)

Offsite Distribution	Number of Copies

Library
Northrop Corporation
3360-82
1 Northrop Avenue
Hawthorne, CA 90250   1

John Steurer
McDonnel Aircraft Company
Dept. 330, Bldg. 33, Level 4 N, Rm 463
PO Box 33
St. Louis, MO 63166   1

Leonard Impellizzeri
McDonnell Aircraft Company
Department 330, Building 33, Level 4 North, Room 463
Post Office Box 516
St Louis, MO 63166   1

E.H. Anderson
McDonnell Aircraft Company
Department 341, Building 32, Room 271
Post Office Box 516
St Louis, MO 63166   1

Fred Whiteford
McDonnell Aircraft Company
Mail Code 102 1311
Post Office Box 516
St Louis, MO 63166   1

David Riley
McDonnell Aircraft Company
Department 341, Building 32, Level 2, Mail Code 0341260
Post Office Box 516
St Louis, MO 63166   1

Mark Drajeske
McDonnell Aircraft Company
Department 341, Building 32, Level 2, Mail Code 0341260
Post Office Box 516
St Louis, MO 63166   1

Technical Library
McDonnell Douglas Corporation
Post Office Box 516
St Louis, MO 63166   1

Distribution List (Continued)

Offsite Distribution	Number of Copies

Technical Library
Douglas Aircraft Company
3855 North Lakewood Boulevard
Long Beach, CA 90401   1

Dr Richard Bradley
General Dynamics Corporation
Mail Zone 2888
Post Office Box 748
Fort Worth, TX 76101   1

Dr Carl Droste
General Dynamics Corporation
Mail Zone 2838
Post Office Box 748
Fort Worth, TX 76101   1

Art Sheridan
General Dynamics Corporation
Post Office Box 748
Fort Worth, TX 76101   1

Technical Library
General Dynamics Corporation
Post Office Box 748
Fort Worth, TX 76101   1

Research Library
General Dynamics Corporation
Post Office Box 80847
San Diego, CA 92138   1

Technical Library
General Dynamics Corporation
1675 West Fifth Street
Pomona, CA 91700   1

Dr John Retelle
Lockheed Corporation
4500 Park Granada Boulevard
Calabasas, CA 91399-0510   1

Dr Lee Nicolai
Lockheed California Company
Post Office Box 551
Burbank, CA 91520   1

Distribution List (Continued)

Offsite Distribution	Number of Copies

Albert Yackle
Lockheed California Company
Department 6905, Building 80, Second Floor
Post Office Box 551
Burbank, CA 91520   1

Clive Whitmore
Lockheed California Company
Department 75-81, B90-1
Post Office Box 551
Burbank, CA 91520   1

Robert Loschke
Lockheed Development Company
PO Box 551
Burbank, CA 91520   1

Information Services Department
Lockheed California Company
Post Office Box 551
2555 North Hollywood Way
Burbank, CA 91520   1

Roy Lange
Lockheed Aeronautical Systems Company
D/72-06, Zone 419
South Cobb Drive
Marietta, GA 30063   1

Technical Library
Lockheed Aeronautical Systems Company
86 South Cobb Drive
Marietta, GA 30063   1

Mark Burgess
Boeing Defense & Space Group
Mail Stop 4C-61
Post Office Box 3707
Seattle, WA 98124-2207   1

Doug Ilgenfrit
Boeing Advanced Systems Division
Mail Stop 33-18
Post Office Box 3707
Seattle, WA 98124   1

Distribution List (Continued)

Offsite Distribution	Number of Copies

Richard Hardy
Boeing Military Airplane Company
Mail Stop 4L-03
Post Office Box 3707
Seattle, WA 98124   1

Daril Hahn
Boeing Aircraft Company
Mail Stop 40-57
Post Office Box 3707
Seattle, WA 98124   1

Technical Library
Boeing Aircraft Company
Post Office Box 3707
Seattle, WA 98124   1

Director, Advanced Systems
Boeing Military Airplane Company
3801 South Oliver
Wichita, KS 67210   1

Technical Library
Boeing Aircraft Company
Wichita, KS 67210   1

Michael Robinson
Rockwell International
Post Office Box 92098
210 N. Douglas St
Los Angeles, CA 90009   1

Bob Bitten
Rockwell International
Mail Code 011-GB02
Post Office Box 92098
Los Angeles, CA 90009   1

Sid Powers
Rockwell International
Dept 736-MCPJ01-805-273-6000-5404
2825 E. Ave P.
Palmdale, CA 93550   1

Distribution List (Continued)

Offsite Distribution	Number of Copies

Ken Dyson
Rockwell International
Mail Code PI23
2825 E Ave P.
Palmdale, CA 93550   1

Fred Knox
Rockwell International
Mail Code PI20
2825 E Ave P.
Palmdale, CA 93550   1

Vice President, Strategic Planning
Rockwell International
2230 East Imperial Highway
El Segundo, CA 90245   1

Technical Library
Rockwell International
Post Office Box 92098
Los Angeles, CA 90009   1

Technical Library
Hughes Aircraft Company
8433 Fallbrook
Canoga Park, CA 91304   1

William Sears
LTV Aircraft Products Group
Post Office Box 65590
Dallas, TX 75265   1

David White
LTV Aircraft Products Group
Mail Stop 19414
Post Office Box 65590
Dallas, TX 75265   1

William Rhoades
LTV Aerospace Defense
PO Box 65590
Mail Stop 194-61
Dallas, TX 75265   1

Distribution List (Continued)

Offsite Distribution	Number of Copies
Technical Library Vought Corporation Post Office Box 225003 1600 Pacific Avenue Dallas, TX 75265-0003	1
Dr Robert Lopina LORAL Aeronautics Ford Road, Bldg 6, Rm H300 PO Box A Newport Beach, CA 92658	1
Technical Library Bendix Aerospace 43 Williams Street Teterboro, NJ 07608	1
Library Pratt & Whitney Aircraft Group Post Office Box 2691 West Palm Beach, FL 33402	1
Robert Flemming Sikorsky Aircraft Mail Stop S317AS 6900 Main Street Stratford, CT 06601	1
Dean Cooper Sikorsky Aircraft Mail Stop S317AS 6900 Main Street Stratford, CT 06601	1
Andy Skow Eidetics International 3415 Lomita Boulevard Torrance, CA 90505	1
Gerald Malcolm Eidectics International 3415 Lomita Boulevard Torrance, CA 90505	1
James Allburn SRS Technologies 1500 Wilson Boulevard Arlington, VA 22209	1

Distribution List (Continued)

Offsite Distribution	Number of Copies
Devere Henderson SRS Technologies 1500 Wilson Boulevard Arlington, VA 22209	1
Guy See SRS Technologies 1500 Wilson Boulevard Arlington, VA 22209	1
William Lamar SRS Technologies 238 Harman Boulevard Dayton, OH 45419	1
Bob Shaw Fighter Command IntUl 1831 Stonewood Dr Beavercreek, OH 45432	1
Avco Corporation Suite 200 333 West First Street Dayton, OH 45402	1
Technical Library Garrett 2525 West 190th Street Torrance, CA 90509	1
Daniel Cichy North American Aero Consultants 2655 Mitzi Drive Columbus, OH 43209	1
Larry Wellman David Taylor Research Center Bethesda, MD 20084-5000	1
Dr Norris Krone, Jr. University Research Foundation Suite 110 6411 Ivy Lane Greenbelt, MD 20770	1
Dr Donald Ward Texas A&M University College Station, TX 77843	1

Distribution List (Concluded)

Offsite Distribution	Number of Copies
Dr Eugene Covert Massachusetts Institute of Technology Room 33-207 Cambridge, MA 02139	1
Steven Hall Massachusetts Institute of Technology Room 33-103 Cambridge, MA 02139	1
Dr Jan Roskam University of Kansas 2004 Learned Hall Lawrence, KS 66045	1
Dr Richard Shevell 151 Stockbridge Ave Atherton, CA 94035	1
Thaddeus Sanford Rockwell International 12214 Lakewood Blvd Mail Code MA40 Downey, CA 90242-2695	1
Finley Barfield Wright Laboratory WL/FIGX Wright-Patterson AFB, OH 45433-6553	1
FTD/SDAA Wright-Patterson AFB, OH 45433-6508	1

Total Copies   226

DEPARTMENT OF THE AIR FORCE
AIR FORCE RESEARCH LABORATORY
WRIGHT-PATTERSON AIR FORCE BASE OHIO 45433

February 1, 2010

MEMORANDUM FOR: Defense Technical Information Center

ATTN: INFORSEC

8725 John J. Kingman, Suite 0944

Ft. Belvoir, VA 22060-6218

FROM: Det. 1 AFRL/WSC (STINFO)

2261 Monahan Way, Bldg.196, Rm 1

Wright-Patterson AFB, OH 45433-7035

SUBJECT: Notice of Change in Technical Report: AFFTC-TR-91-15

1. Distribution statement on the subject report should now be:

DISTRIBUTION STATEMENT A. Approved for public release; distribution is unlimited.

Originator Reference Number: RZ-10-0033
Case Reviewer: Michael Frangipane
Case Number: 88ABW-2010-0399
The material was assigned a clearance of CLEARED on 28 Jan 2010.

2. Point of contact is the undersigned at DSN 785-7415; 937-255-7415.

Annette J. Sheppard, GS11, DAF

Special Collections Librarian

Technical Reports Center